Western Graduate&PostdoctoralStudies

Western University
Scholarship@Western

Electronic Thesis and Dissertation Repository

4-8-2021 2:00 PM

Novel Imaging Tools Reveal the Dynamics of the Myocardial Growth Hormone Secretagogue Receptor in Heart Disease and Heart Failure

Rebecca Sullivan, *The University of Western Ontario*

Supervisor: Dhanvantari, Savita, *The University of Western Ontario*

A thesis submitted in partial fulfillment of the requirements for the Doctor of Philosophy degree in Pathology and Laboratory Medicine

© Rebecca Sullivan 2021

Follow this and additional works at: https://ir.lib.uwo.ca/etd

Part of the Cardiology Commons, Cardiovascular Diseases Commons, Cardiovascular System Commons, Diagnosis Commons, Medical Biophysics Commons, Medical Pathology Commons, and the Pathology Commons

Recommended Citation

Sullivan, Rebecca, "Novel Imaging Tools Reveal the Dynamics of the Myocardial Growth Hormone Secretagogue Receptor in Heart Disease and Heart Failure" (2021). *Electronic Thesis and Dissertation Repository*. 7788.
https://ir.lib.uwo.ca/etd/7788

This Dissertation/Thesis is brought to you for free and open access by Scholarship@Western. It has been accepted for inclusion in Electronic Thesis and Dissertation Repository by an authorized administrator of Scholarship@Western. For more information, please contact wlswadmin@uwo.ca.

Abstract

Heart disease (HD) is the leading cause of mortality worldwide. Currently, diagnosis is based on clinical features, imaging, and circulating cardiac biomarkers. Cardiac imaging technologies, such as echocardiography and cardiac magnetic resonance imaging (cMRI), enable the non-invasive detection of changes in heart function. Although these modalities can detect changes in structure and anatomy, it is usually at later stages, where prevention may not be possible. In conjunction with imaging, circulating biomarkers of heart failure (HF), notably B-type natriuretic peptide (BNP) and cardiac troponin I and T, can be detected with increased levels in the blood. These biomarkers are associated with other comorbidities and may not be specific to cardiac tissue. Thus, there is a critical need to develop imaging agents to detect the biochemical and molecular changes that precede gross structural changes in HD. There is evidence that the growth hormone secretagogue receptor (GHSR) and its ligand ghrelin, could be a potential molecular imaging target where expression is increased in HF. The purpose of my work was to characterize GHSR as a biomarker for the underlying biological mechanisms involved in heart disease and heart.

To characterize GHSR in end stage HF and valvular HD in humans, I used quantitative fluorescence microscopy with a custom far-red ghrelin analog to evaluate changes in the ghrelin-GHSR system and its downstream signalling. In this way, the ghrelin-GHSR system was elevated in HF and showed specific regional changes in HD. The ghrelin-GHSR system was correlated to heart function through left ventricular ejection fraction in HF while this system correlates regionally in only the left atrium in HD and no correlations are present in healthy tissue. Therefore, the ghrelin-GHSR system shows scalability from healthy to HD to HF.

After characterization of ghrelin-GHSR in the human heart, I evaluated this system using *in vivo* imaging techniques to track the heart after a myocardial infarction in canines. A novel molecular imaging agent demonstrated a unique binding pattern in the heart before and after a myocardial infarction. This binding pattern did not simply reflect cardiac perfusion showing specificity and correlated strongly with histological analysis of this system in the heart showing

sensitivity. Therefore, I identified a novel *in vivo* imaging agent to bind specifically and selectively in the canine heart.

In summary, my thesis describes the characterization of the changes in the myocardial ghrelin-GHSR system using novel imaging agents *in situ* and *in vivo*. These findings have important clinical application for the early detection of HD.

Keywords

Heart Disease/ Heart Failure, Biomarkers, Ghrelin - Growth Hormone Secretagogue Receptor, Quantitative Fluorescent Microscopy, Molecular Imaging, Positron Emission Tomography

Summary for Lay Audience

Heart disease is the leading cause of death worldwide. It is defined by any condition that negatively affects the structure or function of the heart. Heart disease may eventually develop into heart failure, which is defined by a weakened or damaged heart muscle that cannot pump blood throughout the body sufficiently. It is a difficult problem as there is no way to predict who will proceed to heart failure, or who will respond to therapies. Currently, heart disease is diagnosed using imaging methods, mainly ultrasound, that detect changes in the heart's anatomy and function. However, these changes are associated with late stages of the disease when prevention may not be possible. In addition to imaging, other signs, or markers, of heart failure can be measured in the blood, although they are not necessarily specific to cardiac tissue. Thus, there is a need to detect heart disease at earlier stages with markers specific to cardiac tissue using non-invasive imaging methods. I have used one such marker, called the growth hormone secretagogue receptor (GHSR), as a tool to develop new methods of imaging the heart. GHSR is known to be beneficial to heart health, as it helps to strengthen the heart muscle and prevents heart tissue from dying. Changes in GHSR levels may indicate early stages of heart disease. The purpose of my work was to identify how GHSR changes in heart disease and heart failure, and to design new imaging methods that target GHSR in the heart. I used advanced microscope techniques to show that GHSR increases in advanced heart failure, and changes to a much smaller extent in mild heart disease. I then developed a non-invasive radioactive imaging method to measure changes in GHSR in dogs before and up to 1 year after a heart attack. I found that GHSR levels decreased in the area of the heart injured in the heart attack, and increased specifically in the area surrounding the injured area immediately after the heart attack, and these changes were sustained for a period of one year. Therefore, I developed a new non-invasive imaging method that can evaluate specific changes in GHSR in the heart. In summary, my thesis describes the changes in GHSR in the heart in human heart disease, and the development of a specific imaging tool to detect these changes in GHSR non-invasively. This is important as alterations in GHSR can indicate early stages of heart disease and therefore will lead to improvements in early detection, which may lead to improved treatments and management of heart disease, thus decreasing the likelihood of progression to heart failure.

Co-Authorship Statement Chapter 2

The experiments in this chapter were performed primarily by Rebecca Sullivan in the laboratory of Dr. Savita Dhanvantari with the assistance of the coauthors listed below. For these experiments, the contribution from Dr. Savita Dhanvantari was of an intellectual nature with respect to experimental design, data analysis/ interpretation and manuscript preparation.

Dr. Varinder Randhawa collected and analyzed all the clinical data along with knowledge in the clinical assessment of clinical heart disease. Drs. Leonard Luyt and Tyler Lalonde developed the custom fluorescent imaging analogue used to target GHSR in this study. Derek Wu and Anne Stokes assisted in staining of some histological cardiac samples. Dr. Bob Kiaii collected the cardiac samples during cardiac surgery from all patients in this study. Dr. Gerald Wisenberg is a clinical cardiologist who helped with patient recruitment and knowledge in the clinical assessment of heart failure.

Co-Authorship Statement Chapter 3

The experiments in this chapter were performed primarily by Rebecca Sullivan in the laboratory of Dr. Savita Dhanvantari with the assistance of the coauthors listed below. For these experiments, the contribution from Dr. Savita Dhanvantari was of an intellectual nature with respect to experimental design, data analysis/ interpretation and manuscript preparation.

Dr. Varinder Randhawa collected and analyzed all the clinical data along with knowledge in the clinical assessment of clinical heart disease. Drs. Leonard Luyt and Tyler Lalonde developed the custom fluorescent imaging analogue used to target GHSR in this study. Tina Yu assisted in some staining of the histological cardiac samples. Dr. Bob Kiaii collected the cardiac samples during cardiac surgery from all patients in this study. Dr. Gerald Wisenberg is a clinical cardiologist who helped with patient recruitment and knowledge in the clinical assessment of heart failure.

Co-Authorship Statement Chapter 4

The experimental analyses in this chapter were performed primarily by Rebecca Sullivan in the laboratory of Dr. Savita Dhanvantari with the assistance of the coauthors listed below. For these experiments, the contribution from Dr. Savita Dhanvantari was of an intellectual nature with respect to experimental design, data analysis/ interpretation and manuscript preparation.

Dr. Jonathan Thiessen and Ben Wilk helped with analysis and knowledge on imaging methodology (both PET and MRI) and programming analysis software. Drs. Leonard Luyt, Jinqiang Hou, and Lihai Yu developed the PET imaging agent used to target GHSR in vivo in this study. Dr. Justin Hicks helped with the generation of PET imaging probes used in this study and the development if initial metabolite analysis. MRI technologists John Butler and Heather Biernaski performed all PET/MRI experiments at all time points. Animal care and anesthesia of animals were performed by the veterinarian technologists Jane Sykes and Lela Deans. The experimental design and all animals were used as part of a bigger project in collaboration with Drs. Frank Prato and Rohan Dharmakumar.

“I am strong. You can’t beat me. I won’t let you win.”

- Rebecca Sullivan

Acknowledgments

To my supervisor, Dr. Savita Dhanvantari, I would like to express my overwhelming gratitude for your unwavering support through my project. Your advice and encouragement have been instrumental in my progress through my doctoral studies. The open and inviting atmosphere you create in your lab has helped to allow your students to grow and learn new things each day. You are an amazing mentor who helped open many doors and you provided incredible opportunities throughout my academic journey. I am forever grateful for the positive and supportive environment you provided during my scientific journey through my doctoral degree.

During my doctoral study, I have been fortunate to receive stipend support through a Lawson Internal Research Fund Studentship, an Alexander Graham Bell Canada Graduate (NSERC) Scholarship, a Frederick Luney Pathology Research Scholarship, as well as travel support from the Collaborative Program in Molecular Imaging. Additionally, the Canadian Institutes of Health Research and Natural Sciences and Engineering research Council of Canada supported my research in Dr. Dhanvantari's laboratory.

I would like to thank my advisory committee members: Dr. Edith Arany who has been incredibly encouraging and supportive in all aspects of my project. You have helped provide advice and assistance I needed extra support and knowledge with my project; and Dr. Gerald Wisenberg who has helped to shape the type and direction of my research project. Your help and guidance have been incredibly important in the progression of my doctoral studies.

To my past and present lab mates, you have been the most supportive and encouraging group of people I could have asked for to tackle this tough journey with. Ahmed, you were with me from day-one and you have shown me what hard work and dedication can lead to. Thank you for being my first friend on this journey. Farzad, you are the nicest person I have ever met, and you have always been there to help me when I am stuck, with anything and at any time of day. Thank you for your continued support through experiments and expert knowledge that helped me instrumentally through my project. Maya, thank you for your friendship and unwavering support through my project and doctoral studies. Thank you all for your continued friendship that I will cherish forever!

I would like to say a special thank you to Ben Wilk for not only helping me through this journey but for a best friend that will stay with me forever. You have helped to shape not only my project, but my academic life more than you can know. I am forever thankful for all that you have done and continue to do for me. Thank you to Sandra Szlapinski for being a crucial support during my project and a friend that I was able to go through this journey with. I will cherish your friendship forever.

Thank you to my friends and family who were there for me throughout my PhD. My amazing friends who put up with my constant talk of research and were sounding boards whenever I needed them: Katie W, Alyssa, Tim, Katie G, Brittany, Emily, and Nina, you have always been there when I need you and you support me in more ways than you know. Thank you for being the best friends I could ask for! To my aunts, uncles, grandparents, and cousins, thank you for everything.

To my boyfriend, James, thank you for allowing me to continuously talk about my work and for putting up with me throughout this journey. I do not know where I would be without your continued love and support.

Most importantly, I would like to thank my parents, Janyce and Joe, and my brother Scott. Thank you for all you have done for me and for always encouraging me to do my best. You have been immensely patient with me through this journey, and I will always be thankful for your eternal support. Thank you all for teaching me the value of hard work and determination. I would not be where I am today without the amazing role models and inspiration that you are in my life. I cannot thank you enough for the love and support you have given me through this tough journey, and I hope that I have made you proud.

Table of Contents

Abstract ii

Summary for Lay Audience iv

Co-Authorship Statement Chapter 2 v

Co-Authorship Statement Chapter 3 vi

Co-Authorship Statement Chapter 4 vii

Acknowledgments ix

Table of Contents xi

List of Tables xvi

List of Figures xvii

List of Supplemental Figures xix

List of Appendices xx

List of Abbreviations, Symbols, and Nomenclature xxi

Chapter 1 1

1 Introduction 1

1.1 Heart Failure Progression 1

1.1.1 Heart Failure Pathophysiology 3

1.1.2 Management of Heart Failure 8

1.2 Diagnosis of Heart Disease and Heart Failure 10

1.2.1 Clinical Diagnosis of HF 10

1.2.2 Echocardiography in Clinical HD 12

1.2.3 Cardiac CT and MRI 15

1.2.4 Cardiac PET Imaging 18

1.2.5 Cardiac Perfusion PET Tracers 20

1.2.6 Inflammation in the Heart with ^{18}F-FDG PET 21

1.2.7 Neuronal Cardiac PET Imaging 23

1.2.8 Emerging Cardiac PET Tracers 24

1.2.9 Simultaneous PET/CT and PET/MR Imaging 25

1.3 Heart Failure and Heart Disease Biomarkers 27

1.3.1 Biomarkers of Cardiomyocyte Stress 27

1.3.2 Biomarkers of Cardiac Damage 29

1.3.3 Inflammatory Biomarkers 31

1.3.4 Specificity of Cardiac Biomarkers 33

1.4 Ghrelin-GHSR as a Novel Biomarker 34

1.4.1 GHSR and Ghrelin Discovery 34

1.4.2 GHSR Signalling in the Heart 36

1.4.3 Argument for GHSR as a Biomarker in Heart Disease and Heart Failure 42

1.4.4 Imaging Agents Targeting GHSR: Fluorescent Probes and PET Tracers 44

1.5 Rationale and Aims of the Study 48

1.6 References 49

Chapter 2 74

2 Dynamics of the Ghrelin-Growth Hormone Secretagogue Receptor System in the Human Heart Before and After Cardiac Transplantation 75

2.1 Introduction 76

2.2 Methods 78

2.2.1 Patient Cohort 78

2.2.2 Immunofluorescence Microscopy 81

2.2.3 Fibrosis Imaging 83

2.2.4 Data Analysis 83

2.3 Results 84

2.3.1 Cardiac Transplant Patient Cohort 84

2.3.2 GHSR and Ghrelin Expression in Cardiomyocytes 84

2.3.3 Metabolic Markers in Cardiac Tissue 86

2.3.4 Cardiac Fibrosis 89

2.4 Discussion 93

2.5 References 99

Chapter 3 104

3 Regional Differences in the Ghrelin-Growth Hormone Secretagogue Receptor Signalling System in Human Heart Disease 104

3.1 Introduction 105

3.2 Methods 107

3.2.1 Patient Cohort 107

3.2.2 Quantitative Fluorescence Microscopy 110

3.2.3 Background Subtraction for Fluorescence Microscopy Imaging 112

3.2.4 Image Acquisition and Analysis 112

3.2.5 Fibrosis Imaging 113

3.2.6 Data Analysis 114

3.3 Results 114

3.3.1 Cardiac Surgery Patient Cohort 114

3.3.2 Correlations Between GHSR and Ghrelin in Diseased Cardiac Tissue .. 115

3.3.3 Relationship of BNP to GHSR and Ghrelin in Diseased Cardiac Tissue 118

3.3.4 Intracellular Colocalization of Ghrelin and BNP in Cardiomyocytes 120

3.3.5 The Relationship of the Cardiac Contractility Biomarker SERCA2a to Ghrelin and GHSR in the diseased Heart 122

3.3.6 Cardiac Fibrosis 124

3.4 Discussion 125

3.5 Supplemental Figures 130

3.6 References 132

Chapter 4 137

4 Hybrid PET-MRI for Spatio-Temporal Tracking of Alterations in GHSR before and after Myocardial Infarction using a Novel ^{18}F-labelled Ghrelin Analogue 137

4.1 Introduction 138

4.2 Methods 139

4.2.1 Production of ^{18}F and Synthesis of ^{18}F-LCE470 139

4.2.2 Animal Use and Surgical Preparation 141

4.2.3 Positron Emission Tomography/ Magnetic Resonance Imaging 141

4.2.4 Tissue Harvesting and Imaging Acquisition 151

4.3 Results 154

4.3.1 ^{18}F-LCE470 Tracer Uptake in the Left Ventricle 154

4.3.2 Perfusion Throughout the Left Ventricle 158

4.3.3 ^{18}F-LCE470 Uptake Does Not Correlate with Perfusion in Remote or Left Circumflex Regions 162

4.3.4 Specificity of ^{18}F-LCE470 Binding in Cardiac Tissue 163

4.3.5 Fibrotic Deposition and Circulating Ghrelin 167

4.3.6 Heart Function Before and After MI 169

4.4 Discussion 170

4.5 Supplemental Figures 180

4.6 References 182

Chapter 5 190

5 Discussion, Future Studies, and Clinical Significance 190

5.1 Cardiac Ghrelin-GHSR System is a Scalable Marker for Heart Disease 190

5.2 Is the Ghrelin-GHSR System a Clinical Diagnostic Biomarker? 192

5.3 In Vivo GHSR PET Tracer Optimization 192

5.4 Can GHSR Imaging be Used for Clinical Diagnosis for Cardiac Impairment? . 194

5.5 Elucidation of the Relationship Between GHSR and Inflammation 195

5.6 References 204

Appendices 209

Curriculum Vitae 215

List of Tables

Table 1.1 Types of Echocardiography Used in Clinic. 14

Table 1.2 Common Cardiac Perfusion Tracer for PET Imaging[80] 20

Table 2.1 Cardiac Transplant Recipient Patient Demographics 79

Table 2.2 Patient Medications Pre- and Post-Cardiac Transplant 80

Table 2.3 Antibody Table – Information on Antibodies Used. 82

Table 2.4 Fibrosis Percentages of explanted hearts and healthy implanted heart biopsies. ... 92

Table 3.1 Cardiac Surgery Patient Demographics. 108

Table 3.2 Patient Medications Post-Heart Surgery. 109

Table 3.3 Antibody Table – Information on Antibodies Used. 111

List of Figures

Figure 1.1 Calcium Regulation and Contractility Signaling in Cardiomyocytes. 37

Figure 1.2 Proposed Biochemical Signalling Cascade of ghrelin-GHSR in Cardiomyocytes. 41

Figure 2.1 Ghrelin and GHSR expression in patients pre- and post- cardiac transplant. 85

Figure 2.2 Cardiac metabolic markers in patients pre- and post-cardiac transplant in entire transplant patient cohort. 87

Figure 2.3 BNP expression in patients pre- and post-cardiac transplant. 88

Figure 2.4 Cardiac fibrosis in patients pre- and post-cardiac transplant. 90

Figure 2.5 Fibrosis and GHSR in human myocardial tissue. 91

Figure 3.1 Representative confocal fluorescence images of all biomarkers. 116

Figure 3.2 GHSR and ghrelin fluorescence intensity in human cardiac tissue. 117

Figure 3.3 BNP correlation to ghrelin-GHSR. 119

Figure 3.4 Intracellular colocalization of ghrelin and BNP in control LV. 121

Figure 3.5 SERCA2a correlation to ghrelin-GHSR and BNP 123

Figure 3.6 Fibrosis deposition in healthy and diseased tissue. 124

Figure 4.1 Stacked HPLC chromatograms. 140

Figure 4.2 PET/MR Imaging Schematic. 142

Figure 4.3 Representative images of LV segmentation. 145

Figure 4.4 Polar map segmentation with manual grouping of segments into 3 regions. 148

Figure 4.5 In vivo ^{18}F-LCE470 in canine model of myocardial infarction (n=4). 155

Figure 4.6 Compartmental modelling of ^{18}F-LCE470 in the left ventricle of canine hearts (n=4)..... 157

Figure 4.7 Analysis of perfusion imaging tracer in dogs (n=4)..... 159

Figure 4.8 Compartmental Modelling of Perfusion Tracer ^{13}N-NH_3 in the left ventricle of canine hearts (n=4)..... 161

Figure 4.9 Correlation of ^{18}F-LCE470 and ^{13}N-NH_3 uptake. 163

Figure 4.10 Tissue Characterization of GHSR in Canine Heart..... 164

Figure 4.11 Cy5-cyclo-ghrelin(1-20) specificity in canine tissue. 165

Figure 4.12 Correlation of GHSR tissue analysis to ^{18}F-LCE470 TBR and distribution volume at end point..... 166

Figure 4.13 Representative qualitative images of fibrosis and hematoxylin and eosin (H&E) are shown in each region..... 168

Figure 4.14 Heart Function Analysis (n=4). 169

Figure 5.1 ^{18}F-FDG imaging in the canine heart after MI. 197

Figure 5.2 Quantification of glucose metabolism with ^{18}F-FDG in canine heart after MI... 200

Figure 5.3 Correlation between inflammation (^{18}F-FDG) and GHSR (^{18}F-LCE470) over time. 201

List of Supplemental Figures

Supplemental Figure 2.S1 Ghrelin and GHSR Correlation in End-Stage HF and Engrafted Heart Biopsies. 98

Supplemental Figure 3.S1 Punctate staining with RenyiEntropy algorithm……. 130

Supplemental Figure 3.S2 Comparison between paraffin embedded control human tissue and frozen healthy heart biopsy samples. 131

Supplemental Figure 4.S1 Time-activity curves showing regional uptake of ^{18}F-LCE470 in infarct, remote, left circumflex area, and blood pool. 180

Supplemental Figure 4.S2 Metabolite Analysis..... 181

List of Appendices

Appendix A 1. Human Ethics Protocol Approval: Cardiac Transplantation and Surgery Study 209

Appendix A 2. Animal Use Protocol Ethics Approval: Cardiac PET/MRI in the Canine Heart 210

Appendix A 3. Permission to Reproduce Sullivan et al. 2019 J. Endocr. Soc. 211

Appendix A 4. Permission to Reproduce Sullivan et al. 2020 CJC Open 213

List of Abbreviations, Symbols, and Nomenclature

α	alpha
β	beta
γ	gamma
κ	kappa
^{11}CHED	11C-meta-hydroxyephiderine
^{11}CPIB	11C-pittsburg
^{13}N-NH3	13N-ammonia
^{15}OH2	15O-water
^{18}F-FDG	18F-fluorodeoxyglucose
^{18}F-NaF	18F-sodium fluoride
2D	two-dimensional
3D	three-dimensional
^{69}Ga-DOTATATE	68Ga-[1,4,7,10-tetraazacyclododecane-N,N',N'',N'''-tetraacetic acid]-d- Phe1,Tyr3-octreotate
^{82}Rb	82-rubidium
ACC	american college of cardiology
ACE	angiotensin converting enzyme
Act A	activin A

AHA	American heart association
Akt	protein kinase B
AMPK	adenosine monophosphate-activated protein kinase
Ang II	angiotensin II
ANOVA	analysis of variance
ANP	atrial natriuretic peptide
AP-1	activator protein-1
ARB	angiotensin II receptor blockers
ARNI	angiotensin receptor-neprilysin inhibitors
ATP	adenosine triphosphate
AU	arbitrary unit
Bi	biopsy
BNP	natriuretic peptide type-B
Ca2+	calcium
CAD	coronary artery disease
CAMKK	calcium-calmodulin-dependent protein kinase kinase
cAMP	cyclic adenosine monophosphate
$\mathbf{C_{bound}}$	concentration bound
CCAC	Canadian council on animal care

C_{free}	concentration free
cGMP	cyclic guanosine mono-phosphate
CHF	chronic heart failure
CHOP	C/EBP homologous protein
CI	confidence interval
cMRI	cardiac magnetic resonance imaging
CO	cardiac output
CorC	correlation coefficient
C_{plasma}	concentration in plasma
CRP	c-reactive protein
CSNA	cardiac sympathetic nerve activity
CT	computed tomography
C_{tissue}	concentration in tissue
cTn	cardiac troponin
cTnI	cardiac troponin I
cTnT	cardiac triponin T
CTP	computed tomography perfusion
DAPI	4',6-diamidino-2-phenylindole
DCM	diabetic cardiomyopathy

DNA	deoxyribonucleic acid
DV	distribution volume
Echo	echocardiography
ERK	extracellular signalling related kinase
ERS	endoplasmic related stress
FA	fatty acid
FA-acyl-CoA	fatty acid acyl-coenzyme A
FITC	fluorescein isothiocyanate
Gd	gadolinium
Gd-DTPA	gadolinium-diethylenetriamine penta-acetic acid
GFP	green fluorescent protein
GHSR	growth hormone secretagogue receptor
GOAT	ghrelin O-acyl transferase
GPCR	g protein-coupled receptor
GPCR39	g protein-coupled receptor 39
GRP78	glucose-regulated protein 78
H&E	hematoxylin and eosin
HD	heart disease
HF	heart failure

H-FABP	heart-type fatty acid-binding protein
HFpEF	heart failure with preserved ejection fraction
HFrEF	heart failure with reduced ejection fraction
HMGB1	high mobility group box 1
hs-CRP	high-sensitivity c-reactive protein
HSP60	heat shock protein 60
I/R	ischemia/ reperfusion
IL-1	interleukin-1
IL-1β	interleukin 1-beta
IL-33	interlerkin-33
IL-6	interleukin-6
Inf	infarct
IP_3	inositol 3 phosphate
IP_3R	inositol 3 phosphate receptor
LA	left atrium
LAD	left anterior descending coronary artery
LAMP-2	lysosomal-activated membrane protein-2
LCX	left circumflex artery
LEAP2	liver-expressed antimicrobial peptide 2

LGE	late gadolinium enhancement
LHSC	London health sciences center
LTCC	L-type calcium channel
LUT	look up tables
LV	left ventricle
LVAD	left ventricular assist device
LVEF	left ventricular ejection fraction
LVH	left ventricular hypertrophy
MAP	mean atrial pressure
MI	myocardial infarction
MPTP	mitochondrial permeability transition pore
MRAC	magnetic resonance attenuation correction
MRI	magnetic resonance imaging
mRNA	messenger ribonucleic acid
MT	Masson's trichrome
mTOR	mechanistic target of rapamycin
NE	norepinephrine
NF-κB	nuclear factor kappa B
NT-ANP	N-terminal atrial natriuretic peptide

NT-proBNP	N-terminal pro-natriuretic peptide type B
NXC	sodium-calcium exchanger
NYHA	New York heart association
OCT	optimal cutting temperature
PBS	phosphate buffer solution
PCC	pearson correlation coefficient
PET	positron emission tomography
PFPN	6-fluoro-2-pentafluorophenyl naphthoate
PKA	protein kinase A
PKC	protein kinase C
PLB	phospholambin B
PLC β	phospholipase C β
PPAR-γ	peroxisome proliferator-activated receptor gamma
PTx	Post-transplantation
RA	right atrium
RAAS	renin angiotensin-aldosterone system
Rem	remote
ROI	region of interest
ROS	reactive oxygen species

RT	room temperature
RV	right ventricle
RyR2	ryanodine 2
SD	standard deviation
SERCA2a	sarcoplasmic reticulum ATPase pump
SGLT2	sodium-glucose cotransporter-2
SPECT	single photon emission computer tomography
SR	sarcoplasmic reticulum
ST2	suppression of tumorigenicity 2
TAC	time activity curve
TBR	tissue to blood ratio
TGF-β1	transforming growth factor beta 1
TLR4	toll-like receptor 4
TNF	tumor necrosis factor
TNFR1	tumor necrosis factor receptor 1
TNFR2	tumor necrosis factor receptor 2
TNF-α	tumor necrosis factor alpha
TPR	total peripheral resistance

Chapter 1

1 Introduction

According to the Heart and Stroke Foundation report (2019) there are currently 2.4 million Canadians living with heart disease (HD)[1]. HD includes impairment and damage to heart muscles or structures that refer to cardiomyopathies including heart wall thickening, severe inflammation, cardiac muscle rigidity, and conductivity derangements. If HD becomes severe, heart function progressively worsens, leading to the clinical syndrome of heart failure (HF). Of the 2.4 million people with HD, over 600,000 are living with HF[2]. HF occurs when the heart cannot pump enough blood to provide sufficient oxygen to the rest of the body, often caused by systolic heart failure where the heart muscle is too weak to pump blood sufficiently[1]. HF places a significant burden on both the patient and the global health care system's limited resources as 40% of people admitted to the hospital are readmitted for adverse cardiac events. Significant advancements in diagnosing and treating patients with HF, specifically caused by myocardial infarction, have reduced the incidence of death but have also led to increased risk of future cardiac events[1,2].

1.1 Heart Failure Progression

The heart is one of the most efficient organs which contains the contractile force to pump blood throughout the body. The wall of the heart is composed of three distinct layers; epicardium (outermost layer of the wall), endocardium (inner most layer), and the myocardium (intermediate and most prominent layer of the heart). The heart contains 4 distinct chambers; the left and right atria, which are small, thin-walled chambers, and the left and right ventricles, the large thick-walled chambers where most of the work is performed. The right atrium (RA) receives blood from the venous system where contraction results in ejection of blood to the right ventricle (RV). The RV pumps blood to

the lungs for oxygenation and is pumped back into the left atrium (LA). The blood is ejected into the left ventricle (LV) which facilitates blood flow throughout the body. Impairment in this process causes cardiac dysfunction; when impairment becomes chronic, it can lead to HF. HF is a clinical syndrome characterized by impaired cardiac output and/or volume overload resulting in the inability to meet the metabolic demands of the body. HF is also commonly associated with structural abnormalities. The two most common forms of HF are: 1) systolic HF where reduced ejection fraction is caused by weakening of the ventricular wall and decreased contractile force; and 2) diastolic HF with preserved ejection fraction and stiffened ventricular walls that are unable to fully relax and fill the chamber with enough blood to pump to the rest of the body[3]. HF can originate from different causes: 1) directly from the heart including congenital heart defects in the valves or chambers of the heart; cardiomyopathies resulting from infection or pressure overload; vasculopathies typically from coronary artery disease and myocardial infarction; and arrythmias caused by electrical failure in the heart, and 2) whole body effects, such as hypertension, lung disease, diabetes complications and drug misuse. In advanced stages of HF, perfusion becomes severely limited, leading to fluid retention in the lungs and peripheral tissues potentially resulting in renal failure. The body compensates through cardio-protective events such as increasing heart rate, sympathetic activation, and up-regulation of hormonal blood pressure through the renin-angiotensin-aldosterone system (RAAS). However, once HF is established in an individual, the functional and structural changes may respond to conventional treatments that manage patient symptoms until the heart deteriorates to the point where advanced therapies/ interventions are needed[4]. Predicting which patients proceed to HF after initial symptoms or trauma remains difficult.

There are many risk factors that are associated with the onset of HF. These include diabetes, smoking, high cholesterol (specifically high low-density lipoprotein levels), high blood pressure, physical inactivity, obesity, age, and previous cardiac conditions[5]. Thus, reduced and preserved ejection fraction (HFrEF and HFpEF, respectively) present with these risk factors which contribute to the progression of HF[3]. HFrEF is usually characterized by an enlarged LV that results in global decreased cardiac output while HFpEF is usually characterized by a normal-sized LV with global impairment of depressed cardiovascular function[6].

HF has become a global health problem where prevalence is on the rise with enormous health care expenditures. In industrialized countries, roughly 0.4-2.2% of the population suffer from HF and rates increasing with age with 9.2 fold increases in prevalence in individuals over 65 years of age[7]. In overall HF incidence, the elderly population accounts for 80% of HF-related hospitalizations and 90% of HF-related deaths[7]. HF presence is increasing in the population largely due to the aging population coupled with the advancements in treatments and diagnostic technology that lead to improved outcomes for patients. Therefore advancements in how HF is diagnosed and treated are necessary[8]. In Sub-Sarharan Africa, cardiovascular disease is progressively taking over infectious disease as the leading cause of mortality with mortality rates range variably from 60 days at 9.5% up to 3 years with 67.1% mortality[9]. With worldwide HF prevalence increasing there is a larger economic burden placed on health care systems both directly and indirectly. Globally, the economic burden of HF is roughly $108 billion[7] with the cost of Canada's health care system being $2.8 billion annually[2]. According to one study that evaluated the readmission rates of Canadians after primary diagnosis of HF in 2015, 18.2% were readmitted within 30 days where older patients were readmitted more frequently than younger patients. Patients who were readmitted had high comorbidity burdens, more hospitalizations in 6-months prior to HF diagnosis, and a longer length of stay at the hospital[10]. With an increasing aging population, there is an expected increase of HF patients with comorbid conditions which could ultimately increase HF mortality. HF rates may also increase due to common trends including increases in physical inactivity, obesity, poor eating habits, and diabetes[11]. Therefore, there is a need for more compelling and innovative strategies to counter the effects of HF on the health care system.

1.1.1 Heart Failure Pathophysiology

Heart failure is a complex clinical syndrome that has a diverse path of progression. When the heart starts to fail, many compensatory mechanisms are initiated, which eventually contribute to the pathophysiology of HF[12]. Compensation occurs as the heart strives to maintain overall cardiac output (CO) as declining mean atrial and ventricular pressures

decrease cardiac perfusion. This increases the left ventricular (LV) end-diastolic pressure with stretching of the myocardial wall and restoration of the CO[13] through mechanisms of sympathetic activation, neurohormonal regulation and cardiac remodeling, along with alterations in biochemical signalling pathways[13]. The main signalling pathways used to compensate for HF include calcium regulation for contractility, cellular death/ survival pathways, and myocardial energy metabolism.

Cardiac output (CO) represents the amount of blood pumped out of the heart as a product of heart rate and stroke volume. CO is also affected by ventricular contraction, chamber wall integrity, and valvular competence[12]. Left ventricular (LV) dysfunction is commonly associated with left atrial (LA) pressure and pulmonary congestion. Right ventricular failure occurs with LV failure and similarly, alterations in right atrial pressures. When the CO along with total peripheral resistance (TPR) decreases, the mean atrial pressure (MAP) and, in turn, tissue perfusion, decrease. The body compensates for decreased CO by increasing the heart rate with subsequent increases in neurohormone secretion[12] and increasing stroke volume via either LV dilation (muscle stretching and thinning) or LV hypertrophy (muscle thickening). Chronically, this process becomes detrimental ultimately resulting in impaired contractility, increases in cell death, a switch in metabolic substrates, initiation of inflammation, all of which lead to further cardiac damage.

Another component of the compensatory mechanism is cardiomyocyte hypertrophy. Since cardiomyocytes lack the ability to divide, cardiomyocyte hypertrophy is a compensatory mechanism to trauma where cells increase in size and mass to normalize wall stress and allow normal function of the heart at rest[14]. This increased size and mass are accompanied by biochemical and molecular mechanism changes to help with cardiomyocyte compensation including contractility, cell survival/ death, and cardiomyocyte metabolism.

The regulation of calcium (Ca^{2+}) homeostasis within cardiomyocytes plays an important role in contractile function (excitation-contraction coupling) in the cardiomyocytes. Contractile function encompasses both contraction (systole) and relaxation (diastole). In contraction, the cell membrane is depolarized through action potentials from neighboring cells allowing for Ca^{2+} to enter the cardiomyocyte through the L-type calcium channel

(LTCC) on the cell membrane. This Ca^{2+} binds to the ryanodine 2 receptor (RyR2) on the sarcoplasmic reticulum (SR) membrane causing an efflux of Ca^{2+} from the SR to the cytosol. The excess of Ca^{2+} in the cell causes contractile proteins to activate. Upon relaxation, the cytosolic Ca^{2+} is pumped back into the SR using SR ATPase pump SERCA2a, and the remaining Ca^{2+} is removed from the cell using the sodium-calcium exchanger (NCX) on the cell membrane[3,15]. In HF, this process is disrupted through either accumulation of excess Ca^{2+} in the cytosol or decreased Ca^{2+} in the SR during the contraction and relaxation processes. Excess amounts of Ca^{2+} can be the result of defects in the LTCC causing too much Ca^{2+} to enter the cell or NCX where Ca^{2+} cannot fully exit the cell[15]. A dysfunction in the RyR2 can cause Ca^{2+} to leak from the SR and accumulate in the cytosol[3] while dysfunction in SERCA2a pump can cause reduced uptake into the SR causing systolic dysfunction. SERCA2a dysfunction can also reduce the speed and quantity of Ca^{2+} transport out of the cytoplasm, thus inhibiting relaxation and causing diastolic dysfunction[3,15,16]. Therefore, Ca^{2+} flux in the cardiomyocytes, specifically in the SR, is highly regulated and can provide therapeutic targets for LV dysfunction.

HF is commonly characterized by increased rates of cell death, commonly through apoptosis, necrosis, or autophagy, ultimately leading to excessive depletion of cardiomyocytes and HF. In the normal functioning heart, cycles of apoptosis and autophagy occur at low basal levels during the process of cardiomyocyte turnover[17]. When these processes become overactive and new cells cannot replace old cells at such rates, the heart starts to fail.

Apoptosis is a highly regulated process of programmed cell death that occurs through extrinsic and intrinsic pathways, characterized by blebbing of the cell membrane, cell shrinkage and formation of apoptotic bodies. In the intrinsic pathway, hypoxia, ischemia/reperfusion, or oxidative stress induce the opening of the mitochondrial permeability transition pore (MPTP) on the mitochondrial membrane. This leads to a release of proteins from inside the mitochondria (cytochrome C, endonuclease G, and apoptosis-inducing factor) to form apoptosomes containing caspase-9, which activate caspase-3 to initiate DNA fragmentation and cell death[18]. This is the most prominent apoptotic process in cell death. The extrinsic pathway involves the “death receptors” Fas

and tumor necrosis factor (TNF) receptors, which are upregulated during myocardial ischemia and HF. When these receptors are bound and activated by their ligands, they form signalling complexes that recruit caspase-8, leading to activation of caspase-3 for cell death. It is still questionable today if apoptosis is the most prominent form of cell death in common types of HF (ischemic and dilated cardiomyopathy)[19].

Cell death in the form of necrosis occurs when there is trauma or damage to the cardiomyocytes usually by nutrient shortage, or exposure to harsh environments. In early stages of necrosis, there is organelle/ cytoplasmic swelling and disrupted cellular functions, eventually leading to rupture of the cell membrane that releases all cellular contents. This is not a form of programmed cell death as there is no formation of apoptotic cell bodies[20]. Necrosis is commonly associated with myocardial infarction, cardiac ischemia/ reperfusion and HF with a prolonged period of restricted blood flow resulting in a lack of nutrients for cellular function[21].

Autophagy is the process of intracellular organelle and protein enzymatic degradation that alters nutrient homeostasis in the cell. Cellular stress triggers degradation of excess organelles and proteins, which would otherwise lead to pressure overload-induced hypertrophy, oxidative stress, and myocardial ischemia which can all lead to HF[20]. In autophagy, deficiency in the lysosomal-activated membrane protein-2 (LAMP-2) causes increased autophagosomes in cardiomyocytes. In a model of Danon's disease (a lysosomal glycogen storage disease) heart dysfunction and HF are common characteristics where defects in autophagy caused by LAMP-2 deficiency in the myocardium causes cardiac dysfunction[22]. The entire process of autophagy is not fully understood although there are known activators, including phosphatidylinositol-3 kinase and Beclin-1, and suppression of these activators causes disruption in the maintenance of metabolic requirements in the cell. Treatments for HF have been developed to target the AMPK/ Akt/ mTOR pathway where autophagic defects are restored and cardiac function is improved[23–25].

Cardiac energy metabolism in the healthy heart encompasses primarily fatty-acid (FA) oxidation used by mitochondria while glucose metabolism is responsible for minimal energy production. FAs oxidation accounts for 60-90% of adenosine triphosphate (ATP)

production in the healthy heart. FAs in the cytoplasm are converted to FA-acyl-coenzyme A (FA-acyl-CoA) by fatty acyl-CoA synthase which gets esterified before entering the mitochondria. Once in the mitochondria, it gets converted back to FA-acyl-CoA for beta-oxidation. This process produces ATP but consumes oxygen in the process[26]. To produce ATP, glucose enters the cell through glucose transporters on cell membranes and proceeds through glycolysis, which uses less oxygen compared to FA oxidation. The products from the glycolysis pathway are transferred to the mitochondria to continue with energy production[27]. This ability to utilize energy substrates based on availability allows the heart some metabolic flexibility through complex regulatory mechanisms.

HF is accompanied by derangements in all aspects of energy metabolism including substrate uptake, utilization, and oxidative phosphorylation which ultimately decreases the rate of ATP synthesis, resulting in LV dysfunction[28]. Substrate uptake and utilization switches from primarily FA to glucose utilization, likely because FA oxidation uses 10-12% more oxygen when compared to glucose metabolism to generate the same amount of ATP. Therefore, FA usage in HF can waste oxygen and increase damage to the heart[26]. In contrast, in advanced HF and in ischemia/reperfusion, there is decreased FA and glucose metabolism which may be explained by decreased activity of mitochondrial enzymes for FA oxidation and mitochondrial dysfunction[27]. It is not fully known whether the altered substrate metabolism in HF is a cause or a consequence of LV dysfunction. It is suggested that the accumulation of FA in the cytosol can lead to toxic lipid species that may contribute to HF, meanwhile, the switch to glucose metabolism is an adaptive process to minimize damage in the failing heart[28]. More research needs to be conducted to evaluate the cause-and-effect relationship with energy metabolism and HF.

In summary, there are many complex and highly regulated signaling processes that function in cardiac homeostasis. In the progression of HF, these processes become dysregulated and can worsen the already present damage to the heart. Overall cardiac output is maintained through regulation of both sympathetic and neurohormonal activation along with LV remodeling and many biochemical signalling pathways (contractility/ calcium homeostasis, cell death, and energy metabolism). Prolonged derangements in these pathways lead to further damage and can be used as targets for HF management.

1.1.2 Management of Heart Failure

Management of HF remains difficult as disease progression and response to therapy are highly variable between patients, and diagnosis is usually made in the later stages of the disease. HF with reduced ejection fraction (HFrEF) has been the largely studied and historically is the most the predominant form of HF. Thus, the management and treatment of HFrEF has improved substantially. HF with preserved ejection fraction (HFpEF) has only recently been studied extensively for its pathophysiology and treatment stradegies[29].

Three classes of drugs have been identified to aid in treatment: angiotensin converting enzyme (ACE) inhibitors/angiotensin II receptor blockers (ARB), aldosterone antagonists/ diuretics, and beta-adrenergic blockers[3]. ACE inhibitors/ARBs prevent the conversion of angiotensin I to angiotensin II and block the actions of angiotensin II to inhibit hypertrophy in vascular tissues and narrowing of coronary vessels leading to decreases in cardiac pressure and workload[30]. ACE inhibitors/ ARB drugs have been shown to improve mortality and reduce hospitalizations, and thus are the first-line drugs for most patients with HF.

Aldosterone antagonists, or diuretics, function to inhibit the production of aldosterone, ultimately preventing aldosterone-induced sodium and water retention and potassium secretion. Subsequent reduction in fluid retention improves kidney function, reduces swelling and bloating, and lowers blood pressure to enhance cardiac function[31].

Beta-adrenergic blockers are usually used in combination with ACE inhibitors/ARB drugs. Beta-adrenergic blockers inhibit the binding of epinephrine to the adrenergic receptors in the heart to reduce heart rate and blood pressure, and relaxes blood vessels to improve blood flow. Beta-blockers have proven to reduce mortality and help regulate heart rate by reduction of sympathetic nervous system activity[32]. ACE inhibitors/ARB and beta blockers are often used together as a first line of HF therapy for all individuals, and aldosterone antagonists/diuretics are used in patients with symptoms of congestion[32].

Some novel and emerging therapies for HFrEF include angiotensin receptor-neprilysin inhibitors (ARNI) and sodium-glucose cotransporter-2 (SGLT2) inhibitors. ARNI are a new class of medications that incorporate blocking of the angiotensin receptors and it inhibits the enzyme neprilysin which degrades protective vasoactive peptides (natriuretic peptides and bradykinin). Entresto is an example of this type of medication which has shown to decrease cardiovascular death and first hospitalization compared to conventional drugs (eg. Enalapril)[33]. SGLT2 inhibitors are approved for the management of type 2 diabetes mellitus and recently have been explored for their use in prevention and treatment of diabetic cardiomyopathy. In diabetic patients with atherosclerosis, prevention with SGLT2 inhibitors have shown to reduce future cases of HF where these results were independent of glucose levels and renal function[34]. Treatment with SGLT2 inhibitors in later stages of HF remain to be fully elucidated. In contrast to these evaluated drug therapies for HFrEF, there is a lack of evidence-based medications for HFpEF and treatment is reliant on the management of comorbidities and symptoms.

If drug therapy is not sufficient for maintaining optimal cardiac function, implantable cardiac devices or extensive surgery may be required. Patients with coronary artery disease (the most common form of HD) that have significant reduction in cardiac output and reduced left ventricular ejection fraction (LVEF) <35%, require cardiac revascularization surgery using a coronary artery bypass graft[35]. This procedure is used to redirect blood flow past blocked arteries and restore normal blood flow to cardiac tissue. Coronary artery bypass graft used in combination with drug therapies lowers mortality rate 2 years after surgery and decreases subsequent myocardial infarctions[36]. Another treatment used is the implantable left ventricular assist device (LVAD) that improves overall heart function by assisting the LV to contract properly and pump sufficient blood across the body. These devices help reduce LV mass and size, reduce levels of renin, angiotensin II, and aldosterone, and improve contractility and subsequently calcium regulation[3]. LVAD implementation has proven to decrease mortality rates and some individuals may even be weaned off the device as the heart strengthens; others may be on the device permanently[37]. In severe cases of end-stage HF, when there are no other options for cardiac improvement, cardiac transplantation may be needed. The limitation with this procedure is the short supply of donor hearts. Upon transplantation, there is a significant improvement in

survival, exercise capacity, and quality of life[4]. In contrast to patients with HFrEF, patients with HFpEF have no current approved device-based therapy for treatment[29].

Novel treatments are emerging that offer new approaches for patients with HF. One promising new technology is gene therapy. This therapy uses viral vectors to target a specific gene that is either over or under expressed. Gene phenotyping can be used to determine any abnormalities in the presence or regulation of genes in the heart[29]. Once phenotyping has been established and a target of interest has been identified, the use of targeted gene therapy could be used[38]. There are many viral delivery methods being evaluated including coronary artery infusion, direct myocardial injection, and injection into pericardial space. A variety of targets have been identified as possible opportunities for treatment including beta-adrenergic receptors, calcium regulation proteins, and G-protein receptor kinases[3]. Additionally, stem cell therapy has been examined for its role in cardiac regeneration. The past decades researchers have examined various cell types and mesenchymal stem cells have shown the most promise[39]. These cells have been tested in animal models and clinical trials to revitalize cardiac stem cells or revascularize the arteries and veins in the heart[40]. Although the idea of this technology is promising, there are major issues including inefficient cell delivery to the target site and low cell retention with minimal effectiveness of the stem cells that do implant in the target area[41]. There are ongoing developments to improve the regenerative capacity of the cells and enhancement of delivery techniques for the target area. Although the idea of gene therapy and cardiac stem-cell regeneration are exciting novel ideas, the technology remains to be optimized to allow for accurate and targeted treatment of HF.

1.2 Diagnosis of Heart Disease and Heart Failure

1.2.1 Clinical Diagnosis of HF

Diagnosis of HF is a very complex process including clinical examination, imaging technology, and the measurement of an array of cardiac biomarkers. Clinical diagnosis of heart failure is commonly initiated with the physical examination which is limited to non-

specific symptoms (age, sex, obesity, smoking and drinking habits, along with other comorbidities), laboratory tests with varying sensitivities, and characteristics not necessarily associated directly with the heart.

The two most common diagnostic methods to evaluate the stage of HF are the New York Heart Association (NYHA)[42] classification and the American College of Cardiology Foundation and American Heart Association (ACC/AHA)[43].

The NYHA classification is based on clinical severity and prognosis with an emphasis on exercise capacity and clinical symptoms. The classification ranges from functional class I (not severe) to IV (most severe). Functional class I includes no limitations to physical activity and no overt symptoms of HF. Functional class II has some limitations of physical activity where ordinary physical activity leads to HF symptoms. Functional class III occurs when less than ordinary activity causes symptoms of HF. Functional class IV refers to patients who are unable to perform physical activity without severe HF symptoms and possible HF symptoms while at rest[43]. One study evaluated the accuracy of this classification method where it correlated with mid- to long-term mortality rates in patients and thus, is a good method for HF classification[42].

The ACC/AHA classification method emphasizes the development and progression of HF and can provide complementary information on diagnosis when combined with NYHA classification. The ACC/AHA classification system recognizes both risk factors and cardiac structure abnormalities associated with HF. Stages range from A, at risk for HF but no structural abnormalities or symptoms of HF; B, structural defects in the heart but no HF symptoms; C, structural HF and prior or current symptoms; D, refractory HF that requires special interventions. Once a patient progresses to the next stage it is not possible to regress and increasing stages is associated with reduced 5-year survival[43]. In 2017, an update to the ACC/AHA guidelines was published to aid in clinical diagnosis along with treatment, medications, and therapies based on a combination of stage and clinical symptoms present[44]. These new guidelines are aimed at diagnosing structural changes at earlier stages (B or C) and targeting treatment to prevent progression of HF and ultimately reduce the morbidity and mortality linked to HF. Although these guidelines have been developed to

aid in early diagnosis, it remains based on patients to identify HF symptoms and a physician to detect based on patient history. In addition, these diagnoses rely on structural and physical changes of the heart which usually occur in the later stages of HF, while early stages of HF progression remain difficult to detect.

1.2.2 Echocardiography in Clinical HD

Echocardiography (Echo) is a commonly used diagnostic tool for cardiac imaging. Echo uses a transducer to send sound waves and generate moving images showing the structure and movement of the heart[43]. It is widely used for its availability to quickly measure the left ventricular size and dysfunction as well as to identify valvular abnormalities non-invasively. Echo is a low-cost technique that is widely available for clinicians to evaluate gross changes in LVEF, cardiac hypertrophy, and valve dysfunction of any patient that presents in the clinic with HD signs and symptoms. There are many forms of echocardiography used in clinic, each with their own advantages and optimal target quantifications (Table 1.1).

Transthoracic Echo is the most common form of Echo used in the clinic for its wide availability and basic cardiac evaluation. Transthoracic Echo uses an ultrasound system transducer to evaluate cardiac structure and function. It can evaluate gross structural abnormalities, valvular disease and any abnormal blood flow through the heart[46]. Doppler Echo is a specialized technique (still using a transducer) that can acquire myocardial velocities and can obtain quantitative information about myocardial motion during the cardiac cycle. Colour M-mode Doppler can also provide spatiotemporal distribution of the velocities across a vertical line for more accurate assessment[47]. Doppler Echo has shown promise in the evaluation of blood flow and cardiac structure in valvular stenosis, valvular regurgitation, blood flow, intracardiac pressures, and intracardiac shunts[48]. This technique is limited due to underestimating the severity of aortic stenosis if the sound beam is not positioned precisely and may not provide accurate diagnosis post-surgery if velocities are abnormally high.

Stress Echo is 2D Echo with stress-induced changes in blood flow to determine severity of coronary artery disease such as in ischemic heart disease and any abnormalities in cardiac blood flow[49]. Stress Echo uses a stressing agent, either through physical exertion/ exercise or a chemical agent (such as dobutamine) to show the function of the heart under these conditions. Echo measurements will be gathered prior to the stress agent and then once again after full stress to the heart is induced. This will allow for clinicians to evaluate the change in blood flow and potential coronary artery disease or ischemic regions in the heart[50]. There are some limitations with this technique that have not yet been fully evaluated including tissue characterization of the myocardial structure, myocardial perfusion with contrast, and regional wall motion quantification with new technologies. New advancements have focused on targeting these limitations to match the data acquired with PET perfusion imaging[50].

One emerging technique that is changing the use of Echo is 3D Echo which measures the geometry and size/ volume of the LV along with valve assessment and functional parameters of the heart. Researchers have evaluated various reconstruction techniques where sequential 2D sliced through the heart have been reconstructed into 3D images to assess better measurements of the heart. Real-time 3D Echo has also been developed to incorporate these reconstructions in real time to more efficiently generate quantitative data[50]. 3D Echo is proposed to generate LV wall thickness and volume measurements comparable to that of cardiac magnetic resonance imaging (cMRI)[51]. New advancements and improvements with clinical studies will help to broaden the applicability of this modality in a variety of cardiovascular diseases. The main limitations with this technique are the user dependence, the extra expense of the probe and software, and the lack of availability in clinical settings.

Table 1.1 Types of Echocardiography Used in Clinic.

	MEASUREMENTS
TRANSTHORACIC ECHOCARDIOGRAPHY	Most common form of echo; measures basic cardiac structure and function
DOPPLER ECHOCARDIOGRAPHY	Used to measure blood flow in the chambers and valves; Can detect abnormal blood flow indicating problems with valves or walls
STRESS ECHOCARDIOGRAPHY	Measures stress induced changes to blood flow and determine severity of CAD; stress agent can be physical exertion or chemically induced
3D ECHOCARDIOGRAPHY	Helpful for identifying problems with heart valves, replacement valves, and the LV; new additional ways to use 3-D echo are being developed

Therefore, echocardiography provides a wide variety of initial measurements for LV size and overall blood flow. After a patient is initially screened with Echo, they may go on to be scanned with cardiac magnetic resonance imaging (cMRI) or cardiac computed tomography (CT) for accurate diagnosis of HF.

1.2.3 Cardiac CT and MRI

Computed tomography (CT) is a technique that allows high-resolution detection of structure and anatomy, thereby enhancing the diagnosis of gross structural changes. CT involves the use of narrow x-ray beams aimed at the target which are quickly rotated to create a combination of cross-sectional planes to generate a 3D image of the specific target of interest[52]. CT provides excellent spatial resolution (0.5-0.625 mm) to evaluate 3D morphological changes in the heart including dimensions and overall heart function. Temporal resolution of CT is limited and poses a challenge with the beating heart[53]. To acquire optimal images using CT, images should be captured between heart beats when movement is lowest. A contrast agent, iodine, can be used to help visualize the difference between adipose and soft muscle tissue as non-contrast CT cannot distinguish between these tissue types. Contrast CT can evaluate the extent of cardiac lesions, myocardial perfusion, and tissue viability[54]. One important consideration with CT imaging is its use with implant devices. CT can be used to image the heart even with implanted devices present although devices near the heart may show an irregular artifact. Although CT imaging uses small doses of radiation, there is no evidence that the radiation disrupts the implanted devices[55].

CT perfusion (CTP) has been shown to improve the specificity and overall accuracy of cardiac CT to detect cardiac blood flow. In CTP, the iodine contrast agent is injected followed by rest and stress scans to evaluate the artery plaque/lesion presence and blood flow[56]. Scans are performed immediately after contrast injection as either static single image scans, or a dynamic set of sequential scans to better visualize perfusion over time[57]. Rest scans are performed with low resting heart rates, <65 beats per minute, where lesions can be detected in the heart. Stress scans are initiated with vasodilator stress agents including adenosine, dipyridamole, or regadenoson followed immediately by a CT scan to enhance defects in perfusion[58]. Rest and stress scans are compared for changes in perfusion which can provide specific information on cardiac defects: 1) hypoperfusion with the same intensity in both stress and rest images indicate regional necrosis; 2) hypoperfusion in stress but normal in rest indicate ischemia; 3) hypoperfusion in stress which decreases in rest show peri-necrosis ischemia; 4) normal perfusion in both rest and stress[58]. Myocardial

blood flow using CTP has been evaluated in porcine hearts before and after a myocardial infarction where decreased perfusion was present specifically in the infarcted region and not in the remote myocardium[59]. CTP imaging is advantageous for cases of suspected coronary artery disease where both blood flow and cardiac anatomy can be examined in one set of images[60]. Further research is needed to evaluate the potential clinical advantages in patient care, treatment costs, and patient outcomes when compared to the current gold standard cardiac PET perfusion imaging.

Cardiac magnetic resonance imaging (cMRI) is an emerging technique that allows for highly reproducible assessment of cardiac dimensions, function, flow, and perfusion. cMRI can recover early structural changes in the heart that comprise many different cardiomyopathies[61]. MRI uses strong magnetic fields to orient protons in the body, then a radiofrequency is applied to detect the location of these protons and can differentiate based on the type of tissue present. MRI provides spatial resolution of 1-2 mm, with temporal resolution of 20-50 milliseconds, and excellent soft-tissue contrast[53]. Due to enhanced resolution of cMRI, sequences have been developed to determine cardiac function, edema, iron deposition, and perfusion[62]. In addition, a gadolinium contrast agent can be used to visualize the morphological changes in the heart and determine cardiomyocyte viability with fibrosis deposition, typically after cardiac ischemia. However, this contrast agent is only able to discern concentrated fibrotic areas and not diffuse regions of fibrosis which is common in some ischemic cardiomyopathies[63]. Therefore, T1 mapping (anatomical images) can be gathered before and after contrast images to accurately determine total fibrotic deposition in the heart. One of the main limitations with cMRI is that patients with magnetic devices or implants near the heart cannot be imaged. Magnetic devices are attracted to the high-powered magnets resulting in damage to the patient and the machine. Additionally, implants near the heart can cause image artifacts and skew images. cMRI provides comprehensive evaluation of HD and is the current gold standard in evaluating ventricular volumes, wall motion and dimensions, and systolic and diastolic function. With the many techniques that encompass cMRI, it detects physical cardiac changes in many forms of HD including: myocardial infarction, dilated and hypertrophic cardiomyopathy, myocarditis, sarcoidosis, and pulmonary hypertension[64]. Overall, cMRI is a robust tool to comprehensively evaluate HD through cardiac anatomy, function, and wall motion.

Hyperpolarized MRI is an emerging technique using ^{13}C to track changes in cardiac metabolism. Hyperpolarized MRI uses a combination of low temperatures and high magnetic fields to allow for high polarization (nearly all electrons are aligned in the same direction). ^{13}C uses this technique to enhance MRI signals[65]. Natural ^{13}C abundance is extremely low in the body (~1.1%) and therefore the use of ^{13}C-tracers have been developed to temporarily enhance the abundance and cause an increase in signal where these tracers are located in the tissue[65]. The most commonly used tracer is ^{13}C-pyruvate where it can measure cellular metabolism through many metabolic processes from energy production to the formation of lactate, alanine and CO_2[66]. A shift in myocardial energy metabolism from primarily fatty acid metabolism to more glucose metabolism is expected to contribute to the development of HF[67]. ^{13}C-pyruvate can be measured through the activity of the pyruvate dehydrogenase complex where increases in its activity show a preference for glucose metabolism. ^{13}C-pyruvate flux through this complex is reduced in the hyperthyroid heart, diabetic heart, and dilated cardiomyopathy while the flux increased in hypertrophic cardiomyopathy[65]. This technology in the heart has only recently been explored and the clinical translatability in heart disease requires further evaluation.

When deciding which imaging tool to use between cMRI or CT, it is important to evaluate each case individually to determine the best one for the patient. cMRI is the gold-standard cardiac imaging technique, however not all patients can safely be imaged (i.e. any patient with metal implants) along with longer scan times as multiple sequences may be used. In evaluation of HD, it is imperative to use accurate and reproducible imaging methods with high temporal, spatial, and contrast resolution[68]. cMRI fulfills all these components in the evaluation of LV function. Recently, new techniques in CT have been developed that approach the function of cMRI by enhancing the temporal resolution. One study evaluated a new dual-source CT technique where temporal resolution (83 milliseconds) results in minimal differences when compared to cMRI[69]. Another study used dual-energy equilibrium contrast-enhanced CT which uses two different x-ray potentials simultaneously to detect both blood and myocardium together in addition to iodine contrast agents measuring fibrosis[70]. The emergence of new cardiac CT imaging techniques can allow for more options when evaluating patients who need diagnostic imaging. Even with many CT techniques being developed to target each aspect of myocardial imaging, cMRI

still remains the gold standard for HD diagnosis. It is important to note that these modalities are used primarily for diagnosis of gross structural changes once HD is already established, and not for the prediction of the onset of HD, prior to overt symptoms. It is imperative to discern changes to the myocardium to be able to facilitate targeted interventions to prevent the progression to HF. One clinical molecular imaging modality that can be used to elucidate the biochemical changes early in HD pathogenesis is positron emission tomography (PET).

1.2.4 Cardiac PET Imaging

Positron Emission Tomography (PET) is a powerful imaging technique that detects molecular and biochemical changes in the body. PET encompasses quantitative non-invasive *in vivo* imaging using positron-emitting radioisotopes (such as ^{11}C, ^{13}N, ^{15}O, ^{18}F, ^{68}Ga, ^{82}Rb) incorporated into biological compounds/ molecules targeted to a specific biological process. Positrons are positively-charged electrons that travel short distances and interact with an electron, causing an annihilation producing two 511 keV gamma rays moving 180° from each other. PET ring detector arrays can detect these gamma rays and determine the original location of the positron which results in sequential high-quality corrected images[71]. PET systems have good temporal resolution and spatial resolution of 4-7 mm which is decreased slightly by movement during image acquisition. Using tracer kinetic modelling with motion and respiratory correction results in high-precision quantitative imaging of targeted biological processes[72]. The main limitation of this technology lies in the limited availability of both PET scanners and a cyclotron facility used to generate the radionuclide compounds for tracers. PET compounds can be useful with drug development, disease diagnosis and monitoring of treatment response based on a specific target. Sensitivity with PET imaging is exceptional as low concentrations of radionucleotide tracers (10^{-11} – 10^{-12} M) are needed to generate precise images[73]. Many tracers have been developed to target overall perfusion and known biological pathways of metabolic processes including fatty acid transport, oxygen consumption, and glucose.

Single photon emission tomography (SPECT) imaging uses radiopharmaceuticals injected into the body where gamma-rays are emitted and detected by collimated radiation detectors. The most common radiopharmaceutical used with SPECT is ^{99}technetium (^{99}Tc) as it has a relatively short half-life of 6 hours. ^{99}Tc-sestamibi (^{99}Tc-MIBI) is a common perfusion tracer that enters cardiomyocytes through passive diffusion and accumulates in the mitochondria. Increased uptake of ^{99}Tc-MIBI demonstrate areas of adequate blood flow while decreased uptake show a loss in perfusion[74]. Evaluation of ^{99}Tc-MIBI in patients with confirmed coronary artery disease showed a diagnostic sensitivity of 90% to evaluate myocardial blood flow and tissue viability[75]. ^{99}Tc-MIBI has shown a demonstrated prognostic value of future acute MI or cardiac death with abnormalities in perfusion imaging[76,77]. Therefore, ^{99}Tc-MIBI may be a useful diagnostic and predictive tool for patients with suspected blood flow abnormalities.

PET imaging shows promise over other radionucleotide imaging techniques, such as single photon emission computer tomography (SPECT), with its superior sensitivity compared to echocardiography/ cMRI, standardized correction of attenuation, and quantitative measurements of tracer uptake[78]. Therefore, PET has begun to be recognized as a useful tool to evaluate biochemical changes throughout the body, including in the heart. In clinical imaging of HD, PET is used primarily to evaluate cardiac perfusion/ tissue viability (ischemia), inflammation, and neuronal activity[71]. Using PET to identify changes in these processes remains an important diagnostic and prognostic tool for evaluation of many forms of HD and HF in patients. Myocardial perfusion tracers (^{13}N-ammonia, ^{15}O-water, ^{82}Rubidium) detect reduced blood flow within the heart and vasculature to determine subclinical coronary stenosis and the severity of both coronary artery disease and ischemia. Inflammation is common in many forms of HD where PET tracers (^{18}F-fluorodeoxyglucose) can measure significant increases of regional inflammation associated with diseases such as endocarditis, sarcoidosis, atherosclerosis, and acute tissue injuries including myocardial ischemia. Neuronal imaging (^{11}C-*meta*-hydroxyephedrine) assesses the severity of HF and post-transplant reinnervation along with arrhythmias in the heart[79]. Therefore, PET is an exciting *in vivo* molecular imaging technique that allows for diagnosis of biochemical processes altered in the severity and type of HD and HF.

1.2.5 Cardiac Perfusion PET Tracers

Myocardial perfusion is an important assessment of coronary artery disease and cardiac ischemia where there is a marked regional reduction in blood flow. PET imaging has emerged as the gold standard for non-invasive myocardial perfusion measurement. The commonly used PET tracers are $^{13}N\text{-}NH_3$, $^{15}OH_2$, and ^{82}Rb, which all have their own strengths and weaknesses (outlined in table 1.2)[80]. All tracers have relatively short half-lives, ranging from 75 seconds to 10 minutes. Although all of these tracers detect perfusion, their mechanisms of action differ. $^{13}N\text{-}NH_3$ passively enters the cardiomyocytes and is incorporated into glutamine through the glutamate synthesis pathway, thereby getting metabolically trapped in the cell. When cardiomyocytes are damaged and the cellular membranes are weakened, $^{13}N\text{-}NH_3$ cannot enter the cells to access myocardial blood flow. Similarly, ^{82}Rb is a potassium analog and enters cardiomyocytes through the sodium/potassium ATP transporter in the cell membrane where it accumulates and gets retained. In cells that are dead or damaged, ^{82}Rb is not taken up and does not accumulate therefore no signal is generated. In contrast, $^{15}OH_2$ is a metabolically inert tracer that freely diffuses across the cell membrane and creates an equilibrium between blood and tissue without significant accumulation in the myocardium. This tends to result in lower count density and overall lower quality images for quantification with this tracer[80,81].

Table 1.2 Common Cardiac Perfusion Tracer for PET Imaging[80].

	$^{13}N\text{-}NH_3$	$^{15}OH_2$	^{82}RB
GENERATION	Cyclotron	Cyclotron	Generator
HALF-LIFE	~10 min	~125 sec	~75 sec
MECHANISM	Trapped in cell	Freely diffuse into cell	Trapped in cell

All these tracers have been evaluated in the forms of HD that are characterized by decreased cardiac perfusion in the myocardium and vasculature. In particular, decreased perfusion reported by $^{13}N\text{-}NH_3$ PET is a strong predictor of adverse cardiac outcomes in HD[82]. Lee *et al.* was able to show that quantitative $^{13}N\text{-}NH_3$ imaging of myocardial blood flow improved detection of coronary artery stenosis and suggested that this *in vivo* imaging method be used to accurately determine disease severity prior to invasive coronary angiography surgery[83]. $^{13}N\text{-}NH_3$ has also been used to detect tissue viability in cardiac ischemia with rest/ stress induced imaging to discern ischemic myocardium from viable tissue[84]. ^{82}Rb has similarly been used in studies evaluating cardiac perfusion where reduced blood flow was an indicator of short-term cardiac events[85,86]. Zampella *et al.* was able to show that ^{82}Rb can detect the extent of calcification and blockage in coronary artery disease patients[86]. $^{15}OH_2$ has also assessed the extent of coronary artery disease[87,88] and detect blood flow in ischemic patients[89]. Taken together, these tracers have been shown to non-invasively correctly identify and diagnose reduced regional blood flow and disease severity in various forms of HD.

1.2.6 Inflammation in the Heart with ^{18}F-FDG PET

Inflammation is commonly associated with HD and HF, and excessive proinflammatory processes may be a predictor of future adverse cardiac events. Inflammation is a common process in the body used to remove dead and damaged cells followed by specific repair mechanisms. Initially after cardiac injury, or reduced cardiac perfusion, an immune response is activated where inflammatory cells including neutrophils, monocytes, and macrophages target the area of interest. This process removes the dead and damaged cells from the area. The immune reaction induces pro-inflammatory cytokine activation including tumor necrosis factor-alpha (TNF-α), interlukin-6 (IL-6), and interlukin-1 (IL-1)[90]. After the pro-inflammatory phase subsides, the anti-inflammatory phase initiates fibroblasts and matrix metalloproteins to deposit fibrotic (scar) tissue in place of the dead/ damaged cells. However, fibrosis deposition may also occur in the presence of chronically

active pro-inflammatory markers where both the pro- and anti-inflammatory phases are active simultaneously[91]. When these pro-inflammatory markers are significantly elevated for prolonged periods of time, they can be a sign of chronic inflammation and can contribute to the progression of HF[92]. A commonly used tracer for inflammation and tissue viability is ^{18}F-fluorodeoxyglucose (^{18}F-FDG). ^{18}F-FDG is a glucose analog that is taken up by viable cardiomyocytes through glucose transporters and promptly gets trapped in the cell as ^{18}F-glucose-6-phosphate via hexokinase. Proinflammatory macrophages have a significant overexpression of glucose transporters which results in increased ^{18}F-FDG uptake[93]. One important thing to note when using ^{18}F-FDG in studies of cardiac inflammation is that normal myocardial glucose uptake should be suppressed to minimize normal tissue uptake. This is usually done with an Intralipid™ infusion in animal studies. Human subjects are required to fast or consume a high fat meal prior to imaging to reduce the extent of myocardial glucose uptake and increase the lipid metabolism in the normal myocardium[94]. One example of imaging cardiac inflammation is the case of cardiac sarcoidosis, an inflammatory disease where granulomas (white blood cells) form in the heart muscle and disrupt normal function. ^{18}F-FDG has been shown to accurately detect it in its early stages where perfusion defects may not yet be present[95]. In patients with suspected unstable angina, ^{18}F-FDG was able to detect angina more sensitively than myocardial perfusion imaging (85.7% vs 52.4% respectively). Therefore, increases in ^{18}F-FDG in angina may indicate angina as an inflammatory condition where ^{18}F-FDG clearly demonstrates the accuracy and sensitivity of non-invasive PET imaging[96]. ^{18}F-FDG PET can also assess the severity of inflammation associated with coronary artery disease (CAD) and atherosclerosis[97,98]. Upon plaque build-up from low-density lipoprotein in the arteries, monocytes, leukocytes, and T-cells are recruited to the plaque area, where monocytes mature into macrophages, the target for ^{18}F-FDG[99]. Therefore, ^{18}F-FDG is a specific clinically relevant tracer to examine the extent of inflammation associated with HD.

^{18}F-FDG is the current clinical gold standard for determination of viable tissue in patients after myocardial infarction and in cardiac dysfunction with accurate assessment of scar presence[75,100]. In addition, ^{18}F-FDG can be used to measure the efficacy of treatments by comparing scans before and after treatment. One study used ^{18}F-FDG to evaluate alcohol septal ablation treatment in patients with hypertropic obstructive cardiomyopathy where

clear reduction of tracer uptake, and associated inflammation, was seen after treatment[101]. Ultimately ^{18}F-FDG is an important non-invasive imaging tool to detect inflammatory heart disease and assess disease severity.

1.2.7 Neuronal Cardiac PET Imaging

Cardiac neuronal imaging is an important tool to evaluate arrythmias associated with HF. In congestive heart failure there are abnormalities in the autonomic nervous system with altered sympathetic traffic (blood pressure) to peripheral vascular areas; however, how this process functions remains largely unknown. ^{11}C-*meta*-hydroxyephedrine (^{11}C-HED) is a norepinephrine (NE) analogue that targets the NE transporter on nerve endings in the sympathetic nervous system, therefore determining NE transporter activity and density[102]. In HF and in arrythmias there are NE transporter abnormalities that can be revealed by ^{11}C-HED PET. Patients with congestive HF had reduced retention of ^{11}C-HED globally in the heart which corresponded to blunted vascular sympathetic responses[103]. Diastolic dysfunction was shown to be associated with impaired sympathetic innervation in the heart using ^{11}C-HED in patients with HF and preserved ejection fraction[104]. ^{11}C-HED imaging may also be used as an alternative for myocardial blood flow imaging in ischemic cardiomyopathy[105]. Additionally, cardiac transplant patients can be imaged with ^{11}C-HED to determine the extent of sympathetic reinnervation of the newly-implanted heart[106]. One study evaluated sympathetic activity in patients at different time points after transplant surgery, and healthy controls. In patients with recent surgery there was a 70% reduction in ^{11}C-HED uptake, which improved to a 59% reduction after 2 years. The authors found that after cardiac transplantation, the sympathetic activity in the heart improved from 30% to 41% activity[107]. Regional and localized ^{11}C-HED retention in the heart can show disease severity and dysfunction in arrhythmias[108]. Overall, ^{11}C-HED can evaluate impairments in cardiac conductivity that are associated with HF and cardiac arrhythmias.

1.2.8 Emerging Cardiac PET Tracers

In addition to these known tracers for cardiac PET imaging, many new tracers are being developed to specifically target aspects of cardiac pathology in HD. One new perfusion tracer that is not yet clinically available is ^{18}F-flurpiridaz, a pyridazinone derivative, which gets metabolically trapped in the cardiomyocytes through the mitochondrial membrane complex-1 and reports cardiac blood flow. ^{18}F-flurpiridaz was able to accurately detect reduction in myocardial blood flow in patients with coronary artery disease (sensitivity 71.9%). ^{18}F-flurpiridaz was superior to SPECT perfusion imaging in image quality, diagnostic certainty, and radiation exposure in human clinical trials[109,110]. Another tracer, ^{11}C-acetate, can indirectly estimate myocardial blood flow and oxygen metabolism where ^{11}C-acetate accumulation in cardiomyocytes refers to low oxygen consumption and blood flow[111]. In a rat model of congestive heart failure, ^{11}C-acetate demonstrated decreased myocardial oxygen consumption with significant correlation to myocardial blood flow, therefore, ^{11}C-acetate can be used as an estimate of cardiac perfusion[112]. Another target for perfusion imaging is the mitochondrial membrane potential which is higher in healthy cardiomyocytes and loss of this signal is associated with cell death. Ammonium and phosphonium cations accumulate in mitochondria and these compounds are targets for potential ^{18}F imaging agents. Many ^{18}F derivatives of tetraphenylphosphonium salt have been developed and tested for detection of cardiac perfusion in animal models[78]. In cardiac amyloidosis, many tracers have been developed to target amyloid depositions including ^{11}C-Pittsburgh B (PIB), ^{18}Florbetapir, and ^{18}Flutemetamol in detecting disease presence and severity[113,114]. In addition, ^{18}F-sodium fluoride (^{18}F-NaF) detects calcification and plaque formation in coronary artery disease and can determine plaque vulnerability along with future cardiac events[115]. An alternative to ^{18}F-FDG for inflammation imaging is ^{68}G-DOTATATE which targets the somatostatin receptor type 2 that is overexpressed in inflammatory macrophages. ^{68}G-DOTATATE can accurately detect inflammation after a myocardial infarction with minimal background uptake[116] and can determine atherosclerotic disease severity by assessing high versus low risk lesions in the vasculature[117]. ^{68}G-pentixafor, targeted to the chemokine receptor CXCR4, can also be used to image inflammation associated with atherosclerosis[118]. With cardiac neuronal

imaging, new ^{18}F-labelled tracers are being developed to target the sympathetic nervous system in the cardiomyocytes. These tracers target the norepinephrine transporter uptake-1 and accumulate in vesicles within the cells. These tracers have similar function to ^{11}C-HED although the longer half-life of ^{18}F aids in the versatility in imaging[119]. In addition to the tracers described above, there are many other new tracers being developed to target specific molecular pathways of HD. These tracers have the potential to be used in an array of imaging profiles to help with diagnosis and targeted treatments of HD.

1.2.9 Simultaneous PET/CT and PET/MR Imaging

To better diagnose and predict adverse cardiac events, simultaneous imaging with PET and CT or MRI can be used to determine both molecular and functional abnormalities in HD. The main limitations with PET imaging alone are the low spatial resolution and lack of anatomical reference. Initially, sequential imaging sessions (PET followed by CT or MRI) were used with co-registration software to integrate the two sets of images. This posed a challenge due to the difference in scanner profiles, patient positioning and organ movement between scans[120]. To overcome these challenges, hybrid systems for both PET/CT and PET/MRI were developed to optimize scan overlay, to lower costs due to multiple scans, and to lower the burden on the patient. Simultaneous imaging poses significant advantages over sequential imaging as the scan duration is minimized and the patients do not have to move, allowing for improved co-registration of the PET images to anatomical imaging of MRI or CT. With PET/CT, an established x-ray (CT) based attenuation correction is used to quantify PET data. PET/MRI is more challenging due to the limited reliability of developed attenuation corrections for PET[121]. The advantages of using PET/CT are the high spatial resolution, shorter study times, can be used with patients with metal implants, and availability. Its disadvantages include extra radiation exposure, possible renal toxicity with large volume of iodine contrast agent (contrast induced nephropathy), limited use in patients with arrhythmias, and functional data acquired retrospectively. In contrast, PET/MRI poses many advantages including temporal resolution, superior soft-tissue contrast, and evaluation of both cardiac anatomy and function. The disadvantages include

inability to scan patients with certain implanted devices, possible renal failure with gadolinium contrast agent (nephrogenic systemic fibrosis), cost, and difficulties with scan duration with patients who have claustrophobia[122]. Overall, PET/MRI can provide more detailed anatomical information with less radiation over PET/CT, but availability is limited in the clinic and patient comfort level should be evaluated.

When performing simultaneous imaging, one study evaluated information provided by PET when using either PET/MRI or PET/CT using the same patient cohort for both modalities. They found the same PET image results regardless of the imaging modality[123]. Therefore, when using simultaneous imaging modalities, the use of CT or MRI should be evaluated based on the choice of diagnostic parameters for the type of HF. In a patient sarcoidosis study with PET/MRI and PET/CT, overall ^{18}F-FDG PET uptake using tissue to blood ratio (TBR) was comparable between imaging methods, although MRI data provided more detailed information in regional fibrotic deposition and edema[124]. Combined PET and MRI supplied complimentary information on disease pathology with both LV and RV abnormalities in cardiac sarcoidosis[125]. In myocarditis, cardiac MRI is widely used for diagnosis and ^{18}F-FDG PET can add more information on the inflammation associated with myocarditis. PET/CT does not provide optimal anatomical information in this disease due to the lack of soft tissue contrast[126]. In patients with myocardial infarction and plaque formation, ^{18}F-NaF PET/MRI and PET/CT were compared to find vulnerable plaques and scar tissue specifically in the myocardium where PET/MRI enabled structural myocardial information that CT was not able to provide. Overall PET/CT data was able to determine scar tissue and plaque presence and these results were comparable with PET/MRI results although anatomy was easier to identify with MRI[127]. Taken together, hybrid imaging with PET and either CT or MRI provides an exceptional amount of information that can improve diagnostic and prognostic accuracy. The choice of PET/CT versus PET/MRI relies on each individual patient and equipment availability.

1.3 Heart Failure and Heart Disease Biomarkers

In addition to clinical examination and imaging, circulating cardiac biomarkers are used to evaluate heart disease. There is a need to develop methods to accurately predict which individuals will proceed to HF, particularly in the early stages when risk factors are present without any measurable deterioration in heart function. Circulating biomarkers can help augment the information provided by imaging and clinical examination.

Circulating cardiac biomarkers are quantifiable biochemical indicators of alterations in cardiac function. Ideally, these biomarkers can be used to determine early molecular changes in the heart that precede the functional changes, as measured by imaging and clinical examination. Elucidating profiles for biomarkers of HD will help to guide therapies and help disease management. An ideal cardiac biomarker would be:

- Quantifiable; able to be accurately and repeatably quantified with quick turnaround times
- Specific; a marker native to cardiac tissue
- Sensitive; shows changes that are scaled to disease severity
- Stable; changes do not degrade prior to detection

The most common clinical biomarkers used to detect damage in the heart are natriuretic peptides and cardiac troponins which measure cardiomyocyte stress and cardiac damage, respectively.

1.3.1 Biomarkers of Cardiomyocyte Stress

Cardiomyocyte stress occurs with extensive pressure and volume overload in the heart. This causes atrial and ventricular diastolic stretching which stimulates natriuresis and vasodilation, and LV relaxation[128]. Natriuretic peptide-B (BNP) is the gold standard biomarker for the diagnosis and prognosis of HF[129], and is produced by primarily ventricular myocytes under conditions of stress. BNP is initially produced as the precursor

molecule pre-pro-BNP and cleaved to generate proBNP. The enzyme corin then cleaves proBNP to the active hormone BNP and the inactive form NT-proBNP (the N-terminal of pro-BNP)[130]. Both BNP and NT-proBNP are released into the blood stream from predominantly the left ventricle upon increased wall stress and neurohormonal activation. Physiologically, BNP promotes diuresis (sodium and water excretion), vasodilation, and attenuate the renin-angiotensin-aldosterone secretion (RAAS). In addition to BNP secreted from the ventricular myocytes, atrial natriuretic peptide (ANP) is produced primarily in the atrial myocytes and is secreted with hypertension and wall stress. The hormones ANP and BNP are eliminated from the body via two methods: receptor internalization, or proteolytic degradation in the excretion organs including kidneys and lungs[130]. The active form BNP has been evaluated in healthy individuals where circulating levels are extremely low. In one study, Tsutamoto *et al.* measured the circulating BNP levels in 85 patients with chronic HF where levels increased in proportion to disease severity. The plasma levels were 5-fold higher in patients who did not survive compared to survivors[131]. Other studies have also evaluated the measurement of plasma BNP in HF severity and found BNP to be an independent predictor of mortality[132]. BNP is also secreted under conditions of severe aortic regurgitation, mitral regurgitation, and aortic stenosis[133]. Another study compared BNP and NT-ANP to echocardiograms where BNP correctly identified HF with a positive predictive value of 84% while NT-ANP's positive predictive value was only 78%. Therefore, BNP is an accurate diagnostic marker of HF[134]. BNP and NT-proBNP have the same cardiac actions which are released upon cardiac stress, although the half-life of NT-proBNP is 5- to 10- fold higher (60-120 min) than BNP (23 min). The threshold values for HF diagnosis with BNP are: <100pg/ml – no HF; 100-400pg/ml – potential HF; >400pg/ml – HF; however, the diagnostic values for NT-proBNP differ significantly based on age: <300pg/ml – no HF; >450pg/ml – HF for patients under 50 years of age; >900pg/ml – HF for ages 50-75; >1800pg/ml – HF for ages over 75[135]. Therefore, due to the longer circulating half-life and age specificity of diagnostic thresholds, NT-proBNP is more commonly measured in a clinical setting.

Although BNP and NT-proBNP are commonly used to diagnose clinical HF, it is important to note that BNP levels are increased or decreased with other comorbidities, most notably renal failure and sepsis, along with age, sex and obesity. BNP, along with all natriuretic

peptides, is elevated with renal failure even when no adverse cardiac events are present[136]. BNP is also elevated in sepsis and other non-cardiac disease states including atrial fibrillation, pulmonary embolism and amyloidosis[137]. BNP levels were significantly lower in obese patients which may be a contributing factor to the higher susceptibility of these individuals to adverse cardiac events[138]. BNP also increases with age[139] and is higher in women compared men[140]. Different assay systems also have different thresholds and ranges which make having a universal threshold difficult[140]. With the multitude of variables present for the measurement of BNP, it is suggested that both BNP and NT-proBNP may not be the most suitable for detection of HF in the entire population.

Suppression of tumorigenicity 2 (ST2) is another measure of mechanical stress in cardiomyocytes[129]. The ligand for the ST2 receptor is interleukin 33 (IL-33) which has anti-hypertrophic and anti-fibrotic benefits in the myocardium, partly due to inhibition of the pro-apoptotic pathway[141]. The soluble form of ST2 (sST2) is secreted from the myocardium and detectable in the circulation under conditions of cardiomyocyte stress. sST2 acts as a decoy receptor for IL-33 to suppress the natural IL-33 pathways which ultimately leads to increases in cardiac apoptosis and fibrosis. Therefore, increases in sST2 indicate increased fibrosis, inflammation, and remodeling, reflecting many hallmarks of several cardiovascular diseases[142]. sST2 levels also appear to increase in acute HF, but unlike BNP, these values were not an independent predictor of mortality[143]. However, when measured with BNP, the prognostic accuracy for HF was greatly improved[141]. Therefore, it is evident that creating a panel of biomarkers to more accurately detect and predict HD is needed.

1.3.2 Biomarkers of Cardiac Damage

Cardiac troponins (cTn) are the leading candidate biomarkers in predicting myocardial damage. It is well established that cardiac troponins T and I levels are significantly elevated in myocardial injury, mainly ischemia[144]. In healthy cardiomyocytes, troponins are essential for regulation of muscle contraction through modulation of calcium-mediated actin and myosin interaction[145]. Cardiac troponin T, I, and C form the cTn complex where

troponin T (cTnT) and I (cTnI) are specific for mediating contractile function[144]. When the cardiomyocyte membrane is disrupted via ischemic (most common) or non-ischemic causes, the cTn complex disaggregates and enters the bloodstream, and therefore, increased levels of cTnI and cTnT correlate with the extent of cellular injury. Studies have observed increases of cTnT and cTnI in many forms of heart disease including coronary heart disease, heart failure, and atherosclerosis[146,147]. It is important to note that cTns are an acute marker of cardiac damage where their half lives in the blood range from 90-120 min with prolonged elevation (3-4 days) indicating severe and irreversible damage to the heart[148]. cTn measurements provided complimentary information to cardiac perfusion imaging to enhance diagnostic accuracy[149]. Some studies have also shown elevations of cTns in other disease states including stroke, pulmonary embolism, sepsis, perimyocarditis and tachycardia[150,151]. Therefore, measurement of cTn is usually evaluated along with clinical examination and imaging to form an accurate diagnosis of cardiac injury.

In addition to troponins, heart-type fatty acid-binding protein (H-FABP) is another measure of cardiac damage. H-FABP is a cytoplasmic protein that transports long-chain fatty acids into the cardiomyocyte and is rapidly released into the bloodstream upon cardiomyocyte membrane damage[129]. Serum H-FABP levels were measured in chronic HF when patients were both admitted and released from the hospital where prolonged elevation at the time of release were associated with significantly higher future cardiac event rates[152]. When circulating levels of H-FABP were measured concurrently with cTn, testing sensitivity was improved in the first 4 hours after admission. However, at later timepoints H-FABP increased the false-positive rate of patients with acute MI[153]. Another study also evaluated H-FABP and cTn in acute coronary artery syndrome where early testing of H-FABP showed increased levels associated with cardiac events in all patients. In contrast to the last group, this group found H-FABP to have a greater predictive capacity for cardiac events within 6 months of initial admission[154]. Due to such differing findings with this biomarker at later stages, further analysis of the predicative value of H-FABP is needed. These studies have shown the importance of using an array of biomarkers in HD for improved prediction of adverse cardiac events and progression to HF.

1.3.3 Inflammatory Biomarkers

Inflammation is a key process that contributes to the progression of many forms of HD. Initially, acute inflammation is a necessary step in the process of healing. However, when the inflammation fails to resolve and becomes prolonged, further tissue damage may occur. Many cardiac biomarkers have been discovered to link to the overall cardiac inflammation in HF. Early studies focused on interleukin-6 (IL-6), tumour necrosis factor alpha (TNF-α), C-reactive protein (CRP) and toll-like receptor 4 (TLR4) with their role in HF progression via adverse effects on vascular endothelium, cardiomyocyte apoptosis, induction of hypertrophy, and left ventricular dilatation[155].

Interleukin-6 (IL-6) is a common inflammatory cytokine that is secreted in response to infections and tissue injuries. It is produced by various cell types and exerts many biological responses through the IL-6 receptor. IL-6 has been reported to play a large role in the process of ischemic HD and HF[156]. In patients with chronic HF, plasma levels of IL-6 increased with diseased severity and could provide prognostic information independent of left ventricular ejection fraction[157]. In a clinical trial from patients with acute coronary syndrome, increased IL-6 levels associated with adverse cardiac outcomes[158] and increased risk of major cardiac events including possible HF[159]. Plasma levels of IL-6 are also elevated after trauma from acute myocardial infarction where prolonged elevation correlates with residual ischemia in the heart[160]. In addition to cardiac ischemia, IL-6 levels increase in dilated or hypertrophic cardiomyopathy and are associated with a higher risk of congestive HF[161]. In contrast to the findings that IL-6 further increases cardiac damage, some studies have shown that IL-6 may play a role in cardio-protection after ischemia/ reperfusion signalling[162] and may even aid in tissue repair[163]. Therefore, IL-6 can be proposed to play a dual role in cardiovascular inflammation. Short term signalling of IL-6 after ischemia can protect the heart from further damage while long term IL-6 elevation plays a role in the development and prediction of future cardiovascular diseases.

Tumour necrosis-alpha (TNF-α) is an inflammatory protein produced primarily by macrophages and released into circulation to elicit an immune response. TNF-α binds to 2 possible receptors, TNFR1 and TNFR2, with each producing divergent responses in HF.

TNFR1 functions through pathological pathways while activation of TNFR2 shows protective effects in the heart. In a mouse model of MI, knockout of TNFR1 indicated attenuated ventricular dysfunction and improved post-MI survival while knockout of TNFR2 exacerbated ventricular dysfunction and cardiac remodeling[164]. Therefore, TNF-α is expected to play a protective role in the heart via the TNFR2-mediated pathway. In the circulation, TNF-α levels have been found to increase in patients with heart disease and heart failure[156]. In patients with coronary artery disease (CAD), TNF-α increased according to disease severity[165]. When both TNF-α and IL-6 were measured in CAD, there was significant predictors of CAD severity while measured together they are an indicator of chronic inflammatory burden and increased atherosclerotic risk[166]. This pattern was also present in patients with LV diastolic dysfunction independent of other cardiac parameters[167]. In mechanistic studies utilizing transgenic mice, overexpression of cardiac TNF-α resulted in LV wall thinning and increased cardiomyocyte apoptosis via loss of cytoprotective factor Bcl-2 and activation of cell death pathways[168]. In isolated perfused rat hearts, TNF-α not only decreased heart rate and contractile force, but activated protein kinase C (PKC) which promotes the development of cardiac dysfunction[169]. High levels of TNF-α can also disrupt contractility through increases of intracellular calcium in cardiomyocytes[170].

The presence of C-reactive protein (CRP) in HF patients was first discovered back in 1956 and since then there has been extensive work on the relationship between CRP and the inflammatory process in HF[130]. In the 1990s a more sensitive test was developed for CRP, namely high-sensitivity CRP (hs-CRP), as testing for this marker of cardiac inflammation became more prevalent[171]. hs-CRP is synthesized in the liver, and with increased vascular inflammatory cytokines in the circulation, hs-CRP is released into the bloodstream which can then be detected in inflammatory HF and atherosclerosis[172]. hs-CRP has a long half-life of about 19 hours with its peak occurring at about 24-48 hours after initial inflammatory response[173]. A large meta-analyses evaluating the circulating levels of hs-CRP showed it to be a predictor of coronary heart disease and future coronary events[174]. Increased levels of this marker are also associated with many risk factors of heart disease including physical ability, smoking, cholesterol levels, body mass index (BMI), and blood pressure[175].

The toll-like receptor (TLR) superfamily plays a crucial role in the innate immune system. Toll like receptor 4 (TLR4) is a membrane-bound receptor in cardiomyocytes and endothelial cells that is upregulated in HF where its activation leads to further inflammatory signalling. TLR4 can be activated by many ligands including endotoxins, heat shock protein 60 (HSP60), reactive oxygen species (ROS) and high mobility group box 1 (HMGB1). Once TLR4 is activated, initiation of both My88-dependent and My88-independent pathways activate many inflammatory transcription factors and proinflammatory cytokines, respectively[176]. Both pathways activate transcription of NF-κB and activator protein-1 (AP-1) which regulate the expression of inflammatory cytokines IL-6 and TNF-α. Compared to all other toll-like receptors TLR4 has the highest expression in inflammatory HD including myocarditis, myocardial infarction, ischemia reperfusion (I/R) injury, HF, valve diseases, hypertension, and atherosclerosis[177]. In HF, many endogenous ligands of TLR4, such as HSP, ROS, and HMGB1, are elevated and mediate myocardial inflammation[176]. Studies in mice showed that TLR4 expression was increased in cardiomyocytes isolated after long-term myocardial infarction (MI)[178], while mice with TLR4 deficiency showed reduced infarct sizes after I/R injury[179]. Cardiac TLR4 expression was also increased in patients with advanced HF[180]. Due to TLR4 overexpression in HD, this pathway has become a target of inhibition to reduce pro-inflammatory responses. Statins have been shown to inhibit TLR4 activity and reduce inflammation in the vascular system[181]. Eritoran is a TLR4 antagonist and has been shown to attenuate I/R injury[182]. Therefore, TLR4 may be a biomarker of myocardial inflammation in several types of HD and vascular diseases.

1.3.4 Specificity of Cardiac Biomarkers

Most of the cardiac biomarkers described above are secreted into the blood and can therefore be measured through a simple blood test. However, they can be associated with other comorbidities that can confound results. Some biomarkers are not even produced by the heart but are secreted by other tissues when cardiac injury or dysfunction occur. Therefore, circulating biomarker levels may not reflect actual cardiac tissue levels which

is a limitation to measuring circulation compared to tissue-specific biomarkers of HD. There is a clear need for the identification and development of ways to non-invasively detect tissue-localized biomarkers. In addition, there is evidence that no one single biomarker can accurately determine HD prognosis. In a study by Jungbauer *et al.* it was suggested that a panel of cardiac biomarkers should be used to more accurately diagnose and predict cardiac outcomes for patients[183]. As HD is a complex syndrome with diverse signs and symptoms, it is imperative to use a large panel of biomarkers to encompass all possible characteristics and aid in better diagnoses. One novel biomarker of interest that reflects cardiac tissue is the growth hormone secretagogue receptor (GHSR) and its endogenous ligand ghrelin. This cardiac system could be an important addition to the already established panel of biomarkers.

1.4 Ghrelin-GHSR as a Novel Biomarker

Upon cardiac biomarker discovery, a new hormone, ghrelin, and its receptor the growth hormone secretagogue receptor (GHSR) have been identified as potential target localized to cardiac tissue. The emerging discovery of this new biomarker has gained traction in HD with the identification of changes in this ghrelin-GHSR system in HF.

1.4.1 GHSR and Ghrelin Discovery

Ghrelin is a peptide hormone that modulates systemic metabolism through activation of orexigenic effects in the body[184]. Ghrelin is a 28-amino acid peptide that is encoded by the preproghrelin gene first discovered in the X/A like cells in the gastric oxyntic cells in the stomach[185]. It is first synthesized as a precursor, preproghrelin, which is cleaved to produce both ghrelin and obestatin. Obestatin has been thought to play a role in food intake and metabolism via the G protein-coupled receptor 39 (GPCR39) although these results have yet to be substantiated[186]. Ghrelin, however, has been extensively studied for its production and secretion in endocrine cells in the gastrointestinal mucosa. Ghrelin is present in cells

in two forms, acylated and un-acylated ghrelin. In the endoplasmic reticulum membrane, proghrelin is acylated on Ser-3 by ghrelin O-acyl transferase (GOAT) prior to its processing to mature ghrelin. Only the acylated form of ghrelin is the natural ligand to GHSR[184]. Although the un-acylated form of ghrelin (des-acyl ghrelin) does not bind GHSR, it also modulates energy metabolism, likely through an unknown receptor[187]. Structure-function studies have shown that the N-terminal 8 amino acids of ghrelin, including the octanoylated group, constitutes the receptor binding domain.

The biologically active receptor for ghrelin is GHSR1a (here termed GHSR), a 366 amino acid, seven transmembrane G-protein coupled receptor that contains an extracellular binding region where active ghrelin binds specifically to transmembrane domains 3 and 6 of GHSR. The splice variant GHSR1b contains only 298 amino acids and is truncated to only contain transmembrane sections 1-5[188]. GHSR1b has been shown to be expressed in the same tissues as GHSR1a as well as adipose tissue, breast, skeletal muscle and prostate[188]. GHSR1b is known to heterodimerize with other G-protein coupled receptors and functions in signalling. GHSR1b may form a heterodimer with GHSR1a in neurons and HEK293 cells where receptor internalization occurs with inhibition of GHSR1a signalling[189,190]. Although GHSR1b has been shown to dimerize with GPCRs, its biological function in the heart is not fully elucidated.

While ghrelin was originally discovered in rat and human stomach[191], it is now known that ghrelin and GHSR are expressed in many other organs; various brain regions; lung, liver, kidney; the epsilon cells of pancreatic islets; and, most importantly, cardiovascular tissues. The presence of GHSR has been demonstrated in human vascular tissues including the aorta, coronary and pulmonary arteries, as well as in the myocardium, indicating that GHSR is present throughout the heart[192]. Ghrelin has been thought to exert paracrine and autocrine effects in the heart where binding of ghrelin to GHSR elicits many cardioprotective responses[193].

1.4.2 GHSR Signalling in the Heart

Activation of GHSR in the heart has been identified through both classical G-protein signaling and G-protein-independent pathways showing the complexity of GHSR activation[194]. Ghrelin activation of GHSR initiates many downstream signalling processes ranging from apoptosis and survival signaling, calcium regulation and contractility signaling, cellular metabolism, and inflammation.

One of the main contributors to cardiac health is cardiomyocyte contractility and regulation of calcium influx/efflux. Calcium (Ca^{2+}) signalling in the cardiomyocyte begins with an influx of calcium into the cell through the L-type calcium channel induced by excitation contraction coupling of the cardiomyocyte membrane. At the same time, Ca^{2+} is released from the sarcoplasmic reticulum (SR) through the ryanodine receptor 2 (RyR_2). Increases in cytoplasmic Ca^{2+} bind to protein kinase C (PKC) and initiate phosphorylation of Ras/Raf, MEK1/2 and ERK1/2[195]. Intracellular Ca^{2+} induces cardiomyocyte contraction through binding to troponin (Tn) C within the actin filament in the sarcomere of the cell. Ca^{2+} is released from the Tn C and actin filament where a signal is sent to the cell to reduce intracellular levels. Stimulation of G-protein coupled receptors (GPCRs) initiate a signalling cascade starting with Gs activating cyclic adenosine monophosphate (cAMP), protein kinase A (PKA) which phosphorylates phospholambin B (PLB) and inhibits binding to sarcoplasmic reticulum calcium ATPase pump (SERCA2a) ultimately allowing for Ca^{2+} uptake into the SR. Furthermore, stimulation of GPCRs activates Gαq, phospholipase C β (PLCβ), inositol 3 phosphate (IP_3) which binds to the IP_3 receptor. This receptor is minimally active in healthy cells and becomes overactive in damaged or stressed cardiomyocytes[196]. Upon relaxation, Ca^{2+} is stored in the SR or removed from the cell through the sodium-calcium exchanger (NCX) on the cell membrane. This process is demonstrated in figure 1.1. The disruption or dysregulation of this process results in cardiac dysfunction[197].

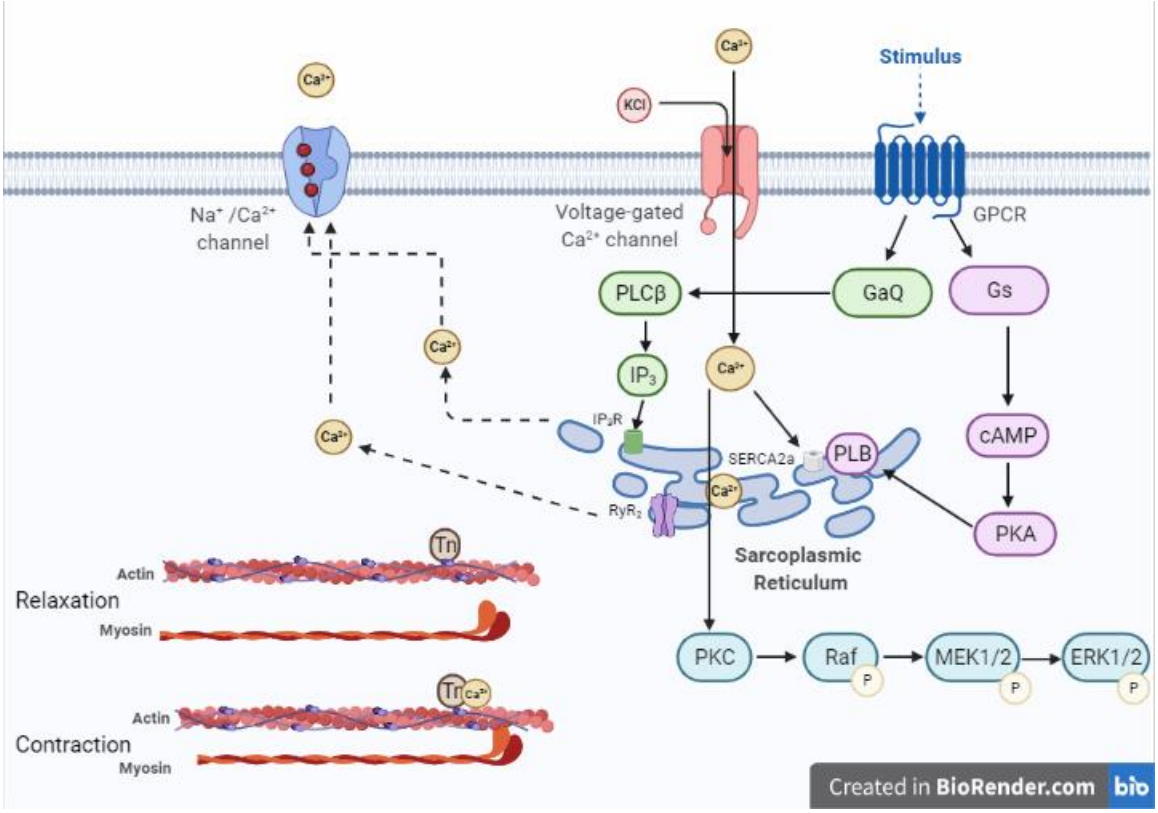

Figure 1.1 Calcium Regulation and Contractility Signaling in Cardiomyocytes.

Calcium (Ca^{2+}) into the cell through the L-type voltage gated calcium channel. Ca^{2+} induces the PKC → MEK → ERK1/2 pathway and stimulates both the opening of the ryonadine receptor 2 (RyR_2) receptors to release stored Ca^{2+} and activation of GPCRs. GPCRs activate Gs → cAMP → PKA → PLB to initiate influx into the sarcoplasmic reticulum along with Gαq → PLCβ → IP_3 and binding to IP_3 receptor (IP_3R). Ca^{2+} is removed from the cytosol through storage in SR via SERCA2a and removed from the cell through the sodium-calcium exchanger (NCX). To induce contraction, Ca^{2+} binds to the troponin (Tn) C on the actin filament where myosin binds to contract the cell. Ca^{2+} and myosin are released from the actin upon relaxation of the cardiomyocyte. *Figure was created in Biorender.*

A number of studies using isolated cardiomyocytes have shown that the ghrelin-GHSR system in the myocardium plays a role in the regulation of Ca^{2+} homeostasis, which is associated with its action in cardioprotection and overall heart function. Treatment of mouse ischemic cardiomyocytes with ghrelin resulted in protection from ischemia/ reperfusion injury, likely from regulation of intracellular Ca^{2+} levels[194]. When ghrelin was administered to rat ventricular cardiomyocytes, a positive inotropic effect was seen through increased intracellular Ca^{2+} transients and increased L-type Ca^{2+} channel current, likely through GHSR-mediated signalling through PKC[198]. The same group evaluated the same parameters of intracellular Ca^{2+} flux on mouse cardiomyocytes with ischemia/ reperfusion (I/R) injury. Activation of GHSR with ghrelin produced a positive inotropic effect again with prevention of Ca^{2+} transient reduction and SR calcium reduction[199]. Therefore, GHSR is expected to protect the heart from I/R injury via the PLB pathway ultimately allowing for maintenance and recovery to normal contractility after cardiac injury[199]. Overall, GHSR is an important regulator of calcium signalling and ultimately contractility in the heart where activation of this system functions as a cardioprotective mechanism for HD.

The inflammatory process plays an important role in the process of HD development. Ghrelin activation of GHSR is known to inhibit pro-inflammatory pathways and activate anti-inflammatory pathways to help protect the heart from further damage. Ghrelin has been shown to act on both immune and endothelial cells to inhibit the leptin- and endotoxin- induced production of pro-inflammatory cytokines, including interleukin 1-β (IL-1β), interleukin-6 (IL-6), and tumour necrosis factor alpha (TNF-α)[200,201]. Further studies evaluated the effect of ghrelin on the toll-like receptor 4 (TLR4)/ NF-κB inflammatory pathway. In the rat heart, ghrelin administration lessened pro-inflammatory signalling through the TLR4/ NF-κB pathway[202]. Additionally, in rats with induced ischemia/reperfusion injury, the increased expression of TLR4, IL-1β, and Caspase-1 were all reduced with the administration of ghrelin[202]. Endogenous ghrelin can also induce anti-inflammation pathways; in ghrelin knockout mice with induced cardiac hypertrophy, the cholinergic anti-inflammatory pathway was suppressed and plasma inflammatory markers (IL-6, IL1-β) were high, compared with wild-type mice[203]. Ghrelin and GHSR also contribute to the inhibition of inflammation via activation of the Akt-activated anti-inflammatory pathway[202]. Therefore, activation of GHSR with ghrelin both inhibits pro-

inflammatory pathways and activates anti-inflammatory pathways to reduce the cardiac damage seen with excessive inflammatory response.

GHSR signalling suppresses apoptosis and promotes survival. One study investigated GHSR signaling in rats with myocardial infarction (MI) and showed a decrease in both apoptosis (metalloproteinase 2 and 9) and inflammation (IL-1β and TNF-α)[204]. GHSR activation promotes pro-angiogenesis, pro-survival and proliferation through Akt and AMP-activated protein kinase (AMPK) in rat cardiomyocytes[205], and extracellular signalling related kinase (ERK) phosphorylation in cardiomyocytes and endothelial cells[206]. Ghrelin has been shown to improve the integrity and decrease shrinkage of rat cardiomyocytes[207]. The ghrelin-GHSR system has been shown to inhibit apoptosis by decreasing pro-apoptotic signalling. In the rat left ventricle, administration of ghrelin decreased the pro-apoptotic factors Bax and Caspase-3 while increasing the anti-apoptotic factors Bcl-2 and Bcl-xL and prevented mitochondrial swelling[208]. In angiotensin II- (Ang II) and isoproterenol-induced HF in rats, activation of AMPK through ghrelin decreased overall apoptosis with decreases in apoptotic factors caspase-3 and caspase-12 [208,209]. GHSR activation has shown to be a cardioprotective marker as it activates many downstream signalling pathways for both decreasing apoptosis and promoting cardiomyocyte survival via a cardioprotective mechanism.

Along with cellular survival, ghrelin acts through GHSR to regulate cellular metabolism, notably glucose metabolism and oxidative stress. In dogs with HF, ghrelin administration enhanced fatty acid oxidation and oxygen consumption and reduced glucose oxidation, thereby partially correcting the metabolic deficiencies from HF[210]. Ghrelin also attenuates the ER stress response to ischemia/reperfusion; in rat hearts with I/R, pre-administration of ghrelin reduced the IR-induced overexpression of mRNA and proteins of the ER stress (ERS) response, glucose-regulated protein78 (GRP78) and C/EBP homologous protein (CHOP)[211]. This group further evaluated the mechanism of ERS activation and determined that ghrelin activates GHSR through the calcium-calmodulin-dependent protein kinase kinase (CAMKK) and AMP-activated protein kinase (AMPK) to ultimately protect the heart from ERS-induced injury[209]. Additionally, ghrelin administration in the mouse heart using adeno-associated virus vectors sustained autophagy and minimized dysfunctional

mitochondria after MI[212]. Taken together, these studies demonstrate the multiple metabolic pathways through which ghrelin activation of GHSR operates to protect against cardiac damage and stress.

Fibrotic deposition is commonly associated with extensive damage and disruption to the myocardium. Many studies have evaluated alterations in scar formation and size after GHSR activation to protect the heart from further injury. Ghrelin has been shown to reduce scar size and volume after MI in mice[213], and ghrelin suppresses collagen I and III mRNA levels in rat cardiomyocytes[214]. In an Ang II-induced model of HF, ghrelin attenuated myocardial fibrosis and expression of fibrotic factors (collagen I, III, TGF-β1) through upregulation of PPAR-γ and inhibition TGF-β1 signalling[215]. The mechanism by which ghrelin inhibits fibrotic deposition was further evaluated in rat ventricular cardiomyocytes where activin A (Act A) levels were significantly increased after a MI. Ghrelin downregulated Act A back to basal levels, thus correcting this Act A imbalance during ventricular remodelling[216]. Therefore, GHSR activation with ghrelin attenuates fibrosis deposition and inhibits fibrotic protein formation to protect the heart from further damage.

The ghrelin-GHSR system is proposed to initiate a cardioprotective mechanism when the myocardium is stressed or damaged. Therefore, studies evaluated cardiac function after activation of this system using ghrelin administration. In healthy humans, ghrelin was injected, and heart function was evaluated acutely after injection. Interestingly, ghrelin dose-dependently enhanced LVEF[217] and vasodilation determined through forearm blood flow[218]. When ghrelin was repeatedly given to CHF patients, there was a drastic improvement in LVEF along with LV mass and end-systolic volume, oxygen capacity and muscle wasting[219]. In human studies, there has been clear evidence that the ghrelin-GHSR system functions to improve cardiac function after myocardial damage. Therefore, these studied have shown the clinical relevance of the ghrelin-GHSR system in HD models.

Overall, these data depict a complex biochemical signalling network upon activation of myocardial GHSR. Cardio-protection via the ghrelin-GHSR system functions to regulate calcium homeostasis and, in turn, contractility; reduce inflammation; inhibit apoptosis and

cell death; regulate cellular metabolism; and reduce fibrosis deposition. These processes are represented in a signalling cascade pathway shown in Figure 1.2.

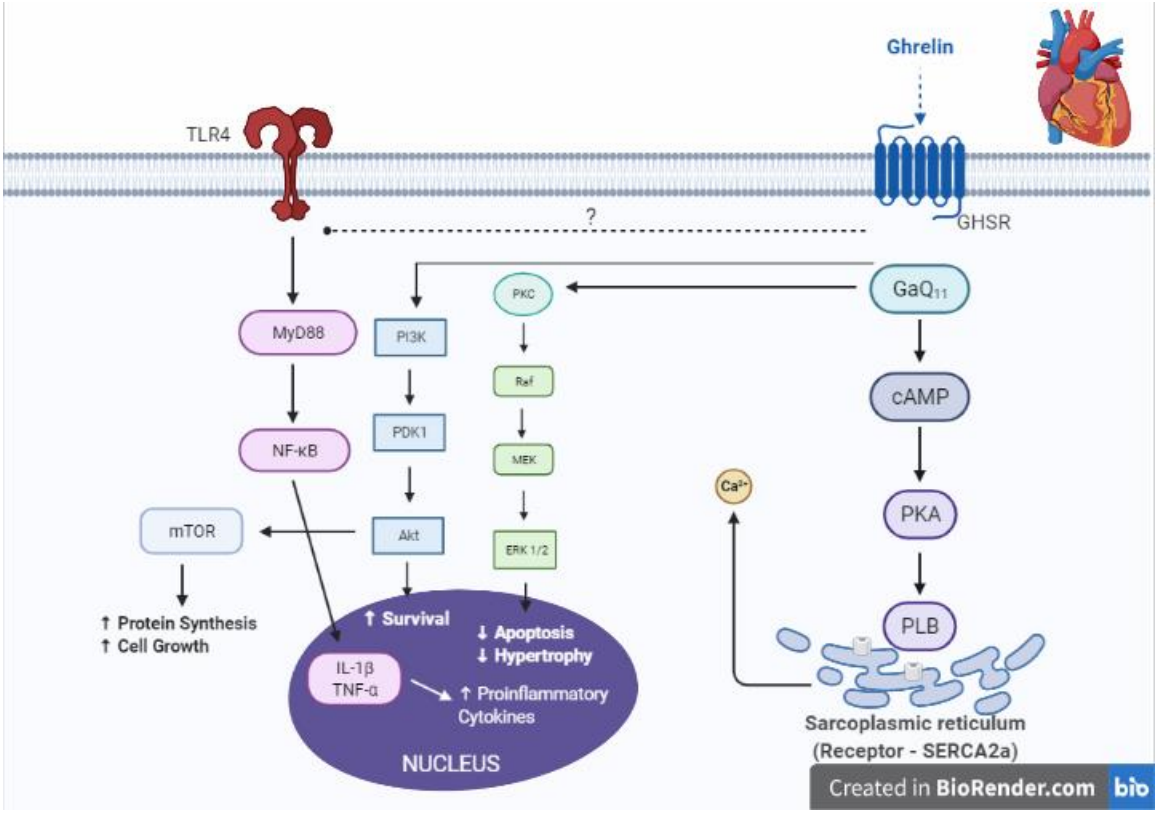

Figure 1.2 Proposed Biochemical Signalling Cascade of ghrelin-GHSR in Cardiomyocytes.

Ghrelin activation of cardiac GHSR initiates downstream signalling pathways for contractility (cAMP → PKA → PLB → SERCA2a and calcium homeostasis); apoptosis/ hypertrophy (PKC → MEK → ERK1/2); cellular survival (PI3K → PDK1 → Akt); protein synthesis and cellular growth (Akt → mTOR); inflammation (TLR4 → MyD88 → NFκB → IL-1β and TNF-α). *Figure was created in Biorender.*

1.4.3 Argument for GHSR as a Biomarker in Heart Disease and Heart Failure

The biology of the myocardial ghrelin-GHSR system has been extensively studied and now the question remains, could this system act as a targeted biomarker for HD and a predictor of HF? Activation of the ghrelin-GHSR system improves overall heart function potentially acting through a cardioprotective mechanism to help mediate the negative effects of HD. The ghrelin-GHSR system dynamics are known to change for different forms of heart disease including diabetic cardiomyopathy, valvular disease, CHF, and MI.

Changes in the ghrelin-GHSR system within the heart may provide clues to the development of HD and HF. The rodent MI model in which the left anterior descending coronary artery is ligated, has revealed some interesting dynamics. Following surgery, myocardial GHSR expression increased over time and ghrelin expression decreased[220]. Additionally, ghrelin serum levels correlated negatively with LV end-diastolic pressure and dimension indicating this ghrelin-GHSR system plays a role in LV function[220]. A rat model of MI was used to evaluate the effects of ghrelin administration on heart function. In rats that were ghrelin-treated post-MI, LV end-diastolic pressure and enlargement were reduced compared to saline controls[214] and overall mortality rates were reduced[221] while cardiac cachexia was reduced[222]. Similarly in a model of MI, isolated rat hearts were administered ghrelin during reperfusion where coronary flow, heart rate, contractility, and left ventricular end systolic and end-diastolic pressures were significantly improved[223]. Similar results were seen in another model of cardiac injury induced by isoproterenol in rats where GHSR and ghrelin mRNA expression increased with cardiac injury and were decreased back to normal levels with ghrelin treatment[224]. Interestingly, in a model of hypoxia/ reperfusion in isolated rat cardiomyocytes, GHSR expression was decreased acutely while ghrelin injection increased the expression of GHSR back to normal cardiomyocyte levels[207]. With Doxorubicin induced cardiotoxicity in mice, there was remarkable mortality and cardiac dysfunction which was ameliorated with ghrelin administration[225]. Our past work in a rodent model of diabetic cardiomyopathy (DCM) showed significant decreases in GHSR expression in acute severe and chronic mild DCM compared to control hearts. This is the first study showing GHSR expression changes in

DCM and significant decreases in GHSR expression in a model of HD. Together these results indicate significant regulation of cardiac function through the ghrelin-GHSR system. Threshold levels for GHSR expression decrease and increase based on the type and severity of heart disease.

Is the ghrelin-GHSR system a clinically meaningful indicator of HD or HF? A few studies have evaluated the expression of both ghrelin and GHSR in human patients with heart disease. In a study by Beiras-Fernandex *et al.*, myocardial tissue from patients with CHF was analyzed for expression of both GHSR and ghrelin and compared to control tissue. The authors found tissue ghrelin levels significantly decreased and levels of GHSR markedly increased in CHF[226]. This was the first study showing changes in both ghrelin and GHSR in the myocardium of patients with HF with association to cardiac function where these changes could reflect a compensatory mechanism. Another study evaluated GHSR density in cardiac vasculature using a labelled ghrelin probe, [^{125}I-*His*^{9}]-ghrelin, where GHSR density increased in atherosclerotic aorta, and coronary arteries and veins. These changes in GHSR density in atherosclerosis vasculature represent a potential therapeutic target in the treatment of cardiovascular disease[227]. Changes in GHSR are also associated with LV mass. *GHSR* gene variant analysis revealed one variant that was common in individuals with highly symptomatic LV hypertrophy. These data suggest that GHSR variants differ based on susceptibility to LVH[228].

Another indicator of cardiac damage is the circulating form of ghrelin where elevations can lead to poor outcomes for patients with cardiac conditions. Chen Y *et al.*, demonstrated a decrease in plasma ghrelin levels in patients with CHF where survival analysis showed that a higher plasma ghrelin level (>85pmol/l) lead to increased 2-year survival rate[229]. Significant correlations were seen between circulating ghrelin levels and NT-proBNP indicating ghrelin could be a predictor of readmission in HF similar to NT-proBNP. Ghrelin also correlated to LVEF, another predictor of readmission, further suggesting lower circulating ghrelin levels could lead to patient readmission and a biomarker of HD and HF[229]. Another study in cardiac hypertrophy patients evaluated the relationship between plasma ghrelin levels and ventricular wall thickness. Higher plasma ghrelin levels correlated to increased wall thickness reflecting a possible compensatory mechanism to

up-regulate ghrelin concentrations and act through the cardiac ghrelin-GHSR system[230]. Plasma ghrelin levels were also correlated to atherosclerotic plaques in atherosclerosis where ghrelin was positively associated with mean artery plaque thickness[231]. Taken all together, these studies indicate that there are thresholds in serum ghrelin levels that are associated with disease severity in HD and HF.

Overall, these data show a clear indication of the cardioprotective effects the ghrelin-GHSR system has on the myocardium and overall cardiac function. The expression of GHSR and ghrelin are altered depending on the type and severity of heart disease present while they ultimately act to improve the biochemical signalling in cardiomyocytes and enhance overall cardiac function. Therefore, the literature supports the use of GHSR as a cardiac localized biomarker of HD and HF and its potential predictive value as serum ghrelin levels and GHSR-associated biochemical signalling occurs early in the progression of cardiac dysfunction.

1.4.4 Imaging Agents Targeting GHSR: Fluorescent Probes and PET Tracers

With the relevance of the ghrelin-GHSR system to not only overall cardiac function but the multitude of biochemical signalling pathways involved in HD progression, this system is a promising target for evaluation of HD. Since ghrelin is produced and secreted from many tissues across the body the use of circulating ghrelin as a biomarker of HD may be confounded. Hence, GHSR may be an optimal target as it is localized to cardiac tissue and GHSR expression levels change significantly in the disease process. Therefore, imaging changes in myocardial GHSR may be an indicator of HD progression.

The detection of GHSR and its associated signalling pathways in tissue has been problematic as antibodies targeting G-protein coupled receptors (GPCRs) are not specific[232]. To overcome this problem, transgenic mouse models of green fluorescent protein (GFP) tagged to GHSR were developed to specifically localize GHSR *in vitro*. In a mouse model of GHSR-GFP, GHSR was regionally localized in the anterior pituitary

with positive GFP fluorescent analysis[233,234]. Although this model accurately identifies GHSR positive cells, there is still the challenge of targeting GHSR in cells that are not transfected with a fluorescent reporter gene. To tackle this issue, fluorescent analogues have been developed targeting GHSR in any histological tissue. One study by Liu M *et al*., developed a fluorescent analogue of full-length human ghrelin where Alexa Fluor 568 was chemically bound to the C-terminal end of ghrelin. This analogue was found to bind GHSR *in vitro* with an IC_{50} of 11nM (comparable to native ghrelin at 3.3nM)[235]. Another study evaluated an endogenous GHSR antagonist, liver-expressed antimicrobial peptide 2 (LEAP2). This group developed a fluorescent LEAP2 analogue termed F-LEAP2 where the fluorescent moiety (F) was conjugated to the N-terminal end and specific binding to GHSR was observed in cells of mouse brain regions with a binding affinity of 3.9nM[236]. More recently, our team has developed fluorescent ghrelin analogues targeted to GHSR. The first fluorescent analogue developed was a truncated 18-amino acid analog of ghrelin tagged with fluorescein isothiocyanate (FITC). The analog was found to bind in mouse cardiac tissue. However, the FITC tag posed a problem as tissue autofluorescence occurs in this fluorescent wavelength in cardiomyocytes[237]. Therefore, we developed a far-red analogue to target GHSR to circumvent the autofluorescence issue. A far-red analogue of truncated ghrelin with a Cy5 fluorescent probe on the C-terminal end, Cy5-Ghrelin(1-19), was developed and tested in P19-derived cardiomyocytes to target GHSR. This analogue bound to GHSR specifically with a binding affinity of 26nM in cardiomyocytes with specificity validated in mouse cardiac tissue[238]. Since then we have developed a second generation of fluorescent peptides targeting GHSR[239]. These peptides have enhanced stability and affinity using a “stapling” method to bridge the peptide, ultimately preserving the cyclic α-helical structure essential for binding. Promising candidates from this array include Sulfo-Cy5-Ghrelin(1-20), Sulfo-Cy5-cyclo-12-Ghrelin(1-20), and Sulfo-Cy5-cyclo-8-ghrelin(1-20) with binding affinities of 11nM, 1.0nM, and 6.2nM respectively[239]. With these new developments in fluorescent ghrelin-derived probes, there are many compounds available to specifically target GHSR *in situ* in cardiac cells and tissues.

Additional to *in situ* imaging analogues, *in vivo* imaging agents have been developed to target GHSR in the body. Initial PET and SPECT imaging agents involved radio-labelling native ghrelin targeting GHSR through *in situ* studies. Studies have demonstrated that the

structure of ghrelin could be highly modified and the n-octanoylated group manipulated while preserving strong affinity to the receptor. This allowed for enhanced stability of the imaging agent to be used for *in vivo* studies[240]. The next stage in GHSR probe development was in 2009 where Rosita *et al.* reported new manipulation of ghrelin peptides including significant truncation and alterations in the octynol side chain of active ghrelin. The lead candidate for PET imaging was a fluorine-bearing 12 carbon aliphatic side chain of the ghrelin(1-14) compound with binding affinity of 28nM while the lead candidate for SPECT imaging was ghrelin(1-14) modified with a rhenium metal complex side chain with binding affinity of 35nM. These analogs show possibilities for future studies with ^{18}F PET and ^{99m}Tc SPECT imaging to noninvasively detect GHSR *in vivo*[241]. Additional SPECT imaging agents was reported by Koźmiński and Gniazdowska where ^{99m}Tc conjugated to CN-Lys-ghrelin was evaluated *in situ* in human prostate cells and *in vivo* in mice. Two promising candidates, $^{99m}Tc(CO)_3L_{s,o}$(CN-Lys-GHR) and $^{99m}Tc(NS_3)$(CN-Lys-GHR), showed strong binding affinities to GHSR (54nM and 45nM respectively) with good stability and minimal tracer degradation in the human serum over time. Although these lead compounds showed promise *in vivo*, there was minimal uptake in the mouse heart[242]. Charron *et al.* developed a [^{68}Ga]-ghrelin analogue, [Dpr^3(octanoyl),Lys^{19}(^{68}Ga-DOTA)]ghrelin(1-19), with a strong affinity to GHSR (5.9 nM) and strong serum stability. This analogue was tested in a xenograft mouse model where the tracer accumulated in the xenograft with excessive uptake in the kidney and minimal uptake in the heart[243]. Due to the limited uptake in the heart with these imaging agents, the labelled ghrelin-peptide may not be optimal for imaging *in vivo* changes in cardiac GHSR density.

To overcome these issues, development of small molecule ligands of GHSR for *in vivo* imaging have been evaluated for increased affinity and serum stability. A study by Chollet *et al.* compared the binding of a ^{68}Ga-NODAGA-ghrelin agonist peptide tracer to a ^{68}Ga-NODAGA-ghrelin small molecule inverse agonist tracer (binds to GHSR with opposite physiological responses). *In vivo* imaging experiments in rats showed increased stability in blood, reasonable clearance in kidneys and liver with both the peptide and small molecule, but higher uptake in the heart with the small molecule inverse agonist compared to the peptide tracer. The small molecule inverse agonist had unspecific diffusion and posed a challenge in understanding GHSR signalling[244]. Another study by Potter *et al.* evaluated a

(S)-stereoisomer of N-methyl piperidine-substituted quinazolinone small molecule derivative of ghrelin was developed to target GHSR with a binding affinity of 22nM. *In vivo* mouse studies demonstrated slight uptake in the heart, however blocking studies showed decreased tracer specificity (38%) and further enhancement of GHSR small molecules should be evaluated[245]. These initial results in ghrelin imaging agents have led to many developments in probes targeting GHSR *in vivo.* PET imaging probes have been developed and optimized by our research team. In a study by Charron *et al*., this group developed an array of ghrelin-derived peptides and small molecules labelled with ^{18}F-fluorine where the lead small molecule analogue, [Inp^{1},Dpr^{3}(6-fluoro-2-naphthoate),1-Nal^{4},Thr^{8}]ghrelin(1−8), had a significantly stronger affinity (0.11nM) to GHSR compared to native ghrelin (3.3nM). This analogue incorporated a 6-fluoro-2-pentafluorophenyl naphthoate (PFPN) group to incorporate ^{18}F and enhance *in vivo* stability[246]. In addition to these developed tracers, work by Abbas *et al.* evaluated a promising peptidomimetic candidate, [1-Nal^{4}, Lys^{5}(4-[^{18}F]-FB)]G-7039, for *in vivo* PET imaging with binding affinity of 69nM. In healthy wild-type mice and mice lacking GHSR, there was no change in tracer uptake in the heart indicating mouse models may not be optimal for imaging GHSR *in vivo*[247]. Therefore, PET tracer development is an ongoing process to target GHSR *in vivo* in the heart.

1.5 Rationale and Aims of the Study

With discovery and identification of the cardiac ghrelin-GHSR system there has been significant evidence of cardioprotective signalling through its activation. GHSR density in cardiac tissue may decrease and increase throughout the progression of HD. GHSR is elevated in end stage heart failure while circulating ghrelin may be a predictor of adverse cardiac events. GHSR activation after cardiac damage may increase pro-survival signalling, boost contractility and maintain calcium regulation, decrease harmful inflammatory effects, and enhance overall cardiac function. Many studies have evaluated the specific biochemical signalling pathways associated with GHSR activation although identification of GHSR density *in situ* and *in vivo* remain difficult. Conventional antibodies targeting GHSR lack specificity with *in situ* histological analysis and thus new targeted fluorescent imaging agents have been developed for GHSR binding and *in vivo* PET imaging agents have been optimized for GHSR detection. In this context, our team has developed and characterized imaging agents targeted to cardiac GHSR. These targeted imaging agents aid in revealing the dynamics of the ghrelin-GHSR system with associated biochemical signalling in HD and HF both *in situ* with quantitative fluorescence microscopy and *in vivo* with PET imaging. Elucidating the role of the ghrelin-GHSR system in the pathophysiological process of HD and HF may aid in clinical diagnosis and targeted therapies.

The hypothesis of my thesis is:

GHSR is a biomarker for the underlying biological mechanisms involved in heart disease and heart failure.

The specific aims of my thesis are:

1) To identify GHSR as a scalable biomarker in human heart failure and heart disease using quantitative fluorescence microscopy
2) To develop and characterize a targeted PET imaging agent for cardiac GHSR in a large animal model of myocardial infarction

1.6 References

1. Heart and Stroke Foundation of Canada. (Dis)connected: How unseen links are putting us at risk. (2019).

2. Foundation, H. and S. *2016 Report on the Health of Canadians*. (2016).

3. Braunwald, E. Heart failure. *JACC Hear. Fail.* **1**, 1–20 (2013).

4. Crespo-Leiro, M. G. *et al.* Advanced heart failure: a position statement of the Heart Failure Association of the European Society of Cardiology. *Eur. J. Heart Fail.* **20**, 1505–1535 (2018).

5. Khatibzadeh, S., Farzadfar, F., Oliver, J., Ezzati, M. & Moran, A. Worldwide risk factors for heart failure: A systematic review and pooled analysis. *Int. J. Cardiol.* **168**, 1186–1194 (2013).

6. Loffredo, F. S., Nikolova, A. P., Pancoast, J. R. & Lee, R. T. Heart failure with preserved ejection fraction: Molecular pathways of the aging myocardium. *Circulation Research* vol. 115 97–107 (2014).

7. Lesyuk, W., Kriza, C. & Kolominsky-Rabas, P. Cost-of-illness studies in heart failure: A systematic review 2004-2016. *BMC Cardiovasc. Disord.* **18**, 74 (2018).

8. Greenberg, B. H. Heart failure epidemic. *Curr. Cardiol. Rep.* **4**, 185 (2002).

9. Nyaga, U. F. *et al.* Data on the epidemiology of heart failure in Sub-Saharan Africa. *Data Br.* **17**, 1218–1239 (2018).

10. Samsky, M. D. *et al.* Trends in Readmissions and Length of Stay for Patients Hospitalized with Heart Failure in Canada and the United States. *JAMA Cardiol.* **4**, 444–453 (2019).

11. Jackson, S. L. *et al.* National Burden of Heart Failure Events in the United States,

2006 to 2014. *Circ. Heart Fail.* **11**, e004873 (2018).

12. Kemp, C. D. & Conte, J. V. The pathophysiology of heart failure. *Cardiovasc. Pathol.* **21**, 365–371 (2012).

13. Michael, Y. Y. Heart Failure in Clinical Practice. in *Heart Failure in Clinical Practice* (2010). doi:10.1007/978-1-84996-153-0.

14. Tham, Y. K., Bernardo, B. C., Ooi, J. Y. Y., Weeks, K. L. & McMullen, J. R. Pathophysiology of cardiac hypertrophy and heart failure: signaling pathways and novel therapeutic targets. *Arch. Toxicol.* **89**, 1401–1438 (2015).

15. Gorski, P. A., Ceholski, D. K. & Hajjar, R. J. Altered myocardial calcium cycling and energetics in heart failure - A rational approach for disease treatment. *Cell Metab.* **21**, 183–194 (2015).

16. Cartwright, E. J., Mohamed, T., Oceandy, D. & Neyses, L. Calcium signaling dysfunction in heart disease. *BioFactors* **37**, 175–181 (2011).

17. Thenappan, S., Raza, J. A., Kreeger, R. W. & Movahed, A. *Clinical cardiac electrophysiology - An overview*. *Integrating Cardiology for Nuclear Medicine Physicians: A Guide to Nuclear Medicine Physicians* (2009). doi:10.1007/978-3-540-78674-0_13.

18. Van Empel, V. P. M. *et al.* Myocyte apoptosis in heart failure. *Cardiovasc. Res.* **67**, 21–29 (2005).

19. Kang, P. M. & Izumo, S. Apoptosis and Heart Failure. *Circ. Res.* **86**, 1107–1113 (2000).

20. Mughal, W. & Kirshenbaum, L. A. Cell death signalling mechanisms in heart failure. *Exp. Clin. Cardiol.* **16**, 102–108 (2011).

21. Zhu, H. & Sun, A. Programmed necrosis in heart disease: Molecular mechanisms and clinical implications. *J. Mol. Cell. Cardiol.* **116**, 125–134 (2018).

22. Saftig, P., Von Figura, K., Tanaka, Y. & Lüllmann-Rauch, R. Disease model: LAMP-2 enlightens Danon disease. *Trends Mol. Med.* **7**, 37–39 (2001).

23. Li, Y. *et al.* AMPK blunts chronic heart failure by inhibiting autophagy. *Biosci. Rep.* **38**, 1–8 (2018).

24. Riquelme, J. A. *et al.* Therapeutic targeting of autophagy in myocardial infarction and heart failure. *Expert Rev. Cardiovasc. Ther.* **14**, 1007–1019 (2016).

25. Zhang, X. *et al.* Tanshinone IIA protects against heart failure post-myocardial infarction via AMPKs/mTOR-dependent autophagy pathway. *Biomed. Pharmacother.* **112**, 108599 (2019).

26. Azevedo, P. S., Minicucci, M. F., Santos, P. P., Paiva, S. A. R. & Zornoff, L. A. M. Energy Metabolism in Cardiac Remodeling and Heart Failure. *Cardiol. Rev.* **21**, 135–140 (2013).

27. Birkenfeld, A. L., Jordan, J., Dworak, M., Merkel, T. & Burnstock, G. Myocardial metabolism in heart failure: Purinergic signalling and other metabolic concepts. *Pharmacol. Ther.* **194**, 132–144 (2019).

28. Bertero, E. & Maack, C. Metabolic remodelling in heart failure. *Nat. Rev. Cardiol.* **15**, 457–470 (2018).

29. Borlaug, B. A. Evaluation and management of heart failure with preserved ejection fraction. *Nat. Rev. Cardiol.* **17**, 559–573 (2020).

30. Bakhle, Y. S. How ACE inhibitors transformed the renin–angiotensin system. *Br. J. Pharmacol.* **177**, 2657–2665 (2020).

31. Marcy, T. R. & Ripley, T. L. Aldosterone antagonists in the treatment of heart failure. *Am. J. Heal. Pharm.* **63**, 49–58 (2006).

32. Osmanska, J. & Jhund, P. S. Contemporary Management of Heart Failure in the Elderly. *Drugs and Aging* **36**, 137–146 (2019).

33. Guidelines and Protocols Advisory Committee. Chronic Heart Failure - Diagnosis and Management. *BC Guidel.* (2015).

34. Lam, C. S. P., Chandramouli, C., Ahooja, V. & Verma, S. SGLT-2 Inhibitors in Heart Failure: Current Management, Unmet Needs, and Therapeutic Prospects. *J. Am. Heart Assoc.* **8**, 1–12 (2019).

35. Elgendy, I. Y., Mahtta, D. & Pepine, C. J. Medical Therapy for Heart Failure Caused by Ischemic Heart Disease. *Circ. Res.* **124**, 1520–1535 (2019).

36. Goyal, A. *et al.* Outcomes Associated With the Use of Secondary Prevention Medications After Coronary Artery Bypass Graft Surgery. *Ann. Thorac. Surg.* **83**, 993–1001 (2007).

37. Birks, E. J. *et al.* Prospective Multicenter Study of Myocardial Recovery Using Left Ventricular Assist Devices (RESTAGE-HF [Remission from Stage D Heart Failure]): Medium-Term and Primary End Point Results. *Circulation* 2016–2028 (2020) doi:10.1161/CIRCULATIONAHA.120.046415.

38. Tilemann, L., Ishikawa, K., Weber, T. & Hajjar, R. J. Gene therapy for heart failure. *Circ. Res.* **110**, 777–793 (2012).

39. Quijada, P. & Sussman, M. A. Making it stick: Chasing the optimal stem cells for cardiac regeneration. *Expert Rev. Cardiovasc. Ther.* **12**, 1275–1288 (2014).

40. Singh, A., Singh, A. & Sen, D. Mesenchymal stem cells in cardiac regeneration: A detailed progress report of the last 6 years (2010-2015). *Stem Cell Res. Ther.* **7**, 1–25 (2016).

41. Lemcke, H., Voronina, N., Steinhoff, G. & David, R. Recent Progress in Stem Cell Modification for Cardiac Regeneration. *Stem Cells Int.* **2018**, (2018).

42. Bredy, C. *et al.* New York Heart Association (NYHA) classification in adults with congenital heart disease: Relation to objective measures of exercise and outcome. *Eur. Hear. J. - Qual. Care Clin. Outcomes* **4**, 51–58 (2018).

43. Yancy, C. W. *et al.* 2013 ACCF/AHA guideline for the management of heart failure: A report of the American college of cardiology foundation/american heart association task force on practice guidelines. *J. Am. Coll. Cardiol.* **62**, (2013).

44. Yancy, C. W. *et al.* 2017 ACC/AHA/HFSA Focused Update of the 2013 ACCF/AHA Guideline for the Management of Heart Failure: A Report of the American College of Cardiology/American Heart Association Task Force on Clinical Practice Guidelines and the Heart Failure Society of Amer. *J. Card. Fail.* **23**, 628–651 (2017).

45. Gandhi, S., Mosleh, W., Shen, J. & Chow, C. M. Automation, machine learning, and artificial intelligence in echocardiography: A brave new world. *Echocardiography* **35**, 1402–1418 (2018).

46. Hillis, G. S. & Bloomfield, P. Basic transthoracic echocardiography. *Br. Med. J.* **330**, 1432–1436 (2005).

47. Garcia, M. J., Thomas, J. D. & Klein, A. L. New doppler echocardiographic applications for the study of diastolic function. *J. Am. Coll. Cardiol.* **32**, 865–875 (1998).

48. NISHIMURA, R. A. *et al.* Doppler Echocardiography: Theory, Instrumentation, Technique, and Application. *Mayo Clin. Proc.* **60**, 321–343 (1985).

49. Lancellotti, P. *et al.* Stress echocardiography in patients with native valvular heart disease. *Heart* **104**, 807–813 (2018).

50. ILICETO, S., CANNONE, M. & RIZZON, P. *Stress Echocardiography*. *Echocardiography* vol. 3 (1986).

51. Inciardi, R. M. *et al.* Echocardiographic advances in hypertrophic cardiomyopathy: Three-dimensional and strain imaging echocardiography. *Echocardiography* **35**, 716–726 (2018).

52. Leipsic, J. *et al.* Core Competencies in Cardiac CT for Imaging Structural Heart

Disease Interventions: An Expert Consensus Statement. *JACC Cardiovasc. Imaging* **12**, 2555–2559 (2019).

53. Lin, E. & Alessio, A. What are the basic concepts of temporal, contrast, and spatial resolution in cardiac CT? *J. Cardiovasc. Comput. Tomogr.* **3**, 403–408 (2009).

54. Woodard, P. K., Bhalla, S., Javidan-Nejad, C. & Gutierrez, F. R. Non-coronary cardiac CT imaging. *Semin. Ultrasound, CT MRI* **27**, 56–75 (2006).

55. Mak, G. S. & Truong, Q. A. Cardiac CT: Imaging of and Through Cardiac Devices. *Curr. Cardiovasc. Imaging Rep.* **5**, 328–336 (2012).

56. Lim, J. W., Lee, H., Her, K., Park, H. W. & Shin, K. E. Myocardial CT perfusion imaging for pre-A nd postoperative evaluation of myocardial ischemia in a patient with myocardial bridging. *Med. (United States)* **96**, (2017).

57. Branch, K. R. *et al.* Myocardial computed tomography perfusion. *Cardiovasc. Diagn. Ther.* **7**, 452–462 (2017).

58. Carrascosa, P. & Capunay, C. Myocardial CT perfusion imaging for ischemia detection. *Cardiovasc. Diagn. Ther.* **7**, 112–128 (2017).

59. So, A. *et al.* Quantitative myocardial perfusion measurement using CT Perfusion: A validation study in a porcine model of reperfused acute myocardial infarction. *Int. J. Cardiovasc. Imaging* **28**, 1237–1248 (2012).

60. Seitun, S. *et al.* CT myocardial perfusion imaging: A new frontier in cardiac imaging. *Biomed Res. Int.* **2018**, (2018).

61. Van Der Geest, R. J. & Reiber, J. H. C. Quantification in cardiac MRI. *J. Magn. Reson. Imaging* **10**, 602–608 (1999).

62. Florian, A., Jurcut, R., Ginghina, C. & Bogaert, J. Cardiac magnetic resonance imaging in ischemic heart disease: a clinical review. *J. Med. Life* **4**, 330–345 (2011).

63. Pereira, R. S., Prato, F. S., Lekx, K. S., Sykes, J. & Wisenberg, G. Contrast-enhanced MRI for the assessment of myocardial viability after permanent coronary artery occlusion. *Magn. Reson. Med.* **44**, 309–316 (2000).

64. Aljizeeri, A., Sulaiman, A., Alhulaimi, N., Alsaileek, A. & Al-Mallah, M. H. Cardiac magnetic resonance imaging in heart failure: where the alphabet begins! *Heart Fail. Rev.* **22**, 385–399 (2017).

65. Wang, Z. J. *et al.* Hyperpolarized 13C MRI: State of the art and future directions. *Radiology* **291**, 273–284 (2019).

66. Kurhanewicz, J. *et al.* Hyperpolarized 13C MRI: Path to Clinical Translation in Oncology. *Neoplasia (United States)* **21**, 1–16 (2019).

67. Cavallari, E. *et al.* The 13C hyperpolarized pyruvate generated by ParaHydrogen detects the response of the heart to altered metabolism in real time. *Sci. Rep.* **8**, 2–10 (2018).

68. Palumbo, A. *et al.* Functional parameters of the left ventricle: comparison of cardiac MRI and cardiac CT in a large population. *Radiol. Medica* **115**, 702–713 (2010).

69. Busch, S. *et al.* Quantitative assessment of left ventricular function with dual-source CT in comparison to cardiac magnetic resonance imaging: Initial findings. *Eur. Radiol.* **18**, 570–575 (2008).

70. Lee, H. J. *et al.* Myocardial extracellular volume fraction with dual-energy equilibrium contrast-Enhanced cardiac ct in nonischemic cardiomyopathy: A prospective comparison with cardiac MR imaging. *Radiology* **280**, 49–57 (2016).

71. MacHac, J. Cardiac positron emission tomography imaging. *Semin. Nucl. Med.* **35**, 17–36 (2005).

72. Saraste, A., Nekolla, S. G. & Schwaiger, M. Cardiovascular molecular imaging: An overview. *Cardiovasc. Res.* **83**, 643–652 (2009).

73. James, M. L. & Gambhir, S. S. A molecular imaging primer: Modalities, imaging agents, and applications. *Physiol. Rev.* **92**, 897–965 (2012).

74. Bucerius, J., Biersack, H. J. & Ahmadzadehfar, H. 99mTc-sestamibi: Clinical applications. *99mTc-Sestamibi Clin. Appl.* 1–194 (2012) doi:10.1007/978-3-642-04233-1.

75. Al Moudi, M. & Sun, Z. H. Diagnostic value of 18F-FDG PET in the assessment of myocardial viability in coronary artery disease: A comparative study with 99mTc SPECT and echocardiography. *J. Geriatr. Cardiol.* **11**, 229–236 (2014).

76. Leslie, W. D. *et al.* Prognostic Value of Automated Quantification of. *J Nucl Med* **46**, 204–211 (2005).

77. Travin, M. I. *et al.* The prognostic value of ECG-gated SPECT imaging in patients undergoing stress Tc-99m sestamibi myocardial perfusion imaging. *J. Nucl. Cardiol.* **11**, 253–262 (2004).

78. Kim, D. Y., Cho, S. G. & Bom, H. S. Emerging Tracers for Nuclear Cardiac PET Imaging. *Nucl. Med. Mol. Imaging (2010).* **52**, 266–278 (2018).

79. Sarikaya, I. Cardiac applications of PET. *Nucl. Med. Commun.* **36**, 971–985 (2015).

80. Driessen, R. S., Raijmakers, P. G., Stuijfzand, W. J. & Knaapen, P. Myocardial perfusion imaging with PET. *Int. J. Cardiovasc. Imaging* **33**, 1021–1031 (2017).

81. Schindler, T. H., Schelbert, H. R., Quercioli, A. & Dilsizian, V. Cardiac PET imaging for the detection and monitoring of coronary artery disease and microvascular health. *JACC Cardiovasc. Imaging* **3**, 623–640 (2010).

82. Fiechter, M. *et al.* Myocardial perfusion imaging with 13N-Ammonia PET is a strong predictor for outcome. *Int. J. Cardiol.* **167**, 1023–1026 (2013).

83. Lee, J. M. *et al.* Integrated Myocardial Perfusion Imaging Diagnostics Improve

Detection of Functionally Significant Coronary Artery Stenosis by 13N-ammonia Positron Emission Tomography. *Circ. Cardiovasc. Imaging* **9**, 1–11 (2016).

84. Benz, D. C. *et al.* Role of quantitative myocardial blood flow and 13 N-ammonia washout for viability assessment in ischemic cardiomyopathy. *J. Nucl. Cardiol.* (2019) doi:10.1007/s12350-019-01684-1.

85. Fukushima, K. *et al.* Prediction of short-term cardiovascular events using quantification of global myocardial flow reserve in patients referred for clinical 82Rb PET perfusion imaging. *J. Nucl. Med.* **52**, 726–732 (2011).

86. Zampella, E. *et al.* Combined evaluation of regional coronary artery calcium and myocardial perfusion by 82Rb PET/CT in the identification of obstructive coronary artery disease. *Eur. J. Nucl. Med. Mol. Imaging* **45**, 521–529 (2018).

87. Kajander, S. A. *et al.* Clinical value of absolute quantification of myocardial perfusion with 15O-water in coronary artery disease. *Circ. Cardiovasc. Imaging* **4**, 678–684 (2011).

88. Danad, I. *et al.* Quantitative assessment of myocardial perfusion in the detection of significant coronary artery disease: Cutoff values and diagnostic accuracy of quantitative [15O]H2O PET imaging. *J. Am. Coll. Cardiol.* **64**, 1464–1475 (2014).

89. Bendix, K., Thomassen, A., Junker, A., Veien, K. T. & Jensen, L. O. 15O-Water Positron Emission Tomography of Myocardial Ischemia in Patients Referred for Percutaneous Coronary Intervention. *Cardiovasc. Revascularization Med.* **21**, 1237–1243 (2020).

90. Anker, S. D. & Von Haehling, S. Inflammatory mediators in chronic heart failure: An overview. *Heart* **90**, 464–470 (2004).

91. Passino, C. *et al.* Markers of fibrosis, inflammation, and remodeling pathways in heart failure. *Clin. Chim. Acta* **443**, 29–38 (2015).

92. Mann, D. L. Innate immunity and the failing heart: The cytokine hypothesis

revisited. *Circ. Res.* **116**, 1254–1268 (2015).

93. Freemerman, A. J. *et al.* Metabolic reprogramming of macrophages: Glucose transporter 1 (GLUT1)-mediated glucose metabolism drives a proinflammatory phenotype. *J. Biol. Chem.* **289**, 7884–7896 (2014).

94. Williams, G. & Kolodny, G. M. Suppression of myocardial 18F-FDG uptake by preparing patients with a high-fat, low-carbohydrate diet. *AJR. Am. J. Roentgenol.* **190**, 151–156 (2008).

95. W., O. *et al.* Usefulness of fasting18F-FDG PET in identification of cardiac sarcoidosis. *J. Nucl. Med.* **45**, 1989–1998 (2004).

96. Dou, K. F. *et al.* Use of resting myocardial 18F-FDG imaging in the detection of unstable angina. *Nucl. Med. Commun.* **36**, 999–1006 (2015).

97. Wykrzykowska, J. *et al.* Imaging of inflamed and vulnerable plaque in coronary arteries with 18F-FDG PET/CT in patients with suppression of myocardial uptake using a low-carbohydrate, high-fat preparation. *J. Nucl. Med.* **50**, 563–568 (2009).

98. Skagen, K. *et al.* Carotid plaque inflammation assessed with 18F-FDG PET/CT is higher in symptomatic compared with asymptomatic patients. *Int. J. Stroke* **10**, 730–736 (2015).

99. Christodoulidis, G., Vittorio, T. J., Fudim, M., Lerakis, S. & Kosmas, C. E. Inflammation in coronary artery disease. *Cardiol. Rev.* **22**, 279–288 (2014).

100. Zhang, X. *et al.* Clinical outcome of patients with previous myocardial infarction and left ventricular dysfunction assessed with myocardial 99mTc-MIBI SPECT and 18F-FDG PET. *J. Nucl. Med.* **42**, 1166–1173 (2001).

101. Aoyama, R. *et al.* Evaluation of myocardial glucose metabolism in hypertrophic cardiomyopathy using 18F-fluorodeoxyglucose positron emission tomography. *PLoS One* **12**, 1–16 (2017).

102. Raffel, D. M., Chen, W., Sherman, P. S., Gildersleeve, D. L. & Jung, Y. W. Dependence of cardiac11C-meta-hydroxyephedrine retention on norepinephrine transporter density. *J. Nucl. Med.* **47**, 1490–1496 (2006).

103. Vesalainen, R. K. *et al.* Cardiac positron emission tomography imaging with [11c]hydroxyephedrine, a specific tracer for sympathetic nerve endings, and its functional correlates in congestive heart failure. *Am. J. Cardiol.* **84**, 568–574 (1999).

104. Aikawa, T. *et al.* Impaired myocardial sympathetic innervation is associated with diastolic dysfunction in heart failure with preserved ejection fraction: 11C-hydroxyephedrine PET study. *J. Nucl. Med.* **58**, 784–790 (2017).

105. Harms, H. J. *et al.* Use of a Single 11C-meta-hydroxyephedrine scan for assessing flow-innervation mismatches in patients with ischemic cardiomyopathy. *J. Nucl. Med.* **56**, 1706–1711 (2015).

106. Münch, G. *et al.* Evaluation of sympathetic nerve terminals with [11C]epinephrine and [11C]hydroxyephedrine and positron emission tomography. *Circulation* **101**, 516–523 (2000).

107. Schwaiger, M. *et al.* Evidence for regional catecholamine uptake and storage sites in the transplanted human heart by positron emission tomography. *J. Clin. Invest.* **87**, 1681–1690 (1991).

108. Mazzadi, A. N. *et al.* Cardiac retention of [11C]HED in genotyped long QT patients: A potential amplifier role for severity of the disease. *Am. J. Physiol. - Hear. Circ. Physiol.* **285**, 1286–1293 (2003).

109. Maddahi, J. *et al.* Phase-III Clinical Trial of Fluorine-18 Flurpiridaz Positron Emission Tomography for Evaluation of Coronary Artery Disease. *J. Am. Coll. Cardiol.* **76**, 391–401 (2020).

110. Moody, J. B. *et al.* Added value of myocardial blood flow using 18F-flurpiridaz PET to diagnose coronary artery disease: The flurpiridaz 301 trial. *J. Nucl.*

Cardiol. (2020) doi:10.1007/s12350-020-02034-2.

111. Magnusson, P. *et al.* Positron emission tomography (15O-water, 11C-acetate, 11C-HED) risk markers and nonsustained ventricular tachycardia in hypertrophic cardiomyopathy. *IJC Hear. Vasc.* **26**, 100452 (2020).

112. Croteau, E. *et al.* [11C]Acetate rest-stress protocol to assess myocardial perfusion and oxygen consumption reserve in a model of congestive heart failure in rats. *Nucl. Med. Biol.* **39**, 287–294 (2012).

113. Lee, S. P. *et al.* 11C-Pittsburgh B PET imaging in cardiac amyloidosis. *JACC Cardiovasc. Imaging* **8**, 50–59 (2015).

114. Kim, Y. J., Ha, S. & Kim, Y. il. Cardiac amyloidosis imaging with amyloid positron emission tomography: A systematic review and meta-analysis. *J. Nucl. Cardiol.* **27**, 123–132 (2020).

115. Dweck, M. R. *et al.* Coronary arterial 18F-sodium fluoride uptake: A novel marker of plaque biology. *J. Am. Coll. Cardiol.* **59**, 1539–1548 (2012).

116. Tarkin, J. M. *et al.* 68Ga-DOTATATE PET Identifies Residual Myocardial Inflammation and Bone Marrow Activation After Myocardial Infarction. *J. Am. Coll. Cardiol.* **73**, 2489–2491 (2019).

117. Tarkin, J. M. *et al.* Detection of Atherosclerotic Inflammation by 68Ga-DOTATATE PET Compared to [18F]FDG PET Imaging. *J. Am. Coll. Cardiol.* **69**, 1774–1791 (2017).

118. Kircher, M. *et al.* Imaging Inflammation in Atherosclerosis with CXCR4-Directed 68Ga-Pentixafor PET/CT: Correlation with 18F-FDG PET/CT. *J. Nucl. Med.* **61**, 751–756 (2020).

119. Kobayashi, R. *et al.* New horizons in cardiac innervation imaging: Introduction of novel 18F-labeled PET tracers. *Eur. J. Nucl. Med. Mol. Imaging* **44**, 2302–2309 (2017).

120. Basu, S. *et al.* Fundamentals of PET and PET/CT imaging. *Ann. N. Y. Acad. Sci.* **1228**, 1–18 (2011).

121. Ratib, O. & Nkoulou, R. Potential applications of PET/MR imaging in cardiology. *J. Nucl. Med.* **55**, 40S-46S (2014).

122. Adenaw, N. & Salerno, M. PET/MRI: Current state of the art and future potential for cardiovascular applications. *J. Nucl. Cardiol.* **20**, 976–989 (2013).

123. Oldan, J. D. *et al.* Do myocardial PET–MR and PET–CT FDG images provide comparable information? *J. Nucl. Cardiol.* **23**, 1102–1109 (2016).

124. Wisenberg, G. *et al.* Same day comparison of PET/CT and PET/MR in patients with cardiac sarcoidosis. *J. Nucl. Cardiol.* **27**, 2118–2129 (2020).

125. Wicks, E. C. *et al.* Diagnostic accuracy and prognostic value of simultaneous hybrid 18 F-fluorodeoxyglucose positron emission tomography/magnetic resonance imaging in cardiac sarcoidosis. *Eur. Heart J. Cardiovasc. Imaging* **19**, 757–767 (2018).

126. Chen, W. & Jeudy, J. Assessment of Myocarditis: Cardiac MR, PET/CT, or PET/MR? *Curr. Cardiol. Rep.* **21**, (2019).

127. Marchesseau, S. *et al.* Hybrid PET/CT and PET/MRI imaging of vulnerable coronary plaque and myocardial scar tissue in acute myocardial infarction. *J. Nucl. Cardiol.* **25**, 2001–2011 (2018).

128. Ravassa, S. *et al.* Biomarkers of cardiomyocyte injury and stress identify left atrial and left ventricular remodelling and dysfunction: A population-based study. *Int. J. Cardiol.* **185**, 177–185 (2015).

129. Takeishi, Y. Biomarkers in heart failure. *Arquivos Brasileiros de Cardiologia* vol. 113 205–206 (2019).

130. Braunwald, E. Biomarkers in heart failure. *New England Journal of Medicine* vol.

358 2148–2159 (2008).

131. Tsutamoto, T. *et al.* Attenuation of compensation of endogenous cardiac natriuretic peptide system in chronic heart failure: Prognostic role of plasma brain natriuretic peptide concentration in patients with chronic symptomatic left ventricular dysfunction. *Circulation* **96**, 509–516 (1997).

132. Vesbianu, D., Vesbianu, C., Bernstein, P. & Kouides, R. Plasma brain natriuretic peptide - an independent predictor of mortality and rehospitalization in congestive heart failure - a meta-analysis. *Congest. Hear. Fail. Symptoms, Causes Treat.* **9842**, 153–162 (2010).

133. Bergler-Klein, J., Gyöngyösi, M. & Maurer, G. The Role of biomarkers in valvular heart disease: Focus on natriuretic peptides. *Can. J. Cardiol.* **30**, 1027–1034 (2014).

134. Doust, J. A., Glasziou, P. P., Pietrzak, E. & Dobson, A. J. A systematic review of the diagnostic accuracy of natriuretic peptides for heart failure. *Arch. Intern. Med.* **164**, 1978–1984 (2004).

135. Mueller, C., Breidthardt, T., Laule-Kilian, K., Christ, M. & Perruchoud, A. P. The integration of BNP and NT-proBNP into clinical medicine. *Swiss Med. Wkly.* **137**, 4–12 (2007).

136. Kasahara, M., Yoshimoto, A., Kamiura, N. & Suzuki, T. Acute renal failure and natriuretic peptides. *Nippon rinsho. Japanese J. Clin. Med.* **62 Suppl 9**, 103–106 (2004).

137. Burke, M. A. & Cotts, W. G. Interpretation of B-type natriuretic peptide in cardiac disease and other comorbid conditions. *Heart Fail. Rev.* **12**, 23–36 (2007).

138. Wang, T. J. *et al.* Impact of Obesity on Plasma Natriuretic Peptide Levels. *Circulation* **109**, 594–600 (2004).

139. Mir, T. S. *et al.* Plasma concentrations of N-terminal brain natriuretic peptide in

healthy children, adolescents, and young adults: Effect of age and gender. *Pediatr. Cardiol.* **27**, 73–77 (2006).

140. Redfield, M. M. *et al.* Plasma brain natriuretic peptide concentration: Impact of age and gender. *J. Am. Coll. Cardiol.* **40**, 976–982 (2002).

141. Friões, F. *et al.* Prognostic value of sST2 added to BNP in acute heart failure with preserved or reduced ejection fraction. *Clin Res Cardiol* **104**, 491–9 (2015).

142. Dieplinger, B. & Mueller, T. Soluble ST2 in heart failure. *Clin. Chim. Acta* **443**, 57–70 (2015).

143. Manzano-Fernndez, S., Mueller, T., Pascual-Figal, D., Truong, Q. A. & Januzzi, J. L. Usefulness of soluble concentrations of interleukin family member ST2 as predictor of mortality in patients with acutely decompensated heart failure relative to left ventricular ejection fraction. *Am. J. Cardiol.* **107**, 259–267 (2011).

144. Kociol, R. D. *et al.* Troponin elevation in heart failure: Prevalence, mechanisms, and clinical implications. *J. Am. Coll. Cardiol.* **56**, 1071–1078 (2010).

145. Wettersten, N. & Maisel, A. Role of Cardiac Troponin Levels in Acute Heart Failure. *Card. Fail. Rev.* **1**, 102 (2015).

146. Saunders, J. T. *et al.* Cardiac troponin T measured by a highly sensitive assay predicts coronary heart disease, heart failure, and mortality in the atherosclerosis risk in communities study. *Circulation* **123**, 1367–1376 (2011).

147. Missov, E., Calzolari, C. & Pau, B. Circulating cardiac troponin I in severe congestive heart failure. *Circulation* **96**, 2953–2958 (1997).

148. Al-Otaiby, M. A., Al-Amri, H. S. & Al-Moghairi, A. M. The clinical significance of cardiac troponins in medical practice. *J. Saudi Hear. Assoc.* **23**, 3–11 (2011).

149. Kontos, M. C. *et al.* Comparison of myocardial perfusion imaging and cardiac troponin I in patients admitted to the emergency department with chest pain.

Circulation **99**, 2073–2078 (1999).

150. Roongsritong, C., Warraich, I. & Bradley, C. Common causes of troponin elevations in the absence of acute myocardial infarction: Incidence and clinical significance. *Chest* **125**, 1877–1884 (2004).

151. Agewall, S., Giannitsis, E., Jernberg, T. & Katus, H. Troponin elevation in coronary vs. non-coronary disease. *Eur. Heart J.* **32**, 404–411 (2011).

152. Niizeki, T. *et al.* Persistently increased serum concentration of heart-type fatty acid-binding protein predicts adverse clinical outcomes in patients with chronic heart failure. *Circ. J.* **72**, 109–114 (2008).

153. Haltern, G. *et al.* Comparison of Usefulness of Heart-Type Fatty Acid Binding Protein Versus Cardiac Troponin T for Diagnosis of Acute Myocardial Infarction. *Am. J. Cardiol.* **105**, 1–9 (2010).

154. Ishii, J. *et al.* Prognostic value of serum concentration of heart-type fatty acid-binding protein relative to cardiac troponin T on admission in the early hours of acute coronary syndrome. *Clin. Chem.* **51**, 1397–1404 (2005).

155. Cheng, J. M. *et al.* Biomarkers of heart failure with normal ejection fraction: A systematic review. *European Journal of Heart Failure* vol. 15 1350–1362 (2013).

156. Bartekova, M., Radosinska, J., Jelemensky, M. & Dhalla, N. S. Role of cytokines and inflammation in heart function during health and disease. *Heart Fail. Rev.* **23**, 733–758 (2018).

157. Tsutamoto, T. *et al.* Interleukin-6 spillover in the peripheral circulation increases with the severity of heart failure, and the high plasma level of interleukin-6 is an important prognostic predictor in patients with congestive heart failure. *J. Am. Coll. Cardiol.* **31**, 391–398 (1998).

158. Fanola, C. L. *et al.* Interleukin-6 and the risk of adverse outcomes in patients after an acute coronary syndrome: Observations from the SOLID-TIMI 52 (stabilization

of plaque using darapladib-thrombolysis in myocardial infarction 52) trial. *J. Am. Heart Assoc.* **6**, (2017).

159. Held, C. *et al.* Inflammatory biomarkers interleukin-6 and c-reactive protein and outcomes in stable coronary heart disease: Experiences from the STABILITY (stabilization of atherosclerotic plaque by initiation of darapladib therapy) trial. *J. Am. Heart Assoc.* **6**, (2017).

160. Kosmala, W., Przewlocka-Kosmala, M. & Mazurek, W. Proinflammatory cytokines and myocardial viability in patients after acute myocardial infarction. *Int. J. Cardiol.* **101**, 449–456 (2005).

161. Parissis, J. T., Adamopoulos, S. N., Venetsanou, K. F., Karas, S. M. & Kremastinos, D. T. Elevated plasma amylase levels in advanced chronic heart failure secondary to ischemic or idiopathic dilated cardiomyopathy: Correlation with circulating interleukin-6 activity. *J. Interf. Cytokine Res.* **23**, 329–333 (2003).

162. Fahmi, A. *et al.* P42/p44-MAPK and PI3K are sufficient for IL-6 family cytokines/gp130 to signal to hypertrophy and survival in cardiomyocytes in the absence of JAK/STAT activation. *Cell. Signal.* **25**, 898–909 (2013).

163. Mayfield, A. E. *et al.* Interleukin-6 mediates post-infarct repair by cardiac explant-derived stem cells. *Theranostics* **7**, 4850–4861 (2017).

164. Monden, Y. *et al.* Tumor necrosis factor-α is toxic via receptor 1 and protective via receptor 2 in a murine model of myocardial infarction. *Am. J. Physiol. - Hear. Circ. Physiol.* **293**, 743–753 (2007).

165. Aydin, M. *et al.* The levels of tumor necrosis factor-alpha and interleukin-6 in patients with isolated coronary artery ectasiae. *Mediators Inflamm.* **2009**, (2009).

166. Gotsman, I. *et al.* Serum Cytokine Tumor Necrosis Factor-Alpha and Interleukin-6 Associated with the severity of Coronary Artery Disease: Indicators of an Active Inflammatory Burden? Israel. *Isr. Med. Assoc. J.* **10**, 494–498 (2007).

167. Dinh, W. *et al.* Elevated plasma levels of TNF-alpha and Interleukin-6 in patients with diastolic dysfunction and glucose metabolism disorders. *Cardiovasc. Diabetol.* **8**, 58 (2009).

168. Haudek, S. B., Taffet, G. E., Schneider, M. D. & Mann, D. L. TNF provokes cardiomyocyte apoptosis and cardiac remodeling through activation of multiple cell death pathways. *J. Clin. Invest.* **117**, 2692–2701 (2007).

169. Jude, B., Vetel, S., Giroux-Metges, M. A. & Pennec, J. P. Rapid negative inotropic effect induced by TNF-α in rat heart perfused related to PKC activation. *Cytokine* **107**, 65–69 (2018).

170. Zhang, M. *et al.* TNF-α as a potential mediator of cardiac dysfunction due to intracellular Ca 2+-overload. *Biochem. Biophys. Res. Commun.* **327**, 57–63 (2005).

171. Shrivastava, A. K., Singh, H. V., Raizada, A. & Singh, S. K. C-reactive protein, inflammation and coronary heart disease. *Egypt. Hear. J.* **67**, 89–97 (2015).

172. Sitepu, N. B. & Harahap, U. The Role Of hs-CRP In Predicting The Likelihood Of Coronary Heart Disease. *Indones. J. Pharm. Clin. Res.* **3**, 51–61 (2020).

173. Casas, J. P., Shah, T., Hingorani, A. D., Danesh, J. & Pepys, M. B. C-reactive protein and coronary heart disease: A critical review. *J. Intern. Med.* **264**, 295–314 (2008).

174. Fong, P. *et al.* New England Journal CREST. *Science (80-.).* 609–619 (2010).

175. Miller, M., Zhan, M. & Havas, S. High attributable risk of elevated C-reactive protein level to conventional coronary heart disease risk factors: The third National Health and Nutrition Examination Survey. *Arch. Intern. Med.* **165**, 2063–2068 (2005).

176. Yu, L. & Feng, Z. The Role of Toll-Like Receptor Signaling in the Progression of Heart Failure. *Mediators Inflamm.* **2018**, 1–11 (2018).

177. Yang, Y. *et al.* The emerging role of toll-like receptor 4 in myocardial inflammation. *Cell Death and Disease* vol. 7 1–10 (2016).

178. Liu, L. *et al.* Up-regulated TLR4 in cardiomyocytes exacerbates heart failure after long-term myocardial infarction. *J. Cell. Mol. Med.* **19**, 2728–2740 (2015).

179. Stapel, H. *et al.* Toll-like receptor 4 modulates myocardial ischaemia-reperfusion injury: Role of matrix metalloproteinases. *Eur. J. Heart Fail.* **8**, 665–672 (2006).

180. Birks, E. J. *et al.* Increased toll-like receptor 4 in the myocardium of patients requiring left ventricular assist devices. *J. Hear. Lung Transplant.* **23**, 228–235 (2004).

181. Gao, W., Xiong, Y., Li, Q. & Yang, H. Inhibition of toll-like receptor signaling as a promising therapy for inflammatory diseases: A journey from molecular to nano therapeutics. *Front. Physiol.* **8**, (2017).

182. Shimamoto, A. *et al.* Inhibition of toll-like receptor 4 with eritoran attenuates myocardial ischemia-reperfusion injury. *Circulation* **114**, 270–274 (2006).

183. Jungbauer, C. G. *et al.* Panel of emerging cardiac biomarkers contributes for prognosis rather than diagnosis in chronic heart failure. *Biomark. Med.* **8**, 777–789 (2014).

184. Müller, T. D. *et al.* Ghrelin. *Molecular Metabolism* vol. 4 437–460 (2015).

185. Poher, A. L., Tschöp, M. H. & Müller, T. D. Ghrelin regulation of glucose metabolism. *Peptides* **100**, 236–242 (2018).

186. Cowan, E., Burch, K. J., Green, B. D. & Grieve, D. J. Obestatin as a key regulator of metabolism and cardiovascular function with emerging therapeutic potential for diabetes. *Br. J. Pharmacol.* 2165–2181 (2016) doi:10.1111/bph.13502.

187. Colldén, G., Tschöp, M. H. & Müller, T. D. Therapeutic potential of targeting the ghrelin pathway. *International Journal of Molecular Sciences* vol. 18 (2017).

188. Callaghan, B. & Furness, J. B. Novel and conventional receptors for ghrelin, desacyl-ghrelin, and pharmacologically related compounds. *Pharmacol. Rev.* **66**, 984–1001 (2014).

189. Navarro, G. *et al.* A significant role of the truncated ghrelin receptor GHS-R1b in ghrelin-induced signaling in neurons. *J. Biol. Chem.* **291**, 13048–13062 (2016).

190. Chow, K. B. S. *et al.* The truncated ghrelin receptor polypeptide (GHS-R1b) is localized in the endoplasmic reticulum where it forms heterodimers with ghrelin receptors (GHS-R1a) to attenuate their cell surface expression. *Mol. Cell. Endocrinol.* **348**, 247–254 (2012).

191. Kojima, M. *et al.* Ghrelin is a growth-hormone-releasing acylated peptide from stomach. *Nature* **402**, 656–660 (1999).

192. Gnanapavan, S. *et al.* The tissue distribution of the mRNA of ghrein and subtypes of its receptor, GHS-R, in humans. **87**, 2988–2991 (2002).

193. Khatib, M., Simkhada, P. & Gode, D. Cardioprotective effects of ghrelin in heart failure: From gut to heart. *Hear. Views* **15**, 74 (2014).

194. YUAN, M. M.-J., HUANG, H. & Huang, C.-X. C. Potential new role of the GHSR-1a-mediated signaling pathway in cardiac remodeling after myocardial infarction (Review). *Oncol. Lett.* **8**, 969–971 (2014).

195. Berridge, M. J., Bootman, M. D. & Roderick, H. L. Calcium signalling: Dynamics, homeostasis and remodelling. *Nature Reviews Molecular Cell Biology* vol. 4 517–529 (2003).

196. Fearnley, C. J., Llewelyn Roderick, H. & Bootman, M. D. Calcium signaling in cardiac myocytes. *Cold Spring Harb. Perspect. Biol.* **3**, (2011).

197. Warbrick, I. & Rabkin, S. W. Effect of the peptides Relaxin, Neuregulin, Ghrelin and Glucagon-like peptide-1, on cardiomyocyte factors involved in the molecular mechanisms leading to diastolic dysfunction and/or heart failure with preserved

ejection fraction. *Peptides* **111**, 33–41 (2019).

198. Sun, Q. *et al.* Effects of GH secretagogues on contractility and Ca2+ homeostasis of isolated adult rat ventricular myocytes. *Endocrinology* **151**, 4446–4454 (2010).

199. Ma, Y., Zhang, L., Edwards, J. N., Launikonis, B. S. & Chen, C. Growth hormone secretagogues protect mouse cardiomyocytes from in vitro ischemia/reperfusion injury through regulation of intracellular calcium. *PLoS One* **7**, (2012).

200. Dixit, V. D. *et al.* Ghrelin inhibits leptin- and activation-induced proinflammatory cytokine expression by human monocytes and T cells. *J. Clin. Invest.* **114**, 57–66 (2004).

201. Li, W. G. *et al.* Ghrelin Inhibits Proinflammatory Responses and Nuclear Factor-κB Activation in Human Endothelial Cells. *Circulation* **109**, 2221–2226 (2004).

202. Wang, Q. *et al.* Ghrelin protects the heart against ischemia/reperfusion injury via inhibition of TLR4/NLRP3 inflammasome pathway. *Life Sci.* **186**, 50–58 (2017).

203. Mao, Y. *et al.* Endogenous Ghrelin Attenuates Pressure Overload-Induced Cardiac Hypertrophy via a Cholinergic Anti-Inflammatory Pathway. *Hypertension* **65**, 1238–1244 (2015).

204. Huang, C.-X. *et al.* Ghrelin inhibits post-infarct myocardial remodeling and improves cardiac function through anti-inflammation effect. *Peptides* **30**, 2286–2291 (2009).

205. Yuan, M.-J. *et al.* GHSR-1a is a novel pro-angiogenic and anti-remodeling target in rats after myocardial infarction. *Eur J Pharmacol.* **788**, 218–225 (2016).

206. Baldanzi, G. *et al.* Ghrelin and des-acyl ghrelin inhibit cell death in cardiomyocytes and endothelial cells through ERK1/2 and PI 3-kinase/AKT. *J. Cell Biol.* **159**, 1029–1037 (2002).

207. Liu, Y., Liu, Y., Li, G., Chen, Z. & Gu, G. Ghrelin protects the myocardium with

hypoxia/reoxygenation treatment through upregulating the expression of growth hormone, growth hormone secretagogue receptor and insulin-like growth factor-1, and promoting the phosphorylation of protein kinase B. *Int. J. Mol. Med.* **42**, 3037–3046 (2018).

208. Eid, R. A. *et al.* Subacute ghrelin administration inhibits apoptosis and improves ultrastructural abnormalities in remote myocardium post-myocardial infarction. *Biomed. Pharmacother.* **101**, 920–928 (2018).

209. Zhang, G. G. *et al.* Ghrelin protects heart against ERS-induced injury and apoptosis by activating AMP-activated protein kinase. *Peptides* **48**, 156–165 (2013).

210. Mitacchione, G. *et al.* The gut hormone ghrelin partially reverses energy substrate metabolic alterations in the failing heart. *Circ. Hear. Fail.* **7**, 643–651 (2014).

211. Zhang, G. G. *et al.* Inhibition of endoplasm reticulum stress by ghrelin protects against ischemia/reperfusion injury in rat heart. *Peptides* **30**, 1109–1116 (2009).

212. Ruozi, G. *et al.* AAV-mediated in vivo functional selection of tissue-protective factors against ischaemia. *Nat. Commun.* **6**, (2015).

213. Han, D. *et al.* Ghrelin improves functional survival of engrafted adipose-derived mesenchymal stem cells in ischemic heart through PI3K/Akt signaling pathway. *Biomed Res. Int.* **2015**, 858349 (2015).

214. Soeki, T. *et al.* Ghrelin suppresses cardiac sympathetic activity and prevents early left ventricular remodeling in rats with myocardial infarction. *Am. J. Physiol. - Hear. Circ. Physiol.* **294**, 5–7 (2008).

215. Wang, Q. *et al.* Ghrelin Ameliorates Angiotensin II-Induced Myocardial Fibrosis by Upregulating Peroxisome Proliferator-Activated Receptor Gamma in Young Male Rats. *Biomed Res. Int.* **2018**, 1–14 (2018).

216. Yang, C. *et al.* Ghrelin suppresses cardiac fibrosis of post-myocardial infarction

heart failure rats by adjusting the activin A-follistatin imbalance. *Peptides* **99**, 27–35 (2018).

217. Enomoto, M. *et al.* Cardiovascular and hormonal effects of subcutaneous administration of ghrelin, a novel growth hormone-releasing peptide, in healthy humans. *Clin. Sci.* **105**, 431–435 (2003).

218. Okumura, H. *et al.* Vasodilatory effect of ghrelin, an endogenous peptide from the stomach. *J. Cardiovasc. Pharmacol.* **39**, 779–783 (2002).

219. Nagaya, N. *et al.* Effects of ghrelin administration on left ventricular function, exercise capacity, and muscle wasting in patients with chronic heart failure. *Circulation* **110**, 3674–3679 (2004).

220. Yuan, M. J. *et al.* Expression of ghrelin and its receptor in rats after coronary artery ligation. *Regul. Pept.* **192**–**193**, 1–5 (2014).

221. Schwenke, D. O. *et al.* Early ghrelin treatment after myocardial infarction prevents an increase in cardiac sympathetic tone and reduces mortality. *Endocrinology* **149**, 5172–5176 (2008).

222. Nagaya, N. *et al.* Chronic administration of ghrelin improves left ventricular dysfunction and attenuates development of cardiac cachexia in rats with heart failure. *Circulation* **104**, 1430–1435 (2001).

223. Chang, L. *et al.* Protective Effects of Ghrelin on Ischemia/Reperfusion Injury in the Isolated Rat Heart. *J. Cardiovasc. Pharmacol.* **43**, 165–170 (2004).

224. Li, L. *et al.* Cardioprotective effects of ghrelin and des-octanoyl ghrelin on myocardial injury induced by isoproterenol in rats. *Acta Pharmacol. Sin.* **27**, 527–535 (2006).

225. Wang, X. *et al.* Ghrelin inhibits doxorubicin cardiotoxicity by inhibiting excessive autophagy through AMPK and p38-MAPK. *Biochem. Pharmacol.* **88**, 334–350 (2014).

226. Beiras-Fernandez, A. *et al.* Altered myocardial expression of ghrelin and its receptor (GHSR-1a) in patients with severe heart failure. *Peptides* **31**, 2222–8 (2010).

227. Katugampola, S. D., Pallikaros, Z. & Davenport, A. P. [125I-His9]-Ghrelin, a novel radioligand for localizing GHS orphan receptors in human and rat tissue; up-regulation of receptors with atherosclerosis. *Br. J. Pharmacol.* **134**, 143–149 (2001).

228. Baessler, A. *et al.* Association of the ghrelin receptor gene region with left ventricular hypertrophy in the general population: Results of the MONICA/KORA Augsburg echocardiographic substudy. *Hypertension* **47**, 920–927 (2006).

229. Chen, Y. *et al.* Prognostic value of plasma ghrelin in predicting the outcome of patients with chronic heart failure. *J Inst Mex Seg Soc.* **45**, 263–9 (2014).

230. Ukkola, O., Pääkkö, T. & Kesäniemi, Y. A. Ghrelin and its promoter variant associated with cardiac hypertrophy. *J. Hum. Hypertens.* **26**, 452–457 (2012).

231. Pöykkö, S. M. *et al.* Plasma ghrelin concentrations are positively associated with carotid artery atherosclerosis in males. *J. Intern. Med.* **260**, 43–52 (2006).

232. Michel, M. C., Wieland, T. & Tsujimoto, G. How reliable are G-protein-coupled receptor antibodies? *Naunyn. Schmiedebergs. Arch. Pharmacol.* **379**, 385–388 (2009).

233. Mani, B. K. *et al.* Neuroanatomical characterization of a growth hormone secretagogue receptor-green fluorescent protein reporter mouse. *J. Comp. Neurol.* **522**, 3644–3666 (2014).

234. Reichenbach, A., Steyn, F. J., Sleeman, M. W. & Andrews, Z. B. Ghrelin receptor expression and colocalization with anterior pituitary hormones using a GHSR-GFP mouse line. *Endocrinology* **153**, 5452–5466 (2012).

235. Liu, M. *et al.* Design, synthesis and characterization of a fluorescently labeled

functional analog of full-length human ghrelin. *Biochem. Biophys. Res. Commun.* **533**, 559–564 (2020).

236. Barrile, F. *et al.* Development of a novel fluorescent ligand of growth hormone secretagogue receptor based on the N-Terminal Leap2 region. *Mol. Cell. Endocrinol.* **498**, 110573 (2019).

237. McGirr, R., McFarland, M. S., McTavish, J., Luyt, L. G. & Dhanvantari, S. Design and characterization of a fluorescent ghrelin analog for imaging the growth hormone secretagogue receptor 1a. *Regul Pept.* **172**, 69–76 (2011).

238. Douglas, G. A. F. *et al.* Characterization of a far-red analog of ghrelin for imaging GHS-R in P19-derived cardiomyocytes. *Regul Pept.* **54**, 81–88 (2014).

239. Lalonde, T., Shepherd, T. G., Dhanvantari, S. & Luyt, L. G. Stapled ghrelin peptides as fluorescent imaging probes. *Pept. Sci.* **111**, (2019).

240. Cameron, K. O., Bhattacharya, S. K. & Loomis, A. K. Small molecule ghrelin receptor inverse agonists and antagonists. *J. Med. Chem.* **57**, 8671–8691 (2014).

241. Rosita, D., Dewit, M. A. & Luyt, L. G. Fluorine and rhenium substituted ghrelin analogues as potential imaging probes for the growth hormone secretagogue receptor. *J. Med. Chem.* **52**, 2196–2203 (2009).

242. Koźmiński, P. & Gniazdowska, E. Synthesis and in vitro/in vivo evaluation of novel mono- and trivalent technetium-99m labeled ghrelin peptide complexes as potential diagnostic radiopharmaceuticals. *Nucl. Med. Biol.* **42**, 28–37 (2015).

243. Charron, C. L., McFarland, M. S., Dhanvantari, S. & Luyt, L. G. Development of a [68Ga]-ghrelin analogue for PET imaging of the ghrelin receptor (GHS-R1a). *Medchemcomm* **9**, 1761–1767 (2018).

244. Chollet, C., Bergmann, R., Pietzsch, J. & Beck-Sickinger, A. G. Design, Evaluation, and Comparison of Ghrelin Receptor Agonists and Inverse Agonists as Suitable Radiotracers for PET Imaging. *Bioconjug. Chem.* **23**, 771–784 (2012).

245. Potter, R. *et al.* Synthesis and in vivo evaluation of (S)-6-(4-fluorophenoxy)-3-((1-[11C]methylpiperidin-3-yl)methyl)-2-o-tolylquinazolin-4(3H)-one, a potential PET tracer for growth hormone secretagogue receptor (GHSR). *Bioorganic Med. Chem.* **19**, 2368–2372 (2011).

246. Charron, C. L. *et al.* Structure-Activity Study of Ghrelin(1-8) Resulting in High Affinity Fluorine-Bearing Ligands for the Ghrelin Receptor. *J. Med. Chem.* **60**, 7256–7266 (2017).

247. Abbas, A. *et al.* Development and Characterization of an 18 F-labeled Ghrelin Peptidomimetic for Imaging the Cardiac Growth Hormone Secretagogue Receptor. *Mol. Imaging* **17**, 1–11 (2018).

2 Dynamics of the Ghrelin-Growth Hormone Secretagogue Receptor System in the Human Heart Before and After Cardiac Transplantation

A version of this chapter has been published.

Sullivan, R. *et al.* Dynamics of the Ghrelin-Growth Hormone Secretagogue Receptor System in the Human Heart Before and After Cardiac Transplantation. *J. Endocr. Soc.* **3**, 748–762 (2019). https://doi.org/10.1210/js.2018-00393

2.1 Introduction

The peptide hormone ghrelin is well-known as a potent orexigenic hormone. It stimulates food intake by activating hypothalamic neurons that regulate normal feeding behaviour[1]. It is the natural ligand of the growth hormone secretagogue receptor (GHSR), a seven transmembrane, G protein-coupled receptor, which, in addition to the hypothalamus, is expressed in other brain regions as well as several endocrine organs, such as the anterior pituitary, pancreatic islets, the intestine, thyroid, and adipose tissue. In addition, ghrelin and GHSR are both expressed in cardiomyocytes where they function through a system that is independent of their role in regulating energy expenditure[2]. Activation of GHSR in cardiomyocytes promotes excitation-contraction coupling by increasing Ca^{2+} flux through both voltage-dependent Ca^{2+} channels[3] and the sarcoplasmic reticulum Ca^{2+}-ATPase pump (SERCA2a)[4–6], and promotes cardiomyocyte growth and survival through extracellular signaling related kinase 1/2 (ERK1/2)[4,5], and phosphatidylinositol-3-kinase / Akt (PI3K/AKT)[5,7]. We[6], and others[3], have recently shown that levels of GHSR are decreased in rodent models of diabetic cardiomyopathy, thus indicating that the dynamics of ghrelin and GHSR change even with mild impairments in left ventricular function.

In contrast, levels of ghrelin and GHSR are dramatically increased throughout the heart in patients with severe heart failure[8], indicating that myocardial GHSR is altered differently in heart failure compared with mild cardiomyopathy. The clinical syndrome of heart failure (HF) is most commonly associated with significant impairment of left ventricular (LV) contractility, leading to elevated intra-cardiac diastolic pressures and extravasation of fluid into the lung parenchyma and other tissues. The early detection and treatment of HF are limited by two issues: a) the specific series of molecular mechanisms leading to impaired contractility remain elusive in patients with idiopathic cardiomyopathies, and b) the responses to guideline-directed medical therapies remain highly variable, such that many patients continue to deteriorate, leading to either the need for cardiac transplantation or ultimately death. Clinically, there is a critical need to prospectively identify groups of patients who will ultimately be at higher risk, particularly in the early stages of left ventricular dysfunction, when the clinical status and ventricular function are not by themselves consistent reliable predictors of disease progression and clinical outcomes.

Circulating biomarkers, such as natriuretic peptide type-B (BNP), particularly the N-terminal form (NT-proBNP), and troponins T and I[9–11], provide some prediction of the progression of HF, by indicating changes within the cardiomyocyte that lead to stress, injury and apoptosis. However, they are produced whenever heart tissue is damaged by any direct or indirect injury to the myocardium, and there may be discordance between tissue and circulating levels of these biomarkers. Therefore, there is a need to identify biomarkers that are localized to the myocardium that reflect the cellular and molecular processes within the heart that underlie the progression of HF.

In this study, we evaluated the role of tissue ghrelin-GHSR levels as a localized biomarker of cardiac dysfunction in a cohort of patients who underwent cardiac transplantation. We examined samples from the diseased explanted heart and biopsies from the same individual's engrafted heart followed through to one-year post-transplantation. In addition, we aimed to determine the relationship between ghrelin-GHSR and BNP to biochemical signaling molecules in cardiac dysfunction. Given the importance of intracellular Ca^{2+} homeostasis in atrial and ventricular contractility and the role of phospho-ERK 1/2 in cardiomyocyte growth, we hypothesized that changes in the ghrelin-GHSR system in myocardial tissue could potentially reflect derangements in cardiomyocyte contractility and initiation of cardiac hypertrophic reprogramming that characterize the progression of heart failure.

2.2 Methods

2.2.1 Patient Cohort

Tissue samples were harvested from 10 patients who underwent cardiac transplantation at the London Health Sciences Center (LHSC) between 2011 and 2013. The protocol for sample dissections was approved by Western University's Health Sciences Research Ethics Board. Samples, roughly 0.5cm to 1.5cm in length, were collected from the right atrium (RA) and left ventricle (LV) of the explanted/diseased heart (DH) from each cardiac transplant patient. Endomyocardial biopsies, roughly 0.1 to 0.3cm in length, from the right ventricle (RV) of the newly grafted heart were also taken at various time-points post-transplantation (PTx), generally weekly for the first 4 weeks, monthly for months 2-6 and then at 1 year PTx. Not all patients had biopsies at all time points listed post transplantation and therefore there are missing data points at some time points stated. Patient demographics, cardiac function (LVEF), and medications pre- and post-transplantation are shown in Tables 2 and 3, respectively. All patient samples and patient data were kept anonymous and all marker analyses was done prior to receiving clinical data.

Table 2.1 Cardiac Transplant Recipient Patient Demographics

Recipient Condition	Number of Patients with Condition (n of 10)
Male gender	6
Mean recipient age (years)	54
Coronary artery disease	5
Hypertension	1
High pulmonary artery pressure	10
Diabetes	0
Assist Device Pre-Transplant	3
LVEF <30% Pre-Transplant	10
LVEF >50% 1 month Post-Transplant	8
LVEF >50% ≥ 6 months Post-Transplant	10

Table 2.2 Patient Medications Pre- and Post-Cardiac Transplant

Medications	Pre-transplant (n of 10)	Post-transplant 1 month (n of 10)	Post-transplant 6 months (n of 10)	Post-transplant 1 year (n of 10)
ACE Inhibitor *	8	2	2	8
Anti-arrhythmic	5	2	0	0
ARB	0	0	0	0
Anti-platelet	5	7	7	8
Coumadin	7	1	0	0
Beta blocker	10	1	0	0
Calcium channel blocker	10	2	4	3
Digoxin	8	0	0	0
Diuretics	10	7	2	2
Statins	5	5	6	6
Nitrates	0	0	0	0
Nitroglycerin	0	0	0	0
Anti-diabetics	0	0	0	0
Inotropic support (Milrinone/ Dobutamine)	1	0	0	0
Tacrolimus	0	9	10	10
Mycophenolate mofetil	0	9	9	9
Prednisone	0	7	9	6

**ACE: Angiotensin Converting Enzyme; ARB: Angiotensin receptor blocker*

2.2.2 Immunofluorescence Microscopy

Samples from both the explanted (diseased) and grafted hearts were frozen and embedded in optimal cutting temperature compound (OCT), and subsequently sectioned at 7 μm thickness, as previously described[4,12]. Immunohistochemistry using primary and fluorophore-conjugated secondary antibodies was conducted as previously described[4,12]. In brief, tissue sections were incubated with primary polyclonal or monoclonal antibodies[13–22] (Table 1) for 1h at room temperature in a humidified chamber. These antibodies were used to identify ghrelin (1:100), BNP (1:1000), pERK1/2 (1:250); SERCA2a (1:300), and collagen I (1:500). Samples were rinsed twice in phosphate buffered solution (PBS) and incubated for 2h at room temperature with secondary antibodies (1:500) (Table 1). To detect GHSR, we used the far-red ghrelin peptide analog, Ghrelin(1-18, Lys^{18}(Cy5), as we have previously done to quantify GHSR *in situ*[4]. This analog binds with high specificity to GHSR in mouse cardiac tissue samples[6]. Following incubation with secondary antibodies, this fluorescent peptide analog was added to tissue sections for 30 min. Sections were washed with PBS, incubated 8 min with DAPI nuclear stain (1:1000), and mounted with ProLong Gold antifade (Life Technologies) to prevent the tissues from photobleaching. Images were captured with a Nikon Eclipse TE2000-S fluorescent microscope. Five random fields of view were acquired for each of 4 tissue sections at 20X magnification (Nikon NIS Elements v. BR 4.50.00) and used for further image analysis. Higher-resolution images were captured using a Nikon A1R confocal microscope at 60x magnification.

Table 2.3 Antibody Table – Information on Antibodies Used.

Antigen	Catalog #	Dilution	Host	Reference #
Ghrelin	sc-10359	1:100	Goat	[13]
Serca2A	ab3625	1:300	Rabbit	[14]
pERK1/2	sc-377400	1:250	Mouse	[15]
BNP	ab19645	1:1000	Rabbit	[16]
Collagen I	ab34710	1:500	Rabbit	[17]
DAPI	62247	1:1000	-	[18]
Alexafluor 488	A11055	1:500	Donkey anti-goat	[19]
Alexafluor 594	A21207	1:500	Donkey anti-rabbit	[20]
Alexafluor 594	A21203	1:500	Donkey anti-mouse	[21]
Alexafluor 488	A21206	1:500	Donkey anti-rabbit	[22]

2.2.3 Fibrosis Imaging

In order to assess fibrosis, heart tissue sections were stained with Masson's Trichrome stain by the core Pathology laboratory at LHSC. Sections were acquired using bright field microscopy at 10X, 20X or 40X magnifications with a Zeiss Axioskop EL-Einsatz microscope and Northern Eclipse software. Fluorescence microscopy was also used to acquire collagen I images as described above.

2.2.4 Data Analysis

Images of GHSR, ghrelin, BNP, SERCA2a and pERK were analyzed with FIJI v. 1.49v, a distribution of ImageJ software (National Institutes of Health, Bethesda). Fluorescence intensities of each section were quantified using a custom FIJI script that integrates raw density images that represent protein expression levels, as we have previously reported[4,6,12,23,24]. Briefly, thresholding was conducted for each image to determine the fluorescence intensity (positive pixel count above threshold minus the background). Fibrosis was analyzed using an online script which quantified the percentage of fibrotic tissue in each sample by distinguishing fibrotic tissue from non-fibrotic tissue[25]. Statistical analyses were performed using GraphPad Prism version 7.02 or IBM SPSS statistics 25, as follows: unpaired student *t* test, a one-way ANOVA with analysis of variance using Tukey *post-hoc* test to compare differences between diseased hearts and biopsies of the grafted hearts; Pearson correlation and logistic linear regression for correlations between markers: and Spearman bivariate correlation for relationships between LVEF and the following markers: GHSR, ghrelin, BNP, pERK1/2 and SERCA2a, all with significance set at $p<0.05$.

2.3 Results

2.3.1 Cardiac Transplant Patient Cohort

Six of the 10 patients who underwent cardiac transplantation were male, with an overall mean age of 54 years (Table 2.1). Five had significant coronary artery disease pre-transplant, and none had diabetes. All patients had elevated pulmonary artery pressures pre-transplant, along with severely reduced left ventricular ejection fraction (LVEF <30%) by echocardiographic assessment. Serial echocardiographic assessment of LV function following cardiac transplant showed LV improvement to an LVEF > 50% in 8 of patients by 1 month PTx. By 6 months PTx, all patients had normal LV function (Table 2.1). Although most patients were receiving HF medications, i.e., angiotensin converting enzyme (ACE) inhibitors/beta blockers/diuretics, prior to transplantation, only a small number continued to receive these medications following surgery. Table 2.2 contains a complete listing of medications pre- and post-Tx.

2.3.2 GHSR and Ghrelin Expression in Cardiomyocytes

In any given cardiac transplant patient, the expression of GHSR and ghrelin in both LV and RA appeared to be elevated in the explanted heart in comparison to their expression PTx in the grafted heart tissue biopsies over time (Figure 2.1 A-C). By logistic regression analysis of all patient specimens, both pre-and post-transplant, the level of GHSR expression demonstrated a strong and highly significant positive linear regression with the level of ghrelin expression ($r = 0.7817$, $p<0.0001$). To examine associations of ghrelin and GHSR with cardiac dysfunction, data were divided into 2 groups of LVEF < 30% (pre-transplant) and LVEF > 50% (post-transplant), as there were no mid-range values of LVEF. In the pre-transplant hearts with LVEF < 30%, expression of GHSR and ghrelin clustered towards the higher end of the regression line, while in grafted heart biopsies at 1 and 6 months (LVEF > 50%), expression of GHSR and ghrelin clustered towards the lower end of the regression line (Figure 2.1 D). To more closely examine correlations between ghrelin-GHSR and cardiac dysfunction, we used a Spearman bivariate correlation test, and showed significant negative correlations between GHSR and LVEF ($p=0.018$) and ghrelin and LVEF ($p=0.004$) (Figure 2.1 E).

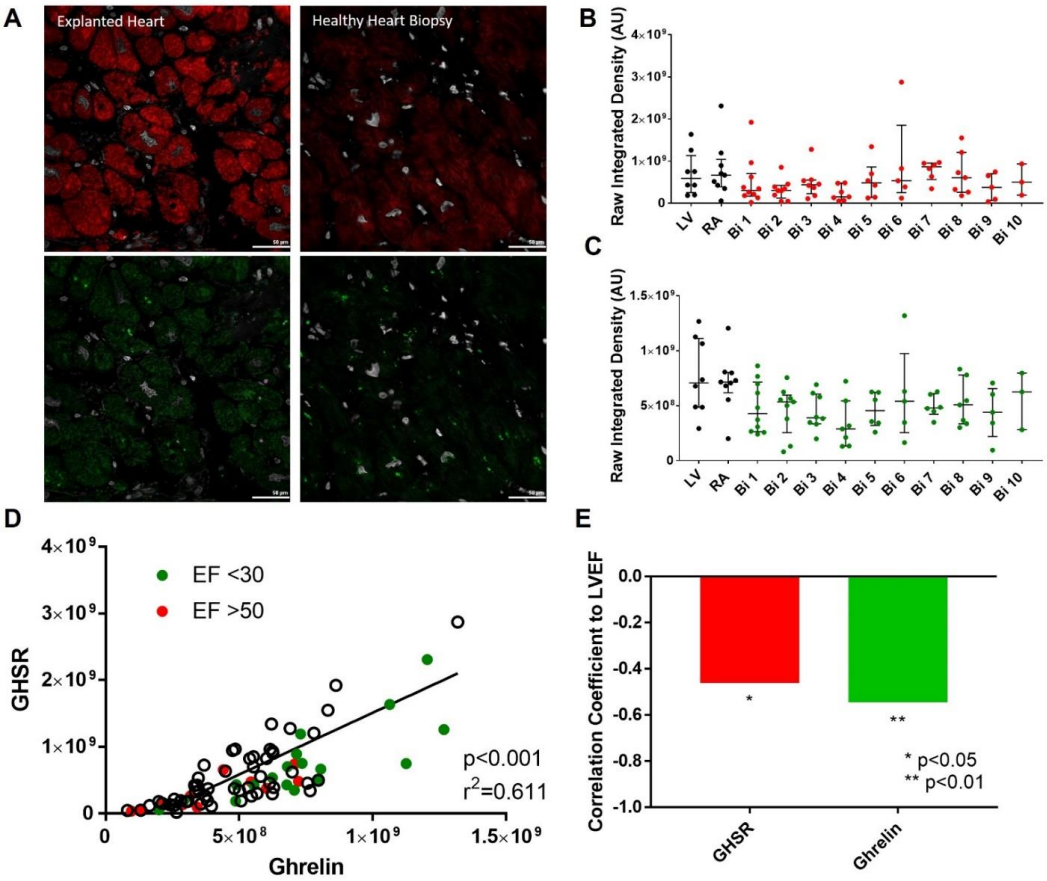

Figure 2.1 Ghrelin and GHSR expression in patients pre- and post- cardiac transplant.

A) Representative fluorescent images of GHSR (red), ghrelin (green), and DAPI (white) are shown in explanted heart tissue (left) and grafted heart biopsies (right) taken from the same patient. B) and C) Quantified fluorescence intensity of GHSR (red) and ghrelin (green) is shown from explanted heart tissue (LV and RA, black dots) and grafted heart biopsies (Bi 1-10, coloured dots). D) Positive linear regression of GHSR and ghrelin expression is shown in the entire cardiac transplant cohort with EF <30 in green and EF>50 in red with white dots representing tissue samples without related EF values. Each dot represents one transplant patient sample. E) Negative correlation between LVEF and GHSR (red) and ghrelin (green). LV: Left Ventricle; RA: Right atrium; Bi 1 – Bi 10: Biopsy 1 – Biopsy 10; EF: ejection fraction.

2.3.3 Metabolic Markers in Cardiac Tissue

The expression of metabolic markers in cardiac tissue that are associated with cardiac dysfunction were measured by immunofluorescence microscopy. We measured the following markers: a) SERCA2a, as an index of cardiomyocyte contractility, b) pERK1/2, as a marker of cardiomyocyte growth/hypertrophy, and c) BNP, as a validated clinical tool used to determine the presence and degree of HF. Representative images of SERCA2a, pERK1/2 and BNP expression are shown in Figures 2.2A and 2.3A, respectively. The expression of SERCA2a was significantly elevated in cardiac tissue from the RA of the diseased heart (Figure 2.2 B) when compared to its expression in endomyocardial biopsies taken at weeks 1, 2, and 3 PTx by 3.2, 2.4, and 2.7 fold, respectively. However, there was no significant difference in SERCA2a expression in the RA after the first month PTx. There were also no significant differences in the expression of SERCA2a in the LV tissue of the diseased heart when compared to the PTx endomyocardial biopsies. pERK1/2 expression was significantly increased in the cardiac tissue of the diseased heart taken from the RA by 1.8-3.1-fold and LV by 1.7-2.9-fold when compared to the grafted heart tissue biopsies taken at any time-point PTx (Figure 2.2 C). The degree of BNP expression (Figure 2.3B) showed similar trends as for GHSR and ghrelin. Logistic regression analyses were performed to determine the association between SERCA2a, pERK1/2, GHSR and ghrelin levels (Figure 2.2D-H). Highly significant and strong positive linear regressions were found between pERK1/2 and SERCA2a ($r = 0.6867$, $p<0.0001$), pERK1/2 and ghrelin ($r = 0.5719$, $p<0.0001$), and SERCA2a and ghrelin ($r = 0.7171$, $p<0.0001$). By contrast, there was a much weaker linear regressions between SERCA2a and GHSR ($r = 0.2320$, $p=0.0483$), and there was no linear regression between pERK1/2 with GHSR. Logistic regression analyses were performed between all metabolic markers and BNP to determine any possible relationships (Figure 2.3 C-F). There was a positive linear regression between ghrelin and BNP ($r = 0.6782$, $p<0.0001$), and SERCA2a and BNP ($r = 0.4838$, $p<0.0001$). However, there were weak linear regressions between GHSR and BNP ($r = 0.2423$, $p=0.0282$), and pERK1/2 and BNP ($r = 0.2745$, $p=0.0196$). Spearman bivariate correlations (correlation coefficients, CorC) were calculated as above and indicated highly significant negative associations between LVEF and SERCA2a ($p<0.001$, CorC = -0.63), and pERK ($p < 0.001$, CorC = -0.814), and between LVEF and BNP ($p < 0.001$, CorC = -0.773).

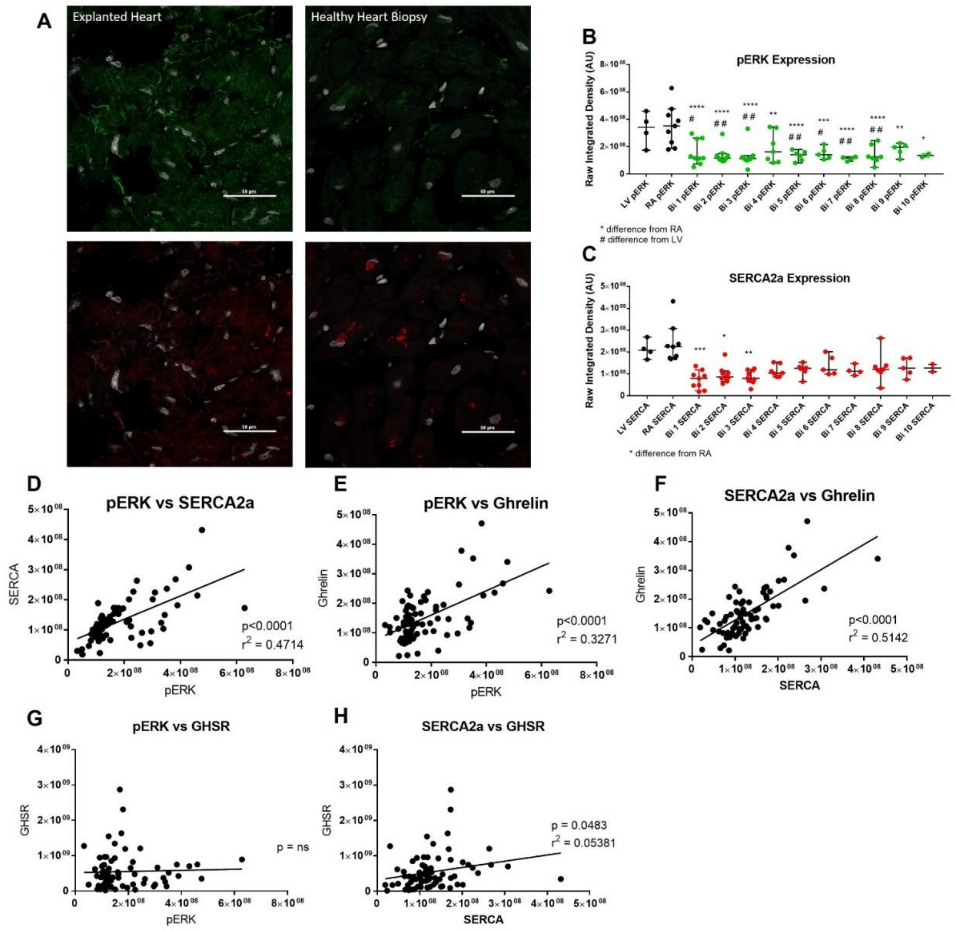

Figure 2.2 Cardiac metabolic markers in patients pre- and post-cardiac transplant in entire transplant patient cohort.

A) Representative fluorescent images of pERK1/2 (green) and SERCA2a (red) are shown from explanted heart tissue (left) and grafted heart biopsies (right) samples taken from the same patient. B and C) Quantified fluorescence intensity of pERK1/2 (green) and SERCA2a (red) are shown for explanted heart tissue (LV and RA, black dots) and grafted heart biopsies (Bi 1-10, coloured dots). D-H) Positive linear regression is seen in the entire cardiac transplant cohort for pERK1/2 vs SERCA2a, pERK1/2 vs ghrelin, SERCA2a vs ghrelin, pERK1/2 vs GHSR, and SERCA2a vs GHSR. Each dot represents one transplant patient sample. LV: Left Ventricle; RA: Right atrium; Bi 1 – Bi 10: Biopsy 1 – Biopsy 10. *p<0.05 from RA; ** p<0.01 from RA; *** p<0.001 from RA; **** p<0.0001 from RA; # p<0.05 from LV; ## p<0.01 from LV.

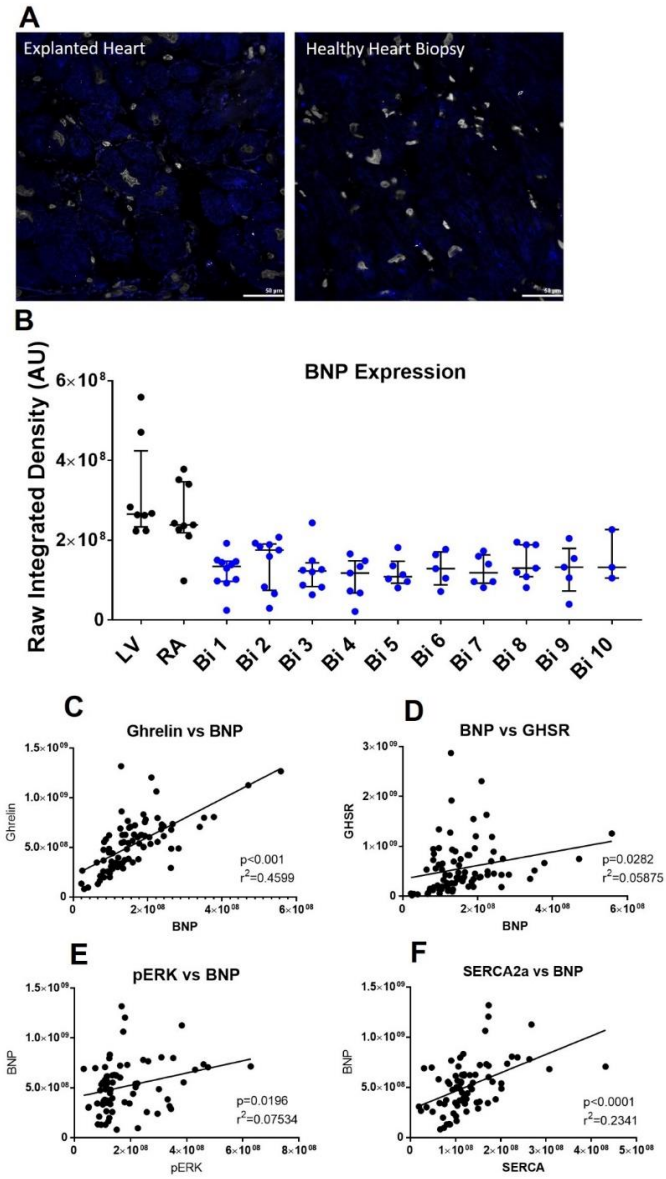

Figure 2.3 BNP expression in patients pre- and post-cardiac transplant.

A) Representative fluorescent images of BNP are shown from explanted heart tissue (left) and grafted heart biopsies (right) taken from the same patient. B) Quantified fluorescence intensity of BNP is shown in explanted heart tissue (LV and RA, black dots) and grafted heart biopsies (Bi 1-10, coloured dots). C-F) Positive linear regression is shown in the entire cardiac transplant cohort for ghrelin vs BNP, BNP vs GHSR, pERK1/2 vs BNP, and SERCA2a vs BNP. Each dot represents one transplant patient sample. LV: Left Ventricle; RA: Right atrium; Bi 1 – Bi 10: Biopsy 1 – Biopsy 10.

2.3.4 Cardiac Fibrosis

Cardiac fibrosis was determined in all patient samples using Masson's trichrome stain which measured the presence of collagen I and III (in blue) and compared that to the non-fibrotic tissue (in red). Quantification of fibrosis is illustrated in Figure 2.4 A, and revealed a high degree of variability both between and within patients from one time point to another (Table 2.4). Representative images showing the high degree of variability between patients taken from a single time-point are shown in Figure 2.4 B where significant fibrosis was seen in one patient with large amounts of collagen I and II (blue) and minimal fibrosis was seen in another patient at the same time-point To determine whether GHSR tissue levels were contributed to by fibrosis, cardiac tissue was examined for colocalization between collagen I and GHSR by fluorescence microscopy (Figure 2.5 A and B). These analyses showed no colocalization between collagen I and GHSR in the human tissue samples (Figure 2.5C and D).

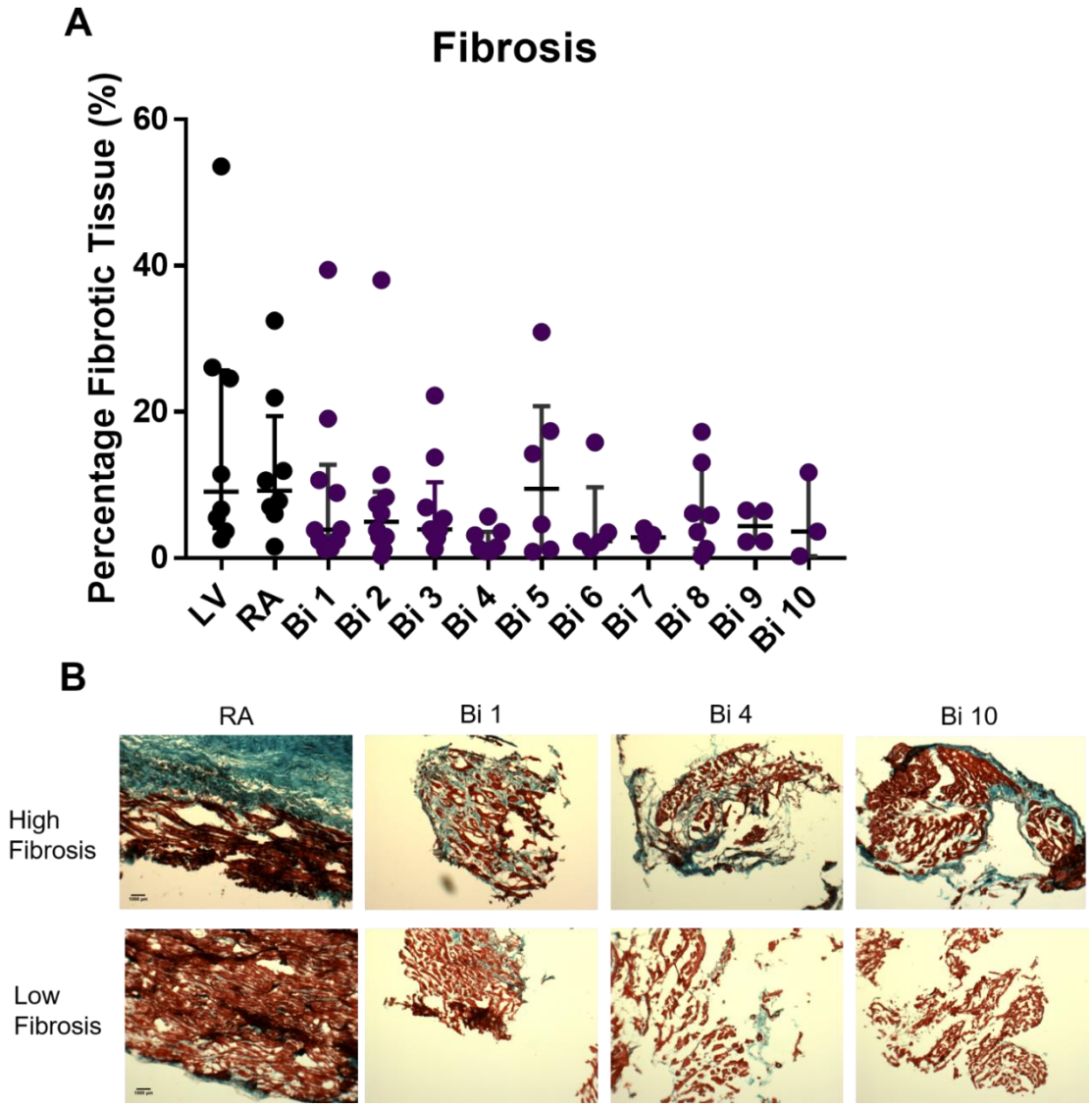

Figure 2.4 Cardiac fibrosis in patients pre- and post-cardiac transplant.

A) Quantified fibrotic data are shown for explanted heart tissue (LV and RA, black dots) and grafted heart biopsies (Bi 1-10, coloured dots). B) Representative images of the fibrotic variability between patients showing high levels of fibrosis (top) and low levels of fibrosis (bottom) where blue is fibrotic tissue (collagen I and III) and red is healthy cardiac tissue. Images of the RA, Bi 1, Bi 4, Bi 10 showing different patients at same time point pre- and post-cardiac transplant. LV: Left Ventricle; RA: Right atrium; Bi 1 – Bi 10: Biopsy 1 – Biopsy 10.

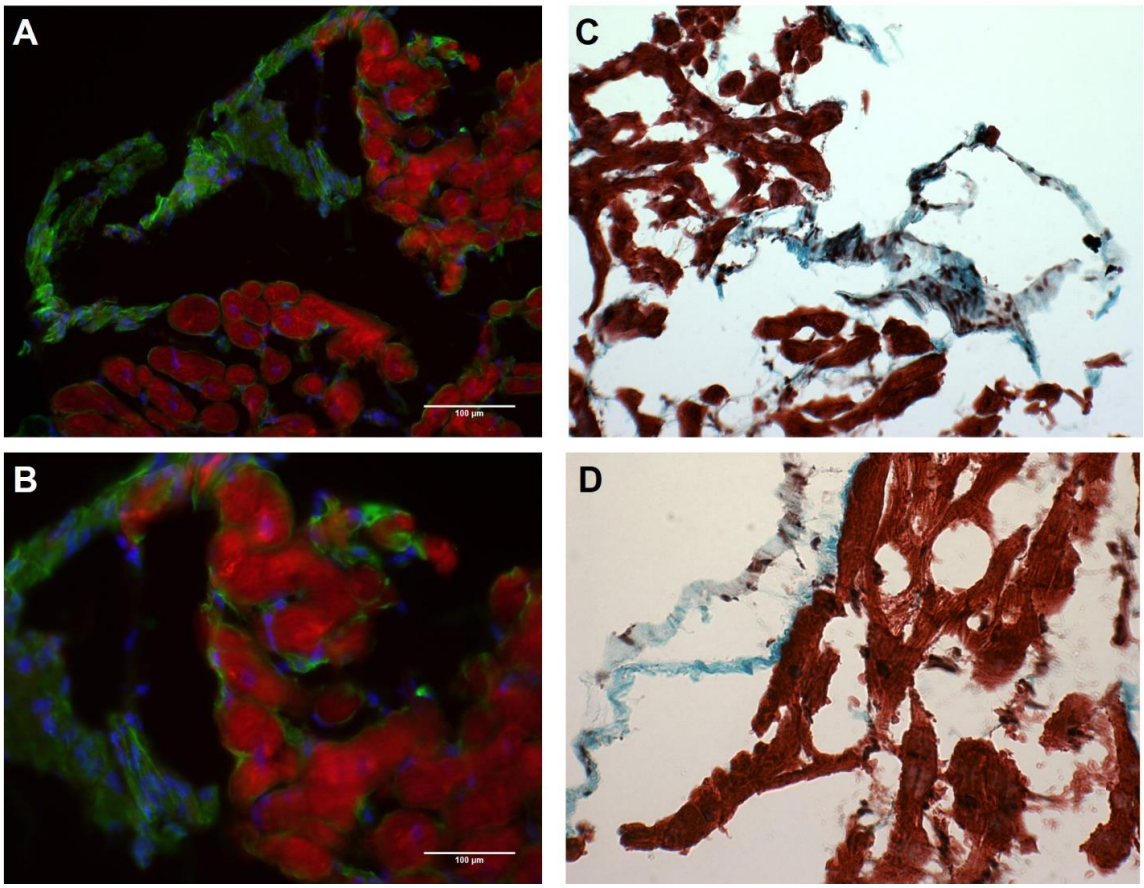

Figure 2.5 Fibrosis and GHSR in human myocardial tissue.

Representative images from grafted heart biopsy 1 showing the same patient sample in all images. A and B show no colocalization of GHSR (red) and collagen I (green) with DAPI showing nuclei (blue). C and D show Masson's trichrome staining of same patient sample as in A and B where blue is fibrotic tissue (collagen I and III) and red is healthy tissue. A and C show 10X magnification where B and D show 20X magnification.

Table 2.4 Fibrosis Percentages of explanted hearts and healthy implanted heart biopsies.

(RA and LV of explanted heart; Biopsy 1-10 of grafted heart). All values listed in percentages (%).

	LV	RA	Bi 1	Bi 2	Bi 3	Bi 4	Bi 5	Bi 6	Bi 7	Bi 8	Bi 9	Bi 10
Patient 1	26.1	10.6	1.3	2.9	5.4	1.5	15.8	2.2	1.3	-	-	-
Patient 2	24.6	6.0	19.1	3.8	3.8	5.7	-	-	-	-	-	-
Patient 3	-	7.0	3.9	11.4	22.2	0.9	-	-	-	3.6	2.2	-
Patient 4	2.6	32.5	1.2	0.3	-	3.9	4.6	-	-	13.1	-	-
Patient 5	53.6	-	2.4	7.3	3.9	1.3	-	-	-	-	-	-
Patient 6	3.7	7.8	2.4	38.0	1.3	-	-	-	4.1	5.9	2.3	11.7
Patient 7	5.5	-	39.4	2.9	2.7	3.1	17.4	3.5	1.8	6.1	6.4	0.3
Patient 8	7.6	1.6	10.7	1.1	6.9	3.6	0.9	1.3	2.8	0.3	6.6	3.6
Patient 9	-	21.9	8.9	6.1	3.5	-	1.2	2.3	-	17.3	-	-
Patient 10	11.5	11.9	3.8	8.3	13.8	0.9	30.9	2.2	3.2	-	-	-

2.4 Discussion

This study is the first comprehensive and longitudinal study to examine tissue GHSR, ghrelin and subsequent downstream biochemical signaling molecules involved in cardiomyocyte contractility and growth, over time, in the same patients with two different hearts. Our findings have demonstrated a relationship between cardiac function, as measured by LVEF, and the expression of both ghrelin and GHSR, suggesting that the cardiac ghrelin-GHSR system may represent a new cardiac-localized biomarker in HF. Our findings further showed an association between some signaling proteins and their relationship to LVEF. Our results demonstrate relationships between GHSR, ghrelin, and biochemical signaling molecules in human cardiac tissues and their relationship to LV function, therefore providing substantial new findings related to this myocardial ghrelin-GHSR system.

Currently the "gold standard" cardiac biomarkers of heart failure are BNP and NT-proBNP, which are markers of myocardial stress. Historically, past studies using BNP have focused on characterizing HF with reduced EF as associated with and directly linked to elevated circulating BNP levels[11,26]. More recent studies have also attempted to understand the mechanisms leading to HF in the setting of preserved EF. To explore this and other etiologies of HF, a variety of biomarkers including hormones (growth hormone)[27,28], extracellular matrix proteins (matrix metalloproteinase, galectin-3); oxidative stress proteins (8-hydroxy-2,-deoxyguanosine, neopterin); and inflammatory molecules (c-reactive protein, pentraxin 3)[29] have been identified and their association with the presence and degree of heart failure investigated. Further, circulating biomarkers of HF continue to be discovered through proteomic and gene sequencing of blood serum analyses[30–32]. Many novel serum biomarkers are currently being identified[33,34], and the ghrelin-GHSR system may provide a complementary cardiac tissue-localized indicator of LV function in HF. Certainly, biomarkers that are intimately involved in the different pathological processes in HF would help to both enhance diagnosis and might have the potential to optimize targeted therapies[29,35]. We propose that the ghrelin-GHSR system represents the first cardiac-localized indicator of HF.

A prior study has also shown that levels of myocardial GHSR are elevated in chronic heart failure in humans[8]. In contrast to our findings, where both GHSR and ghrelin were elevated, that study also reported a decrease in ghrelin expression in chronic heart failure. The difference in the degree of ghrelin expression between these two studies may be due to the different tissues being compared. Beiras-Fernandez et al[8] compared tissue obtained from HF patients to those obtained from young adult subjects with no previous history of heart disease. In contrast, our study compared levels of GHSR and ghrelin at end stage HF with serial biopsies from the engrafted heart under the effects of immunosuppressive therapy taken up to a year after transplant surgery. Furthermore, there were significant relationships between LVEF and tissue ghrelin and GHSR levels in two hearts from the same patient. Similar to Beiras-Fernandez et al, our sample size is relatively small, and may provide challenges in making broad generalizations on increases or decreases in the cardiac ghrelin-GHSR system. Now that we have established that higher levels of GHSR and ghrelin associate with LVEF in the very low range, these results set the stage for a larger study examining changes in cardiac GHSR and ghrelin in patients with a range of LVEF values that reflect the evolution of heart failure.

Strong positive linear regressions between GHSR and ghrelin were present in the entire patient cohort as shown in Fig 2.1D indicating the potential regulation of this ghrelin-GHSR system in human HF. Additionally, we examined linear regressions between GHSR and ghrelin in both the end-stage HF and engrafted heart biopsies separately (Supplemental Fig 2.S1) where there are still highly significant positive linear regressions in both these individual cohorts. This may provide information about the engrafted heart as this ghrelin-GHSR system is still increased up to 1 year after cardiac transplantation. Other cardiac markers, such as BNP, are known to be chronically elevated after transplantation which demonstrates ongoing active cardiac structural remodeling, vascular injury, and inflammation in the engrafted heart[36]. The correlation of the ghrelin-GHSR system in engrafted heart biopsies may provide more information on the biochemical processes that are activated in the engrafted heart after cardiac transplantation.

Ghrelin is produced in a variety of cardiovascular cell types, including endothelial cells, inflammatory cells and cardiomyocytes[37]. Ghrelin down-regulates pro-inflammatory and

up-regulates anti-inflammatory signalling pathways in attenuating cardiac hypertrophy[38], post-infarct cardiac remodeling[39], and sepsis[40]. Although we did not study inflammatory signalling pathways, it is possible that the higher levels of ghrelin-GHSR in the diseased heart may indicate up-regulation in response to the inflammatory environment of heart failure. The post-transplant immunosuppressive regimen may also affect myocardial ghrelin levels and ghrelin-GHSR signalling, particularly through anti-inflammatory pathways.

Circulating ghrelin may also be a potential single biomarker of HF, and from a prognostic perspective, a level of 85 pmol/l or higher was predictive of increased survival [41]. However, circulating ghrelin levels are also elevated in the fasting state, and are decreased in both the elderly population and with patients who have a higher BMI[42], therefore skewing this prognostic cut-off level. While we did not obtain blood samples for measurement of circulating ghrelin, our data in cardiac tissue samples provide the first direct measure of the ghrelin-GHSR system being elevated in the human myocardium. These data further strengthen the case for the use of ghrelin-GHSR as a novel cardiac-localized biomarker of HF. However, how tissue levels of ghrelin-GHSR change with age or BMI in humans is not known.

As mentioned above, circulating BNP and NT-pro BNP are the currently used clinical biomarkers of HF, as levels rise with decreasing LVEF[43–45]. Our results indicate that levels of BNP in human cardiac tissue trend towards an increase when LVEF is in the very low range and was more strongly correlated with LVEF than was ghrelin, suggesting that tissue levels of BNP could also be a sensitive biomarker for severe HF. Interestingly, in our study, levels of both GHSR and ghrelin were also associated with LVEF, indicating that the ghrelin-GHSR system may also be a good cardiac biomarker of LV function. As discussed below, ghrelin showed stronger correlations with biochemical signalling molecules, indicating that tissue ghrelin is more closely associated than is BNP with the biochemical mechanisms that underlie the development of HF.

To better understand the potential mechanisms underlying HF, we examined the downstream signaling pathways that link the ghrelin-GHSR system to cardiomyocyte

contractility and growth. The significant elevation of pERK1/2 levels we observed in end-stage HF is consistent with the reported elevations in pERK1/2 in cardiac tissue in mouse and rat models of HF[46]. Signalling through pERK1/2 is associated with pressure overload-induced myocardial hypertrophy, and thus indicates maladaptive alterations under conditions of persistent myocardial stress. Interestingly, *ghrelin* and *GHSR* gene variants are also associated with LV hypertrophy[47,48]. Therefore, our data suggest a new upregulated ghrelin-GHSR-pERK1/2 pathway that may mediate HF in humans through myocardial hypertrophy.

The strong positive correlation between ghrelin and SERCA2A is in accordance with the role of ghrelin in the improvement of Ca^{2+} dynamics in cardiomyocytes isolated from rodents with ischemia-reperfusion myocardial injury[49]. In this study, activation of GHSR by either ghrelin or hexarelin increased SERCA2a expression and activity through increased phosphorylation of its regulatory binding protein, phospholamban, thus replenishing Ca^{2+} stores in the sarcoplasmic reticulum. However, our results indicating that SERCA2a levels are actually elevated in end-stage HF are in sharp contrast to the literature documenting a decrease in SERCA2a expression and activity in the failing human myocardium[50]. In contrast to the literature, we compared SERCA2a expression between end-stage heart disease and engrafted hearts, and not to healthy controls. The relative decrease in SERCA2a expression in biopsies taken at earlier time points may reflect a subclinical immune response, as a recent study has suggested that decreases in tissue SERCA2a correlate with graft rejection[51].

Cardiac fibrosis due to a deposition of extracellular matrix proteins including fibroblasts and collagen, occurs in all etiologies of heart disease and heart failure and is a marker of increased heart failure severity[52,53]. Our results indicate increased collagen I and III deposition in the diseased hearts, although there was significant variability both between and within patients. The variability could be a consequence of sampling location; a high presence of fibrosis in the apparently healthy implanted hearts likely indicates a considerable degree of geographic heterogeneity within any given patient's heart. Traditionally biopsies are acquired from the RV, as what was done here, although a recent study found LV biopsies to be not only possible with low risk via radial access, but

preferable for determination of heart function through immunohistochemistry and molecular analyses[54]. In our study, values of RV used a surrogate measure of LV dysfunction as RV failure is commonly associated with LV dysfunction and these biopsies were collected with preserved LV function (seen with preserved LVEF). Since there was such a large degree of variability in the amount of fibrotic tissue in both pre-transplant hearts and grafted heart tissue, there was a possibility that GHSR expression originated within the fibrotic tissue, thus potentially skewing our results. However, we have shown that GHSR was found only in non-fibrotic tissue; therefore, the variability in expression likely lies in HF type and severity, and not in sampling location. Since the diseased heart tends to have larger amounts of collagen deposition, the positive fluorescent signal is only originating from a limited, non-fibrotic component of the whole tissue section. Therefore, the measurement of GHSR which we used was affected by the extent of collagen deposition within any given sample, with samples with higher degrees of fibrosis having an artificially depressed measurement of "myocardial" levels.

The present study characterized changes in myocardial GHSR and ghrelin before and after cardiac transplantation. The engrafted hearts were subjected to immunosuppressive therapy, and we did not measure the degree of inflammation or subclinical indicators of rejection in these biopsies. However, that four of these patients were followed up to a year after transplant, with normal EFs, and no dramatic changes in GHSR, ghrelin, SERCA2a, pERK1/2 and fibrosis from the first through to the last biopsy, suggests a normally functioning and stable engrafted heart during this time period. Our next step is to characterize the ghrelin-GHSR system in cardiac tissue obtained from human donors with no history of heart disease.

Overall, we have identified the ghrelin-GHSR system as a cardiac-localized biomarker of cardiac dysfunction in human heart failure. This system was demonstrated to have a higher sensitivity to the downstream signaling molecules linked to cardiomyocyte contractility and hypertrophy when compared to BNP, the gold standard biomarker of HF used clinically. Cardiac fibrosis was highly variable both within and between patients and GHSR was not expressed in fibrotic tissue. We are currently examining the expression and relationship of ghrelin-GHSR signaling that contribute to defective cardiomyocyte

programming in other types of heart disease in humans, as well as in healthy human hearts. Our ongoing work will help to identify the role of myocardial ghrelin-GHSR as a biomarker that may be used to determine the progression of HF at earlier stages.

2.5 Supplemental Figures

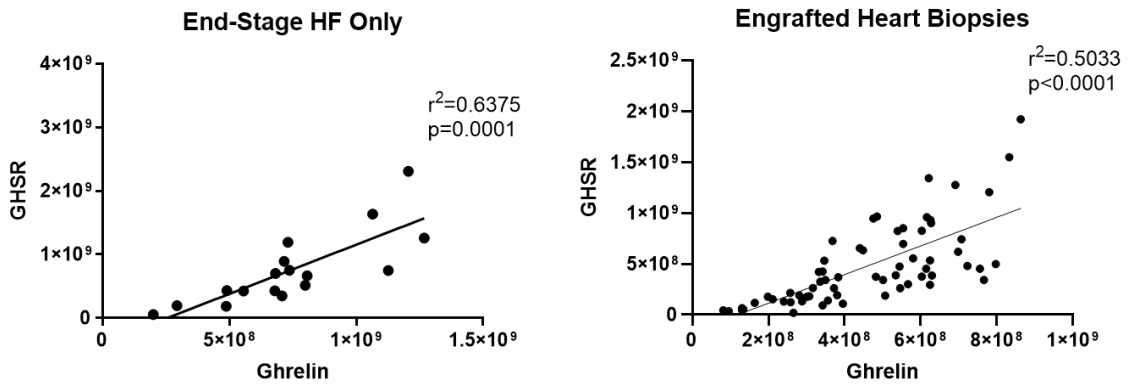

Supplemental Figure 2.S1 Ghrelin and GHSR Correlation in End-Stage HF and Engrafted Heart Biopsies.

Positive linear regression of GHSR and ghrelin expression is shown separated out into end-stage HF and in engrafted heart biopsies where string significance of p=0.0001 is seen in both these cohorts. Each dot represents individual patient values.

2.6 References

1. Yanagi, S., Sato, T., Kangawa, K. & Nakazato, M. The Homeostatic Force of Ghrelin. *Cell Metab.* **27**, 786–804 (2018).

2. Kishimoto, I., Tokudome, T., Hosoda, H., Miyazato, M. & Kangawa, K. Ghrelin and cardiovascular diseases. *Int J Cardiol.* **59**, 8–13 (2012).

3. Sun, Q. *et al.* Effects of GH secretagogues on contractility and Ca2+ homeostasis of isolated adult rat ventricular myocytes. *Endocrinology* **151**, 4446–4454 (2010).

4. Douglas, G. A. F. *et al.* Characterization of a far-red analog of ghrelin for imaging GHS-R in P19-derived cardiomyocytes. *Regul Pept.* **54**, 81–88 (2014).

5. Baldanzi, G. *et al.* Ghrelin and des-acyl ghrelin inhibit cell death in cardiomyocytes and endothelial cells through ERK1/2 and PI 3-kinase/AKT. *J. Cell Biol.* **159**, 1029–1037 (2002).

6. Sullivan, R. *et al.* Changes in the Cardiac GHSR1a-Ghrelin System Correlate With Myocardial Dysfunction in Diabetic Cardiomyopathy in Mice. *J. Endocr. Soc.* **2**, 178–189 (2018).

7. Yuan, M.-J. *et al.* GHSR-1a is a novel pro-angiogenic and anti-remodeling target in rats after myocardial infarction. *Eur J Pharmacol.* **788**, 218–225 (2016).

8. Beiras-Fernandez, A. *et al.* Altered myocardial expression of ghrelin and its receptor (GHSR-1a) in patients with severe heart failure. *Peptides* **31**, 2222–8 (2010).

9. Gaggin, H. K. & Januzzi, J. L. Biomarkers and diagnostics in heart failure. *Biochimica et Biophysica Acta - Molecular Basis of Disease* vol. 1832 2442–2450 (2013).

10. Van Kimmenade, R. R. J. & Januzzi, J. L. Emerging biomarkers in heart failure. *Clinical Chemistry* vol. 58 127–138 (2012).

11. Braunwald, E. Biomarkers in heart failure. *New England Journal of Medicine* vol. 358 2148–2159 (2008).

12. McGirr, R., McFarland, M. S., McTavish, J., Luyt, L. G. & Dhanvantari, S. Design and characterization of a fluorescent ghrelin analog for imaging the growth hormone secretagogue receptor 1a. *Regul Pept.* **172**, 69–76 (2011).

13. RRID: AB_2111733. http://antibodyregistry.org/search?q=AB_2111733.

14. RRID: AB_303961. http://antibodyregistry.org/search?q=AB_303961.

15. RRID: AB_2762850. http://antibodyregistry.org/search?q=AB_2762850.

16. RRID: AB_445037. http://antibodyregistry.org/search?q=AB_445037.

17. RRID: AB_731684. http://antibodyregistry.org/search?q=AB_731684.

18. RRID: AB_2629482. http://antibodyregistry.org/search?q=AB_2629482.

19. RRID: AB_2534102. http://antibodyregistry.org/search?q=AB_2534102.

20. RRID: AB_141637. http://antibodyregistry.org/search?q=AB_141637.

21. RRID: AB_141633. http://antibodyregistry.org/search?q=AB_141633.

22. RRID: AB_141708. http://antibodyregistry.org/search?q=AB_141708.

23. Abbas, A. *et al.* Development and Characterization of an 18 F-labeled Ghrelin Peptidomimetic for Imaging the Cardiac Growth Hormone Secretagogue Receptor. *Mol. Imaging* **17**, 1–11 (2018).

24. Guizzetti, L., McGirr, R. & Dhanvantari, S. Two dipolar α-helices within hormone-encoding regions of proglucagon are sorting signals to the regulated secretory pathway. *J. Biol. Chem.* **289**, 14968–14980 (2014).

25. Kennedy, D. J. *et al.* Central role for the cardiotonic steroid marinobufagenin in the pathogenesis of experimental uremic cardiomyopathy. *Hypertension* **47**, 488–

495 (2006).

26. Friões, F. *et al.* Prognostic value of sST2 added to BNP in acute heart failure with preserved or reduced ejection fraction. *Clin Res Cardiol* **104**, 491–9 (2015).

27. Arcopinto, M. *et al.* Multiple hormone deficiencies in chronic heart failure. *Int. J. Cardiol.* **184**, 421–423 (2015).

28. Arcopinto, M. *et al.* Growth hormone deficiency is associated with worse cardiac function, physical performance, and outcome in chronic heart failure: Insights from the T.O.S.CA. GHD study. *PLoS One* **12**, e0170058 (2017).

29. Takeishi, Y. Biomarkers in heart failure. *Arquivos Brasileiros de Cardiologia* vol. 113 205–206 (2019).

30. Senthong, V., Kirsop, J. L. & Tang, W. H. W. Clinical Phenotyping of Heart Failure with Biomarkers: Current and Future Perspectives. *Current Heart Failure Reports* vol. 14 106–116 (2017).

31. Meder, B. *et al.* Epigenome-Wide Association Study Identifies Cardiac Gene Patterning and a Novel Class of Biomarkers for Heart Failure. *Circulation* **136**, 1528–1544 (2017).

32. Xuan, L. *et al.* Circulating long non-coding RNAs NRON and MHRT as novel predictive biomarkers of heart failure. *J. Cell. Mol. Med.* **21**, 1803–1814 (2017).

33. Stenemo, M. *et al.* Circulating proteins as predictors of incident heart failure in the elderly. *Eur. J. Heart Fail.* **20**, 55–62 (2018).

34. van Boven, N. *et al.* Serially measured circulating microRNAs and adverse clinical outcomes in patients with acute heart failure. *Eur. J. Heart Fail.* **20**, 89–96 (2018).

35. Bishu, K. & Redfield, M. M. Acute heart failure with preserved ejection fraction: Unique patient characteristics and targets for therapy. *Curr. Heart Fail. Rep.* **10**, 190–197 (2013).

36. Mehra, M. R. *et al.* Gene expression profiles and B-type natriuretic peptide elevation in heart transplantation: More than a hemodynamic marker. *Circulation* **114**, (2006).

37. Müller, T. D. *et al.* Ghrelin. *Molecular Metabolism* vol. 4 437–460 (2015).

38. Mao, Y. *et al.* Endogenous Ghrelin Attenuates Pressure Overload–Induced Cardiac Hypertrophy via a Cholinergic Anti-Inflammatory Pathway. *Hypertension* **65**, 1238–1244 (2015).

39. Huang, C.-X. *et al.* Ghrelin inhibits post-infarct myocardial remodeling and improves cardiac function through anti-inflammation effect. *Peptides* **30**, 2286–2291 (2009).

40. Wu, R. *et al.* Ghrelin down-regulates proinflammatory cytokines in sepsis through activation of the vagus nerve. *Ann. Surg.* **245**, 480–6 (2007).

41. Chen, Y. *et al.* Prognostic value of plasma ghrelin in predicting the outcome of patients with chronic heart failure. *J Inst Mex Seg Soc.* **45**, 263–9 (2014).

42. Rigamonti, A. E. *et al.* Plasma ghrelin concentrations in elderly subjects: comparison with anorexic and obese patients. *J Endocrinol.* **175**, 1–5 (2002).

43. Karakilic, E. *et al.* The relationship between B-type natriuretic peptide levels and echocardiographic parameters in patients with heart failure admitted to the emergency department. *Anadolu Kardiyol. Dergisi/The Anatol. J. Cardiol.* **10**, 143–149 (2010).

44. Jiang Yanxia, M. C., Yanxia, J., Xingjun, C., Xintao, T. & Lei, S. The Correlation between Left Ventricular Ejection Fraction and Peripheral Blood MCP-1 NT-Pro BNP in Patients with Acute Coronary Syndrome. *Intern. Med. Open Access* **04**, 1–4 (2014).

45. Belagavi, A. C., Rao, M., Pillai, A. Y. & Srihari, U. S. Correlation between NT proBNP and left ventricular ejection fraction in elderly patients presenting to

emergency department with dyspnoea. *Indian Heart J.* **64**, 302–4 (2012).

46. Bueno, O. F. & Molkentin, J. D. Involvement of extracellular signal-regulated kinases 1/2 in cardiac hypertrophy and cell death. *Circ. Res.* **91**, 776–781 (2002).

47. Baessler, A. *et al.* Association of the ghrelin receptor gene region with left ventricular hypertrophy in the general population: Results of the MONICA/KORA Augsburg echocardiographic substudy. *Hypertension* **47**, 920–927 (2006).

48. Ukkola, O., Pääkkö, T. & Kesäniemi, Y. A. Ghrelin and its promoter variant associated with cardiac hypertrophy. *J. Hum. Hypertens.* **26**, 452–457 (2012).

49. Ma, Y., Zhang, L., Edwards, J. N., Launikonis, B. S. & Chen, C. Growth hormone secretagogues protect mouse cardiomyocytes from in vitro ischemia/reperfusion injury through regulation of intracellular calcium. *PLoS One* **7**, (2012).

50. Gorski, P. A., Ceholski, D. K. & Hajjar, R. J. Altered myocardial calcium cycling and energetics in heart failure - A rational approach for disease treatment. *Cell Metab.* **21**, 183–194 (2015).

51. Tarazón, E. *et al.* SERCA2a: A potential non-invasive biomarker of cardiac allograft rejection. *J. Hear. Lung Transplant.* **36**, 1322–1328 (2017).

52. Majumder, R., Nayak, A. R. & Pandit, R. Nonequilibrium Arrhythmic States and Transitions in a Mathematical Model for Diffuse Fibrosis in Human Cardiac Tissue. *PLoS One* **7**, e45040 (2012).

53. Boldt, A. *et al.* Fibrosis in left atrial tissue of patients with atrial fibrillation with and without underlying mitral valve disease. *Heart* **90**, 400–405 (2004).

54. Frey, N., Meder, B. & Katus, H. A. Left Ventricular Biopsy in the Diagnosis of Myocardial Diseases. *Circulation* **137**, 993–995 (2018).

Chapter 2

3 Regional Differences in the Ghrelin-Growth Hormone Secretagogue Receptor Signalling System in Human Heart Disease

A version of this chapter has been published.

Sullivan, R. *et al*. Regional Differences in the Ghrelin-Growth Hormone Secretagogue Receptor Signalling System in Human Heart Disease. *CJC Open* **4**, 1-13 (2020). https://doi.org/10.1016/j.cjco.2020.10.015

3.1 Introduction

Ghrelin is a peptide hormone that has well-known orexigenic effects on the body. Ghrelin is an endogenous 28 amino acid peptide that is a natural ligand of the growth hormone secretagogue receptor (GHSR) 1a, a seven transmembrane G-protein coupled receptor. More recently, ghrelin has been studied for its effects and role in cardiac energetics through activation of myocardial GHSR. Specifically within cardiomyocytes, the binding of ghrelin to GHSR activates downstream signalling pathways that lead to cardioprotective effects, such as maintenance of contractility[1,2], suppression of inflammation[3,4], and promotion of growth and survival[5]. Cardiac GHSR activation promotes excitation-contraction coupling, increasing Ca^{2+} flux through the sarcoplasmic reticulum ATPase pump (SERCA2a) and the voltage gated Ca^{2+} channels, which produces a positive inotropic effect and protects against ischemia/reperfusion injury in cardiomyocytes[2]. Ghrelin also regulates inflammation in the heart through the protein kinase B (Akt) pathway, decreasing expression of the pro-inflammatory markers[6] IL1-β, TNF-α, and IL-6, and upregulating the tumour necrosis factor α/ nuclear factor kappa-light-chain-enhancer of activated B cells (NFκB) pathways[3]. Ghrelin has been shown to protect the heart through the toll like receptor 4 pathway (TLR4)[4]. Apoptosis is decreased upon GHSR activation through extracellular signal-related kinases 1/2 (ERK1/2) and Akt serine kinases[5,6] and inhibition of caspase-3 and 9[7]. Fibrosis deposition is also minimized in the heart after ghrelin administration[8,9]. Therefore, the ghrelin-GHSR system within the myocardium plays a critical role in the maintenance of cardiomyocyte function and survival.

The discovery of the myocardial ghrelin-GHSR system and its role in cardiomyocyte function and health has prompted studies on its dynamics in heart failure and cardiomyopathy. We and others have shown that myocardial GHSR is elevated in heart failure (HF)[10,11]. Additionally, we showed that the cardiac ghrelin-GHSR system was abnormally up-regulated in end-stage HF compared to endomyocardial biopsies from engrafted hearts[11], thus suggesting that tissue levels of ghrelin and GSHR could be indicators of the health of transplanted hearts. In contrast, one study has reported decreased GHSR in tissue from patients with dilated cardiomyopathy, which negatively correlated with LVEF[12]. We[13] and others[14] have shown that tissue GHSR also decreased in mouse

models of diabetic cardiomyopathy, suggesting that the dynamics of the myocardial ghrelin-GHSR system may differ in earlier stages of myocardial decompensation as compared with end-stage heart failure.

Some potential causes of heart failure include coronary artery disease (an accumulation of cholesterol (plaques) in the vessel walls) or aortic stenosis (progressive restriction of the opening of the aortic valve)[15], and there has been some clinical investigation into correlations with serum ghrelin levels and the effects of ghrelin administration on heart function in these conditions. In humans with coronary artery disease and with diabetes-associated coronary atherosclerosis, serum levels of ghrelin decreased significantly compared to healthy controls[16,17]. Another study also showed an inverse relationship between serum ghrelin and coronary artery disease (CAD) detected by angiography that was independent of other cardiovascular risk factors[16], suggesting that a reduction in ghrelin-GHSR signalling may be correlated with progressively more severe CAD. Ghrelin administration in rats with aortic stenosis reduced calcification buildup in the myocardium in a dose-dependent manner[18], and attenuated aortic calcium deposition both *in vivo* and *in vitro*[19]. Therefore, investigating the dynamics of the ghrelin-GHSR system and signaling within cardiomyocytes may provide further insight into the potential use of ghrelin as a therapy for myocardial dysfunction (heart failure).

In this study, towards the goal of determining the potential of ghrelin-GHSR as a biomarker of heart disease, we examined their levels in a cohort of patients who underwent elective cardiac valve replacement surgery and compared their expression levels to control heart tissues. We also determined the correlation of ghrelin-GHSR with an array of biomarkers including natriuretic peptide type-B (BNP), sarcoplasmic reticulum ATPase (SERCA2a), and toll-like receptor 4 (TLR4). With these data, we hope to obtain further insights into the distinct molecular signalling patterns associated with the progression of heart disease.

3.2 Methods

3.2.1 Patient Cohort

Tissue samples were harvested from 25 patients who underwent aortic valve replacement surgery for aortic stenosis at the London Health Sciences Center (LHSC) between 2013 and 2014. Twenty-four of these patients had aortic stenosis and one had mitral valve impairment. Of these 25 patients, 11 concurrently had coronary artery disease and received coronary artery bypass grafts. Sixteen patients were male and nine were female, with an overall average age of 66 years. Twenty-three patients had normal ejection fractions (>45%) prior to surgery, and two patients had reduced ejection fractions (35-40%). The protocol for obtaining tissue samples was approved by Western University's Health Sciences Research Ethics Board. Tissue samples, roughly 0.2cm to 0.5cm in length, were collected from the left atrium (LA) and left ventricular (LV) myocardium from each patient. The left atrial samples were obtained from the posterior left atrial wall just on the left atrial side of the inter-atrial septum (close to the right atrium but technically the left atrium). The left ventricular samples were taken from the posterior left ventricular wall, just below the mitral valve. Patient demographics, cardiac function (LVEF), and medications are shown in Tables 3.1 and 3.2. All patient samples and patient data were kept anonymous and all biomarker analyses were completed prior to receiving clinical data.

In order to provide a reference non-diseased control, paraffin-embedded and sectioned samples of cardiac tissue (n=10) were obtained from the tissue archives of the Department of Pathology, London Health Sciences Centre. These tissue samples had been obtained from the LV of patients who had died from non-cardiac causes at the time of post-mortem, 24-48 h after the patient was pronounced dead. Of these 10 patients, 5 were male and 5 were female. The average age of all ten patients was approximately 59 years. Analysis of these tissues was compared to the analysis derived from the surgery patients for overall marker fluorescence intensity and differences in biomarker relationships.

Table 3.1 Cardiac Surgery Patient Demographics.

Patient Condition	Number of Males with Condition (n of 16)	Number of Females with Condition (n of 9)
Age range (years)	49 – 84	45 – 77
Mean age (years)	69	60
Coronary artery disease	9	2
Moderate – Severe Aortic Stenosis	14	8
Hypertension	8	2
High pulmonary artery pressure	10	7
Diabetes	2	1
LVEF <45%	2	0
LVEF >45%	14	9

Table 3.2 Patient Medications Post-Heart Surgery.

Patient Medication	Number of Males with Use (n of 16)	Number of Females with Use (n of 9)
ACE Inhibitor	1	2
Anti-arrhythmic	1	2
Angiotensin receptor blocker (ARB)	6	1
Coumadin	4	2
Beta blocker	5	5
Calcium channel blocker	2	3
Diuretics	8	3
Statins	11	3

3.2.2 Quantitative Fluorescence Microscopy

Samples were fixed, frozen and embedded in optimal cutting temperature compound (OCT), and subsequently sectioned at 6-7 μm thickness, as previously described[20,21]. Immunohistochemistry using primary and fluorophore-conjugated secondary antibodies was conducted as previously described[20,21]. In brief, tissue sections were incubated with blocking buffer in 10% serum for 30 minutes at room temperature followed by incubation with primary polyclonal or monoclonal antibodies (Table 3.3) for 1h at room temperature in a humidified chamber. These antibodies were used to identify ghrelin (1:100) [Santa Cruz Biotechnology], BNP (1:1000) [Abcam], SERCA2a (1:300) [Abcam], and TLR4 (1:250) [Abcam]. Samples were rinsed twice in phosphate buffered saline (PBS) and incubated for 2h at room temperature with secondary antibodies (1:500) (Table 3.3). To detect GHSR, we used the far-red ghrelin peptide analog, [Dpr^3(n-octanoyl),Lys^{19}(sulfo-Cy5)]ghrelin(1-19), referred to as Cy5-ghrelin(1-19), as we have previously done to quantify GHSR *in situ*[21]. This analog binds with high specificity to GHSR in mouse and human cardiac tissue samples[11,13]. After incubation with secondary antibodies, Cy5-ghrelin(1-19) was added to tissue sections for 30 min. Sections were washed twice with PBS, incubated 8 min with DAPI nuclear stain (1:1000), and mounted with ProLong Diamond antifade (Life Technologies) to prevent the tissues from photobleaching. N numbers for each biochemical marker were different due to the limited amount of tissue available at the time of staining.

For control cardiac tissue, all sections were deparaffinized with decreasing concentrations of alcohol solutions (95%-70%). Samples were then stained as previously stated for the following biomarkers: ghrelin (1:100) [Santa Cruz Biotechnology], BNP (1:1000) [Abcam], SERCA2a (1:300) [Abcam], and TLR4 (1:250) [Abcam] and GHSR (1:100) using Cy5-ghrelin(1-19).

Table 3.3 Antibody Table – Information on Antibodies Used.

Antigen	Catalog Number	Dilution	Host
Ghrelin	sc-10359	1:100	Goat
BNP	ab19645	1:1000	Rabbit
SERCA2a	ab3265	1:300	Rabbit
TLR4	ab22048	1:250	Mouse
DAPI	62247	1:1000	-
Alexa Fluor 488	A11055	1:1000	Donkey anti-goat
Alexa Fluor 594	A21207	1:1000	Donkey ant-rabbit
Alexa Fluor 488	A21206	1:1000	Donkey anti-rabbit
Alexa Fluor 594	A21203	1:1000	Donkey anti-mouse

3.2.3 Background Subtraction for Fluorescence Microscopy Imaging

To ensure specificity of the fluorescent signal for GHSR, background subtraction was performed, as GHSR has a diffuse staining pattern. To calculate the background signal, tissue sections were first incubated with 100µM hexarelin, a GHSR ligand[22] known to competitively displace Cy5-ghrelin(1-19)[21], for 1 hour at room temperature prior to incubation with 10µM Cy5-ghrelin(1-19) as described above. Tissues were then stained for DAPI (1:1000), washed and mounted with ProLong Diamond antifade as described above. For control tissue samples, background fluorescence intensity values were calculated in 5 separate control samples, and the average value of these intensities was subtracted from the total fluorescence intensities of GHSR in each of the 10 original tissue samples. For diseased tissue samples, background values were calculated from 5 fields of view in one slide from each patient, and the average value of this slide was calculated as the background fluorescence. These values were subtracted from the total fluorescence intensities of non-blocked tissue from that patient to obtain specific Cy5-ghrelin(1-19) signal in the diseased tissue.

3.2.4 Image Acquisition and Analysis

High resolution images of both the diseased and control tissues were captured with a Nikon A1R Confocal Microscope at 60x magnification using an oil immersion lens. Five random fields of view were acquired for each of 2 tissue sections per patient sample with the exposure time, gain and high/ow look up tables set the same for all tissue sections. Therefore, each patient sample (reported as data points in all graphs) reflects an average of 2 technical replicates.

Images of GHSR, ghrelin, BNP, SERCA2a, and TLR4 were analyzed with FIJI 1.49v, a distribution of ImageJ software (National Institutes of Health, Bethesda). Algorithms built into ImageJ were used to quantify different staining patterns in the tissue. Punctate staining patterns were quantified using the RenyiEntropy algorithm, an entropy-based approach that distinguishes the positive punctate signals within the cells from the background. The

integrated density represents the mean intensity of the positive signal above a certain threshold in scaled units divided by the area in pixels. The integrated density threshold was set such that the entropies of distributions above and below the set threshold are maximized. Therefore, this algorithm only captured the high intensity punctate staining patterns and did not calculate any background staining of these images. A representation of what the algorithm identified as positive versus background is shown in Supplemental Figure 3.S1.

For diffuse staining patterns, the Li algorithm was used to quantify the specific fluorescence signal after background subtraction as described above. All images for diffuse staining were quantified using the built-in ImageJ Li algorithm with the integrated density (stated above) determined for each tissue.

3.2.5 Fibrosis Imaging

To assess fibrosis, heart tissue sections were stained with Masson's Trichrome stain by the core Pathology Laboratory at LHSC. Sections of both the diseased and control tissue were acquired using bright field microscopy at 10X and 20X magnifications with a Zeiss Axioskop EL-Einsatz microscope and Northern Eclipse software as described previously[11,13]. Images were acquired for the entire tissue section and quantification was performed on the entire tissue.

Fibrosis was analyzed using an online script in the program ImageJ Fiji which quantified the percentage of fibrotic tissue in each sample by distinguishing fibrotic tissue (blue) from non-fibrotic tissue (red), as previously described[23]. Briefly, this script divides the RBG image into each of its channels which thresholds the image for positive pixels in either the red or blue channels. All tissue sections were set at the same threshold for both the fibrotic and non-fibrotic tissue. The fibrosis was then quantified based on the fibrotic tissue compared to the total area of tissue to determine the average percentage of fibrosis in each of the diseased or control tissue samples.

3.2.6 Data Analysis

Data from biomarkers (GHSR, ghrelin, BNP, SERCA2a, and TLR4) were disaggregated by cardiac region using a post-hoc analysis. Statistical analyses were performed using GraphPad Prism version 8. Unpaired student *t*-tests were used to compare overall biomarker expression differences between the diseased and control tissue. Within the diseased tissue cohort, a one-way analysis of variance (ANOVA) with analysis of variance using Tukey *post-hoc* test was used to determine regional differences. Linear regression was used to determine correlations between the following biomarkers: GHSR, ghrelin, BNP, SERCA2a and TLR4. Linear regression analysis was used to compare biomarker fluorescence intensities based on the following categories: entire patient cohort and regional differences (left atrium and left ventricle). Pearson correlation was used to determine colocalization between ghrelin and BNP in both diseased (LA and LV) and control tissue. All statistical analyses were completed with significance set at $p<0.05$.

3.3 Results

3.3.1 Cardiac Surgery Patient Cohort

Of the twenty-five patients who underwent cardiac surgery, 16 were male and 9 were female with mean ages of 69 and 60 respectively (Table 3.1). The patients had a range of moderate to severe aortic stenosis while 11 also had coronary artery disease. In the patients with coronary artery disease, there were no linear regressions between any markers evaluated in this study (GHSR and ghrelin – r=0.3942 p=0.1826; GHSR and BNP – r=0.0596 p=0.8467; ghrelin and BNP – r=0.1769 p=0.8850; SERCA2a and GHSR – r=0.4132 p=0.2354; SERCA2a and ghrelin – r=0.5175 p=0.1256; SERCA2a and BNP – r=0.4315 p=0.2131). Sixteen patients had elevated estimated pulmonary artery pressures, based on their pre-operative echocardiograms and only two patients had a reduced ejection fraction prior to surgery (30-40%). After cardiac surgery, 10 patients were on beta blockers, 11 were on diuretics and 14 were on statins (Table 3.2).

3.3.2 Correlations Between GHSR and Ghrelin in Diseased Cardiac Tissue

Fluorescence intensities of both GHSR and ghrelin were variable in any given cardiac tissue sample in both the diseased and control cohort (Fig 3.1A & C). Overall GHSR expression was not significantly different between the diseased and control groups (Fig 3.1B) while tissue ghrelin was significantly lower ($p<0.0001$) in the diseased cohort in both the LA and the LV (Fig 3.2 D). Linear regression analysis of GHSR vs. ghrelin showed a positive relationship in the overall cardiac surgery cohort ($r = 0.3995$; $p=0.0318$) (Fig 3.2 C). Regionally, this linear regression persisted only in the left atrium ($r = 0.4859$; $p=0.0299$) and not in the left ventricle ($r = 0.01730$; $p=0.7562$) (Fig 3.2D). There was no significant linear regression between GHSR and ghrelin in the control tissues ($r = 0.1105$; $p=0.3480$) (Fig 3.2B).

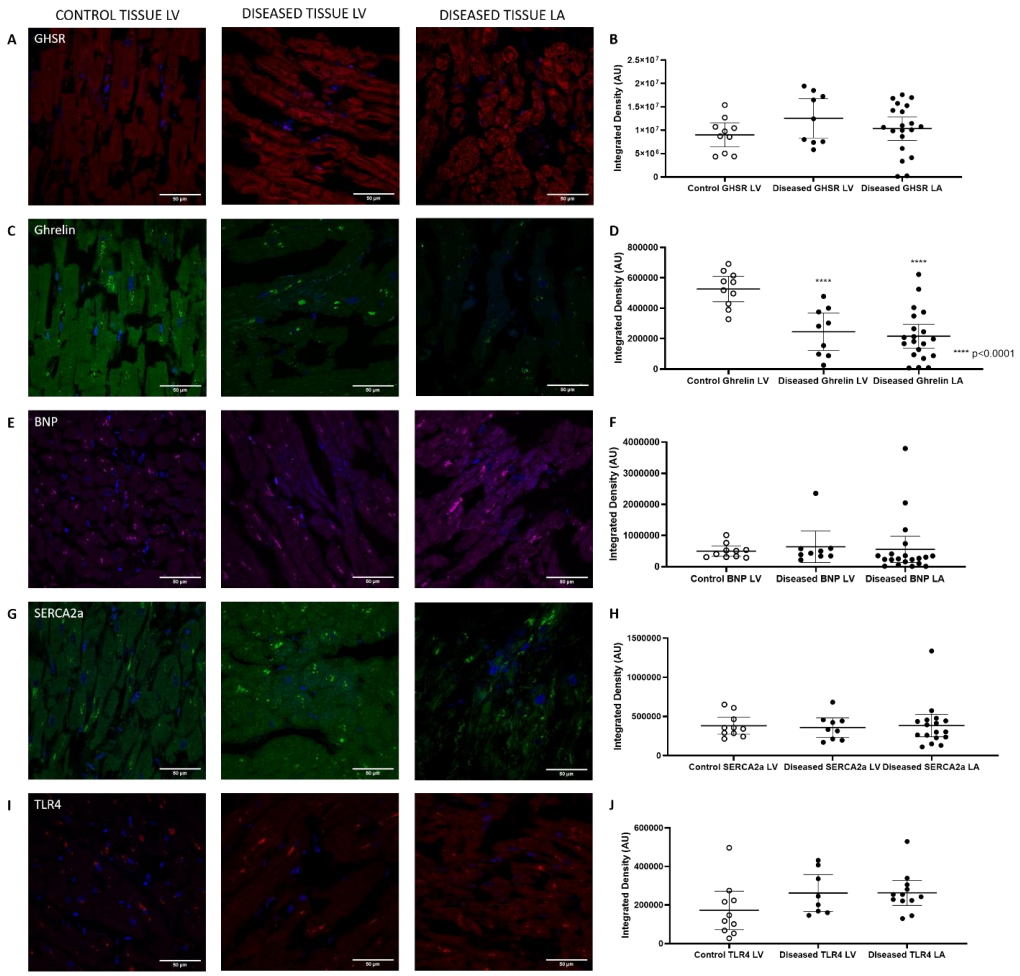

Figure 3.1 Representative confocal fluorescence images of all biomarkers.

(A) [Dpr^{3}(n-octanoyl),Lys^{19}(sulfo-Cy5)]ghrelin(1-19): red, (C) ghrelin: green, (E) BNP: magenta, (G) SERCA2a: green, (I) toll-like receptor 4 [TLR4]; red) in the control tissue left ventricle (LV; left column) and diseased tissue LV (middle column) and LVA (right column). All images indicate DAPI nuclear stain in blue. Graphs represent quantification of fluorescent images as means ± 95% CI of integrated densities for each biomarker with each dot representing one patient sample. There were no significant differences in fluorescence intensities of (B) Cy5-ghrelin(1-19) [control LV n=10, LV n=9, LA=20], (F) BNP [control LV n=10, LV n=9, LA=20], (H) SERCA2a [control LV n=10, LV n=9, LA=17] or (J) TLR4 [control LV n=10, LV n=8, LA=12]. There was a significant decrease in the fluorescence intensities detecting (D) ghrelin ($p<0.0001$) [control LV n=10, LV n=9, LA=20] in the diseased cohort compared to the control tissues.

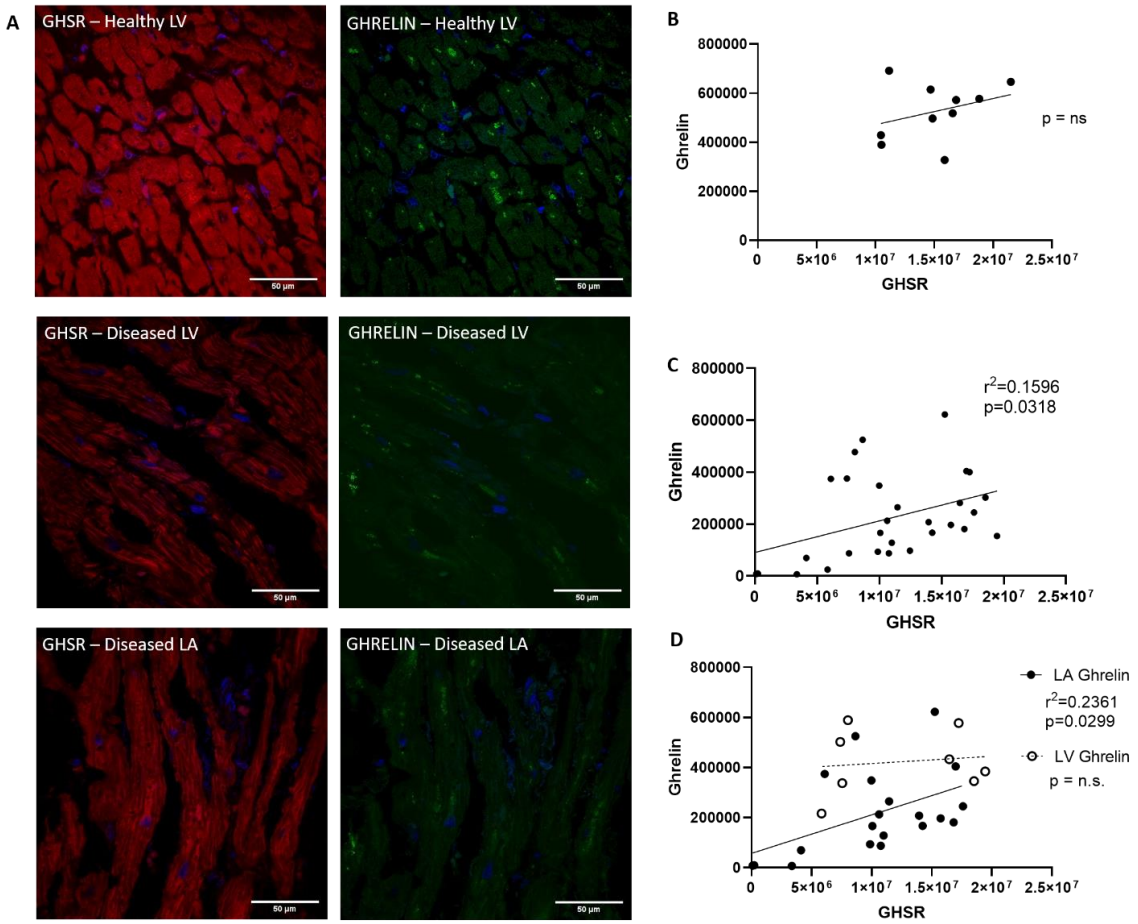

Figure 3.2 GHSR and ghrelin fluorescence intensity in human cardiac tissue.

(A) Representative confocal images of [Dpr^{3}(n-octanoyl),Lys^{19}(sulfo-Cy5)]ghrelin(1-19) (red), and ghrelin (green) in diseased control left ventricle (LV, top), diseased LV (middle) and diseased LA (bottom). DAPI (blue) indicates nuclear localization in cardiomyocytes. Graphs indicate quantification of integrated densities using linear regression between Cy5-ghrelin(1-19) and ghrelin. In control tissue, there was no linear regression between Cy5-ghrelin(1-19) and ghrelin (p=ns) [n=10] (B). Linear regression between Cy5-ghrelin(1-19) and ghrelin (r = 0.3995; p=0.0318) in the entire patient cohort [n=29] where each dot represents one patient sample (C). Regional analysis showed a significant linear regression of Cy5-ghrelin(1-19) and ghrelin in the LA (r = 0.4859; p=0.0299) [n=20] but not the LV (p=ns) [n=9] (D). LA, Left Atrium; LV, Left Ventricle.

3.3.3 Relationship of BNP to GHSR and Ghrelin in Diseased Cardiac Tissue

Fluorescence images indicated the localization of BNP within the diseased and control heart tissue (Figure 3.1E). Analysis of these images indicated no significant difference in immunofluorescence (p=ns) in the disease cohort compared to the control tissues (Fig 3.1F). Linear regression analysis indicated a strong and significant positive relationship between BNP and GHSR (r = 0.5633; p=0.0034); this relationship was strong within the LA (r = 0.6751; p=0.0029) but not the LV (r = 0.0127; p=0.9784) (Fig 3.3 C – D). There was also a significant positive relationship between BNP and ghrelin in the entire cohort (r = 0.5008; p=0.0108). This relationship, however, differed by region: LV (r = 0.9152; p=0.0014), LA (r = 0.394 p=0.1177) (Fig 3.3 E – F). Again, no relationship was seen between BNP and GHSR or ghrelin in the control cardiac tissue (r = 0.2465; p=0.4923 and r = 0.1236; p=0.7337 respectively).

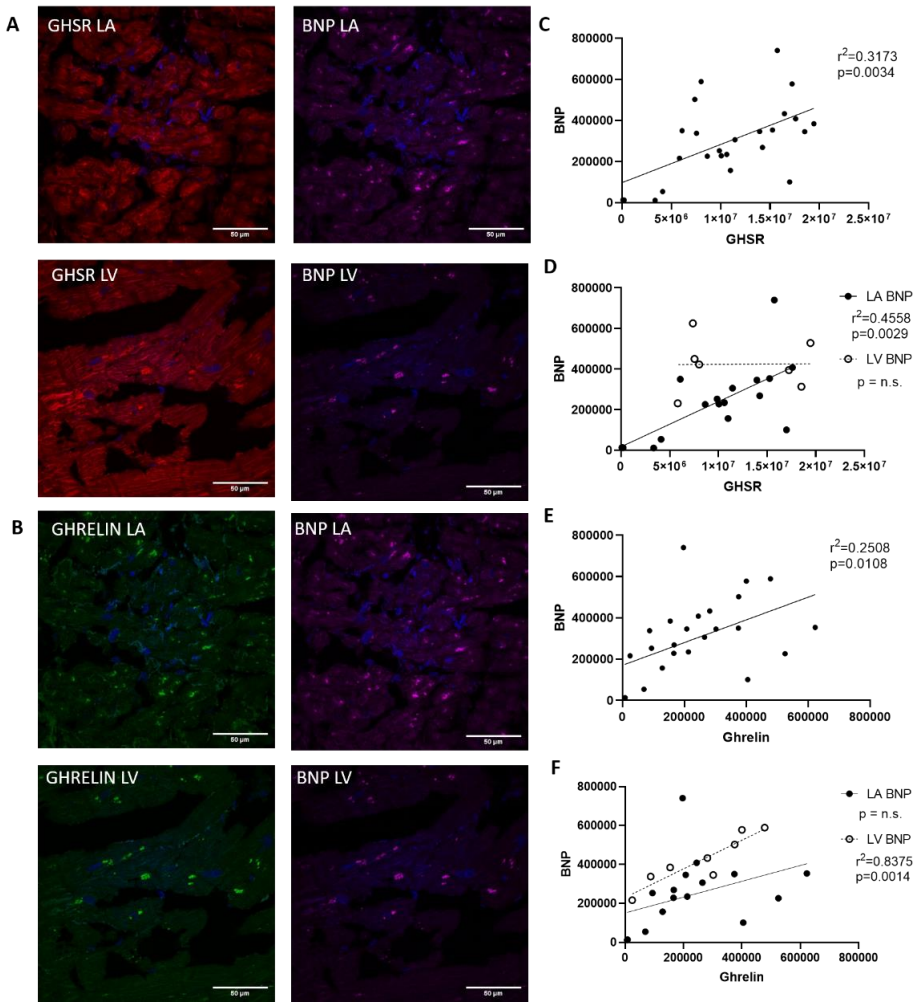

Figure 3.3 BNP correlation to ghrelin-GHSR.

Representative fluorescent confocal images of[Dpr^{3}(n-octanoyl),Lys^{19}(sulfo-Cy5)]ghrelin(1-19) (red), ghrelin (green) and BNP (magenta) in human cardiac tissue in the LA and LV (A & B). Nuclei were visualized with DAPI (blue). Graphs show linear regression analysis of quantified integrated densities with each dot representing an individual patient sample. There was significant linear regression of Cy5-ghrelin(1-19) vs BNP (r = 0.5633; p=0.0034) in the entire patient cohort [n=25] (C). When data were disaggregated by region, a significant linear regression was found in the LA (r = 0.6751; p=0.0029) [n=17] but not the LV (p=ns) [n=8] (D). Ghrelin and BNP were correlated in the entire patient cohort (r = 0.5008; p=0.0108) [n=25] (E). Linear regression analysis between ghrelin and BNP indicate linear regressions in the LV (r = 0.9152; p=0.0014) [n=17] but not the LA (p=ns) [n=9] (F). LA, Left Atrium; LV, Left Ventricle.

3.3.4 Intracellular Colocalization of Ghrelin and BNP in Cardiomyocytes

Ghrelin and BNP appeared to be spatially localized to the same intracellular compartment within cardiomyocytes. In the control tissue, ghrelin and BNP appeared as larger ordered punctate areas mainly surrounding the nucleus (Fig 3.4A) while in the diseased tissue these colocalized areas of ghrelin and BNP were smaller and scattered more diffusely throughout the cell, and are not focused primarily around the nucleus (Fig 3.4B – C). The Pearson Correlation Coefficient was strong for both diseased LA (PCC=0.76) and LV (PCC=0.83) and control (PCC=0.86) while there was a significantly higher correlation in the control tissues compared to the LA (p=0.00169) diseased tissue but not LV (p=0.2923) (Fig 3.4D).

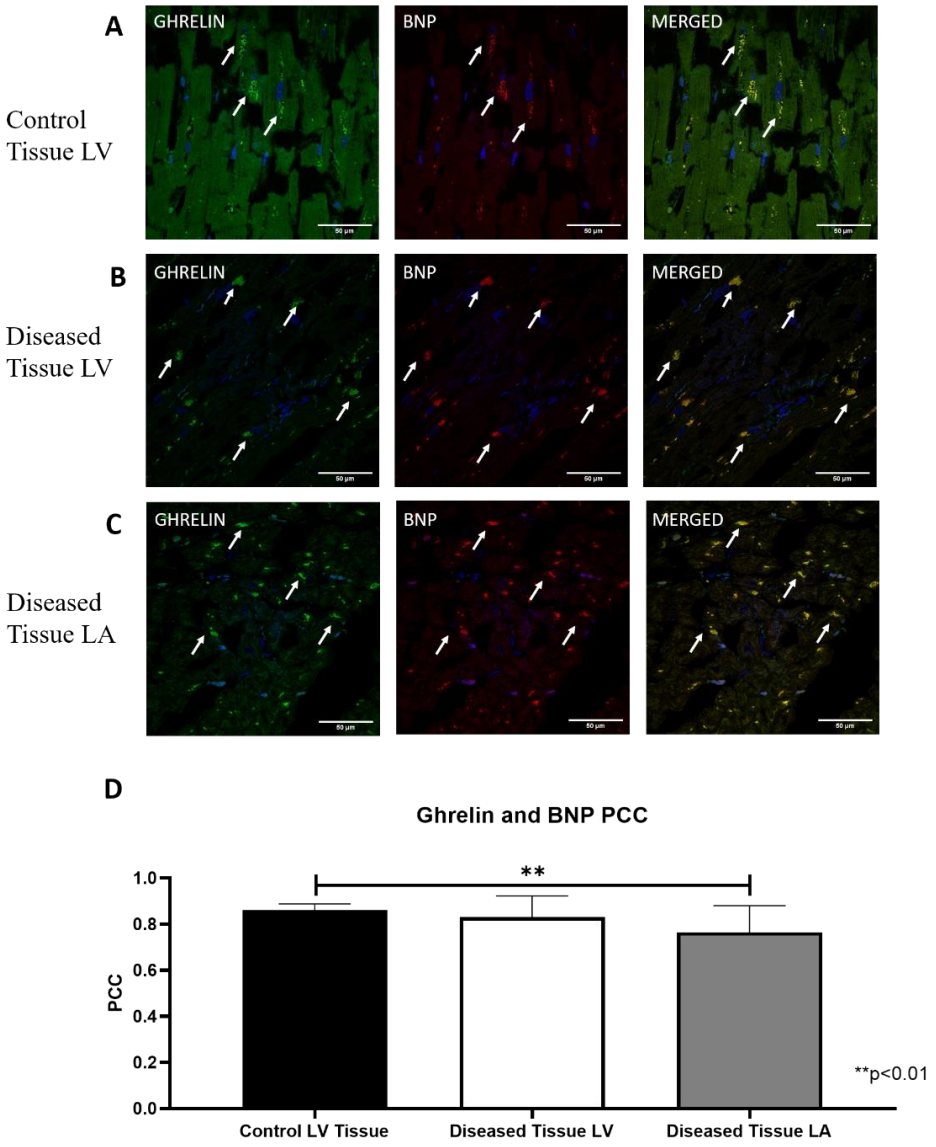

Figure 3.4 Intracellular colocalization of ghrelin and BNP in control LV.

(A) and diseased tissue LV (B) and LA (C). (A-C) Representative confocal fluorescent images of ghrelin (green) and BNP (red) in healthy and diseased tissue shows linear regression of ghrelin and BNP in the merged images. DAPI (blue) indicates nuclear staining. White arrows indicate areas of punctate staining and colocalization in the merged images. (D) Pearson Coefficient Correlation (PCC) values indicate a stronger correlation in the healthy tissue [n=10] compared to the diseased tissue in the left atrium (p=0.0040) [n=29] but not the left ventricle (p=ns) [n=29]. Values are means ± SD.

3.3.5 The Relationship of the Cardiac Contractility Biomarker SERCA2a to Ghrelin and GHSR in the diseased Heart

Quantitative fluorescence microscopy was used to measure SERCA2a in the control and diseased cohorts with representative images shown in Fig 3.1G. No differences in overall expression were seen between the diseased and control cohorts (Fig 3.1H). Linear regression analysis showed that SERCA2a had a positive relationship to GHSR, ghrelin and BNP (Fig 3.5C – E) but only in the LV ($r = 0.7893$, $p=0.0348$; $r = 0.7315$, $p=0.0392$; $r = 0.8401$, $p=0.0180$ respectively) and not the LA. Quantification of overall expression of toll-like receptor 4 (TLR4) showed no differences between the diseased and control cohorts (Fig 3.1J). No relationships were present in the control group between SERCA2a and any other biomarker [GHSR ($r = 0.0936$; $p=0.7970$), ghrelin ($r = 0.0089$; $p=0.9385$), BNP ($r = 0.2492$; $p=0.4875$)].

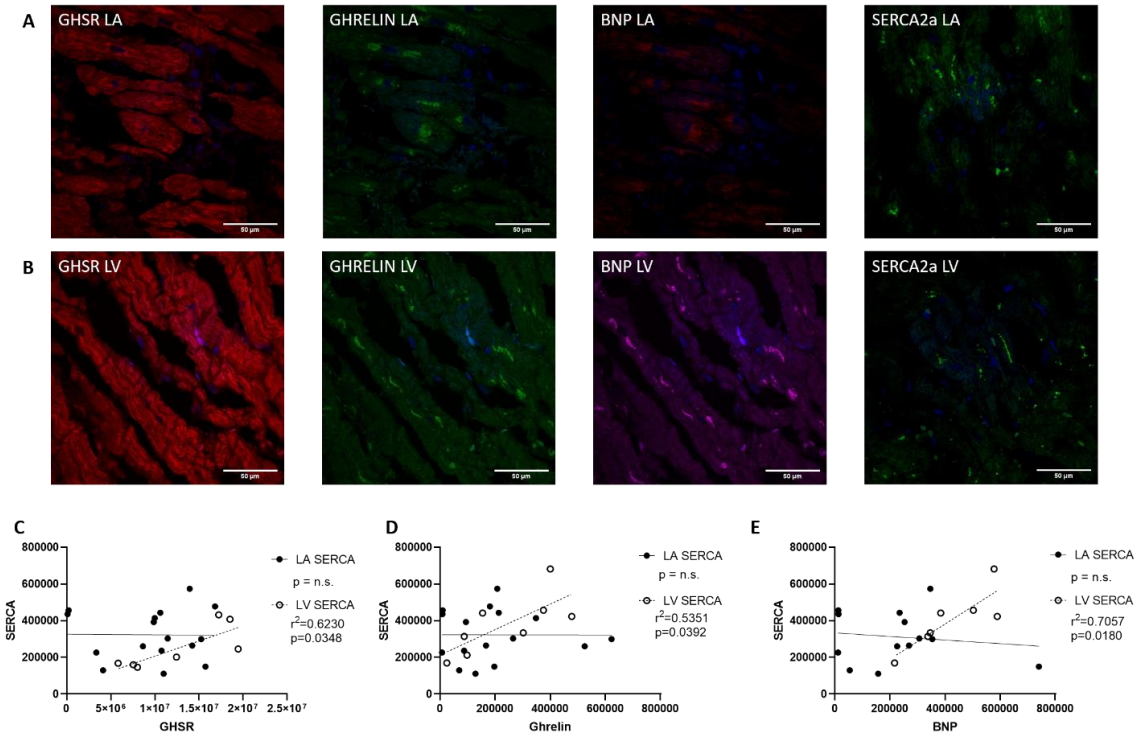

Figure 3.5 SERCA2a correlation to ghrelin-GHSR and BNP

(A) Representative fluorescent confocal images of Cy5-ghrelin(1-19) (red), ghrelin (green), BNP (magenta), and SERCA2a (green) in cardiac tissue of the LA (A in top panels) and the LV (B middle panels). DAPI (blue) nuclear stain in all images. Graphs indicate fluorescence intensities represented by integrated densities where each dot represents one patient sample. A significant linear regression is present in only the LV between SERCA2a and (C) Cy5-ghrelin(1-19) (r = 0.7893; p=0.0348) [LA n=15, LV n=8], (D) ghrelin (r = 0.7315; p=0.0392) [LA n=15, LV n=8], and (E) BNP (r = 0.8401; p=0.0180) [LA n=14, LV n=7]. LA, Left Atrium; LV, Left Ventricle.

3.3.6 Cardiac Fibrosis

Masson's trichrome staining was used to determine the extent of fibrosis in all cardiac tissue samples. There were highly variable amounts of fibrotic deposition (blue) in samples of diseased tissue compared to the non-fibrotic tissue (red) in any given cardiac surgery patient sample but not in the control tissue (Fig 3.6A – C). Quantification of fibrotic tissue showed a significantly higher amount of collagen deposition in diseased tissues of the LA (p=0.0034) but not of the LV (p=0.0509) compared to the control tissues (Fig 3.6D).

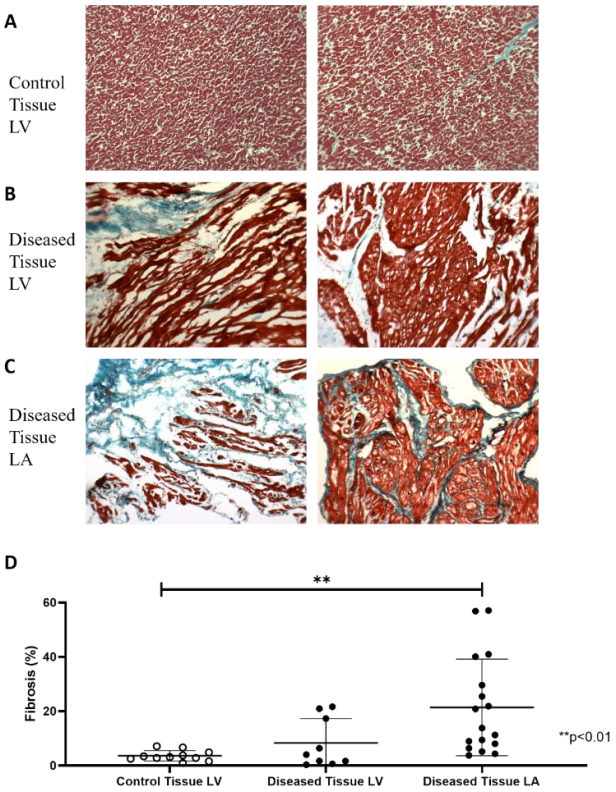

Figure 3.6 Fibrosis deposition in healthy and diseased tissue.

Representative images of fibrotic (blue) and non-fibrotic tissue (red) in control tissue LV (A) and diseased tissues of the LV (B) and the LA (C) show variability in fibrotic deposition in the diseased tissue while not in the control tissue. (D) Graph shows mean ± 95% CI of percentage fibrotic tissue with significantly less fibrotic deposition in the control tissue [n=10] compared to the left atrium (p=0.0034) [n=17] but not the left ventricle (p=ns) [n=11].

3.4 Discussion

In this study, we used our fluorescent ghrelin analog, Cy5-ghrelin(1-19), to examine the expression of myocardial GHSR in relation to that of ghrelin and other known markers of downstream signaling pathways in tissue obtained from patients with valvular heart/ coronary artery disease but without reduced LVEF. We also measured these markers in control, non-diseased, cardiac tissue. In patients with valvular heart disease (±coronary artery disease), there were positive correlations between GHSR and ghrelin which were regionally constrained to the left atrium. Similarly, there were regionally divergent correlations between GHSR and BNP (the gold standard marker of HF) and ghrelin and BNP. The positive correlations with the contractility marker SERCA2a were specific to the left ventricle. In contrast, no correlations between GHSR and ghrelin, or any other biochemical marker were observed in the control tissue. Additionally, we found that both ghrelin and BNP localized to the same intracellular compartment within cardiomyocytes, and this colocalization was slightly disrupted in the left atrium in the heart disease (HD) cohort. Therefore, there was an emergence of region-specific patterns in the myocardial ghrelin-GHSR signalling system in patients with valvular disease despite the absence of measurable changes in heart function.

We have previously shown that GHSR and ghrelin are positively correlated in tissue samples from patients with end-stage heart failure and are correlated negatively with LVEF[11]. Results from other studies also indicate changes in the dynamics of the ghrelin-GHSR system in end-stage heart failure[10] and dilated cardiomyopathy[12], suggesting this cardioprotective ghrelin-GHSR system is abnormally up-regulated when there is injury or stress to the heart[11]. Our present results also show a positive correlation between ghrelin and GHSR in patients with heart disease, but this time in the absence of a decrease in LVEF. As this correlation was not observed in tissue samples from the control group, we suggest that changes in the myocardial ghrelin-GHSR system occur early in the progression of heart disease, (in this study, in hearts subject to increased LV systolic pressures secondary to aortic stenosis) prior to measurable changes in heart function, as defined by the global LVEF.

Post-hoc disaggregation of data by region showed that the positive correlation between ghrelin and GHSR was maintained in the left atrium (LA) but not the left ventricle (LV). Interpretation of these data is very limited as we did not collect data on the LA pressures which are commonly elevated in valvular diseases due to stretching of the atrial wall. We did, however, observe a very slight but significant negative correlation between GHSR in the left atrium and LV diastolic pressure ($r = 0.6887$, $p = 0.0402$). Left ventricular diastolic pressure is elevated in valve disease which is associated with increased LA pressure[24]. In one study by Schwarz *et al.*, in patients with aortic valve disease, there was an elevation in end-diastolic left ventricular pressure and mean left atrial pressure along with significant correlations with myocardial cell diameter[25]. Therefore, in our study of patients with aortic stenosis, it is expected that with the increased LV diastolic pressure, left atrial pressures are also increased. The increased LA pressures may be related to the strong correlation between ghrelin and GHSR. The positive ghrelin-GHSR correlation in the LA but not the LV may also represent a compensatory up-regulation under conditions of mild stress and trauma of the LA without any measurable changes in the heart function as measured by the LVEF. An up-regulation may be increased through GHSR signalling in the LA, which promotes cardiomyocyte survival (through Akt and phosphorylated extracellular signal-related kinase)[5], contractility (through SERCA2a)[26], and inhibits signalling through pro-inflammatory proteins and apoptosis[6,27]. More robust data will be required to establish a concrete relationship between alterations in the ghrelin-GHSR system and onset of LA dysfunction.

In addition to the myocardium, ghrelin and GHSR are also present in the endothelial cells of the aorta, coronary arteries, and pulmonary arteries and veins[28]. Ghrelin is known to have vasoconstrictive effects in the coronary arteries and dose-dependently increases coronary perfusion pressure in a calcium-dependent manner thereby enhancing arteriole contractility[29]. The density of GHSR is increased in the atherosclerotic coronary artery and the saphenous vein compared to the corresponding non-diseased artery and vein[30], indicating that up-regulation of ghrelin-GHSR signalling may occur within the diseased vasculature. In the same study, no differences in GHSR density were observed in the LA or the LV between the ischemic heart disease or dilated cardiomyopathy to the control tissues[30]. Our findings also showed no changes in myocardial GHSR as measured by Cy5-

ghrelin(1-19), and a relatively weak correlation with ghrelin, suggesting that more dramatic changes in GHSR may occur at the site of vascular tissue injury or dysfunction.

The secretion of both natriuretic peptide type-B (BNP) and its N-terminal form (NT-proBNP), the current "gold standard" clinical heart failure (HF) biomarkers, are increased under conditions of cardiomyocyte stress and pressure overload. Circulating BNP levels are also increased in patients with aortic stenosis and mitral regurgitation, and can be used as a potential indication for valve replacement in patients with normal ejection fraction[31]. However, myocardial BNP mRNA does not change in patients who had aortic valve stenosis[32]. In our current study in patients with valvular disease, we also did not find a change in the tissue expression of BNP in either the LA or the LV. If tissue levels of BNP do not change, but levels of circulating BNP increase in valvular disease, it may suggest that the rate of post-translational processing of pro-BNP, rather than transcription or translation, increases in cardiomyocytes.

Interestingly, we found that BNP and ghrelin correlated in the left ventricle, and furthermore, strongly co-localized to the same intracellular compartment within ventricular cardiomyocytes. In healthy individuals, BNP is predominantly localized in the atrium; in heart failure, BNP appears to localize primarily in the ventricles[33]. In aortic stenosis, the endocrine profile of aortic valves, which includes natriuretic peptides, their receptors and processing enzymes, is altered [32]; taken together with our results, we suggest that a regional shift in myocardial endocrine programming may be part of the progression of heart disease to heart failure. This regional shift may extend to other genetic programs as well; in dogs exposed to prolonged rapid ventricular pacing, there were drastic changes in genes expressing apoptosis, cell structure and mobility, and inflammation in the left atrium, while genes involved in metabolism and Ca^{2+} signalling changed only in the left ventricle[34,35]. Therefore, there are clear regional differences in the genetic programs that underlie cardiomyocyte function in heart disease. Further studies will determine the intracellular dynamics of ghrelin and BNP during the progression of heart disease.

We also evaluated GHSR signalling pathways involving contractility and inflammation. We were particularly interested in correlations with SERCA2a, a common marker of

contractility, as it has been shown to be activated through the GHSR signalling pathway, reducing intracellular Ca^{2+} levels and improving LVEF after myocardial infarction[2]. Additionally, we have previously found strong relationships between ghrelin and SERCA2a in both a mouse model of cardiomyopathy[13] and human heart failure[11]. In the present study, we observed a positive correlation between SERCA2a and ghrelin-GHSR only in the left ventricle, which may indicate the importance of contractility signalling in the left ventricle, as it is the predominant chamber for contractile force. Activation of GHSR is known to regulate calcium handling and cardiomyocyte relaxation. This positive correlation in the LV may indicate the promotion of contractile function in the heart through GHSR by enhancing SERCA2a function. GHSR activation causes Gαq11 to activate the protein kinase A/calmodulin-dependent phosphokinases pathway through phosphorylation of phospholamban (PLB) from SERCA2a on the sarcoplasmic reticulum (SR) membrane thereby eliminating the inhibitory effect of PLB on SERCA2a uptake[26]. Removal of this inhibition increases the calcium flux in the SR thereby decreasing intracellular calcium and promoting contractility[2,26]. Additionally, SERCA2a and BNP were also correlated only in the left ventricle. Through binding natriuretic peptide receptor-A, BNP activates cyclic guanosine mono phosphate (cGMP) signalling, which is coupled to L-type calcium channels and intracellular calcium levels through SERCA2a in ventricular cardiomyocytes[36]. As LVEF was unchanged in most of the patients, it is likely that alterations in the relationships between SERCA2a, ghrelin-GHSR, and BNP within left ventricular cardiomyocytes occurs prior to any overt functional changes as detected by echocardiography.

Toll-like receptor 4 (TLR4) is a marker of inflammation elevated in the myocardium in end stage heart failure[37,38], and ghrelin has been shown to attenuate the pro-inflammatory effects of TLR4 in HF[4,39]. In this study, we did not find any significant correlations between TLR4 and GHSR or ghrelin or other biomarkers, which may indicate the TLR4-mediated pro-inflammatory system is not co-regulated with the ghrelin-GHSR system at this point in valvular heart disease.

Another measure of cardiac damage is the presence of fibrosis (collagen and fibroblast deposition) in the myocardium, which increases with HD severity[40,41]. Our results indicate

a significant increase in the fibrotic deposition in only the left atrium of HD patients when compared to the control heart tissues. The apparent lack of left ventricular fibrosis is consistent with the preserved LVEF of this cohort[42]. This accumulation of fibrosis present in the left atrium may be associated to the downstream signalling pathway changes seen in ghrelin-GHSR in this cohort as increased fibrosis deposition is common in the heart during the later stages of heart failure and is a sign of cardiomyocyte damage. However, these results are a bit difficult to interpret due to the large degree of variability in fibrosis in the patient cohort. This result is not surprising due to the heterogenous nature of fibrosis deposition in the myocardium and the subsequent difficulty in obtaining representative biopsy specimens[43].

There are a few limitations to our study to note. Our study was conducted with a small sample size that limited effective disaggregation of the data by region. It is important to note that the control and diseased tissues were embedded differently (paraffin wax vs fixed frozen respectively), although all samples were stained with the same protocols for each marker tested. Quantification of both paraffin and frozen healthy heart tissue is shown in Supplemental Figure 3.S2 where there was no difference in the quantification between either tissue storage method. In addition, control LV tissue was obtained up to 1-3 days post-mortem which could allow for potential protein degradation between time of death and when the tissue samples were put in fixative during autopsy. Finally, we did not obtain blood samples from the patients, which would have provided useful insight into the relationship between myocardial and circulating levels of ghrelin and BNP.

To conclude, we have identified changes in the myocardial ghrelin-GHSR system in human valvular heart disease as compared to control cardiac tissues. The correlation between ghrelin and BNP and the colocalization in the myocardium of these peptides may suggest a regional shift in myocardial endocrine programming of cardiac cells in valvular heart disease. We have shown that the contractility marker SERCA2a was selectively correlated in the left ventricle, potentially as a cardioprotective mechanism prior to decreased LVEF. Our ongoing work will help to characterize GHSR-associated biochemical changes present in early stages of heart disease.

3.5 Supplemental Figures

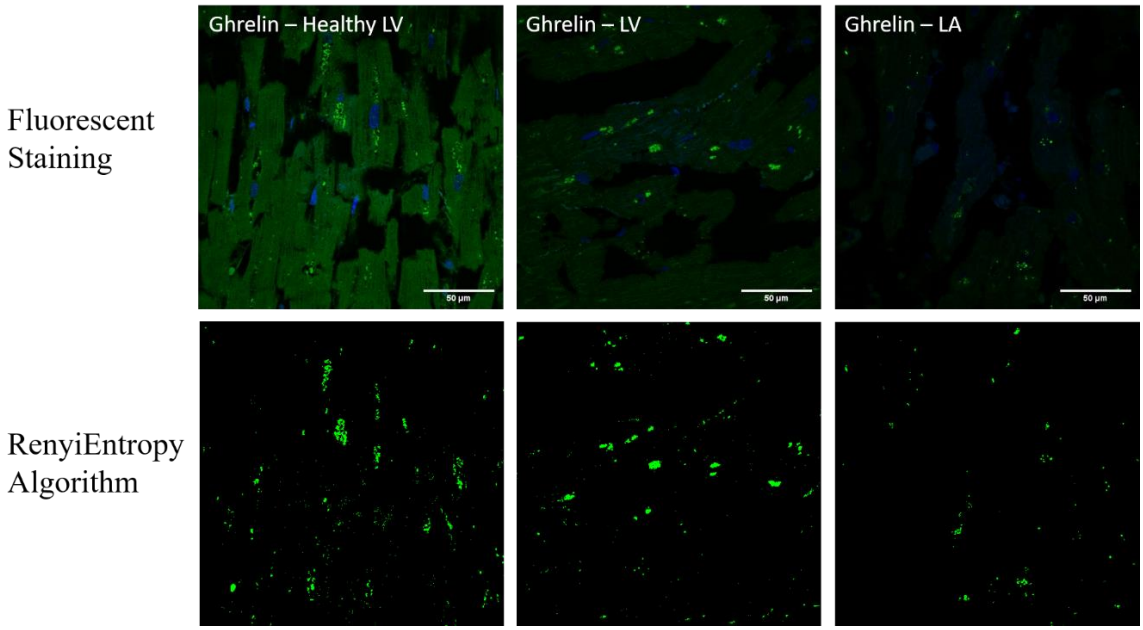

Supplemental Figure 3.S1 Punctate staining with RenyiEntropy algorithm.

Top panel shows representative fluorescent staining of healthy, diseased left atrium (LA) and diseased left ventricle (LV) tissue. Bottom panels show what the RenyiEntrophy algorithm considers positive staining (green) and what is background staining (black) for all types of tissues.

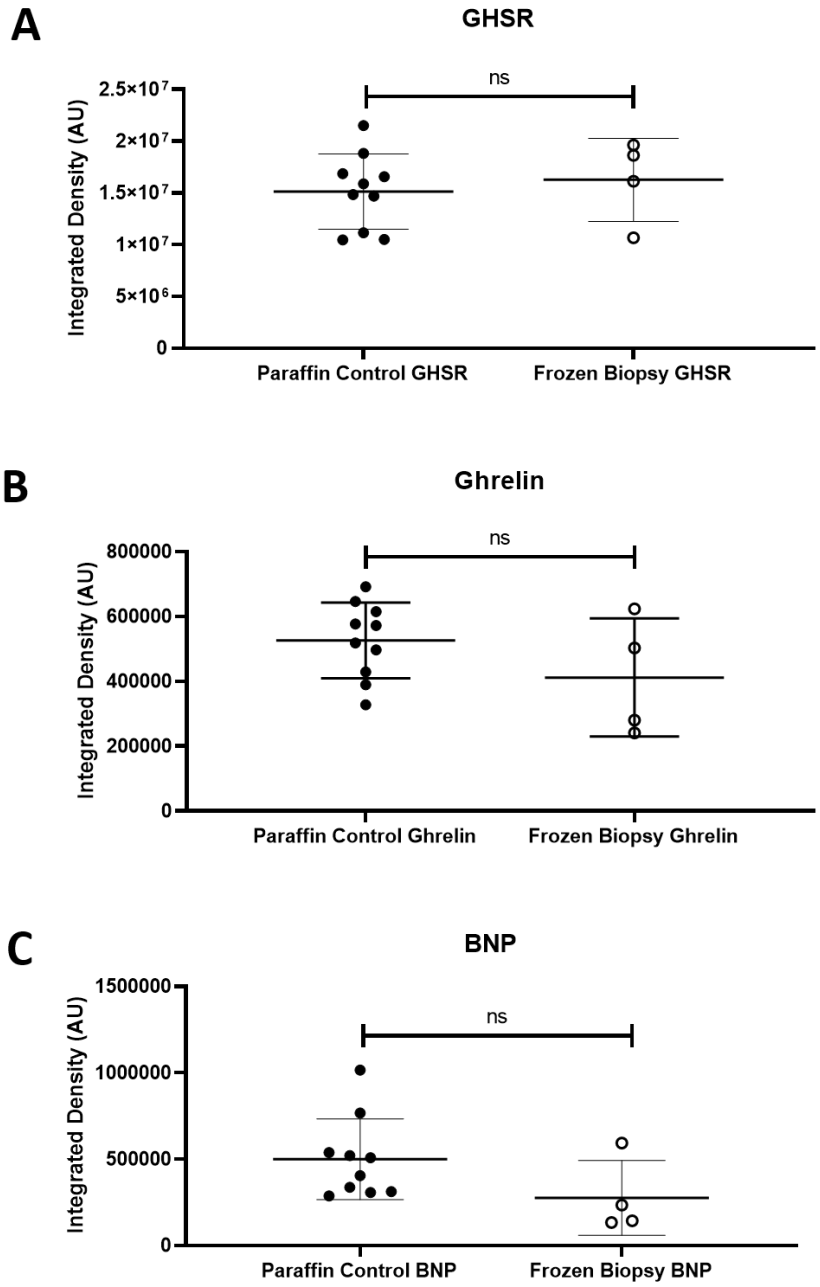

Supplemental Figure 3.S2 Comparison between paraffin embedded control human tissue and frozen healthy heart biopsy samples.

Marker comparison between GHSR (A), Ghrelin (B), and BNP (C) indicated no significant difference in quantification between methods of tissue storage.

3.6 References

1. Ma, Y., Zhang, L., Launikonis, B. S. & Chen, C. Growth hormone secretagogues preserve the electrophysiological properties of mouse cardiomyocytes isolated from in Vitro ischemia/reperfusion heart. *Endocrinology* **153**, 5480–5490 (2012).

2. Ma, Y., Zhang, L., Edwards, J. N., Launikonis, B. S. & Chen, C. Growth hormone secretagogues protect mouse cardiomyocytes from in vitro ischemia/reperfusion injury through regulation of intracellular calcium. *PLoS One* **7**, (2012).

3. Raghay, K., Akki, R., Bensaid, D. & Errami, M. Ghrelin as an anti-inflammatory and protective agent in Ischemia/Reperfusion injury. *Peptides* **124**, (2019).

4. Wang, Q. *et al.* Ghrelin protects the heart against ischemia/reperfusion injury via inhibition of TLR4/NLRP3 inflammasome pathway. *Life Sci.* **186**, 50–58 (2017).

5. Baldanzi, G. *et al.* Ghrelin and des-acyl ghrelin inhibit cell death in cardiomyocytes and endothelial cells through ERK1/2 and PI 3-kinase/AKT. *J. Cell Biol.* **159**, 1029–1037 (2002).

6. Huang, C.-X. *et al.* Ghrelin inhibits post-infarct myocardial remodeling and improves cardiac function through anti-inflammation effect. *Peptides* **30**, 2286–2291 (2009).

7. Yang, C., Liu, Z., Liu, K. & Yang, P. Mechanisms of ghrelin anti-heart failure: Inhibition of Ang II-induced cardiomyocyte apoptosis by down-regulating AT1R expression. *PLoS One* **9**, (2014).

8. Wang, Q. *et al.* Ghrelin Ameliorates Angiotensin II-Induced Myocardial Fibrosis by Upregulating Peroxisome Proliferator-Activated Receptor Gamma in Young Male Rats. *Biomed Res. Int.* **2018**, 1–14 (2018).

9. Yang, C. *et al.* Ghrelin suppresses cardiac fibrosis of post-myocardial infarction heart failure rats by adjusting the activin A-follistatin imbalance. *Peptides* **99**, 27–35 (2018).

10. Beiras-Fernandez, A. *et al.* Altered myocardial expression of ghrelin and its receptor (GHSR-1a) in patients with severe heart failure. *Peptides* **31**, 2222–8 (2010).

11. Sullivan, R. *et al.* Dynamics of the Ghrelin/Growth Hormone Secretagogue Receptor System in the Human Heart Before and After Cardiac Transplantation. *J. Endocr. Soc.* **3**, 748–762 (2019).

12. Aleksova *et al.* Ghrelin Derangements in Idiopathic Dilated Cardiomyopathy: Impact of Myocardial Disease Duration and Left Ventricular Ejection Fraction. *J. Clin. Med.* **8**, 1152–1172 (2019).

13. Sullivan, R. *et al.* Changes in the Cardiac GHSR1a-Ghrelin System Correlate With Myocardial Dysfunction in Diabetic Cardiomyopathy in Mice. *J. Endocr. Soc.* **2**, 178–189 (2018).

14. Pei, X. M. *et al.* Protective effects of desacyl ghrelin on diabetic cardiomyopathy. *Acta Diabetol.* **52**, 293–306 (2015).

15. Fox, K. F. *et al.* Coronary artery disease as the cause of incident heart failure in the population. *Eur. Heart J.* **22**, 228–236 (2001).

16. Kadoglou, N. P. E. *et al.* Serum levels of apelin and ghrelin in patients with acute coronary syndromes and established coronary artery disease-KOZANI STUDY. *Transl. Res.* **155**, 238–246 (2010).

17. Zhang, M. *et al.* Plasma ghrelin levels are closely associated with severity and morphology of angiographically-detected coronary atherosclerosis in Chineses patients with diabetes mellitus. *Acta Pharmacol. Sin.* **33**, 452–458 (2012).

18. Wang, F. *et al.* Ghrelin reduces rat myocardial calcification induced by nicotine and vitamin D3 in vivo. *Int. J. Mol. Med.* **28**, 513–519 (2011).

19. Li, G. Z. *et al.* Ghrelin blunted vascular calcification in vivo and in vitro in rats. *Regul. Pept.* **129**, 167–176 (2005).

20. McGirr, R., McFarland, M. S., McTavish, J., Luyt, L. G. & Dhanvantari, S. Design and characterization of a fluorescent ghrelin analog for imaging the growth hormone secretagogue receptor 1a. *Regul Pept.* **172**, 69–76 (2011).

21. Douglas, G. A. F. *et al.* Characterization of a far-red analog of ghrelin for imaging GHS-R in P19-derived cardiomyocytes. *Regul Pept.* **54**, 81–88 (2014).

22. Locatelli, V. *et al.* Growth hormone-independent cardioprotective effects of hexarelin in the rat. *Endocrinology* **140**, 4024–4031 (1999).

23. Kennedy, D. J. *et al.* Central role for the cardiotonic steroid marinobufagenin in the pathogenesis of experimental uremic cardiomyopathy. *Hypertension* **47**, 488–495 (2006).

24. Braunwald, E. *et al.* The Hemodynamics of the Left Side of the Heart as Studied by Simultaneous Left Atrial, Left Ventricular, and Aortic Pres- sures; Particular Reference to Mitral Stenosis. *Circulation* **XII**, 69–81 (1955).

25. Schwarz, F., Flameng, W., Schaper, J. & Hehrlein, F. Correlation between myocardial structure and diastolic properties of the heart in chronic aortic valve disease: Effects of corrective surgery. *Am. J. Cardiol.* **42**, 895–903 (1978).

26. Warbrick, I. & Rabkin, S. W. Effect of the peptides Relaxin, Neuregulin, Ghrelin and Glucagon-like peptide-1, on cardiomyocyte factors involved in the molecular mechanisms leading to diastolic dysfunction and/or heart failure with preserved ejection fraction. *Peptides* **111**, 33–41 (2019).

27. YUAN, M. M.-J., HUANG, H. & Huang, C.-X. C. Potential new role of the GHSR-1a-mediated signaling pathway in cardiac remodeling after myocardial infarction (Review). *Oncol. Lett.* **8**, 969–971 (2014).

28. Papotti, M. *et al.* Growth hormone secretagogue binding sites in peripheral human tissues. *J. Clin. Endocrinol. Metab.* **85**, 3803–3807 (2000).

29. Pemberton, C. J. *et al.* Ghrelin induces vasoconstriction in the rat coronary

vasculature without altering cardiac peptide secretion. *Am. J. Physiol. - Hear. Circ. Physiol.* **287**, 1522–1529 (2004).

30. Katugampola, S. D., Pallikaros, Z. & Davenport, A. P. [125I-His9]-Ghrelin, a novel radioligand for localizing GHS orphan receptors in human and rat tissue; up-regulation of receptors with atherosclerosis. *Br. J. Pharmacol.* **134**, 143–149 (2001).

31. Bergler-Klein, J., Gyöngyösi, M. & Maurer, G. The Role of biomarkers in valvular heart disease: Focus on natriuretic peptides. *Can. J. Cardiol.* **30**, 1027–1034 (2014).

32. Peltonen, T. O. *et al.* Distinct downregulation of C-type natriuretic peptide system in human aortic valve stenosis. *Circulation* **116**, 1283–1289 (2007).

33. Hystad, M. E. *et al.* Regional cardiac expression and concentration of natriuretic peptides in patients with severe chronic heart failure. *Acta Physiol. Scand.* **171**, 395–403 (2001).

34. Cardin, S. *et al.* Marked differences between atrial and ventricular gene-expression remodeling in dogs with experimental heart failure. *J. Mol. Cell. Cardiol.* **45**, 821–831 (2008).

35. Pelouch, V., Milerová, M., Ošťádal, B., Hučín, B. & Šamánek, M. Differences between atrial and ventricular protein profiling in children with congenital heart disease. *Mol. Cell. Biochem.* **147**, 43–49 (1995).

36. Rose, R. A. & Giles, W. R. Natriuretic peptide C receptor signalling in the heart and vasculature. *J. Physiol.* **586**, 353–366 (2008).

37. Yu, L. & Feng, Z. The Role of Toll-Like Receptor Signaling in the Progression of Heart Failure. *Mediators Inflamm.* **2018**, 1–11 (2018).

38. Yang, Y. *et al.* The emerging role of toll-like receptor 4 in myocardial inflammation. *Cell Death and Disease* vol. **7** 1–10 (2016).

39. Liu, S. P. *et al.* Octanoylated Ghrelin Inhibits the Activation of the Palmitic Acid-

Induced TLR4/NF- κ B Signaling Pathway in THP-1 Macrophages. *ISRN Endocrinol.* **2012**, 1–8 (2012).

40. Barasch, E. *et al.* The Association Between Elevated Fibrosis Markers and Heart Failure in the Elderly: The Cardiovascular Health Study. *Circ. Hear. Fail.* **2**, 303–10 (2009).

41. Travers, J., Kamal, F., Robbins, J., Yutzey, K. & Blaxall, B. Cardiac fibrosis. *Circ. Res.* **118**, 1021–1040 (2016).

42. Burlew, B. S. & Weber, K. T. Cardiac fibrosis as a cause of diastolic dysfunction. *PLoS One* **27**, 92–98 (2002).

43. Nagaraju, C. K. *et al.* Myofibroblast Phenotype and Reversibility of Fibrosis in Patients With End-Stage Heart Failure. *J. Am. Coll. Cardiol.* **73**, 2267–2282 (2019).

Chapter 3

4 Hybrid PET-MRI for Spatio-Temporal Tracking of Alterations in GHSR before and after Myocardial Infarction using a Novel ^{18}F-labelled Ghrelin Analogue

4.1 Introduction

Detection of heart disease (HD) is limited by the current clinically used imaging modalities and circulating cardiac biomarkers. Echocardiography is commonly used to evaluate heart structure and function[1,2] while cardiac magnetic resonance imaging (cMRI) evaluates the heart anatomy, edema, and fibrosis deposition[3]. These modalities can provide information on structural and functional changes when the disease has advanced to a level to become clinically manifest, by which time, prevention and therapy are difficult. Circulating biomarkers may be used as an adjunct to imaging to determine the state of cardiac distress via a blood test. The gold standard biomarkers are natriuretic peptide type-B (BNP)[4,5], secreted from the myocardium upon pressure and volume overload in cardiac tissue, and troponin T and I[6], released into the circulation when the myocardium is damaged. However, limitations of the use of these circulating biomarkers include normal variations due to age, sex, and weight; their association with other comorbidities; and their short half lives in the blood. Therefore, there is a need for the use of *in vivo* molecular imaging techniques to detect HD earlier, when structural changes are not yet prominent, perhaps even prior to clinical symptoms, using a biomarker localized and specific to the cardiac tissue.

One particular marker of interest is the growth hormone secretagogue receptor (GHSR) and its ligand ghrelin. Ghrelin and GHSR form an independent system in the myocardium, and GHSR signalling is associated with cardioprotection through anti-apoptosis[7], anti-inflammation[8,9], contractility[10,11] and cell growth[12]. Their expression levels and associated downstream signalling events are altered in both HD (initial or acute structural and functional changes in cardiac output), and HF (severe function and structural damage to the heart). Myocardial tissue expression of GHSR in patients is elevated in end stage heart failure [13] and cardiac transplantation[14]. In patients with valvular disease there was a decrease in myocardial ghrelin expression with minimal changes in GHSR expression[15]. In rat myocardium after myocardial infarction (MI) the expression of GHSR increased over time as an expected compensatory mechanism for the heart[16]. Therefore, GHSR may be a potential molecular imaging target for detecting molecular changes in the HD process.

Positron emission tomography (PET) imaging is a highly sensitive imaging modality that can be potentially be used to image changes in GHSR *in vivo*. Radiolabelled PET tracers based on the structure of ghrelin have been developed to target GHSR in tissues[17]. More recently, ^{18}F-labelled peptidomimetic and small molecule GHSR agonists have been developed[18,19] with the overall purpose of imaging the dynamics of GHSR expression as a clinically relevant means of detecting disease.

In this study, we characterized a new ^{18}F-tracer targeting GHSR for its ability to evaluate regional dynamics of GHSR over time in a canine model of moderately extensive anterior MI. Using simultaneous multi-tracer PET/MRI, we were able to determine the relationships between GHSR, perfusion and heart function before and after myocardial infarction. Our ^{18}F-tracer was found to bind sensitively and specifically in the left ventricle of the heart, independent of perfusion tracer distributions and global cardiac function.

4.2 Methods

4.2.1 Production of ^{18}F and Synthesis of ^{18}F-LCE470

The [$^{18}F^-$]anion was produced by the PET cyclotron (St. Joseph's Health Care London Ontario, Canada) as a result of the $^{18}O(p,n)^{18}F$ reaction involving proton bombardment of [^{18}O]H_2O. A Waters Sep-Pak® Accell™ PlusLight (46 mg) QMA Carbonate cartridge was pre-activated by slowly treating with EtOH (10 ml) and Milli-Q® water (10 ml) and then flushing with air. The radioactive [$^{18}F^-$] anion was then trapped by drawing up the [^{18}O]H_2O solution containing it through the Sep-Pak.

To potassium carbonate (3.0 mg) and Kryptofix 222 (10.0 mg) was added water (200 µl) and MeCN (800 µl) and the resulting solution used to elute the Sep-Pak® containing [^{18}F]fluoride into a glass vial. The mixture was dried azeotropically (120 °C). The drying step was repeated twice more after the drop-wise addition of anhydrous MeCN (1 ml). The precursor with tosylate (2.0 mg in 0.5 mL of MeCN) was added to the aforementioned mixture, and the mixture was heated at 100ºC for 10 min under sealed conditions. 0.5ml of water containing 0.1% TFA as added. The radiolabelled compound LCE470 was purified

by semi-prep HPLC using 40-80% MeCN in Water (0.1% TFA, flow rate: 4.5ml/min, 15min run, 2min wash).

Radioligand	[^{18}F] LCE470
Radiochemical Yield (%)	42±10
Radiochemical Purity (%)	≥99
Total Synthesis Time (mins)	71±1

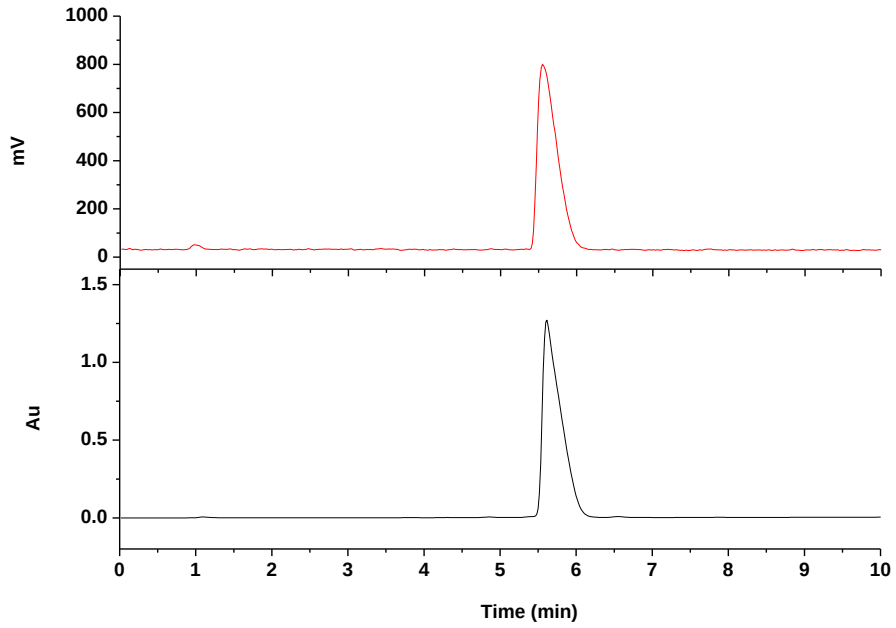

Figure 4.1 Stacked HPLC chromatograms.

(λ = 254 nm) (bottom line) and radio chromatograms (top line) for **LCE470** and **[^{18}F] LCE470**

4.2.2 Animal Use and Surgical Preparation

All animals used in this study were treated in accordance with ethical guidelines of the Canadian Council on Animal Care (CCAC). Animal protocol #2017-006 was approved by the Animal Use Subcommittee at Western University for the experiments described herein.

Four bred-for-research female hounds (19-22kg) were obtained at 10-11 months of age. Anesthesia for surgery was induced using Propofol and maintained with 1.5 – 2.0% isoflurane. The heart was exposed through a left thoracotomy where the mid portion of the left anterior descending coronary artery (LAD) was isolated and occluded for two hours by a snare ligature, a type of ligature to allow for release externally, to induce a myocardial infarction (MI). After the 2-hour occlusion, the ligature was released causing reperfusion in the infarcted area. After MI surgery all animals were allowed to recover for 24 hours before next imaging session and simultaneous PET/MR imaging was performed at multiple time-points over a period of 1.5 years along with one timepoint one week prior to surgery to establish a baseline. All dogs were administered an oral iron chelator (to reduce iron deposition from blood and hemorrhaging in the heart) twice daily for 30 days after MI starting on the day of surgery.

4.2.3 Positron Emission Tomography/ Magnetic Resonance Imaging

Hounds were anesthetized as described above (induced with Propofol and maintained at 1.5 – 2.0% isoflurane) and placed onto the bed of a 3T Biograph mMR (Siemens Medical Solutions, Erlangen, Germany). A hind leg catheter was inserted prior to imaging to allow for injection of tracers and contrast agents. All hounds were imaged with simultaneous PET/MRI for either ^{18}F-LCE470 or ^{13}N-NH_3 at specified time points pre-post and surgery (illustrated in Fig 4.2). Due to technical difficulties, not all tracers were imaged on all days. Technical difficulties include: data corruption of either the PET or cMRI sequences, tracers failed to generate at specific timepoints in the study, or early sacrifice for one animal at 6 months.

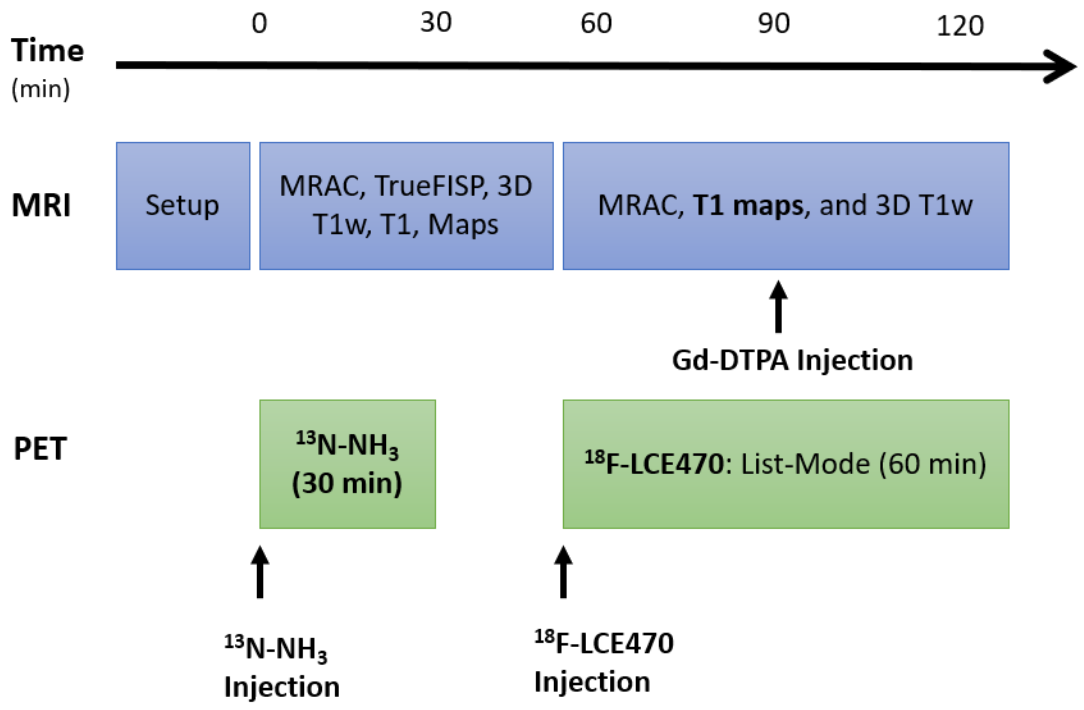

Figure 4.2 PET/MR Imaging Schematic.

Injection of ^{13}N-NH_3 tracer followed by 30 min scan and 50 min after injection the ^{18}F-LCE470 tracer was injected and scanned for 60 min. Simultaneous MRI sequences acquired include: MR attenuation correction (MRAC), TrueFISP cine images to determine heart function and T1 images and 3D T1 weighted images to determine anatomy of the heart. Gadolinium DTPA contrast was injected during the ^{18}F-LCE470 scan to determine scar location and volume.

4.2.3.1 Imaging Perfusion with ^{13}N-NH_3

The PET-MR imaging protocol is illustrated in Figure 4.2. Hounds were imaged at the following time points post-surgery: Day 21 (n=3), Week 16 (n=4), Month 11(n=3). A 30-minute dynamic list-mode PET acquisition was initiated simultaneously with a bolus injection of 6.5 – 7 MBq/kg of ^{13}N-NH_3 (produced in-house at the Lawson Cyclotron Facility). PET data was reconstructed using a 3D Ordered Subset Expectation Maximization reconstruction (3 iterations, 21 subsets, 172 x 172 x 127 matrix size, zoom of 2, and 4 mm Gaussian filter) in the following segments: 12 frames x 10 seconds, 2 frames x 30 seconds, 1 frame x 60 seconds, 1 frame x 360 seconds. An MR-based attenuation correction was used from a two-point Dixon MRI sequence that was segmented into water, fat, lung, and air with constant attenuation coefficients for each tissue listed. PET voxel size was 2.09 x 2.09 x 2.03mm.

4.2.3.2 Imaging GHSR with the Novel PET tracer ^{18}F-LCE470

Fifty minutes following ^{13}N-NH_3 imaging, hounds were imaged with ^{18}F-LCE470 at the following time points: baseline (n=3), day 3 (n=4), Day 21 (n=3), Week 16 (n=4), Month 11(n=3). A 60-minute dynamic list mode PET acquisition was started simultaneously with injection of 6.5 – 7 MBq/kg of ^{18}F-LCE470 in the hind leg catheter. PET data was reconstructed using OSEM as above in the following segments for a dynamic scan: 12 frames x 10 seconds, 6 frames x 30 seconds, 5 frames x 60 seconds, 10 frames x 300 seconds. PET data was also reconstructed using the last 15 minutes to generate a static scan for additional analysis. An MR-based attenuation correction was used as stated above. PET voxel size was 2.09 x 2.09 x 2.03mm.

4.2.3.3 Cardiac MR Imaging

MR imaging was initiated at the beginning of the first PET scan (^{13}N-NH_3 or ^{18}F-LCE470) and continued throughout the full imaging session. MR sequences included short axis cine stacks of the left ventricle synchronized to the Echo signal (true fast imaging with steady-

state free precession (TrueFISP), slice thickness of 6 mm, 356 x 216 voxels with voxel size of 1.09 x 1.09 mm, 10-12 second acquisition time, based in heart rate) with each slice acquired during a breath hold where the ventilator was manually turned off for 10 seconds to allow for image acquisition. To determine the scar formation in the left ventricle, gadolinium diethylenetriamine penta-acetic acid (Gd-DTPA) contrast agent was injected (44 mmol/kg, Gadovist, Bayer) as a bolus at the 30-min time point of the ^{18}F-LCE470 scan. A 3D T1 weighted image was used with LGE to create scar images (Echo triggered inversion recovery sequence with respiratory gating, 256 x 200 x 112 voxels, voxel size 0.625 x 0.625 x 0.99 mm, 4-minute acquisition time, based on heart and respiratory rate). T1 maps (Echo triggered modified Lock-Locker inversion recovery sequence, slice thickness 6 mm, 256 x 144 voxels, voxel size 1.09 x 1.09, 12 second acquisition time, based on heart rate) were generated in a single breath hold to acquire 2- and 4- chamber views (Siemens Work In Progress).

4.2.3.4 TBR Analysis

Static acquisitions were used for the assessment of tracer uptake via calculation of standardized uptake values (SUV) and tissue to blood ratios (TBR) of both ^{18}F-LCE470 and ^{13}N-NH_3, using the online software 3D Slicer 4.8.1 (https://www.slicer.org/). To obtain the TBR for each tracer, the PET and gadolinium-enhanced T1 MR images were uploaded and regions of interest (ROIs) were manually drawn onto the MR images. The regions specified were the infarct region, the left circumflex region, remote tissue of the septal wall, and blood pool. The 2D ROIs were then transferred to the corresponding PET slices. The SUVs were determined where the tissue activity (MBq/ml) was divided by the injected dose (MBq) all multiplied by the body weight (g). To determine the TBR, the SUV of each tissue region (infarct, remote, left circumflex) were divided by the SUV of the blood pool. TBR was automatically calculated for each hound at each time point using the following formula:

(1):

$$TBR: \frac{SUV_{tissue}\left(\frac{g}{ml}\right)}{SUV_{blood\ pool}\left(\frac{g}{ml}\right)}$$

4.2.3.5 Compartmental Modelling of PET Data

Compartmental modelling of both tracers was done by uploading the dynamic list mode scan data to the online software package Carimas 2.10.0.0 (Turku Pet Center, Hospital District of Southwest Finland, https://turkupetcentre.fi/carimas/). For ^{18}F-LCE470, the reconstructed dynamic data from the left ventricle was used to segment the area of the LV automatically (Fig 4.3). Manual corrections were made based on tissue localization in each axis (coronal short axis, vertical long axis, horizontal long axis) and slice.

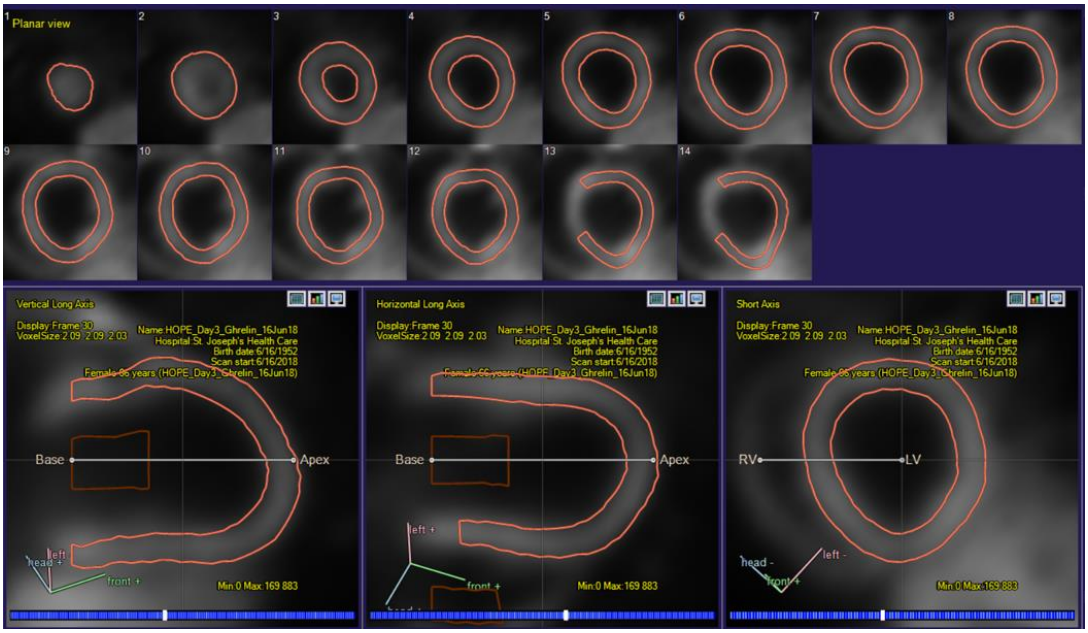

Figure 4.3 Representative images of LV segmentation.

Manual corrections were performed to delineate LV tissue, right ventricle, base and apex of the heart to orientate the program for analysis.

An image-derived arterial input function was extracted from the time-activity curve measured in the blood pool of the left ventricle. This input function, along with the tissue time-activity curves, was used to solve for the kinetics of the tracer uptake in heart tissue using a two-compartment Logan model that accounts for free and bound components of ^{18}F-LCE470[20], as we expect a receptor-ligand reversible interaction based on the natural ghrelin-GHSR system present in the heart. From the Logan analysis, we calculated the distribution volume of ^{8}F-LCE470, and a full tracer kinetic analysis can determine the binding potential and receptor density.

The following equation (2) illustrates the formula of Logan analysis where C_{tissue} represents the pixel-wise time activity curves of the target tissue tracer concentration measured by PET, C_{plamsa} is the tracer concentration in plasma, DVt is the slope of the resulting line, V is the y-intercept or initial concentration ratio at time 0 of the graph. The distribution volume (DV), total distribution for ^{18}F-LCE470 in the tissue, is calculated using a 2-tissue reversible compartmental model shown in the equation (2 – 3) where C_{plasma} is the concentration is tracer in the blood plasma, C_{free} is the concentration of unbound tracer in the tissue, and C_{bound} is the concentration of specifically bound tracer to the receptor. The distribution volume using the kinetic rate constants in equation 3 is represented by equation 4 where BP is the binding potential and AF is the binding affinity of the ligand.

2) $$\frac{\int_0^t C_{tissue}(s)ds}{C_{tissue}(t)} = DVt\ \frac{\int_0^t C_{plasma}(s)\,ds}{C_{tissue}(t)} + V$$

3) 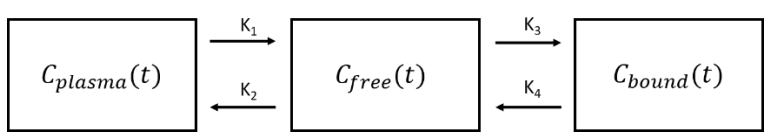

4) $$DV = \left(\frac{K_1}{K_2}\right)\left(1 + \frac{K_3}{K_4}\right) + V_p; BP = \frac{K_3}{K_4}; BP = receptor\ density * AF$$

The Logan analysis generates a polar map of the left ventricle partitioned into 17 individual segments where the outer part of polar map represents the base of the heart and the center is the apex. These segments were manually grouped into three regions: infarct, left circumflex tissue, and remote non-infarcted tissue. The distribution volume (ml plasma/ml tissue) was determined for each of these three regions to calculate the overall tracer distribution in the LV. The segments assigned to each of the three regions was variable for each dog due to differences in infarct size. Within each individual dog, grouped segments were maintained for all timepoints to maintain consistency for all regions. Fig 4.4 shows the 17 segmented polar maps with the three delineated regions outlined for all dogs at day 3.

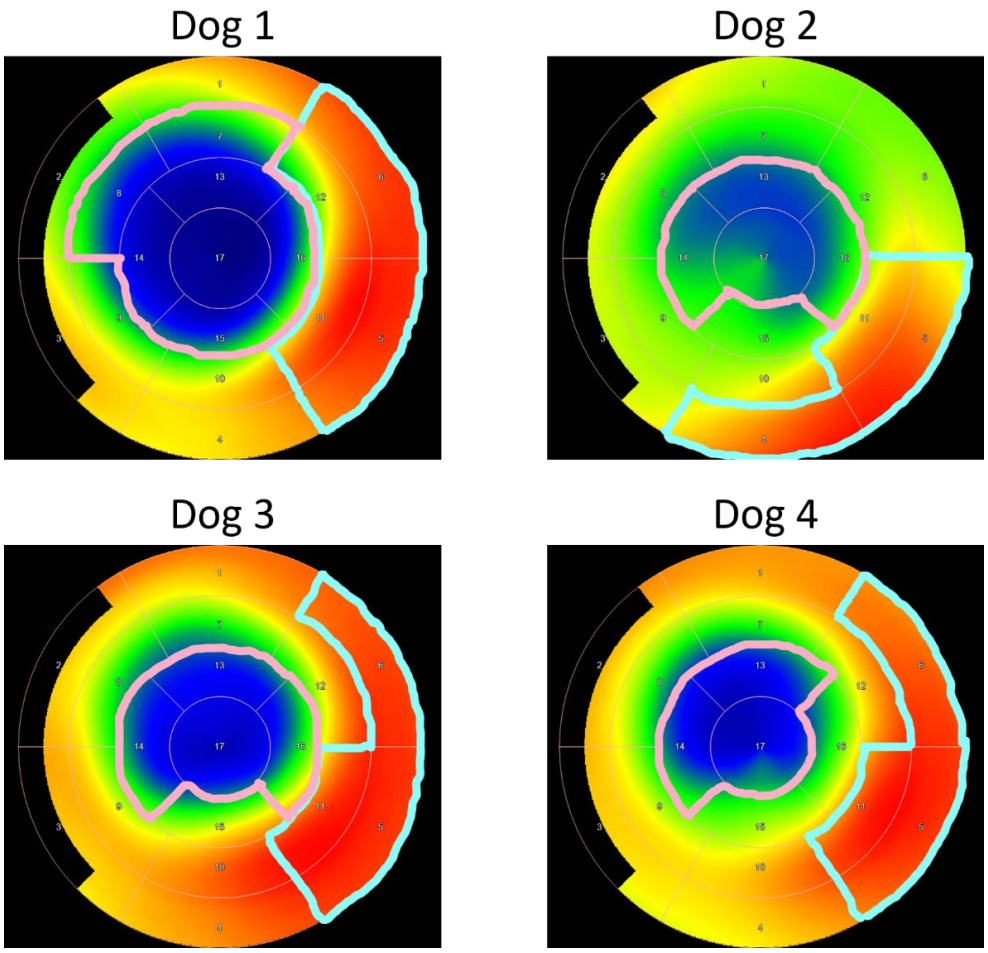

Figure 4.4 Polar map segmentation with manual grouping of segments into 3 regions.

Left circumflex region (in light blue), infarct region (in pink), and remote tissue (all other segments not outlined). All dogs show variability in infarct size and left circumflex tissue.

For more precise mapping of tracer movement over time of the dynamic scan, the three regions (infarct, remote, left circumflex, blood pool) were manually delineated using Matlab R2020a software with custom scripts, and separate time-activity curves were generated for the blood pool in the left ventricle and the 3 tissue regions (Supplemental Fig 4.S1).

For ^{13}N-NH_3 the 30-minute data was segmented automatically in the left ventricle and manual correction was performed as stated for ^{18}F-LCE470. Compartmental modelling for ^{13}N-NH_3 used a 1-tissue compartment model (5) as demonstrated by Degrado *et al*[21] where a polar map was generated and the left ventricle was segmented into 17 individual segments as was done for ^{18}F-LCE470. The rate of tracer movement into the tissue is defined by K1 and is represented as the flow of tracer in the heart. The equation used to generate this compartmental model is illustrated in the following equation (6). C_{tissue} is the concentration in the myocardial tissue, C_{plasma} is the concentration in the blood plasma, FBV is the fractional blood volume in tissue coming from blood plasma and $\otimes$ is the convolution operator.

5) 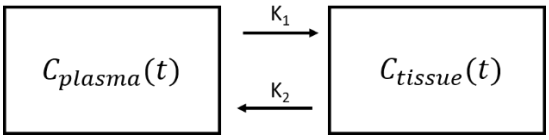

6) $$C_{tissue}(t) = (FBV)\left(C_{plasma}(t)\right) + (1 - FBV)K_1 C_{plasma}(t) \otimes e^{-K_2 t}$$

The K1 (ml/g*min)) and K2 (min^{-1}) values were generated for each segment and segments were grouped into 3 regions in the left ventricle as stated above. These grouped segments were maintained for all timepoints and for each hound to maintain consistency for all regions amongst time.

4.2.3.6 Correlation of ^{18}F-LCE470 and ^{13}N-NH_3 Uptake

In order to determine the relationship between ^{18}F-LCE470 uptake and myocardial perfusion, linear regressions were performed between TBRs of ^{18}F-LCE470 and ^{13}N-NH_3 and between ^{18}F-LCE470 distribution volumes and K1 values of ^{13}N-NH_3. Values from remote and left circumflex areas were selected for analysis; values from the infarct region were not used as tracer uptake in this area was significantly decreased and would therefore skew the regression analysis. Data from day 21, week 16 and month 11 were selected, as these were the time points at which both tracers were injected.

4.2.3.7 MRI Data Analysis

A commercial cardiovascular image analysis software Circle CVI42 (Circle cardiovascular Imaging Inc, Calgary) was used to calculate the following parameters of heart function: left ventricular ejection fraction, stroke volume, end systolic and diastolic volume, and end systolic and diastolic mass. Short axis TrueFISP image series were uploaded and automated segmentation for systole and diastole were generated. Manual adjustments were made when needed to correct for LV segmentation and to select slices in the series at systole and diastole for calculating functional parameters. Slices in the series were excluded due to poor image quality, if the aorta or left atrium were visible, or if they were past the apex. Based on proper segmentation of the series, all cardiac function values were calculated automatically in the online software.

4.2.3.8 Statistical Analyses of PET and MR Imaging Data

Statistical analysis was performed with GraphPad Prism Version 8.2.0 (GraphPad Software, San Diego, California USA, www.graphpad.com). For TBR and compartmental modelling analysis, a repeated measures analysis of variance (ANOVA) for both ^{18}F-LCE470 and ^{13}N-NH_3 were used to determine regional differences at any given time point pre- and post- myocardial infarction. Corrections for multiple comparisons were performed using Tukey's *post-hoc* test. Statistical analysis of functional MR data was calculated using

an ANOVA with Tukey's *post-hoc* test for multiple comparisons based on each imaging time point. All statistical analyses were completed with significance set at $p<0.05$. PET and MR Images were generated using 3D Slicer software where MR and PET images were optimized with individual window/levelling for each individual dog at each time point.

4.2.4 Tissue Harvesting and Imaging Acquisition

At 1.5 years after MI, animals were sacrificed, and tissue was obtained for histological analysis. Immediately after sacrifice the chest was opened and the entire heart was removed. Myocardial tissue samples (roughly 1 cm^3) were collected in duplicate from areas within the left ventricle including center of infarct, remote (non-infarcted) tissue, and the territory served by the left circumflex artery. Tissue was immediately snap frozen in liquid nitrogen and kept at -80°C until use. Frozen tissue blocks were embedded in optical cutting temperature medium (OCT) and left to freeze at -80°C overnight. Tissue was cryosectioned at 5-6 µm and adhered to positively charged microscope slides. All tissue sections were stored at -80°C until use. Tissue sections were subsequently fixed using ice cold acetone for 15 minutes at room temperature (RT). All tissues were then stained for GHSR using our custom-made far-red ghrelin analogue (cyclo 12,16)-[Dpr_3(octanoyl),Lys_{20}(SulfoCy5)] ghrelin(1-20)[22], termed Cy5-cyclo-ghrelin(1-20), at a 20 µM concentration for 1 hour at RT. We have previously used [Dpr^3(n-octanoyl),Lys^{19}(sulfo-Cy5)]ghrelin(1-19) to detect GHSR in human[14] and mouse cardiac tissue[23]. Cy5-cyclo-ghrelin (1-20) has a greatly improved affinity towards GHSR (1.0 nM). Samples were then stained with 4',6-diamidino-2-phenulindole (DAPI) at a concentration of 300 nM for 6 minutes at RT followed by mounting with ProLong Diamond Antifade (Life Technologies) to prevent photobleaching.

High resolution images were captured with a Nikon A1R Confocal Microscope at 60x magnification using an oil immersion lens. For each tissue location in the heart (technical replicate of 2), five random fields of view were captured with microscope parameters (exposure time, gain and LUT) set the same for all tissue sections.

In addition, we evaluated regional fibrosis deposition using Masson's Trichrome and tissue morphology using hematoxylin and eosin (H&E). Adjacent sections were stained with Masson's Trichrome and H&E by the Molecular Pathology Department at Robarts Research Institute. Images of all cardiac tissue (infarct, edge of infarct, remote, left circumflex) were acquired using bright field microscopy at 10X, 20X and 40X magnifications with a Zeiss Axioskope EL-Einsatz microscope and Northern Eclipse software as described previously[14,15].

Blood plasma was obtained at all time points prior to imaging to evaluate circulating levels of ghrelin. Samples of whole blood were added to tubes containing a complete mini protease inhibitor (Sigma Aldrich) to inhibit degradation of active circulating biomarkers. The blood was centrifuged at 3000rpm for 10 min at 4°C to separate red blood cells from plasma. The plasma was kept at -80°C until end of the study for analysis. Levels of canine ghrelin (CGTMAG-98K-02 - Millipore Sigma) were measured using multiplexed immunoassay kits according to manufacturers' instructions (R&D Systems, Minneapolis, MN). A Bio-Plex 200 readout system was used (Bio-Rad), which utilizes Luminex® xMAP fluorescent bead-based technology (Luminex Corporation, Austin, TX). Levels were automatically calculated from standard curves using Bio-Plex Manager software (v. 6.1, Bio-Rad).

4.2.4.1 Tissue Image Analysis

Images of tissue GHSR were analyzed with FIJI v. 1.49v, a distribution of ImageJ software (National Institutes of Health). An algorithm built into ImageJ, Percentile[24], was used to quantify regional distribution of GHSR in cardiac tissue. The value assumes the threshold of all foreground pixels is 0.5 and therefore quantifies the integrated density of the positively stained tissue. The integrated density represents the mean intensity of the positive signal above the threshold in scaled units divided by the area in pixels. Therefore, this algorithm only captured foreground images and calculated the intensity values based on a percentile value of 0.5.

4.2.4.2 Correlation of ^{18}F-LCE470 Uptake and Distribution Volume to Tissue GHSR and Plasma Ghrelin

In order to determine the sensitivity of the GHSR-targeted PET tracer ^{18}F-LCE470 to GHSR tissue levels, both TBR and distribution volumes obtained at the final imaging session (18 months) were correlated with fluorescence intensities of Cy5-cyclo-ghrelin(1-20). Values from all tissue regions were pooled to obtain a robust sample size.

To determine the impact of circulating ghrelin on LCE470 tracer binding in the heart, plasma ghrelin levels were compared to LCE470 distribution volume at all time points from baseline to 12 months post MI. Linear regression of plasma ghrelin and ^{18}F-LCE470 distribution volume were compared based on region (infarct, remote, circumflex).

4.2.4.3 Statistical Analyses

Statistical analysis was performed with GraphPad Prism Version 8.2.0 (GraphPad Software, San Diego, California USA, www.graphpad.com). Unpaired student t-tests and a one-way ANOVA analyses were used to compare overall GHSR expression in tissue based on region in the left ventricle. Correlation analyses of tissue and PET values were performed using linear regression analysis. All statistical analyses were completed with significance set at $p<0.05$.

4.3 Results

4.3.1 ^{18}F-LCE470 Tracer Uptake in the Left Ventricle

Standardized uptake value ratios (TBR) for ^{18}F-LCE470 were calculated at baseline, day 3, day 21, week 16 and month 11 post-MI overall for all dogs (n=4). TBR was significantly elevated in the left circumflex region compared to both the remote (p=0.0348) and infarct (p=0.0003) regions over time (Fig 4.5a). TBR in the infarct region was significantly decreased over time compared to the remote tissue (p=0.0365). Representative PET/MR images from one dog are shown in Fig 4.5b at all time points analyzed in TBR analysis. The PET signal in the LV at baseline shows a uniform distribution of tracer binding. After MI, the tracer uptake decreases in the infarct area compared to the remote and circumflex regions and this pattern is present at acute and chronic time points.

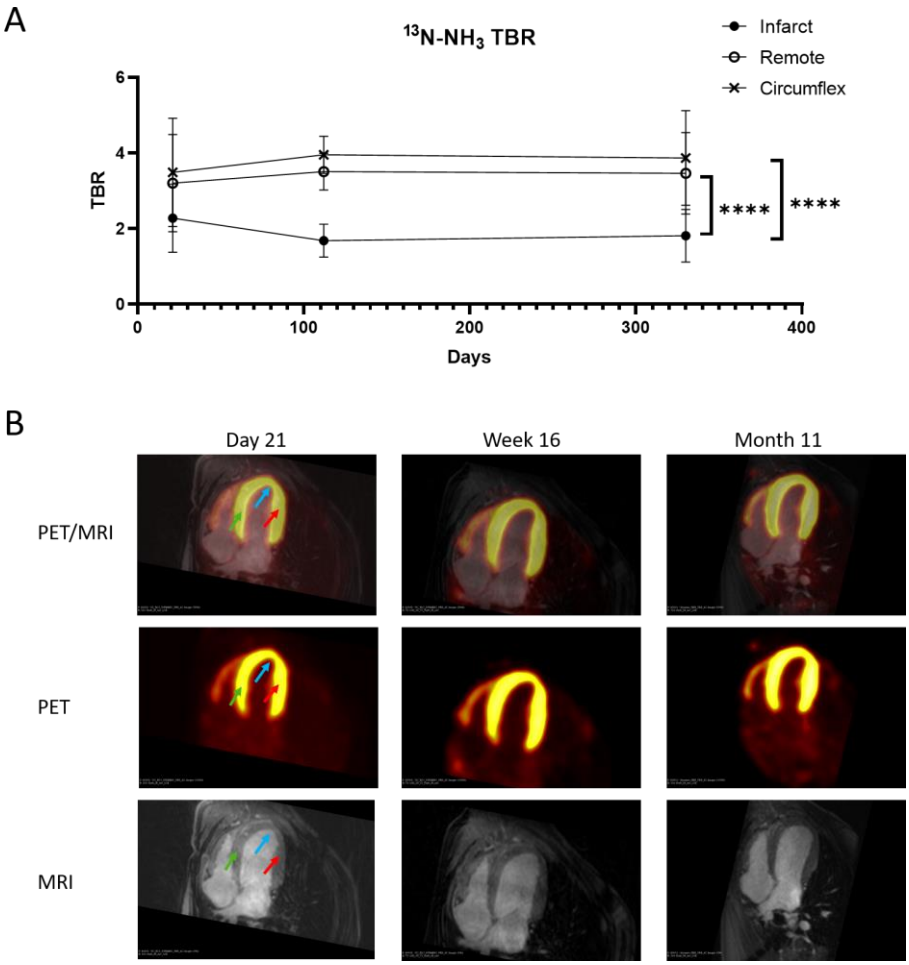

Figure 4.5 In vivo ^{18}F-LCE470 in canine model of myocardial infarction (n=4).

A) Tissue to Blood Ratio (TBR) for tracer ^{18}F-LCE470 over time in the left ventricle from baseline to 330 days post-myocardial infarction. Values calculated from static scan at 45-60 min post-injection where three regions were delineated: infarct, remote non-infarcted tissue, left circumflex tissue. For overall canine TBR values there was a significant difference between infarct and remote regions (*p=0.0365); remote and circumflex regions (*p=0.0348); infarct and circumflex regions (***p=0.0003). B) Representative images of the four-chamber view of the left ventricle from one dog depicting the PET, MRI, and fused PET/MR images for all timepoints shown in the graph above. Arrows point to the 3 regions of interest including: Infarct (blue), Remote (green), Circumflex (red). After MI there is minimal uptake of tracer in the infarct while remote and circumflex increase. This pattern is present at both acute and chronic time points.

The regional dynamics of GHSR is represented by the distribution volume of ^{18}F-LCE470 and is presented at all time points for each individual dog to show regional patterns in tracer uptake in the LV (Fig 4.6a). Similar to the TBR analysis, ^{18}F-LCE470 distribution volume in the area of infarct was significantly decreased compared to the left circumflex area at any given time point post-MI in all dogs ($p<0.001$). There was a slight decrease in tracer uptake in the infarct region in dogs 2 and 4 only. One pattern that emerged in dogs 1, 2 and 3 was a significant increase ($p<0.05$) in ^{18}F-LCE470 distribution volumes in the left circumflex region compared to the remote tissue at week 16 and month 11 post-MI, a difference that was not present at baseline. Interestingly, this pattern was also observed in dogs 2 and 3 at acute time point day 3. Polar maps (Fig 4.6b) were generated for a visual representation of how the LV volume was segmented for the calculation of distribution volume in the different regions of the left ventricle. Distribution volume in polar maps indicated a lower uptake in the center of infarct (shown in green) while there is increased tracer binding in the remote area (yellow to orange colour) and left circumflex tissue increased in uptake even further (dark orange to red colours).

Dynamic ^{18}F-LCE470 tracer uptake over time was evaluated based on region (infarct, remote, left circumflex area, blood pool) at all time points including baseline, day 3, day 21, week 16, and month 11 (Supplemental Fig 4.S1). Tracer uptake in the infarct slightly decreased after Mi compared to baseline while both remote and left circumflex regions increased in tracer uptake after MI. Tracer in the blood showed quick washout with rapid decreased uptake.

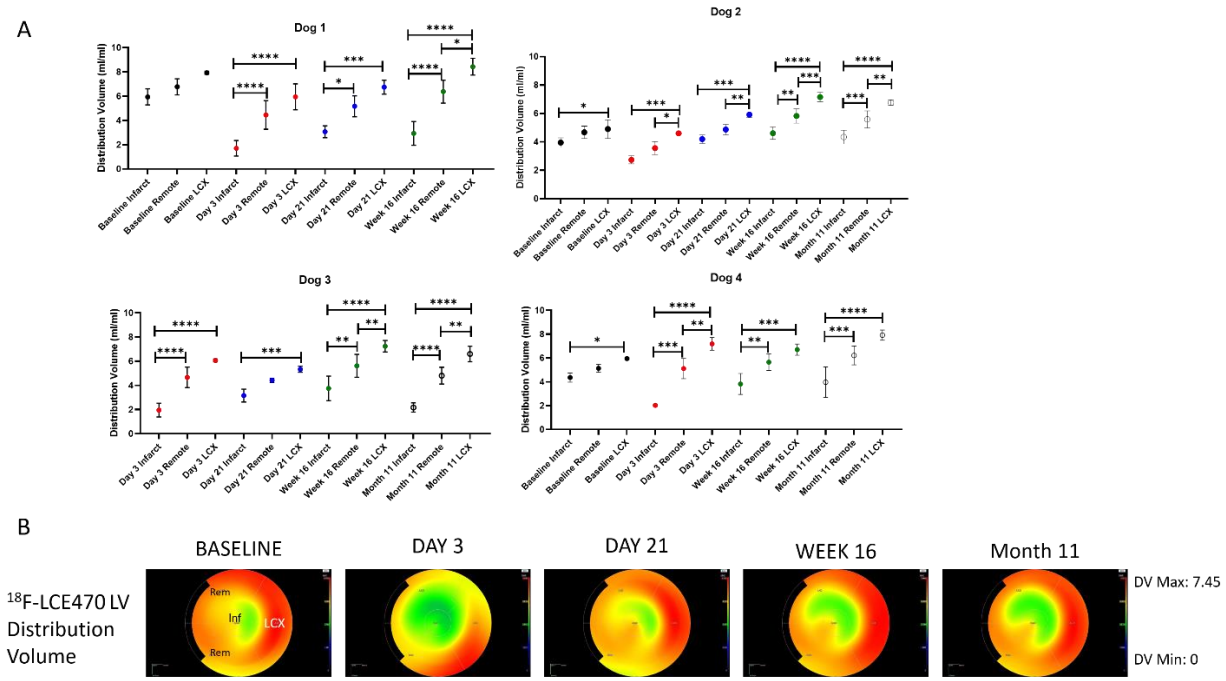

Figure 4.6 Compartmental modelling of ^{18}F-LCE470 in the left ventricle of canine hearts (n=4).

A reversible receptor-ligand interaction (Logan analysis) was used for compartmental modelling of this novel tracer. A) The distribution volume was calculated for all dogs shown in each graph. The left ventricle was segmented into 3 regions for each timepoint: infarct, remote non-infarcted region, left circumflex region. [Black – Baseline; Red – Day 3; Blue – Day 21; Green – Week 16; White – Month 11] Significant differences were seen between all regions at most timepoints, particularly between infarct and remote and infarct and circumflex while these differences were not seen at baseline. (*p<0.05; **p<0.01; ***p<0.001; ****p<0.0001) B) Representative polar maps of the left ventricle for one dog at all time points imaged with the ^{18}F-LCE470 tracer. All images are scaled the same with maximum DV of 7.45 and minimum DV 0. Images depict the binding pattern of the tracer in the left ventricle showing the lower uptake in the apex/infarct of the heart at the center of the map (green colour), with moderate uptake in the remote tissue (yellow - orange colour), and increased uptake in the left circumflex area at the right middle to bottom (red). [LCX – left circumflex tissue; Rem – remote tissue; Inf – infarct]

4.3.2 Perfusion Throughout the Left Ventricle

$^{13}N\text{-}NH_3$ was used to determine changes in regional perfusion in the LV using TBR at day 21, week 16 and month 11 post-MI overall for all dogs (n=4) (scans at baseline and day 3 post-MI were not obtained). As expected, TBR was significantly decreased in the area of infarct ($p<0.0001$) at all time points compared to the remote and left circumflex regions; however, there were no differences in TBR between the remote and left circumflex tissue at any time point (Fig 4.7a). Representative PET/MR images from one dog are shown in Fig 4.7b. The PET signal in the LV after MI shows decreased tracer uptake in the infarct area compared to the remote and circumflex regions. This pattern is present at acute and chronic time points.

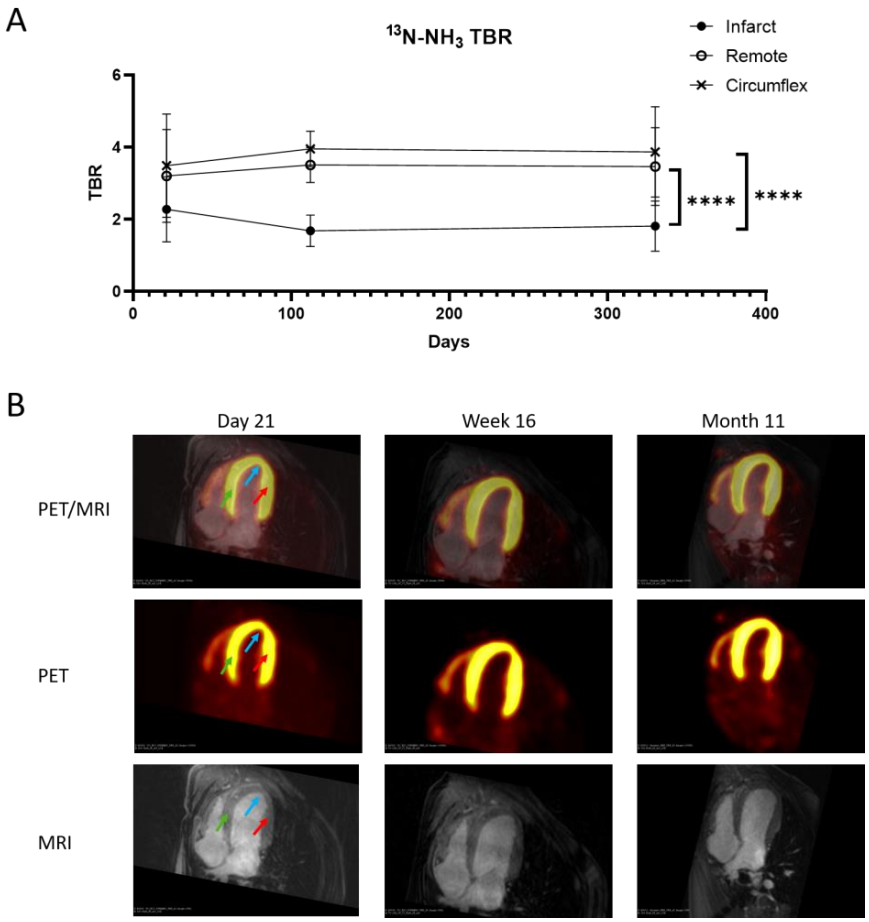

Figure 4.7 Analysis of perfusion imaging tracer in dogs (n=4).

Due to technical difficulties perfusion imaging was only initiated at day 21. A) Tissue to Blood Ratio (TBR) for tracer ^{13}N-NH$_3$ over time in the left ventricle from day 21 to 330 days post-myocardial infarction. Values calculated from static scan of 9-15 min where three regions were delineated: infarct, remote non-infarcted tissue, left circumflex tissue. For overall canine TBR values there was a significant difference between infarct and remote regions (****$p<0.0001$); infarct and circumflex regions (****$p<0.0001$); but no significant difference between remote and circumflex regions. B) Representative images of the for-chamber view of the left ventricle from one dog depicting the PET, MRI, and fused PET/MR images for all timepoints shown in the graph above. Regions are delineated by coloured arrows including infarct (blue), remote tissue (green), left circumflex tissue (red). The PET images have decreased distribution of ammonia in the infarct region compared to the remote and circumflex regions at all time points.

The rate of $^{13}N\text{-}NH_3$ uptake (K1) into the tissue was determined at all timepoints for each individual dog to allow for visualization of perfusion patterns (Fig 4.8a). There were significant differences in the rate of tracer perfusion pattern between the infarct and both the remote ($p<0.05$) and left circumflex ($p<0.05$) tissues at week 16 and month 11 in dogs 2 and 3, and at day 21 and week 16 in dog 1. There were no significant differences in K1 in dog 4. There was also no difference in K1 between the remote and left circumflex regions at any time points in any dog. A visual representation of the regional rate of tracer perfusion pattern in the LV is shown in polar maps representative of one dog (Fig 4.8b). These polar maps demonstrate the 3 regions evaluated (left circumflex region, remote tissue, infarct) where there was a decreased perfusion pattern in infarct (green to yellow) and an increased perfusion pattern in the remote and circumflex regions (orange to red). There appeared to be no visual differences between perfusion patterns in the remote or circumflex regions.

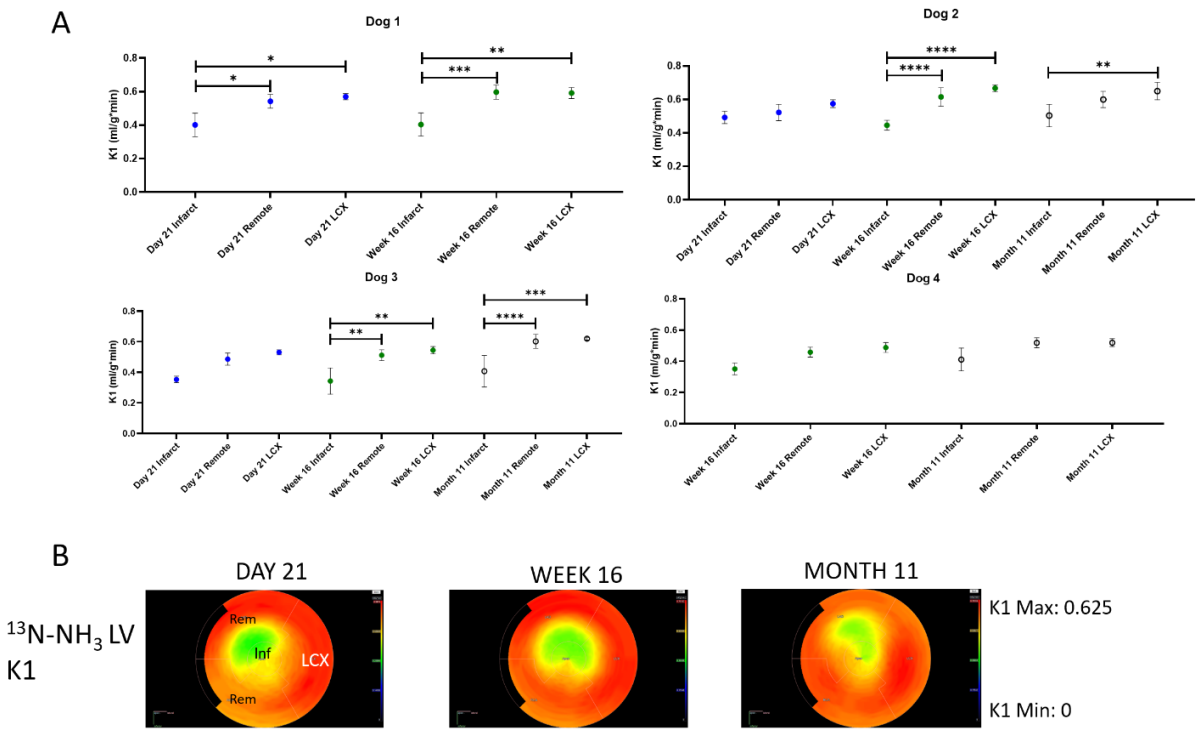

Figure 4.8 Compartmental Modelling of Perfusion Tracer ^{13}N-NH$_3$ in the left ventricle of canine hearts (n=4).

A 1-Tissue compartment model was used for this tracer in the canine heart. A) The K1 values were calculated for all dogs shown in each graph. The left ventricle was segmented into 3 regions for each timepoint: infarct, remote non-infarcted region, left circumflex region. [Blue – Day 21; Green – Week 16; White – Month 11] Significant differences were seen at some time points between infarct and remote and infarct and circumflex while no differences were seen between remote and circumflex at any timepoint. (*p<0.05; **p<0.01; ***p<0.001; ****p<0.0001) B) Representative polar maps of the left ventricle for one dog at all time points imaged with the ^{13}N-NH$_3$ tracer. All images were normalized for maximum flow (0.625) to the minimum flow (0). Images depict the rate of tracer movement in the left ventricle showing the lower perfusion in the apex/infarct of the heart at the center of the map (green colour), with moderate perfusion in the remote tissue (orange - red colour), and no differences in colour perfusion of the left circumflex area right middle to bottom (orange - red). [LCX – left circumflex tissue; Rem – remote tissue; Inf – infarct]

4.3.3 ^{18}F-LCE470 Uptake Does Not Correlate with Perfusion in Remote or Left Circumflex Regions

To assess whether the regional flux of ^{18}F-LCE470 could be accounted for by perfusion alone, linear regression analysis was applied for TBR values of both tracers (Figure 4.9A), and to the distribution volumes of ^{18}F-LCE470 (representing GHSR density) and adjusted K1 values for ^{13}N-NH_3 (representing the rate of perfusion (Figure 4.9B). Linear regressions were separated by day of scanning and were limited to the time points at which ^{13}N-NH_3 scans were acquired (Day 21, Week 16 and Month 11 post-infarct), and to the remote and left circumflex regions. There were no significant linear regressions at any time point between TBR values of the tracers (Fig 4.9a). There were also no significant linear regressions between GHSR density and the rate of perfusion at any time point (Fig 4.9b).

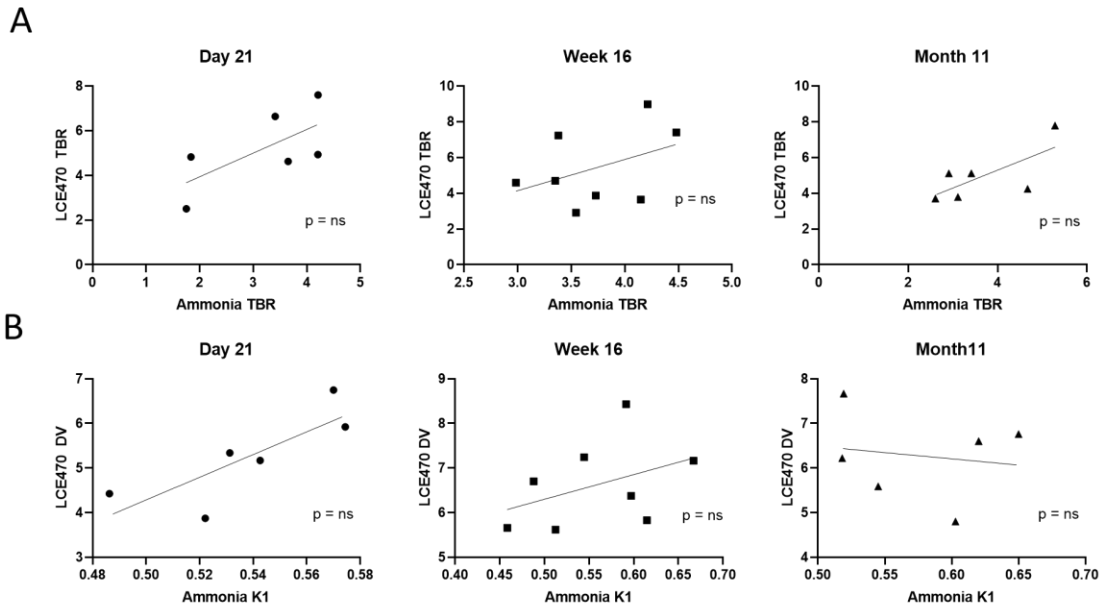

Figure 4.9 Correlation of ^{18}F-LCE470 and ^{13}N-NH$_3$.

Data derived from the remote and left circumflex tissues from all dogs were pooled. A) Linear regression analysis of TBR values showed no correlation at any given time point. B) Linear regression analysis showed no correlation between tracer patterns in the remote and circumflex areas at any time point.

4.3.4 Specificity of ^{18}F-LCE470 Binding in Cardiac Tissue

Tissue quantification of GHSR was determined with quantitative fluorescence microscopy using the fluorescent ghrelin analogue Cy5-cyclo-ghrelin(1-20)[22]. Representative images of the infarct, remote and left circumflex regions are shown in Fig 4.10a, and quantification of fluorescence in each region for each individual dog (n=3) is shown in Fig 4.10b. In all dogs, Cy5 fluorescence in the left circumflex region was significantly increased compared to the infarct region ($p<0.0001$). Interestingly, there was a significant increase in fluorescence in the left circumflex region compared to the remote region in two of three dogs ($p<0.001$). Tissue specificity was demonstrated through a blocking study with hexarelin (GHSR blocking agent) shown in Fig 4.11 where blocking showed a drastic decrease in fluorescent signal in the canine myocardial tissue.

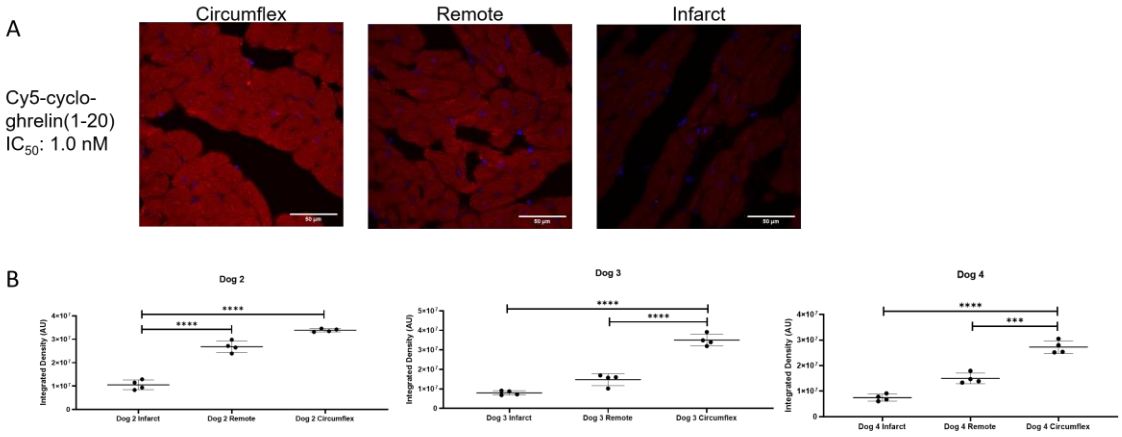

Figure 4.10 Tissue Characterization of GHSR in Canine Heart.

A) Representative fluorescent images of GHSR in the canine heart with the novel imaging agent Cy5-ghrelin stapled peptide. Tissue gathered from 3 regions of the heart at sacrifice: infarct, remote non-infarcted tissue, left circumflex tissue with red stain showing diffuse staining of GHSR in the heart and DAPI nuclear stain in blue. B) Quantification of fluorescent images for each dog (n=3) at end point. Significant differences seen between infarct and remote, remote and circumflex. (***$p<0.001$; ****$p<0.0001$)

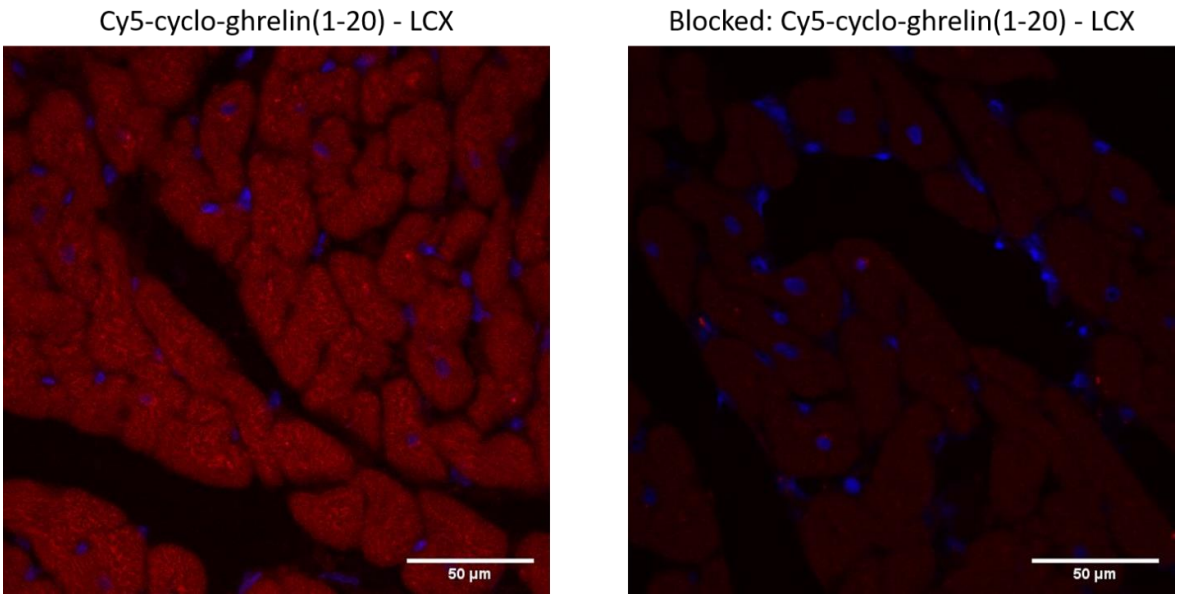

Figure 4.11 Cy5-cyclo-ghrelin(1-20) specificity in canine tissue.

Tissue shown without blocking agent on left and with blocking agent (hexarelin) on right. Blocked tissue showed decrease in fluorescence signal in the LCX region. LCX: left circumflex tissue.

We then determined the sensitivity of the GHSR-targeted PET tracer ^{18}F-LCE470 by linear regression to Cy5-cyclo-ghrelin(1-20)[22] fluorescence in the left ventricle by pooling data from the infarct, remote and left circumflex regions (Fig 4.12). There was a significant positive linear regression between tissue Cy5-cyclo-ghrelin(1-20) fluorescence and ^{18}F-LCE470 TBR values (p=0.0070, r=0.8185). Tissue Cy5-cyclo-ghrelin(1-20) fluorescence was also positively and significantly correlated to ^{18}F-LCE470 distribution volume (p-0.0054, r=0.8318).

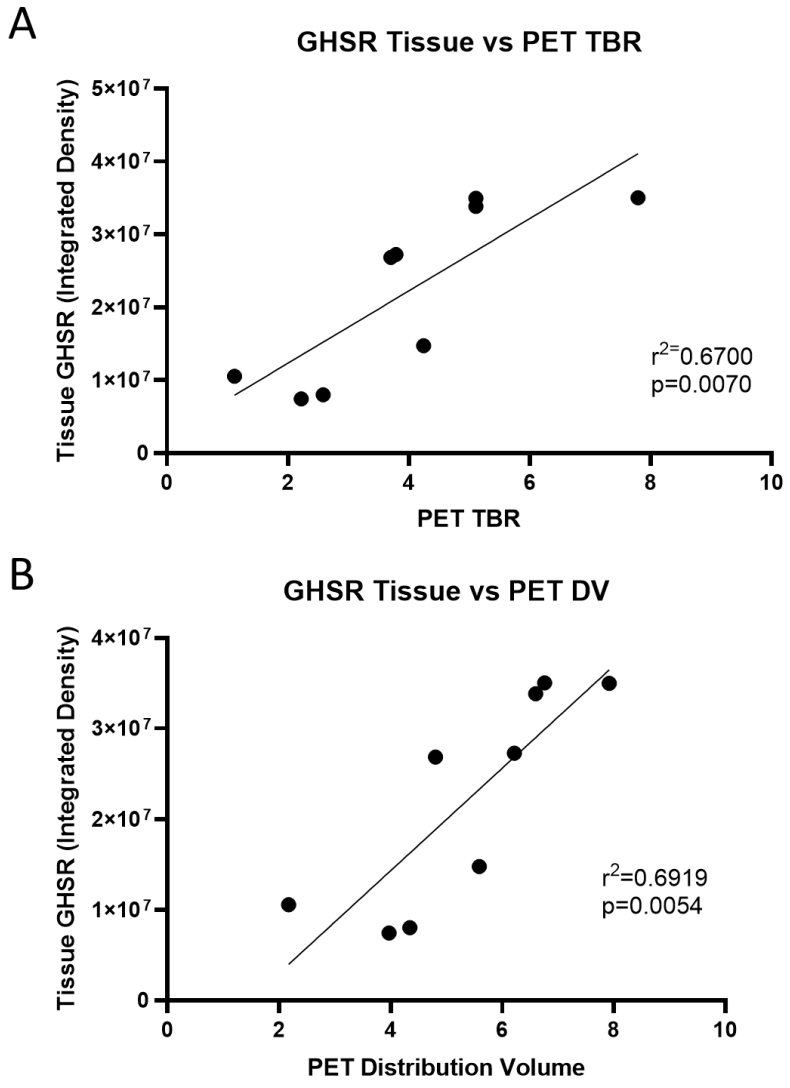

Figure 4.12 Correlation of GHSR tissue analysis to ^{18}F-LCE470 TBR and distribution volume at end point.

A) Linear regression of tissue GHSR values and PET TBR for all dogs (n=3) at endpoint. There was a significant linear regression between tissue and PET with r = 0.8185 and p=0.0070. B) Tissue GHSR linear regression with ^{18}F-LCE470 distribution volume (DV) showing significant linear regression, r = 0.8318 and p=0.0054.

4.3.5 Fibrotic Deposition and Circulating Ghrelin

Fibrotic deposition was determined regionally in the left ventricle using Masson's trichrome stain (Fig 4.13a). Qualitative images show a large amount of fibrosis (blue) in the infarct while the remote and left circumflex areas were predominantly non-infarcted areas (red). Hematoxylin and eosin (H&E) stain also qualitatively showed the distinct changes in tissue morphology and type between in the infarct and both remote and left circumflex areas. These images clearly show the extensive fibrotic deposition in the infarct.

Circulating ghrelin levels were evaluated at all time points and correlated to the LCE470 distribution volume tracer binding (Fig 4.13b). There were no significant linear regressions in any region evaluated (infarct, remote, circumflex) where changes in circulating ghrelin levels did not change with LCE470 tracer uptake.

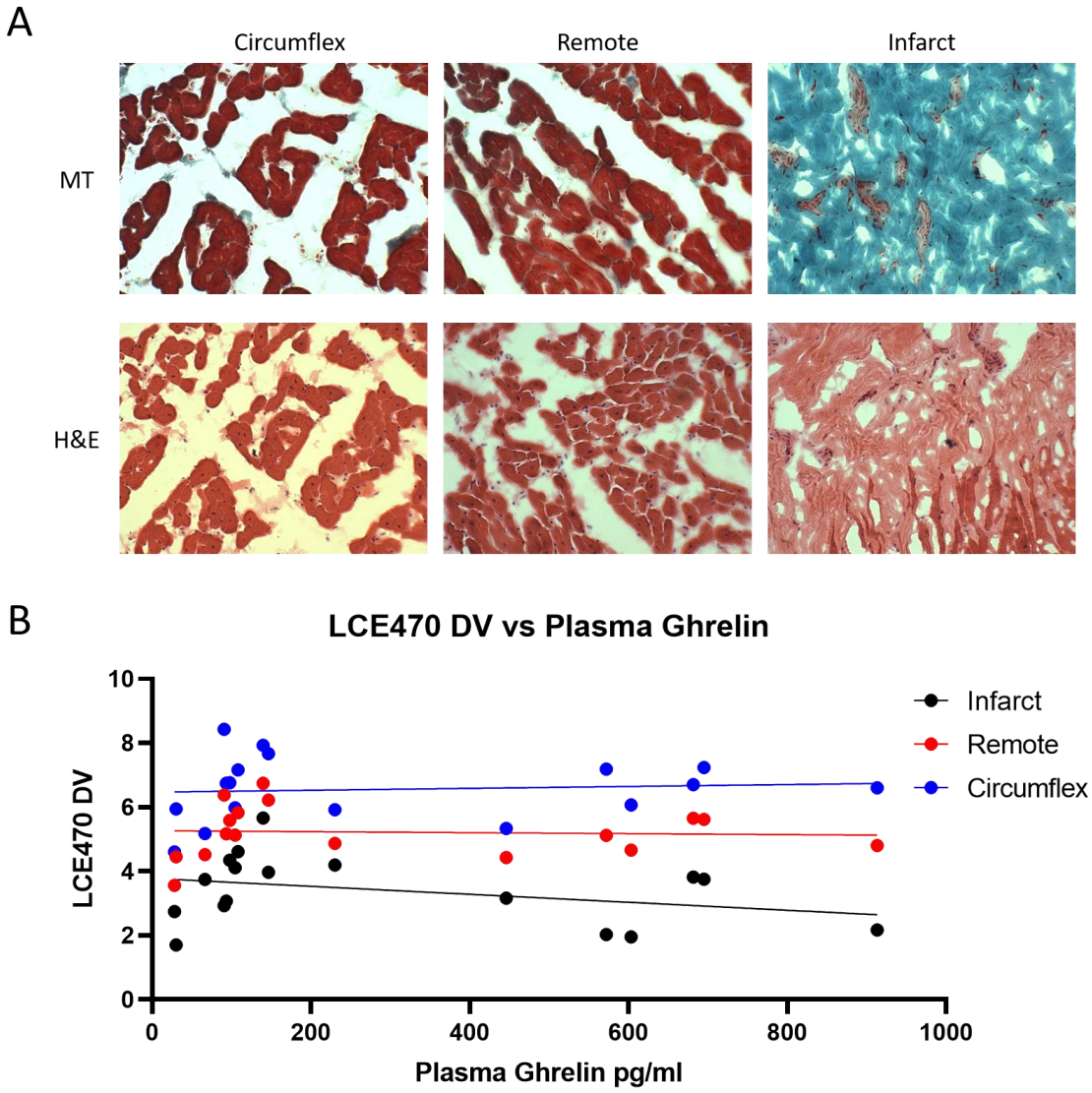

Figure 4.13 Representative qualitative images of fibrosis and hematoxylin and eosin (H&E) are shown in each region.

A) Masson's trichrome (MT) stained for fibrosis (blue) and non-fibrotic tissue (red) where there were significant amounts of fibrosis in the infarct compared to the remote and circumflex tissue regions (A top). H&E stain confirmed differences in tissue distribution and type as seen in fibrosis (A bottom). B) Linear regression between LCE470 distribution volume and circulating plasma ghrelin levels based on region (infarct, remote, circumflex). There were no significant linear regressions in any region where circulating ghrelin did not alter the binding of LCE470 regionally in the heart.

4.3.6 Heart Function Before and After MI

Parameters of heart function were determined from the cardiac MRI sequence short axis TrueFISP series (10-11 slices through the LV) and generates a 3D representation of the left ventricle. The short axis TrueFISP sequences were acquired at all time points, from baseline to 11 months post-infarct. Heart function parameters evaluated were left ventricular ejection fraction, stroke volume, diastolic and systolic volume, and end diastolic and end systolic mass. There were no significant differences in any measured parameter at any given time point (Fig 4.14).

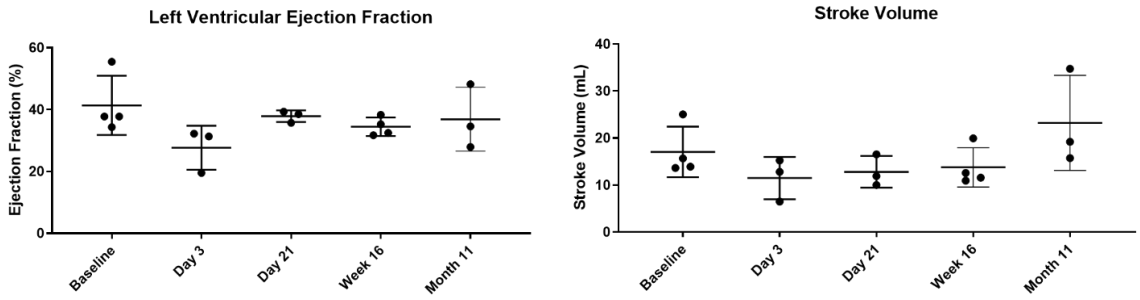

Figure 4.14 Heart Function Analysis (n=4).

Calculation of MR images of Echo triggered short axis TrueFISP image series was used to calculate heart function parameters including left ventricular ejection fraction (LVEF) and stroke volume. No significant differences were seen in overall heart function at any given timepoint: baseline, day 3, day 21, week 16, or month 11.

4.4 Discussion

In this study, we characterized a new PET tracer, ^{18}F-labelled small molecule GHSR ligand termed ^{18}F-LCE470 to examine GHSR density in the heart *in vivo* with simultaneous PET/MR imaging in a canine model of MI. We used TBR to calculate tracer uptake and quantitative PET to determine the distribution volume of ^{8}F-LCE470, which is a measure of GHSR in three regions of the LV: area of infarct, the territory of the left circumflex artery, and remote myocardium, where we revealed a unique pattern of uptake of ^{18}F-LCE470 in the left ventricle that persisted over time. This work is extremely novel as it follows tracer distribution out for 18 months after MI including timepoints before and both acutely and chronically after MI. The regional distribution of ^{18}F-LCE470 in the LCX territory and remote myocardium differed from that of the perfusion tracer, ^{13}N-NH_3, suggesting potential specificity to binding GHSR. As well, both TBR and distribution volume of ^{18}F-LCE470 significantly correlated with levels of tissue GHSR as determined by Cy5-cyclo-ghrelin(1-20)[22] fluorescence in tissue obtained at the end of the study. Heart function (global LVEF and stroke volume) as determined by cMRI did not change significantly over the one-year period of the study, although regional changes may have occurred but were not formally assessed in this study. Therefore, we have characterized the specificity and sensitivity of ^{18}F-LCE470 in detecting myocardial GHSR and shown that regional GHSR distribution is altered after MI independently of changes in perfusion and global LV function.

Specifically, for the entity of heart failure (HF) diagnosis, there is a need for the development of new targets for *in vivo* imaging that are specific for cardiac tissue and can directly detect molecular changes in disease pathophysiology. Such imaging may allow early detection of altered disease patterns, and the fashioning of targeted interventions that may improve patient outcomes. The current promising cardiac PET tracers have been developed for the purpose of tracking the biological processes that underlie HD. In particular ^{13}N-ammonia (^{13}N-NH_3) is commonly used after a MI to determine the extent of diminished cardiac perfusion and damaged myocardium[21]. ^{13}N-NH_3 freely diffuses across the cell membrane and is utilized in glutamine synthesis via glutamate synthase. ^{13}N-NH_3 only enters viable cells and therefore regional perfusion patterns in the myocardium

directly detects blood flow and tissue viability. Another common clinically used PET tracer is a glucose analogue, ^{18}F-fluorodeoxy glucose (^{18}F-FDG) which primarily measures the rate of glucose metabolism in cells. ^{18}F-FDG enters cells through glucose transporters, gets phosphorylated by hexokinase and is trapped in the cell. Changes in ^{18}F-FDG uptake are primarily related to the upregulation or downregulation of glucose transporters on cellular membranes. With an appropriate protocol that suppresses normal myocardial glucose uptake, ^{18}F-FDG can be used to detect inflammation, mediated by primarily pro-inflammatory macrophages[25]. Glucose transporters are upregulated in pro-inflammatory macrophages; therefore, increased ^{18}F-FDG signal can be used to detect the extent of inflammation in HD[26,27]. In addition, ^{18}F-FDG can measure changes in myocardial substrate metabolism from predominantly fatty acid metabolism to glucose metabolism as seen in congestive HF[28]. ^{11}C-*meta*-hydroxyephedrine (HED) is a norepinephrine (NE) analogue that targets the NE receptor to evaluate regional changes in cardiac neuronal activity which can help assess HF presence and reinnervation commonly present in arrythmias[29]. In addition to these common cardiac PET tracers used in research, there have been many recent discoveries in developing PET tracers targeting cardiac transporters, receptors, and proteases that change in HD[30,31]. An emerging perfusion tracer is ^{18}F-flurpiridaz, a pyridazinone derivative, which gets metabolically trapped in cardiomyocytes through the mitochondrial membrane complex-1 and determines cardiac blood flow. ^{18}F-flurpiridaz was able to accurately detect coronary artery disease using cardiac perfusion PET imaging[32,33]. When detecting cardiac inflammation, ^{68}G-DOTATATE targets the somatostatin receptor 2 that is overexpressed in inflammatory macrophages. It can accurately detect inflammation after a myocardial infarction with minimal background uptake[34] and can determine atherosclerotic disease severity[35]. Lastly, there is emergence of ^{68}Ga labelled fatty acid analogues (^{68}Ga–NOTA–undecanoic acid) that target fatty acid transporters and can detect abnormalities of fatty-acid oxidation in myocardial disease[36]. Therefore, there are several ongoing efforts at generating novel molecular imaging agents that target a number of cardiac biomarkers of heart disease.

To optimize new targeted PET tracer development, there are many important factors to consider. First, for improved plasma stability, small molecule ligands are preferable to peptide analogues or natural ligands. Second, binding affinity that is improved from that

of the natural ligand would be ideal for *in vivo* studies specifically. Finally, labelling with a clinically used radioisotope, such as ^{18}F can allow for easy clinical translation. These considerations have led our team to develop small molecule PET probes targeting GHSR, specifically ^{18}F-CE470, with strong binding affinities to the receptor (0.11nM). We have developed an ^{18}F-labelled ghrelin octapeptide analogue from N-terminal 8 amino acids of native ghrelin, [Inp^{1},Dpr^{3}(6-fluoro-2-naphthoate),1-Nal^{4},Thr^{8}]ghrelin(1−8), termed ^{18}F-LCE470, which had a significantly stronger affinity (0.11nM) to GHSR compared to native ghrelin (3.3nM) with *in vitro* studies[37]. The next step for this analogue is to evaluate *in vivo* binding. We also characterized the efficacy of ^{18}F-G-7039, a ghrelin peptidomimetic (binding affinity 69nM), in healthy mice where minimal tracer uptake was present in the heart[18]. Therefore, we concluded mouse models may not be optimal for imaging GHSR *in vivo.* We also determined that small molecules (low molecular weight organic compound with minimal resemblance to the ligand) are optimal for tracer binding compared to both peptidomimetics (combination of amino acids to resemble ligand which have been manipulated for better binding) and analogues (truncated versions of natural ligands).

We then evaluated our new PET tracer, ^{18}F-LCE470, using both a semi-quantitative TBR method to determine regional tracer uptake and quantitative kinetic modelling reflecting GHSR distribution. It is important to note here that one limitation with our kinetic modelling is the lack of plasma metabolite analysis that corrects the image-derived arterial input function for metabolic degradation of the tracer over the image acquisition period. Initial results in one dog showed that ^{18}F-LCE470 was fairly stable, with the parent compound decreasing at a linear rate by approximately 40% 60 minute after injection (Supplemental Fig 4.S2). While this result may indicate relative stability of ^{18}F-LCE470 in canine plasma over time, we need more robust data in canine plasma to accurately determine the metabolite correction for this tracer and thus did not use metabolite correction for this study[38].

Typically, in humans, after a MI occurs, there are significant remodeling changes in the left ventricle that result from both the acute and chronic phases of remodeling. This pattern of remodeling also occurs in the canine heart after MI[39]. After the initial infarct, the acute remodeling phase involves the myocardium surrounding the infarct, termed border

myocardium, with infarct expansion and the initiation of adaptive biochemical processes to preserve LVEF and stroke volume[40]. One such adaptive process is the upregulation of the $G_{q\alpha}$/Phospholipase C β (PLCβ) pathway which play a role in cardio-protection, cardiac hypertrophy and fibrosis deposition[41]. This pathway is also known to be activated by GHSR in cardiomyocytes in the regulation of calcium homeostasis and contractility[10,42]. Therefore, the border myocardium may be essential in cardiac remodeling after injury. In late stage remodeling, the LV is globally involved in progressive dilatation and scar enlargement, along with distortion of shape and contractile function[43]. Importantly, in later stages of remodeling, the border myocardium plays a large role in cardio-protection to minimize the scar enlargement and reduce damage to heart structure and function[44]. In our study, the border myocardium is represented by the left circumflex (LCX) tissue which surrounds the edge of the infarct.

We evaluated uptake of ^{18}F-LCE470 in the LV semi-quantitatively through TBR values. There were some significant regional changes in TBR of ^{18}F-LCE470 post-MI compared with pre-MI. The sustained post-MI decrease in ^{18}F-LCE470 uptake in the infarct area compared to the remote and LCX tissue likely suggests a significant and sustained decrease in GHSR expression over time after MI. Similarly, the slight decrease of ^{18}F-LCE470 in the remote tissue could also be due to a slight decrease in receptor density, and the sustained uptake in the LCX region suggests that GHSR expression is maintained in this region. Interestingly, the decrease in ^{18}F-LCE470 TBR specifically in the infarct region could also be due to a lack of perfusion not allowing the tracer to enter this area. To better determine the actual dynamics of GHSR distribution after MI, we used kinetic modelling to examine changes in distribution volume.

Kinetic modelling revealed highly individual responses to MI regarding GHSR distribution. One pattern that emerged was increased distribution volume in the LCX border region compared to the remote and infarcted tissue, similar to the pattern of TBR. These results suggest that one mechanism by which the border myocardium is cardioprotective is through GHSR signalling. Activation of GHSR in the myocardium is known to function through the $G_{\alpha q}$/PLCβ pathway to regulate contractility through calcium homeostasis[11] along with decreasing inflammatory and fibrotic signalling[45], reducing

apoptosis[12], and promoting cellular metabolism[46]. This pathway is likely upregulated to compensate for the reduced contractile stress of this area acutely after MI[47]. Such a mechanism may also operate to a lesser extent in the remote myocardium, as suggested by the elevated distribution volumes compared to the area of infarct. In one study evaluating the strain and stiffness of tissue from baseline to day 28 post MI, increased diastolic stiffness was initially observed in the infarct and border myocardium at day 3 post MI but not until day 14 post MI in remote tissue[44]. In addition apoptosis after MI is increased extensively in border myocardium and to a lesser extent in remote tissue which is sustained for 4 weeks[48]. This provides evidence that there is milder dysregulation of processes in the remote tissue compared to border tissue. In a proteomic and histological analysis of signalling in a porcine MI model, 4 weeks after I/R injury the border myocardium had decreases in proteins for energy metabolism and mitochondrial dysfunction, while proteins for endothelial growth and apoptosis increased. These results may provide a mechanism for increased angiogenesis seen in LV remodeling after MI and for increased apoptosis in the expansion of the infarct when the compensatory mechanisms fail[48]. Acutely after an infarct necrosis of cardiomyocytes initiate an intense inflammatory and immune response where monocytes, neutrophils, and leukocytes clear dead cells out of the infarcted area. An anti-inflammatory response is then initiated at about 3-4 weeks post MI where fibroblasts deposit extracellular matrix proteins and cross-linked collagen while granulation tissue becomes apoptotic[49]. We have previously shown that GHSR is not expressed in fibrotic deposition, specifically collagen I and III[14]. However, GHSR expression is present in fibroblasts[50,51] which may explain the lower ^{18}F-LCE470 distribution in the infarct region since as the scar matures, the density of cardiac fibroblasts is greatly reduced[52]. GHSR and ghrelin are also expressed in macrophages[53] which are chronically present in the infarct and border myocardium at lower levels[48], again attributing to part of the weakened ^{18}F-LCE470 signal in the infarct. It is important to note that a lack of perfusion in the infarct area can be physiology linked to the changes in receptor availability. The calculations derived from kinetic modeling are not biased due to this as changes in perfusion are reflected in the plasma-to-tissue influx and efflux. The binding potential of the tracer is not dependent on these rate constants, rather to the tracer binding and disassociating to the receptor. The concept of tracer binding to receptors independently of altered delivery

(perfusion), have been validated in multiple PET studies. These overall changes in GHSR binding and activation in the border myocardium to infarct region may prove optimal targets for increasing angiogenesis and decreasing apoptosis/ scar expansion chronically.

To better evaluate if these changes in infarct and border myocardium are attributed to actual changes in distribution volume or cardiac perfusion, we determined regional cardiac perfusion post-MI. Perfusion in the LV was measured using $^{13}N\text{-}NH_3$[21,54,55] which functions through entering the cardiomyocytes by diffusion and incorporation into the glutamine synthesis pathway[56], and is thus metabolically trapped within the cardiomyocyte. This pathway of uptake and retention does not operate if the cell membrane is damaged, and therefore $^{13}N\text{-}NH_3$ detects only viable myocardium[21,54]. In our study, the pattern of $^{13}N\text{-}NH_3$ TBR indicated persistently lower perfusion in the area of infarct for the duration of the study compared with the remote and LCX myocardium. Interpretation of this difference is limited by the lack of perfusion data before MI and immediately after. However, it is known that, in this particular model, perfusion of the infarct area significantly decreases immediately after MI[57,58]. The MI biology changes dramatically acutely (up to 4 weeks post-MI) versus chronically (4 weeks onwards). In the acute phase post-MI, the inflammatory and immune response initiate the removal of dead tissue and begin formation of new vasculature to restore blood flow to this area. Until this revascularization occurs, blood flow to the infarcted area is highly limited[49]. Once fibrotic tissue is deposited and angiogenesis is present in the infarct area, perfusion is restored while $^{13}N\text{-}NH_3$ binding remains minimal. Therefore, the decreased $^{13}N\text{-}NH_3$ binding in infarct area shows a lack of tracer access to infarcted area acutely, while chronically it represents scar formation. When analyzing trends in perfusion imaging after MI, decreased perfusion with $^{13}N\text{-}NH_3$ in patients with HD symptoms were predictive of adverse cardiac outcomes[59,60]. Therefore, these acute immune and inflammatory processes may prove to be ideal therapeutic targets for HD patients.

There is a notable divergence in the perfusion pattern of $^{13}N\text{-}NH_3$ in the remote and LCX areas when compared with uptake of ^{18}F-LCE470, in that $^{13}N\text{-}NH_3$ TBR was the same in these two regions, whereas ^{18}F-LCE470 TBR were different. These results suggest that uptake of ^{18}F-LCE470 is independent of perfusion in the remote myocardium. This is

further supported by the lack of correlation of both TBRs and that of the distribution volume of ^{18}F-LCE470 and K1 of ^{13}N-NH_3 in these two areas. Therefore, uptake and distribution volume of ^{18}F-LCE470 is likely due to binding to GHSR, and not due to changes in perfusion. In lieu of a blocking study we compared the TBRs and distribution volumes of ^{18}F-LCE470 to the kinetics of perfusion (blood flow) to determine tracer specificity.

We acknowledge that the specificity of LCE towards cardiac GHSR would be further confirmed through a blocking study, in which an excess of unlabeled ghrelin would be administered before or during tracer injection. To date, there has been no GHSR antagonists administered to humans. The most commonly used GHSR antagonists are [D-Lys-3]-GHRP-6 and YIL781 which have primarily been used in energy metabolism studies in rodents[61]. However, there is evidence that increased concentrations of [D-Lys-3]-GHRP-6 injected in rats show adverse cardiac events including elevated mean atrial pressure and heart rate[62]. There has also not been any toxicity study performed for these antagonists in canines and administering large doses is likely to cause significant adverse cardiac events, similar to what was seen in rats. Therefore, with these important considerations, we did not use a bocking study to determine tracer specificity.

To validate our *in vivo* findings, and to further demonstrate that ^{18}F-LCE470 yields a readout of GHSR, we measured GHSR expression in all three LV regions using Cy5-cyclo-ghrelin(1-20)[22]. Fluorescent signal intensity was significantly increased in tissue from the LCX area compared to the infarct region, and in most dogs, the LCX tissue had higher fluorescence intensity compared to the remote. These results indicate the relative differences in the presence of GHSR in LCX, remote and infarct areas, and mirror the distribution of ^{18}F-LCE470 in each of these regions. In the chronic stages after MI, late-stage remodeling occurs in both the remote and border myocardium which encompasses decreased LV function and global apoptosis. As discussed above, activation of GHSR in the border myocardium could contribute to enhanced cardioprotective signalling in the failing cardiac muscle[41,63]. There is also a significant amount of fibrosis (collagen deposition) in the infarct area, which may explain the low GHSR signal in this region, as we have previously shown that GHSR is not expressed in the collagen deposition of fibrotic

tissue[14]. GHSR is also known to have increased expression in HF[13,14] and after MI[16] which reflects the pattern of GHSR expression present here in cardiac tissue at 18 months post-MI. In addition, the lack of GHSR in infarct tissue provides further evidence that the decreased ^{18}F-LCE470 distribution in the infarct is due to a lack of GHSR uptake and not solely due to decreased perfusion in that area.

In order to examine the sensitivity of ^{18}F-LCE470 in binding GHSR, we determined the relationship between TBR and DV values obtained during the final imaging session and tissue fluorescence intensities. The strong significant positive correlations between TBR and fluorescence intensity, and between distribution volume and fluorescence intensity, demonstrates high tracer sensitivity targeting GHSR density in the heart. One limitation to note is that tissue was only collected upon sacrifice, and thus tissue GHSR expression could only be compared to *in vivo* image analysis at 11 months. Other ^{18}F PET tracers have been validated for diagnostic accuracy using histological analysis with known positive and negative samples[64–66]. The histological analysis in our study used a custom Cy5-cyclo-ghrelin(1-20)[22] to accurately determine GHSR presence in the tissue. This method is superior as we measured GHSR protein in the tissue and we used a fluorescent analogue instead of antibodies. Traditional GPCR antibodies have shown to have low specificity whereas our fluorescent analogue demonstrated a high specificity to the receptor as shown through significant decreases in fluorescence after added blocking agent (supplemental Fig 4.11). Nonetheless, the strong correlation between tissue fluorescence of GHSR and ^{18}F-LCE470 uptake indicates the high specificity of ^{18}F-LCE470 binding to GHSR in the LV.

Surprisingly, heart function as determined by MR did not significantly change over time between baseline and both acute and chronic time points after MI. There was a slight but not significant decrease in both LVEF and stroke volume observed at day 3 post-MI in the overall cohort. Normally after a MI, heart function is significantly reduced at acute time points and can either return to normal, pre-MI levels of heart function, or continue to decrease and proceed to HF[67]. The main explanation for no significant functional changes over time is due to the use of global function rather than regional function. Global heart function can be an insensitive marker as hypercontractility in non-infarcted tissue will compensate for the hypocontractility in the infarct. Another possibility for why we are not

seeing significant changes could be due to the small cohort of dogs used in this study. In addition, an iron chelator was given to these dogs twice a day from days 1-30 post MI. Iron chelation has shown to reduce the amount of iron deposition in hemorrhages after acute MI[68] and reduce adverse remodeling such as ventricular enlargement and myocardial hypertrophy[69]. The iron chelation agent used in this study could have had similar effects on LVEF. Even with these variables present, we were still able to demonstrate clear significant regional changes in both *in vivo* PET imaging with ^{18}F-LCE470 and tissue GHSR fluorescence in the absence of any functional changes seen in the heart.

The main limitation to this study is the lack of metabolite-corrected arterial input function for compartmental modelling of our new ^{18}F-LCE470 tracer. Metabolite corrections are used to determine the rate of tracer decay over time[70]. Our initial results indicate that the tracer appears to be relatively stable in the blood over the image acquisition time (supplemental Fig 4.S2), and more studies need to be completed to show reproducibility. Other forms of metabolite correction include a mathematical model of correction and population-based correction. To use the mathematical model, an optimal model must be selected based on the quality of data and reliability of results. In studies with unknown or too many parameters, the fitting may be poor[71]. Metabolite correction based on population can only be used with a large number of available samples and the population used to correct must be diverse. This method is rarely possible due to the extensive testing and validation required for each individual tracer[71]. Alternatively, a tissue reference region that does not contain the receptor could be used to generate ratios of tracer uptake with distribution volume for accurate analysis[70]. This option is difficult for our particular tracer, since GHSR is present in both atrial and ventricular myocytes, and vascular endothelial cells of the aorta, coronary, pulmonary, and arcuate arteries in human tissue[72]. If we assume the binding patterns in canine cardiovascular tissue follow those of humans and rats, there is no appropriate reference region in the heart. There is also evidence that GHSR expression is present in lung tissue, thereby excluding them as a suitable reference region[73]. Therefore, as of now, there is no accurate tissue reference region in the heart with this canine model.

To conclude, we have characterized a novel PET tracer, ^{18}F-LCE470, to sensitively and specifically target GHSR *in vivo*. ^{18}F-LCE470 had a unique, specific binding pattern in the

canine heart after MI, which did not fully reflect changes in cardiac perfusion. Tissue GHSR showed a strong correlation to ^{18}F-LCE470 *in vivo* PET imaging, further supporting the sensitivity of our tracer to GHSR density. While changes in ^{18}F-LCE470 tracer uptake were present in the LV, there were no significant changes to the overall heart function indicating ^{18}F-LCE470 may reflect the molecular and biochemical changes that occur in the absence of functional changes after MI. Our ongoing work will help to further characterize the *in vivo* changes to the ghrelin-GHSR system throughout the progression of HD.

4.5 Supplemental Figures

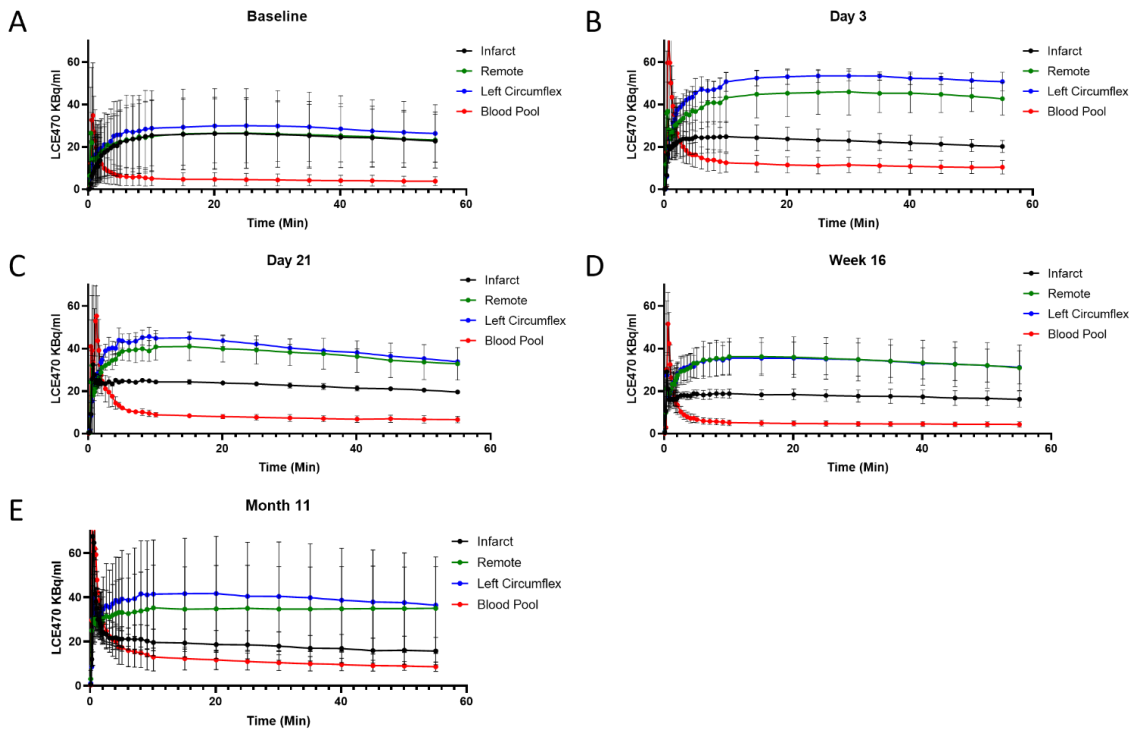

Supplemental Figure 4.S1 Time-activity curves showing regional uptake of ^{18}F-LCE470 in infarct, remote, left circumflex area, and blood pool.

A) Baseline; B) Day 3; C) Day 21; D) Week 16; E) Month 11. Regional uptake decreased slightly in the infarct after MI compared to baseline while both remote and left circumflex tissues drastically increased after MI.

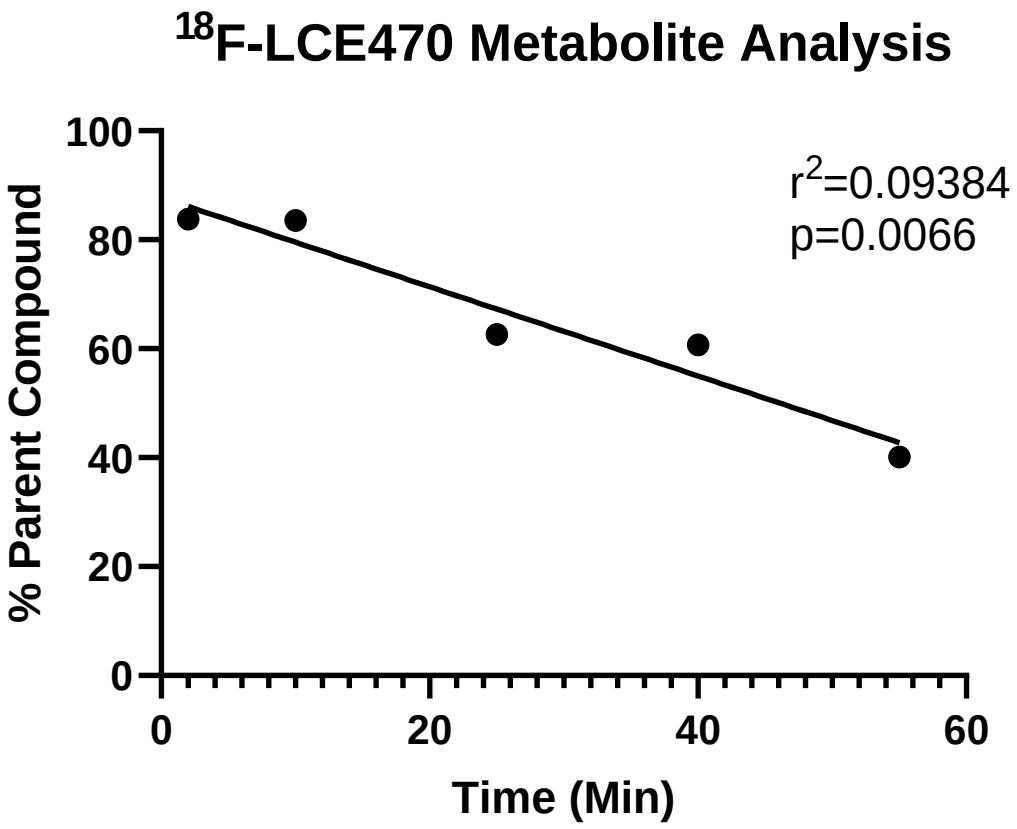

Supplemental Figure 4.S2 Metabolite Analysis.

Preliminary metabolite analysis on one dog where parent tracer compound decreases 40% by 60 minutes after injection. Metabolite analysis indicates the tracer degrades 40% over 60 minutes although more robust data needs to be collected for accurate correction.

4.6 References

1. Balluz, R., Liu, L., Zhou, X. & Ge, S. Real time three-dimensional echocardiography for quantification of ventricular volumes, mass, and function in children with congenital and acquired heart diseases. *Echocardiography* **30**, 472–482 (2013).

2. Dunn, F. G., Chandraratna, P., deCarvalho, J. G. R., Basta, L. L. & Frohlich, E. D. Pathophysiologic assessment of hypertensive heart disease with echocardiography. *Am. J. Cardiol.* **39**, 789–795 (1977).

3. Wieben, O., Francois, C. & Reeder, S. B. Cardiac MRI of ischemic heart disease at 3 T: Potential and challenges. *Eur. J. Radiol.* **65**, 15–28 (2008).

4. Berger, R. *et al.* B-type natriuretic peptide predicts sudden death in patients with chronic heart failure. *Circulation* **105**, 2392–2397 (2002).

5. Redfield, M. M. *et al.* Plasma brain natriuretic peptide concentration: Impact of age and gender. *J. Am. Coll. Cardiol.* **40**, 976–982 (2002).

6. Peacock IV, W. F. *et al.* Cardiac troponin and outcome in acute heart failure. *N. Engl. J. Med.* **358**, 2117–2126 (2008).

7. Zhang, G. G. *et al.* Ghrelin protects heart against ERS-induced injury and apoptosis by activating AMP-activated protein kinase. *Peptides* **48**, 156–165 (2013).

8. Rusu, C. C. *et al.* Ghrelin and acyl ghrelin levels are associated with inflammatory and nutritional markers and with cardiac and vascular dysfunction parameters in hemodialysis patients. *Int. Urol. Nephrol.* **50**, 1897–1906 (2018).

9. Wang, Q. *et al.* Ghrelin protects the heart against ischemia/reperfusion injury via inhibition of TLR4/NLRP3 inflammasome pathway. *Life Sci.* **186**, 50–58 (2017).

10. Sun, Q. *et al.* Effects of GH secretagogues on contractility and Ca2+ homeostasis

of isolated adult rat ventricular myocytes. *Endocrinology* **151**, 4446–4454 (2010).

11. Ma, Y., Zhang, L., Edwards, J. N., Launikonis, B. S. & Chen, C. Growth hormone secretagogues protect mouse cardiomyocytes from in vitro ischemia/reperfusion injury through regulation of intracellular calcium. *PLoS One* **7**, (2012).

12. Baldanzi, G. *et al.* Ghrelin and des-acyl ghrelin inhibit cell death in cardiomyocytes and endothelial cells through ERK1/2 and PI 3-kinase/AKT. *J. Cell Biol.* **159**, 1029–1037 (2002).

13. Beiras-Fernandez, A. *et al.* Altered myocardial expression of ghrelin and its receptor (GHSR-1a) in patients with severe heart failure. *Peptides* **31**, 2222–8 (2010).

14. Sullivan, R. *et al.* Dynamics of the Ghrelin/Growth Hormone Secretagogue Receptor System in the Human Heart Before and After Cardiac Transplantation. *J. Endocr. Soc.* **3**, 748–762 (2019).

15. Sullivan, R. *et al.* Regional Differences in the Ghrelin-Growth Hormone Secretagogue Receptor Signalling System in Human Heart Disease. *CJC Open* **4**, 1–13 (2021).

16. Yuan, M. J. *et al.* Expression of ghrelin and its receptor in rats after coronary artery ligation. *Regul. Pept.* **192**–**193**, 1–5 (2014).

17. Rosita, D., Dewit, M. A. & Luyt, L. G. Fluorine and rhenium substituted ghrelin analogues as potential imaging probes for the growth hormone secretagogue receptor. *J. Med. Chem.* **52**, 2196–2203 (2009).

18. Abbas, A. *et al.* Development and Characterization of an 18 F-labeled Ghrelin Peptidomimetic for Imaging the Cardiac Growth Hormone Secretagogue Receptor. *Mol. Imaging* **17**, 1–11 (2018).

19. Hou, J., Kovacs, M. S., Dhanvantari, S. & Luyt, L. G. Development of Candidates for Positron Emission Tomography (PET) Imaging of Ghrelin Receptor in Disease:

Design, Synthesis, and Evaluation of Fluorine-Bearing Quinazolinone Derivatives. *J. Med. Chem.* **61**, 1261–1275 (2018).

20. Logan, J. Graphical analysis of PET data applied to reversible and irreversible tracers. *Nucl. Med. Biol.* **27**, 661–670 (2000).

21. Wu, H. M. *et al.* Quantification of myocardial blood flow using dynamic nitrogen-13-ammonia PET studies and factor analysis of dynamic structures. *J. Nucl. Med.* **36**, 2087–2093 (1995).

22. Lalonde, T., Shepherd, T. G., Dhanvantari, S. & Luyt, L. G. Stapled ghrelin peptides as fluorescent imaging probes. *Pept. Sci.* **111**, (2019).

23. Sullivan, R. *et al.* Changes in the Cardiac GHSR1a-Ghrelin System Correlate With Myocardial Dysfunction in Diabetic Cardiomyopathy in Mice. *J. Endocr. Soc.* **2**, 178–189 (2018).

24. Doyle, W. Operations Useful for Similarity-Invariant Pattern Recognition. *J. ACM* **9**, 259–267 (1962).

25. Williams, G. & Kolodny, G. M. Suppression of myocardial 18F-FDG uptake by preparing patients with a high-fat, low-carbohydrate diet. *AJR. Am. J. Roentgenol.* **190**, 151–156 (2008).

26. W., O. *et al.* Usefulness of fasting18F-FDG PET in identification of cardiac sarcoidosis. *J. Nucl. Med.* **45**, 1989–1998 (2004).

27. Wykrzykowska, J. *et al.* Imaging of inflamed and vulnerable plaque in coronary arteries with 18F-FDG PET/CT in patients with suppression of myocardial uptake using a low-carbohydrate, high-fat preparation. *J. Nucl. Med.* **50**, 563–568 (2009).

28. Taylor, M. *et al.* An Evaluation of Myocardial Fatty Acid and Glucose Uptake Using PET with [18 F] Fluoro-6- Thia-Heptadecanoic Acid and [18 F] FDG in Patients with Congestive Heart Failure. *J. Nucl. Med.* **42**, 55–62 (2001).

29. Magnusson, P. *et al.* Positron emission tomography (15O-water, 11C-acetate, 11C-HED) risk markers and nonsustained ventricular tachycardia in hypertrophic cardiomyopathy. *IJC Hear. Vasc.* **26**, 100452 (2020).

30. Kopka, K., Schober, O. & Wagner, S. 18F-labelled cardiac PET tracers: Selected probes for the molecular imaging of transporters, receptors and proteases. *Basic Res. Cardiol.* **103**, 131–143 (2008).

31. Kim, D. Y., Cho, S. G. & Bom, H. S. Emerging Tracers for Nuclear Cardiac PET Imaging. *Nucl. Med. Mol. Imaging (2010).* **52**, 266–278 (2018).

32. Maddahi, J. *et al.* Phase-III Clinical Trial of Fluorine-18 Flurpiridaz Positron Emission Tomography for Evaluation of Coronary Artery Disease. *J. Am. Coll. Cardiol.* **76**, 391–401 (2020).

33. Moody, J. B. *et al.* Added value of myocardial blood flow using 18F-flurpiridaz PET to diagnose coronary artery disease: The flurpiridaz 301 trial. *J. Nucl. Cardiol.* (2020) doi:10.1007/s12350-020-02034-2.

34. Tarkin, J. M. *et al.* 68Ga-DOTATATE PET Identifies Residual Myocardial Inflammation and Bone Marrow Activation After Myocardial Infarction. *J. Am. Coll. Cardiol.* **73**, 2489–2491 (2019).

35. Tarkin, J. M. *et al.* Detection of Atherosclerotic Inflammation by 68Ga-DOTATATE PET Compared to [18F]FDG PET Imaging. *J. Am. Coll. Cardiol.* **69**, 1774–1791 (2017).

36. Jain, A., Mathur, A., Pandey, U., Dev, H. & Dash, A. Bioorganic & Medicinal Chemistry Letters Ga labeled fatty acids for cardiac metabolic imaging : Influence of different bifunctional chelators. *Bioorg. Med. Chem. Lett.* **26**, 5785–5791 (2016).

37. Charron, C. L. *et al.* Structure-Activity Study of Ghrelin(1-8) Resulting in High Affinity Fluorine-Bearing Ligands for the Ghrelin Receptor. *J. Med. Chem.* **60**, 7256–7266 (2017).

38. McGirr, R. *et al.* Towards PET imaging of intact pancreatic beta cell mass: A transgenic strategy. *Mol. Imaging Biol.* **13**, 962–972 (2011).

39. Jugdutt, B. I. The Dog Model of Left Ventricular Remodeling After Myocardial Infarction. **8**, 472–475 (2002).

40. St. John Sutton, M. G. & Sharpe, N. Left ventricular remodeling after myocardial infarction: Pathophysiology and therapy. *Circulation* **101**, 2981–2988 (2000).

41. Ju, H., Zhao, S. & Tappia, P. S. Expression of G q and PLC- in Scar and Border Tissue in Heart Failure Due to Myocardial Infarction. *Circ. Basic Sci. Rep* **97**, 892–899 (1998).

42. Pose, M. L. Characterization of the intracellular signaling mechanisms activated by ghrelin through GHSR-1a: role of β-arrestins. (UNIVERSIDAD DE SANTIAGO DE COMPOSTELA, 2011).

43. French, B. A. & Kramer, C. M. Mechanisms of postinfarct left ventricular remodeling. *Drug Discov. Today Dis. Mech.* **4**, 185–196 (2007).

44. Torres, W. M. *et al.* Regional and temporal changes in left ventricular strain and stiffness in a porcine model of myocardial infarction. *Am. J. Physiol. - Hear. Circ. Physiol.* **315**, H958–H967 (2018).

45. Cao, Y. *et al.* Cardioprotective Effect of Ghrelin in Cardiopulmonary Bypass Involves a Reduction in Inflammatory Response. *PLoS One* **8**, (2013).

46. Mitacchione, G. *et al.* The gut hormone ghrelin partially reverses energy substrate metabolic alterations in the failing heart. *Circ. Hear. Fail.* **7**, 643–651 (2014).

47. Wenk, J. F. *et al.* First evidence of depressed contractility in the border zone of a human myocardial infarction. *Ann. Thorac. Surg.* **93**, 1188–1193 (2012).

48. Yang, L. *et al.* Quantitative Proteomics and Immunohistochemistry Reveal Insights into Cellular and Molecular Processes in the Infarct Border Zone One

Month after Myocardial Infarction. *J. Proteome Res.* **16**, 2101–2112 (2017).

49. Prabhu, S. D. & Frangogiannis, N. G. The biological basis for cardiac repair after myocardial infarction. *Circ. Res.* **119**, 91–112 (2016).

50. Ma, J. *et al.* Effects of ghrelin on the apoptosis of rheumatoid arthritis fibroblast-like synoviocyte MH7A cells. *Biol. Pharm. Bull.* **42**, 158–163 (2019).

51. Nokhbehsaim, M. *et al.* Effect of interleukin-1β on ghrelin receptor in periodontal cells. *Clin. Oral Investig.* **23**, 113–122 (2019).

52. Frangogiannis, N. G., Michael, L. H. & Entman, M. L. Myofibroblasts in reperfused myocardial infarcts express the embryonic form of smooth muscle myosin heavy chain (SMemb). *Cardiovasc. Res.* **48**, 89–100 (2000).

53. Waseem, T., Duxbury, M., Ito, H., Ashley, S. W. & Robinson, M. K. Exogenous ghrelin modulates release of pro-inflammatory and anti-inflammatory cytokines in LPS-stimulated macrophages through distinct signaling pathways. *Surgery* **143**, 334–342 (2008).

54. Rauch, B., Helus, F. & Grunze, M. Kinetics of 13N-ammonia uptake in myocardial single cells indicating potential limitations in its applicability as a marker of myocardial blood flow. *Circulation* **71**, 387–393 (1985).

55. Bol, A., Melin, J. A., Vanoverschelde, J. & Baudhuin, T. Direct Comparison of [13N] Ammonia and [150] Water Estimates of Perfusion With Quantification of Regional Myocardial Blood Flow by Microspheres. *Circulation* **87**, 512–525 (1993).

56. Cooper, A. J. L. 13N as a tracer for studying glutamate metabolism. **59**, 456–464 (2012).

57. Hansen, H. *et al.* Sustained regional abnormalities in cardiac metabolism after transient ischemia in the chronic dog model. *J. Am. Coll. Cardiol.* **6**, 336–347 (1985).

58. Jr, J. M. C. & Suzuki, G. Journal of Molecular and Cellular Cardiology Myocardial perfusion and contraction in acute ischemia and chronic ischemic heart disease ☆. *J. Mol. Cell. Cardiol.* **52**, 822–831 (2012).

59. Herzog, B. A. *et al.* Long-Term Prognostic Value of 13N-Ammonia Myocardial Perfusion Positron Emission Tomography. Added Value of Coronary Flow Reserve. *J. Am. Coll. Cardiol.* **54**, 150–156 (2009).

60. Fiechter, M. *et al.* Myocardial perfusion imaging with 13N-Ammonia PET is a strong predictor for outcome. *Int. J. Cardiol.* **167**, 1023–1026 (2013).

61. Muller, A. F., Kopchick, J. J., Flyvbjerg, A. & Van Der Lely, A. J. Growth hormone receptor antagonists. *J. Clin. Endocrinol. Metab.* **89**, 1503–1511 (2004).

62. Vlasova, M. A., Järvinen, K. & Herzig, K. H. Cardiovascular effects of ghrelin antagonist in conscious rats. *Regul. Pept.* **156**, 72–76 (2009).

63. Yuan, M.-J. *et al.* GHSR-1a is a novel pro-angiogenic and anti-remodeling target in rats after myocardial infarction. *Eur J Pharmacol.* **788**, 218–225 (2016).

64. Schirrmeister, H. *et al.* Fluorine-18 2-deoxy-2-fluoro-D-glucose PET in the preoperative staging of breast cancer: Comparison with the standard staging procedures. *Eur. J. Nucl. Med.* **28**, 351–358 (2001).

65. Chen, W. *et al.* 18F-FDOPA PET imaging of brain tumors: Comparison study with 18F-FDG PET and evaluation of diagnostic accuracy. *J. Nucl. Med.* **47**, 904–911 (2006).

66. Kayani, I. *et al.* Functional imaging of neuroendocrine tumors with combined PET/CT using 68Ga-DOTATATE (Dota-DPhe1, Tyr3-octreotate) and 18F-FDG. *Cancer* **112**, 2447–2455 (2008).

67. Gómez, A. M., Guatimosim, S., Dilly, K. W., Vassort, G. & Lederer, W. j. Heart failure after myocardial infarction: altered excitation-contraction coupling. *Circulation* **104**, 688–693 (2001).

68. Dharmakumar, R. “Rusty Hearts” Is it time to rethink iron chelation therapies in post-myocardial-infarction setting. *Circ. Card. Imaging* **9**, 1–3 (2016).

69. Behrouzi, B. *et al.* Action of iron chelator on intramyocardial hemorrhage and cardiac remodeling following acute myocardial infarction. *Basic Res. Cardiol.* **115**, 1–18 (2020).

70. Logan, J. *et al.* Distribution Volume Ratios Without Blood Sampling from Graphical Analysis of PET Data. *J. Cereb. Blood Flow Metab.* **16**, 834–840 (1996).

71. Tonietto, M. *et al.* Plasma radiometabolite correction in dynamic PET studies: Insights on the available modeling approaches. *J. Cereb. Blood Flow Metab.* **36**, 326–339 (2016).

72. Katugampola, S. D., Pallikaros, Z. & Davenport, A. P. [125I-His9]-Ghrelin, a novel radioligand for localizing GHS orphan receptors in human and rat tissue; up-regulation of receptors with atherosclerosis. *Br. J. Pharmacol.* **134**, 143–149 (2001).

73. Volante, M. *et al.* Ghrelin expression in fetal, infant, and adult human lung. *J. Histochem. Cytochem.* **50**, 1013–1021 (2002).

Chapter 4

5 Discussion, Future Studies, and Clinical Significance

5.1 Cardiac Ghrelin-GHSR System is a Scalable Marker for Heart Disease

To optimize diagnosis for heart disease (HD) and prediction towards the development of heart failure (HF), a better understanding of the underlying biological mechanisms through the evolution of HF is needed. My work has revealed some dynamics of ghrelin and GHSR in the human myocardium that may be a key factor in this understanding. GHSR expression is abnormally elevated in end-stage heart failure[1] and activation of this system elicits many cardioprotective mechanisms, including preservation of calcium homeostasis/ contractiliy[2], decreasing inflammatory and fibrotic signalling[3], reducing apoptosis[4], and promoting cellular metabolism[5]. Because many of these effects occur before the onset of structural changes that define HD, myocardial GHSR may be an optimal target for HD diagnosis in its earlier stages. In Chapter 2, I used a novel far-red fluorescently labelled ligand of GHSR to examine the dynamics of the ghrelin-GHSR system. It is important to note that the expression of GHSR shown with this fluorescent ligand is not necessarily a demonstration of biological activity in the myocardium. It is better demonstrated by an increase in production of the receptor that is expressed both on the membrane and within the cardiomyocytes. This is the first study that evaluated GHSR and ghrelin expression in human cardiac tissue in patients before and up to 1 year after cardiac transplantation. I demonstrated that both GHSR and ghrelin were slightly elevated in end-stage HF compared to serial biopsies of the newly transplanted heart, and both ghrelin and GHSR were correlated negatively with LVEF. Changes in the ghrelin-GHSR system were associated with cardioprotective mechanisms as reflected by significant correlations to biochemical markers of contractility and cell survival/ hypertrophy. My work suggested that ghrelin-GHSR may be a more sensitive indicator of alterations in these signalling pathways of

contractility and hypertrophy than BNP, the gold standard HF biomarker[6]. Additionally, GHSR was not expressed in fibrotic tissue, specifically within areas of collagen deposition, which can provide more information on the exact types of tissues express GHSR and the biological composition of damaged tissue in this area. Therefore, ghrelin-GHSR can provide significant information about HF biology.

To further understand the dynamics of how ghrelin-GHSR changes in the heart, this system was measured in tissue obtained from patients with valvular heart disease with preserved ejection fraction. These patients had not been diagnosed with HF, but had some significant risk factors, such as valvular impairments, hypertension, coronary artery disease, and medications including diuretics and ACE/ARB inhibitors. In Chapter 3, I evaluated the expression and biology of the ghrelin-GHSR system using our fluorescently labelled ghrelin ligand in control non-diseased cardiac tissue and in tissue obtained from different regions of the heart from patients undergoing valve replacement surgery. A positive correlation between ghrelin and GHSR was present in tissue from the left atrium but not the left ventricle. In contrast, no correlations were present in the control tissue, which was sampled from the left ventricle. Taken together with the correlations in end-stage HF, the weak regional correlation of ghrelin and GHSR in the absence of measurable changes in LVEF could indicate the scalability of this marker from control → HD → HF. Further assessment of biochemical changes associated with GHSR activation in valvular disease indicated a significant positive correlation with SERCA2a, a marker of Ca^{2+}-dependent contractility, only in the LV. That this relationship was also present in the absence of measurable changes in LVEF suggests subclinical alterations in GHSR-associated signalling in the LV. Therefore, I have demonstrated specific, regional changes in the ghrelin-GHSR system and associated biochemical signalling pathways at different stages in the progression of HD. The scalability of this system can help provide clues to understanding to the underlying evolution of HD and the development of HF.

5.2 Is the Ghrelin-GHSR System a Clinical Diagnostic Biomarker?

Heart disease (HD) is a diverse clinical syndrome with no one specific path of progression. This makes diagnosis extremely difficult in the evolution of HD as current biomarkers can only detect at late stages. Here, we suggest the ghrelin-GHSR system as a potential new cardiac-localized biomarker of cardiac dysfunction. My work has demonstrated a significant relationship between ghrelin-GHSR and overall heart function indicating increases in this system in late stages of HF. This system clearly shows its scalability with disease severity progressing from no correlations in healthy tissue, to weak correlations in HD with preserved ejection fraction, to strong correlations in end stage HF. This scalability also translates with GHSR-associated biochemical signalling as there is no correlation of GHSR with markers of signalling pathways in control tissue, weak correlations in the HD cohort, and strong correlations in HF. That these specific alterations in GHSR-associated signalling occur in both the presence and absence of reduced LVEF indicates subclinical changes in contractile function may occur prior to overt derangements in cardiac function and structure. This work is unique in its development and use of a novel fluorescent optical imaging tool to specifically target expression of GHSR as conventional antibodies lack specificity. This imaging tool was evaluated in human cardiac tissue, demonstrating the clinical relevance of ghrelin-GHSR in cardiovascular disease and heart failure. The next step was to develop a novel *in vivo* imaging tool to target and track changes in GHSR in the heart. We then developed a targeted PET tracer for GHSR that can track changes in tracer distribution in HD and HF.

5.3 In Vivo GHSR PET Tracer Optimization

In the past decade there have been developments for targeting GHSR *in vivo* with PET imaging. The first study in designing GHSR-targeted probes was in 2009 by Rosita *et al.* where the structure of the ghrelin peptide was significantly modified to carry SPECT and PET radioisotopes, while maintaining binding to GHSR. They determined that ghrelin

could be truncated to ghrelin(1-14) and modified on the Ser-3 side chain to carry SPECT and PET isotopes and still maintain GHSR binding similar to that of native ghrelin. The lead PET analog, ghrelin(1-14)-12C-F, had a fluorine addition with a strong binding affinity to GHSR of 28nM. They showed that binding to GHSR could be preserved even though the octanoyl side chain on Ser3, which comprises the receptor binding domain of ghrelin, had been altered. In another study by Charron *et al*., a [^{68}Ga]-ghrelin analogue ([Dpr^{3}(octanoyl),Lys^{19}(Ga-DOTA)]ghrelin(1- 19)) showed strong affinity to GHSR (5.9nM) in a xenograft mouse model. This analogue was tested *in vivo* where there was significant uptake in the xenograft although no uptake was seen in the cardiovascular system[7]. This study confirmed the manipulation and radiolabeling of ghrelin to target GHSR *in vivo* with motivation to further optimize tracers for GHSR PET imaging. Up until this point, peptide derivates of ghrelin had been used to target GHSR *in vivo* but peptides are inherently unstable in circulation. To generate tracers with improved plasma stability, small molecule ligands to GHSR have been developed. A small molecule developed by Chollet *et al*[8], N$^{\alpha}$-NODAGA(^{68}Ga)-KwFwLL-CONH$_2$, was evaluated *in vivo* in rats. This compound exhibited high stability in the blood, good clearance in kidneys and liver, and detectable but minimal uptake in the heart. Therefore, the tracer profile should be further developed for optimal detection of cardiac GHSR[8]. Another study by Potter *et al.* evaluated a small molecule labelled with ^{11}C, (S)- 6-(4-fluorophenoxy)-3-((1-[^{11}C]methylpiperidin-3-yl)methyl)-2-o-tolylquinazolin-4(3H)-one, targeted to GHSR where there was increased stability and clearance with significant uptake in the brain region but minimal uptake in the mouse heart[9]. With these improvements in ghrelin analogues, our team developed targeted analogues for GHSR. Previously, we developed and tested a peptidomimetic, [1-Nal^{4},Lys^{5}(4-[^{18}F]-FB)]G-7039, for GHSR binding (69nM) in wildtype mice and mice lacking GHSR. There was no significant difference in tracer accumulation in the heart between mouse models indicating mouse models may not be optimal for imaging cardiac GHSR *in vivo*[10]. The next generation of tracer development incorporated small molecules where the lead candidate, ^{18}F-LCE470, showed improved binding affinity to GHSR of 0.11nM when compared to native ghrelin (3.3nM) with *in vitro* studies[11].

For my project, I evaluated the sensitivity and specificity of this new small molecule tracer, ^{18}F-LCE470, in targeting cardiac GHSR *in vivo*. In chapter 4, I used ^{18}F-LCE470 to

measure the regional distribution of GHSR density before and after a myocardial infarction (MI) using simultaneous PET/MRI. My work suggested that the uptake and distribution of ^{18}F-LCE470 are altered immediately (3 days) after a MI, with increases in uptake in the left circumflex region and significant decreases in the infarct region, and this pattern persisted for 11 months. The increased tracer uptake in the circumflex tissue surrounding the infarct suggests that GHSR activation may play a role in the mechanism of cardioprotection within the border myocardium in the weakening heart. To evaluate tracer specificity, patterns of cardiac perfusion measured through ^{13}N-NH_3 were compared to binding patterns in ^{18}F-LCE470. There was a unique binding pattern of ^{18}F-LCE470 in the LV of the canine heart when compared to cardiac perfusion (blood flow) as demonstrated by ^{13}N-NH_3. I then evaluated tracer sensitivity by correlating ^{18}F-LCE470 to tissue GHSR expression at end point (1.5 years after MI) using a custom far-red ghrelin analog, Cy5-cyclo-ghrelin(1-20), in infarct, remote, and LCX regions. The overall tissue GHSR expression strongly correlated to GHSR density as measured by ^{18}F-LCE470, showing the sensitivity of tracer binding in the canine heart. These specific regional changes in GHSR density show molecular alterations in the heart independently of changes in perfusion and overall LV function. Therefore, I have characterized a novel PET tracer, ^{18}F-LCE470, to sensitively and specifically detect molecular GHSR changes the heart in the absence of overall cardiac dysfunction.

5.4 Can GHSR Imaging be Used for Clinical Diagnosis for Cardiac Impairment?

Diagnosis of HD remain difficult as pathogenesis occurs in a variety of forms. The current diagnostic tests commonly encompass cardiac biomarkers and cardiac imaging. Conventional cardiac imaging, in the form of echocardiography, CT and MRI, detects functional and structural changes that are characteristic of the later stages of HD development while molecular imaging can target specific receptors or signalling pathways to measure the subclinical changes in the heart. My work suggests that a novel molecular PET imaging agent, ^{18}F-LCE470, may report increases in GHSR density *in vivo* in regions

surrounding a MI in the canine heart in the absence of overt global cardiac dysfunction. The increase in GHSR density may indicate GHSR-associated subclinical biochemical changes, as my results in human tissue biopsies showed that upregulation of GHSR is correlated with specific signalling pathways that induce cardioprotective responses through enhancing contractility, hypertrophy, and cell survival[6,12]. Alterations in cardiomyocyte biochemical signalling are known to occur early in the progression of HD and therefore early detection of these changes can provide significant advancements in diagnosis[13]. Additionally, we have demonstrated the scalability of the ghrelin-GHSR system in HD and hence, ^{18}F-LCE470 has the potential to track specific regional changes in GHSR density in the evolution of HD and HF. With the development of this novel PET imaging tool, we can detect molecular changes of GHSR through imaging which can be a useful tool in early diagnosis of clinical HD.

5.5 Elucidation of the Relationship Between GHSR and Inflammation

Now that we have validated ^{18}F-LCE470 sensitivity and specificity to GHSR *in vivo* in the canine model of MI, we want to evaluate the biochemical mechanisms associated with GHSR *in vivo*. One important process of interest is the relationship between GHSR and inflammation in the injured and failing heart. After cardiac injury, an intense acute immune and pro-inflammatory process is activated where monocytes, neutrophils, and leukocytes migrate to the site of injury to remove dead and damaged cells. This process specifically includes high numbers of pro-inflammatory macrophages in which glucose transporters have been upregulated due to their high energy demand[14]. About 3-4 weeks after injury, the pro-inflammatory response subsides, and the anti-inflammatory response is initiated. During this process, fibroblasts deposit extracellular matrix proteins and cross-linked collagen while granulation tissue becomes apoptotic and is cleared[15]. As discussed in the Introduction, GHSR functions through both an inhibitory effect of the pro-inflammatory response[16,17] and activation of the anti-inflammatory response[18,19] to protect the heart from further injury and adverse cardiac events induced by a prolonged inflammatory response.

We can measure potential *in vivo* relationships between GHSR and inflammation using PET imaging techniques.

Many PET tracers have been developed to target different aspects of the cardiac inflammatory process[20]. ^{68}Ga-[1,4,7,10-tetraazacyclododecane-N,N',N'',N'''-tetraacetic acid]-d- Phe1,Tyr3-octreotate (DOTATATE) is a common PET tracer that targets the somatostatin receptor 2 which is overexpressed in inflammatory macrophages. ^{68}G-DOTATATE can accurately detect inflammation after a myocardial infarction with minimal background uptake[21] and can determine atherosclerotic disease severity by differentiating high versus low risk lesions in the vasculature[22]. Another target for inflammation is the receptor C-X-C motif chemokine receptor 4 (CXCR4) which is upregulated on macrophage and T-cells associated with the pro-inflammatory process. ^{68}G-pentixafor, targeted to CXCR4, has been used to detect the increase in pro-inflammatory cells and vasculature lesions associated with atherosclerosis[23]. Another emerging target is the mitochondrial translocator protein TSPO, which is upregulated in most macrophages and lymphocytes; however, all cells express TSPO on the mitochondrial membrane, thereby creating background uptake in the myocardium[24]. Many tracers have been developed to target TSPO, and tracers that target TSPO specifically in cardiac inflammation include ^{18}F-flutriciclamide (^{18}F-GE180)[25], ^{11}C-PK11195[26], and ^{18}F-FEDAA1106[27]. ^{18}F-GE180 has been shown to be elevated globally in inflammatory macrophages acutely after an MI[25], and ^{11}C-PK11195 was elevated in inflammation associated with vulnerable/ symptomatic plaques in atherosclerosis[28]. Therefore, increased uptake of tracers that target TSPO measures increases in activated inflammatory cells and mitochondrial dysfunction in failing cardiomyocytes[24].

The most common clinically used tracer to detect inflammation in the heart is ^{18}F-fluorodeoxyglucose (^{18}F-FDG). Proinflammatory macrophages have significant overexpression of glucose transporters resulting in increased ^{18}F-FDG uptake[14]. One important thing to note when using ^{18}F-FDG in studies of inflammation is that normal myocardial glucose uptake needs to be suppressed to minimize background signal. This is usually done with an Intralipid™ infusion in animal studies, or by requiring human subjects to fast or have a high fat meal prior to imaging to reduce glucose metabolism and increase

the lipid metabolism in the normal myocardium[29]. It is uncommon for suppression to be ineffective; however, there may be variability in effectiveness. An example of such variability shown in Figure 5.1 where suppression was effective at the day 28 and week 8 time points after MI. However, suppression did not work effectively at month 6, as there is a significant amount of PET signal throughout the entire heart without any discernable cardiac region. Regardless, ^{18}F-FDG is clinically used to determine inflammation associated with HD such as endocarditis, sarcoidosis, and atherosclerosis. Additionally, ^{18}F-FDG is currently the clinical gold standard for determination of viable tissue in patients after myocardial infarction and in cardiac dysfunction with accurate assessment of scar presence[30,31]. Therefore, ^{18}F-FDG is an optimal tracer to evaluate the relationship between inflammation and GHSR *in vivo* in the heart.

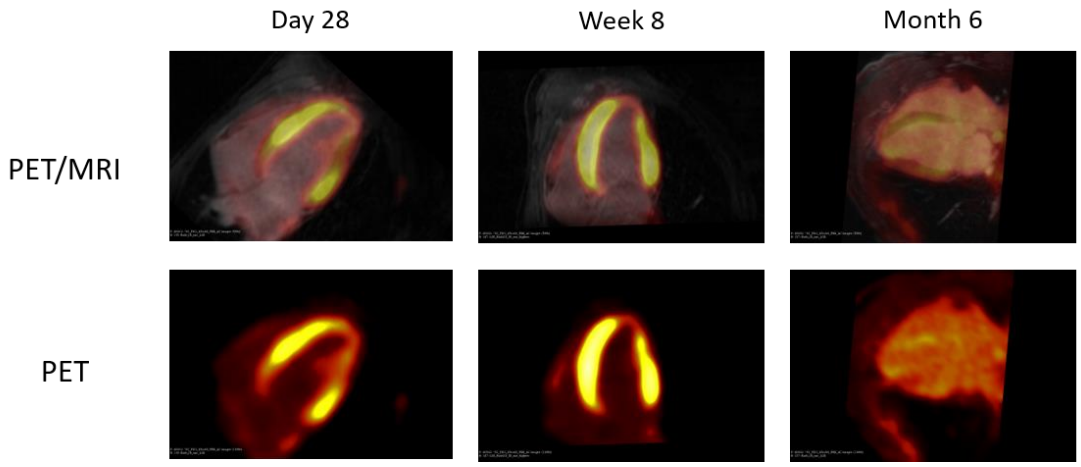

Figure 5.1 ^{18}F-FDG imaging in the canine heart after MI.

Canine heart after MI using Intralipid™ suppression to reduce background myocardial glucose uptake with PET imaging. Day 28 and week 8 demonstrate effective Intralipid™ suppression while month 6 indicates ineffective suppression with no clear discernible cardiac region.

We have performed preliminary analysis of ^{18}F-FDG uptake in the same dogs described in Chapter 4 with Intralipid™ suppression from day 1 to 1-year post-MI to evaluate the temporal dynamics of glucose metabolism in inflammation. We used kinetic modeling with Patlak analysis, an established method to quantify glucose metabolism[32,33], to determine the regional Ki values (net influx rate of the tracer). The Ki values of ^{18}F-FDG were determined for three different regions including the remote, infarct and left circumflex at days 1,7, 28, week 8, months 6 and 12 (Fig 5.2a). There was a significant increase in Ki values in the area of infarct compared to both the remote and circumflex tissue during the acute inflammatory phase of macrophage infiltration at days 1 and 7. We observed increased inflammation in the infarct region acutely and there is evidence in the literature of abundant macrophage, monocyte, and leukocyte infiltration in acute myocardial damage that can account for this increased signal we observed[15]. There was no significant inflammatory process in the remote or circumflex tissues acutely (days 1 and 7 post MI) as there was minimal ^{18}F-FDG uptake in these areas. The minimal ^{18}F-FDG uptake persisted around the same level through the chronic phase of MI (day 28 - 1 year post MI) which may be indicative of the lack of inflammatory processes in these areas chronically. However, there was a significant reduction of ^{18}F-FDG uptake in the infarct region in the chronic phase of MI (day 28 - 1 year post MI). It is known that the chronic phase of inflammation encompasses fibroblasts deposition of extracellular matrix proteins and cross-linked collagen with minimal macrophage presence[15] which likely accounts for the chronic decreased ^{18}F-FDG uptake in the infarct region. Therefore, changes in ^{18}F-FDG uptake help to provide a better understanding of the biology of the infarct region acutely and chronically.

We also measured levels of circulating cardiac inflammatory marker C-reactive protein (CRP), which is an indicator of inflammation associated with stressed and damaged myocardium, at the same time points as ^{18}F-FDG imaging sessions. CRP is released from the liver upon activation by a pro-inflammatory IL-6 specific response to cardiac stress and injury[34]. In cardiac inflammation, CRP exacerbates the pro-inflammatory response by binding to damaged cell membranes to enhance macrophage recruitment and phagocytosis[35]. In our study, there was a significant increase in plasma CRP in the pro-inflammatory phase (days 1, 3, and 7) after cardiac injury followed by reduced

inflammation back to baseline levels by day 21 (Fig 5.2b). That the peak of circulating CRP coincides with the peak of ^{18}F-FDG uptake suggests there is a significant increase in macrophage presence in the infarct at these time points, as ^{18}F-FDG is known to have significant uptake in macrophages while CRP recruits them to the site of cardiac inflammation. The enhancement of both ^{18}F-FDG and CRP acutely after MI provides a better understanding of the pro-inflammatory temporal timeline and the cell types present in the infarct region. Further elucidating the regional inflammatory biology composition and biochemical activation will help with understanding the evolution of HD.

To evaluate the relationship between inflammation and GHSR in the heart, we conducted linear regression analysis with ^{18}F-FDG Ki values and ^{18}F-LCE470 DV values in both the acute and chronic phases after MI (Fig 5.3). There was no correlation between GHSR density and glucose metabolism in the acute phase; however, there was a significant positive correlation in the chronic phase. GHSR is shown to have increased expression in tissue that is stressed[1], such as the region surrounding the infarct, no expression in dead and fibrotic tissue[6], and low expression in macrophages[36]. GHSR signalling is also known to activate cardioprotective responses, including anti-inflammatory responses, in cardiac tissue[18,19]. The lack of correlation between GHSR density and glucose metabolism acutely could be due to significant increases in macrophages where GHSR density is known to be low but ^{18}F-FDG uptake is increased. This lack of correlation acutely supports no significant relationship between GHSR and pro-inflammatory signaling in this model of MI. In contrast in the chronic phase (day 28 – 1 year post MI), macrophage presence is known to be decreased which is supported by decreased ^{18}F-FDG uptake in the area of infarct in our study. The positive correlation of ^{18}F-FDG and GHSR density chronically could be due to a cardioprotective response through GHSR in non-infarcted tissue. After MI, increases in inflammation in the heart are commonly associated with increase LV wall stress especially in the border myocardium[37]. The LV dilates as a compensatory mechanism to improve overall cardiac output[38]. GHSR is expected to be activated in the border myocardium after MI and induce cardioprotective mechanisms and help improve cardiac function[39,40]. Therefore, increased GHSR expression chronically after MI is likely due to cardioprotective mechanisms, partly due to inflammation associated to LV wall stress and dilation. To fully evaluate the relationship between GHSR and inflammation, *in vivo* PET

results should be compared to circulating inflammatory markers and histological samples of cardiac tissue.

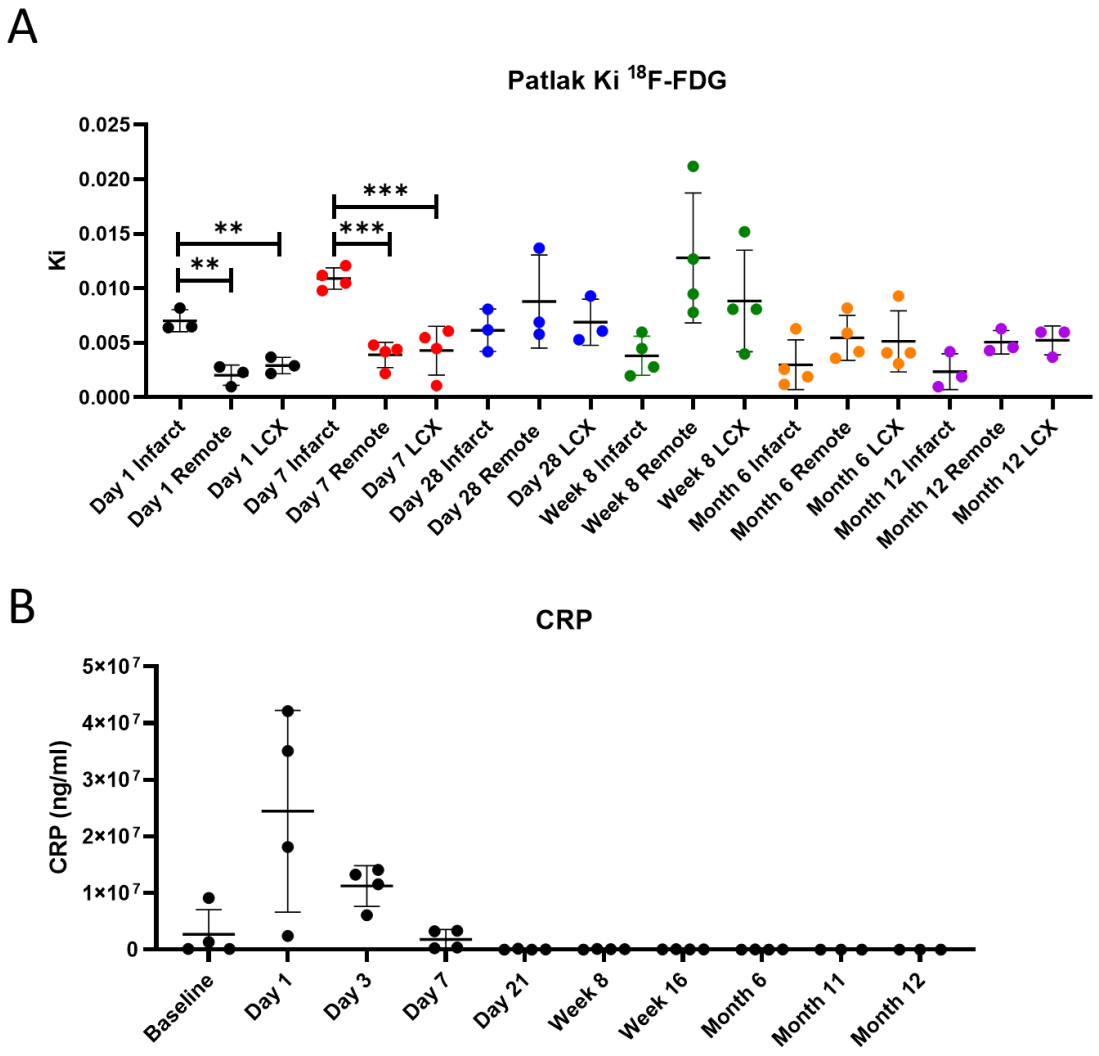

Figure 5.2 Quantification of glucose metabolism with ^{18}F-FDG in canine heart after MI.

A) Ki values increased in acute pro-inflammatory phase in the infarct at days 1 and 7. In the chronic anti-inflammatory phase, there was no significant differences between regions. B) Circulating CRP (cardiac specific inflammatory marker) levels which increased acutely and decreased back to low levels in the chronic inflammatory phase.

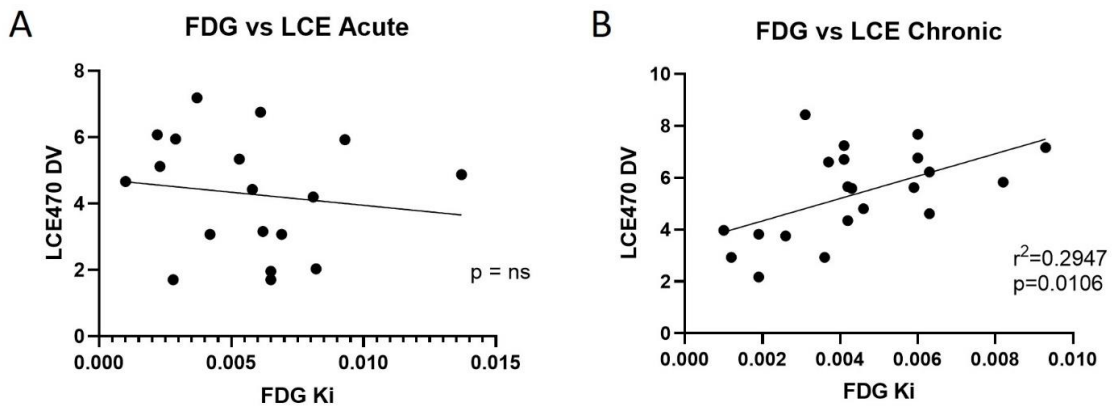

Figure 5.3 Correlation between inflammation (^{18}F-FDG) and GHSR (^{18}F-LCE470) over time.

A) Acute (days 1 and 7 post MI) inflammatory response shows no linear regression with GHSR *in vivo.* B) Chronic (day 28, week 8, month 6, and 1-year post MI) inflammatory response indicates a positive linear regression with GHSR *in vivo* in the canine heart after MI.

Our preliminary results outline a potential relationship between GHSR and inflammation after MI, and this process should be investigated in subsequent studies. To further determine the connections between cardiac inflammation and the regional distribution of GHSR, baseline ^{18}F-FDG imaging, before MI, is needed for accurate comparison of changes to both the acute and chronic inflammatory processes. The baseline images will help determine the extent of the pro- and anti-inflammatory phases and how long each phase persists. The change in ^{18}F-FDG uptake from baseline can then be correlated to the change in ^{18}F-LCE470 uptake at the same time points. To better compare GHSR to inflammation signalling, ^{18}F-LCE470 could be further characterized for quantitative PET imaging. A complete metabolite analysis should be conducted to generate a metabolite-corrected image-derived input function for precision quantitative imaging of GHSR dynamics. Although the quantitative values may change with metabolite correction, the pattern of tracer uptake should remain consistent. In addition to the GHSR-inflammation

relationship with PET imaging, circulating levels of inflammatory markers CRP and IL-6 along with HF markers BNP/NT-proBNP and high sensitive-Troponin T and I, should be correlated to circulating ghrelin levels to show the temporal relationships in the blood between ghrelin and both inflammation and HF. Furthermore, to accurately examine the regional and temporal relationship between GHSR and inflammation, endomyocardial biopsies of cardiac tissue, from baseline up to 1 year, should be analyzed for tissue markers of pro- and anti- inflammation along with GHSR expression. Additionally, changes in signalling pathways associated with contractility, metabolism, survival, and apoptosis should be measured in these tissue samples. These analyses will provide a more complete picture of the biology underlying the progression of cardiac dysfunction after MI.

In summary, my project successfully identified GHSR as a scalable biomarker in human heart failure and heart disease using quantitative fluorescence microscopy. I demonstrated specific regional changes in both the ghrelin-GHSR system and GHSR-associated signalling. These molecular and biochemical changes were present prior to the development of overt cardiac dysfunction. I then developed and characterized a targeted PET imaging agent for cardiac GHSR in a large animal model of myocardial infarction. I determined this PET tracer to sensitively and specifically bind to GHSR before and up to one year post-MI. This work not only demonstrated significant advancement in elucidating the biology of the myocardial ghrelin-GHSR system, but I have identified a novel *in vivo* imaging tool to accurately identify specific regional changes in cardiac tissue. The myocardial ghrelin-GHSR system can be a unique tool to non-invasively determine alterations in the molecular and biochemical processes associated with early stages of HD.

My project focused on three specific types of HD including end-stage HF, aortic stenosis, healthy heart, and cardiac remodeling after MI. In these specific models the ghrelin-GHSR system correlated in a scalable manner. It is still unknown how the ghrelin-GHSR system changes in all types of HD and therefore this system must be explored in all disease states. There is currently no universal biomarker of HD or HF and ghrelin-GHSR must be explored to determine which disease states have increased or decreased GHSR expression in the myocardium. *In vivo* imaging has allowed for detection of GHSR changes in the heart which can be quantified with compartmental modelling. The next step for this system

is to determine a quantitative threshold where GHSR is elevated, likely at earlier stages when HF is still treatable with medications or surgery. This biomarker, GHSR, can be used in conjunction with a panel of biomarkers to help predict which patients may proceed to HF. This system may ultimately help to diagnose HD earlier in its progression, resulting in favourable outcomes for more patients.

5.6 References

1. Beiras-Fernandez, A. *et al.* Altered myocardial expression of ghrelin and its receptor (GHSR-1a) in patients with severe heart failure. *Peptides* **31**, 2222–8 (2010).

2. Ma, Y., Zhang, L., Edwards, J. N., Launikonis, B. S. & Chen, C. Growth hormone secretagogues protect mouse cardiomyocytes from in vitro ischemia/reperfusion injury through regulation of intracellular calcium. *PLoS One* **7**, (2012).

3. Cao, Y. *et al.* Cardioprotective Effect of Ghrelin in Cardiopulmonary Bypass Involves a Reduction in Inflammatory Response. *PLoS One* **8**, (2013).

4. Baldanzi, G. *et al.* Ghrelin and des-acyl ghrelin inhibit cell death in cardiomyocytes and endothelial cells through ERK1/2 and PI 3-kinase/AKT. *J. Cell Biol.* **159**, 1029–1037 (2002).

5. Mitacchione, G. *et al.* The gut hormone ghrelin partially reverses energy substrate metabolic alterations in the failing heart. *Circ. Hear. Fail.* **7**, 643–651 (2014).

6. Sullivan, R. *et al.* Dynamics of the Ghrelin/Growth Hormone Secretagogue Receptor System in the Human Heart Before and After Cardiac Transplantation. *J. Endocr. Soc.* **3**, 748–762 (2019).

7. Charron, C. L., McFarland, M. S., Dhanvantari, S. & Luyt, L. G. Development of a [68Ga]-ghrelin analogue for PET imaging of the ghrelin receptor (GHS-R1a). *Medchemcomm* **9**, 1761–1767 (2018).

8. Chollet, C., Bergmann, R., Pietzsch, J. & Beck-Sickinger, A. G. Design, Evaluation, and Comparison of Ghrelin Receptor Agonists and Inverse Agonists as Suitable Radiotracers for PET Imaging. *Bioconjug. Chem.* **23**, 771–784 (2012).

9. Potter, R. *et al.* Synthesis and in vivo evaluation of (S)-6-(4-fluorophenoxy)-3-((1-[11C]methylpiperidin-3-yl)methyl)-2-o-tolylquinazolin-4(3H)-one, a potential PET tracer for growth hormone secretagogue receptor (GHSR). *Bioorganic Med.*

Chem. **19**, 2368–2372 (2011).

10. Abbas, A. *et al.* Development and Characterization of an 18 F-labeled Ghrelin Peptidomimetic for Imaging the Cardiac Growth Hormone Secretagogue Receptor. *Mol. Imaging* **17**, 1–11 (2018).

11. Charron, C. L. *et al.* Structure-Activity Study of Ghrelin(1-8) Resulting in High Affinity Fluorine-Bearing Ligands for the Ghrelin Receptor. *J. Med. Chem.* **60**, 7256–7266 (2017).

12. Sullivan, R. *et al.* Regional Differences in the Ghrelin-Growth Hormone Secretagogue Receptor Signalling System in Human Heart Disease. *CJC Open* **4**, 1–13 (2021).

13. Ashrafian, H., Frenneaux, M. P. & Opie, L. H. Metabolic mechanisms in heart failure. *Circulation* **116**, 434–448 (2007).

14. Freemerman, A. J. *et al.* Metabolic reprogramming of macrophages: Glucose transporter 1 (GLUT1)-mediated glucose metabolism drives a proinflammatory phenotype. *J. Biol. Chem.* **289**, 7884–7896 (2014).

15. Prabhu, S. D. & Frangogiannis, N. G. The biological basis for cardiac repair after myocardial infarction. *Circ. Res.* **119**, 91–112 (2016).

16. Li, W. G. *et al.* Ghrelin Inhibits Proinflammatory Responses and Nuclear Factor-κB Activation in Human Endothelial Cells. *Circulation* **109**, 2221–2226 (2004).

17. Dixit, V. D. *et al.* Ghrelin inhibits leptin- and activation-induced proinflammatory cytokine expression by human monocytes and T cells. *J. Clin. Invest.* **114**, 57–66 (2004).

18. Huang, C.-X. *et al.* Ghrelin inhibits post-infarct myocardial remodeling and improves cardiac function through anti-inflammation effect. *Peptides* **30**, 2286–2291 (2009).

19. Raghay, K., Akki, R., Bensaid, D. & Errami, M. Ghrelin as an anti-inflammatory and protective agent in Ischemia/Reperfusion injury. *Peptides* **124**, (2019).

20. Wu, C., Li, F., Niu, G. & Chen, X. PET imaging of inflammation biomarkers. *Theranostics* **3**, 448–466 (2013).

21. Tarkin, J. M. *et al.* 68Ga-DOTATATE PET Identifies Residual Myocardial Inflammation and Bone Marrow Activation After Myocardial Infarction. *J. Am. Coll. Cardiol.* **73**, 2489–2491 (2019).

22. Tarkin, J. M. *et al.* Detection of Atherosclerotic Inflammation by 68Ga-DOTATATE PET Compared to [18F]FDG PET Imaging. *J. Am. Coll. Cardiol.* **69**, 1774–1791 (2017).

23. Kircher, M. *et al.* Imaging Inflammation in Atherosclerosis with CXCR4-Directed 68Ga-Pentixafor PET/CT: Correlation with 18F-FDG PET/CT. *J. Nucl. Med.* **61**, 751–756 (2020).

24. Thackeray, J. T. & Bengel, F. M. Molecular Imaging of Myocardial Inflammation With Positron Emission Tomography Post-Ischemia: A Determinant of Subsequent Remodeling or Recovery. *JACC Cardiovasc. Imaging* **11**, 1340–1355 (2018).

25. Thackeray, J. T. *et al.* Myocardial Inflammation Predicts Remodeling and Neuroinflammation After Myocardial Infarction. *J. Am. Coll. Cardiol.* **71**, 263–275 (2018).

26. Tarkin, J. M., Joshi, F. R. & Rudd, J. H. F. PET imaging of inflammation in atherosclerosis. *Nat. Rev. Cardiol.* **11**, 443–457 (2014).

27. Cuhlmann, S. *et al.* In vivo mapping of vascular inflammation using the translocator protein tracer 18F-FEDAA1106. *Mol. Imaging* **13**, 1–11 (2014).

28. Gaemperli, O. *et al.* Imaging intraplaque inflammation in carotid atherosclerosis with 11C-PK11195 positron emission tomography/computed tomography. *Eur. Heart J.* **33**, 1902–1910 (2012).

29. Williams, G. & Kolodny, G. M. Suppression of myocardial 18F-FDG uptake by preparing patients with a high-fat, low-carbohydrate diet. *AJR. Am. J. Roentgenol.* **190**, 151–156 (2008).

30. Al Moudi, M. & Sun, Z. H. Diagnostic value of 18F-FDG PET in the assessment of myocardial viability in coronary artery disease: A comparative study with 99mTc SPECT and echocardiography. *J. Geriatr. Cardiol.* **11**, 229–236 (2014).

31. Zhang, X. *et al.* Clinical outcome of patients with previous myocardial infarction and left ventricular dysfunction assessed with myocardial 99mTc-MIBI SPECT and 18F-FDG PET. *J. Nucl. Med.* **42**, 1166–1173 (2001).

32. Yao, S. *et al.* Simplified Protocol for Whole Body Patlak Parametric Imaging with 18 F-FDG PET/CT: Feasibility and Error Analysis . *Med. Phys.* (2020) doi:10.1002/mp.14187.

33. Nakajo, M. *et al.* Value of Patlak Ki images from 18F-FDG-PET/CT for evaluation of the relationships between disease activity and clinical events in cardiac sarcoidosis. *Sci. Rep.* **11**, 1–10 (2021).

34. Sitepu, N. B. & Harahap, U. The Role Of hs-CRP In Predicting The Likelihood Of Coronary Heart Disease. *Indones. J. Pharm. Clin. Res.* **3**, 51–61 (2020).

35. Sproston, N. R. & Ashworth, J. J. Role of C-reactive protein at sites of inflammation and infection. *Front. Immunol.* **9**, 1–11 (2018).

36. Gnanapavan, S. *et al.* The tissue distribution of the mRNA of ghrelin and subtypes of its receptor, GHS-R, in humans. *J. Clin. Endocrinol. Metab.* **87**, 2988–2991 (2002).

37. Jackson, B. M. *et al.* Border zone geometry increases wall stress after myocardial infarction: Contrast echocardiographic assessment. *Am. J. Physiol. - Hear. Circ. Physiol.* **284**, 475–479 (2003).

38. Westman, P. C. *et al.* Inflammation as a Driver of Adverse Left Ventricular

Remodeling after Acute Myocardial Infarction. *J. Am. Coll. Cardiol.* **67**, 2050–2060 (2016).

39. Ju, H., Zhao, S. & Tappia, P. S. Expression of G q and PLC-[illegible] in Scar and Border Tissue in Heart Failure Due to Myocardial Infarction. *Circ. Basic Sci. Rep* **97**, 892–899 (1998).

40. Pose, M. L. Characterization of the intracellular signaling mechanisms activated by ghrelin through GHSR-1a: role of β-arrestins. (UNIVERSIDAD DE SANTIAGO DE COMPOSTELA, 2011).

Appendices

Appendix A 1. Human Ethics Protocol Approval: Cardiac Transplantation and Surgery Study

Western Research

Date: 31 August 2020

To: Gerry Wisenberg

Project ID: 102992

Study Title: Assessment of ghrelin in cardiac tissue sample

Application Type: Continuing Ethics Review (CER) Form

Review Type: Delegated

REB Meeting Date: September 15 2020

Date Approval Issued: 31/Aug/2020

REB Approval Expiry Date: 04/Sep/2021

Dear Gerry Wisenberg,

The Western University Research Ethics Board has reviewed the application. This study, including all currently approved documents, has been re-approved until the expiry date noted above.

REB members involved in the research project do not participate in the review, discussion or decision.

Western University REB operates in compliance with, and is constituted in accordance with, the requirements of the TriCouncil Policy Statement: Ethical Conduct for Research Involving Humans (TCPS 2); the International Conference on Harmonisation Good Clinical Practice Consolidated Guideline (ICH GCP); Part C, Division 5 of the Food and Drug Regulations; Part 4 of the Natural Health Products Regulations; Part 3 of the Medical Devices Regulations and the provisions of the Ontario Personal Health Information Protection Act (PHIPA 2004) and its applicable regulations. The REB is registered with the U.S. Department of Health & Human Services under the IRB registration number IRB 00000940.

Please do not hesitate to contact us if you have any questions.

Sincerely,

The Office of Human Research Ethics

Note: This correspondence includes an electronic signature (validation and approval via an online system that is compliant with all regulations).

Appendix A 2. Animal Use Protocol Ethics Approval: Cardiac PET/MRI in the Canine Heart

eSirius3G

Western

PI :	Prato, Frank
Protocol #	2017-006
Status :	Approved (w/o Stipulation)
Approved :	06/01/2017
Expires :	06/01/2021
Title :	"PET/MR Based Myocardial Tissue Characterization in Health and Ischemic Heart Disease"

Table of Contents

- Animal Use Protocol Overview
- Funding Source List
- Purpose of Animal Use
- Hazardous Materials
- Animal Movement Between Sites
- Animal Groups and Experimental Timelines Overview
- Dog
  - Break
  - Justification for Choice of Species
  - the 3Rs: Replace, Reduce, Refine
  - Species Strains
  - Animal Transfers
  - Environmental Enrichment
  - Animal Holding/Housing and Use Location Information
  - Holding beyond 12 hours
  - Acclimatization Period & Quarantine
  - Physical Restraint Devices List
  - Experimental Agents Information
  - SOP List
  - Procedures Checklist for Reporting and Training
  - Procedures Narrative
  - Procedural Consequences & Monitoring
  - Endpoint Method Information
  - Animal Numbers Requested
- Personnel List

Appendix A 3. Permission to Reproduce Sullivan et al. 2019 J. Endocr. Soc.

ENDOCRINE SOCIETY

Dynamics of the Ghrelin/Growth Hormone Secretagogue Receptor System in the Human Heart Before and After Cardiac Transplantation

Author: Sullivan, Rebecca; Randhawa, Varinder K
Publication: Journal of the Endocrine Society
Publisher: Oxford University Press
Date: 2019-02-14

Copyright © 2019, Oxford University Press

Review Order

Please review the order details and the associated terms and conditions.

No royalties will be charged for this reuse request although you are required to obtain a license and comply with the license terms and conditions. To obtain the license, click the Accept button below.

Licensed Content

Licensed Content Publisher	Oxford University Press
Licensed Content Publication	Journal of the Endocrine Society
Licensed Content Title	Dynamics of the Ghrelin/Growth Hormone Secretagogue Receptor System in the Human Heart Before and After Cardiac Transplantation
Licensed Content Author	Sullivan, Rebecca; Randhawa, Varinder K
Licensed Content Date	2019-02-14
Licensed Content Volume	3
Licensed Content Issue	4

Order Details

Type of Use	Thesis/Dissertation
Requestor type	Author of this OUP content
Format	Print and electronic
Portion	Text Extract
Number of pages requested	10
Will you be translating?	No

About Your Work

Additional Data

About Your Work

Title	Dynamics of the Ghrelin/Growth Hormone Secretagogue Receptor System in the Human Heart Before and After Cardiac Transplantation
Institution name	Western University
Expected presentation date	Apr 2021

Additional Data

Portions	I want to reuse my article in my thesis.

Requestor Location

Requestor Location	Miss. Rebecca Sullivan 268 Grosvenor Street London, ON N6A4V2 Canada Attn: Lawson Health Research Institute and Western University

Tax Details

Publisher Tax ID	GB125506730

$ Price

Total	0.00 USD

☑ I agree to these terms and conditions.
☑ I understand this license is for reuse only and that no content is provided.

Customer Code(if supplied) Apply Code

Total: 0.00 USD

BACK DECLINE HOLD QUOTE ACCEPT

Please click accept only once.

Dear Miss. Rebecca Sullivan,

Thank you for placing your order through Copyright Clearance Center's RightsLink® service.

Order Summary

Licensee:	Miss. Rebecca Sullivan
Order Date:	Feb 5, 2021
Order Number:	5002671362348
Publication:	Journal of the Endocrine Society
Title:	Dynamics of the Ghrelin/Growth Hormone Secretagogue Receptor System in the Human Heart Before and After Cardiac Transplantation
Type of Use:	Thesis/Dissertation
Order Total:	0.00 USD

View or print complete details of your order and the publisher's terms and conditions.

Sincerely,

Copyright Clearance Center

Appendix A 4. Permission to Reproduce Sullivan et al. 2020 CJC Open

FW: Rights and Access form completed for your article [CJCO_220]

Dear Miss. Sullivan,

Thank you for completing the Rights and Access Form for your article *Regional Differences in the Ghrelin-Growth Hormone Secretagogue Receptor Signalling System in Human Heart Disease* on November 10, 2020.

The Order Summary is attached to this email.
Your article is free for everyone to read online at https://doi.org/10.1016/j.cjco.2020.10.015

If you have any questions, please do not hesitate to contact us. To help us assist you, please quote our article reference CJCO220 in all correspondence.

Now that your article has been accepted, you will want to maximize the impact of your work. Elsevier facilitates and encourages authors to share their article responsibly. To learn about the many ways in which you can share your article whilst respecting copyright, visit: www.elsevier.com/sharing-articles.

Kind regards,
Elsevier Researcher Support

Copyright Clearance Center | RightsLink®

Home | Help | Email Support | Sign in | Create Account

Regional Differences in the Ghrelin-Growth Hormone Secretagogue Receptor Signalling System in Human Heart Disease

Author: Rebecca Sullivan,Varinder K. Randhawa,Tyler Lalonde,Tina Yu,Bob Kiaii,Leonard Luyt,Gerald Wisenberg,Savita Dhanvantari
Publication: CJC Open
Publisher: Elsevier
Date: Available online 4 November 2020

© 2020 Canadian Cardiovascular Society. Published by Elsevier Inc.

Journal Author Rights

Please note that, as the author of this Elsevier article, you retain the right to include it in a thesis or dissertation, provided it is not published commercially. Permission is not required, but please ensure that you reference the journal as the original source. For more information on this and on your other retained rights, please visit: https://www.elsevier.com/about/our-business/policies/copyright#Author-rights

BACK | CLOSE WINDOW

© 2021 Copyright - All Rights Reserved | Copyright Clearance Center, Inc. | Privacy statement | Terms and Conditions
Comments? We would like to hear from you. E-mail us at customercare@copyright.com

ELSEVIER

About Elsevier | Products & Solutions | Services | Shop & Discover | Search

Preprint | Accepted manuscript | Published journal article | Help and support

Published Journal Article

Policies for sharing published journal articles differ for subscription and gold open access articles:

Subscription articles

- If you are an author, please share a link to your article rather than the full-text. Millions of researchers have access to the formal publications on ScienceDirect, and so links will help your users to find, access, cite, and use the best available version
- If you are an author, you may also share your Published Journal Article (PJA) privately with known students or colleagues for their personal use
- Theses and dissertations which contain embedded PJAs as part of the formal submission can be posted publicly by the awarding institution with DOI links back to the formal publications on ScienceDirect
- If you are affiliated with a library that subscribes to ScienceDirect you have additional private sharing rights for others' research accessed under that agreement. This includes use for classroom teaching and internal training at the institution (including use in course packs and courseware programs), and inclusion of the article for grant funding purposes
- Otherwise sharing is by agreement only
- The Published Journal Article cannot be shared publicly, for example on ResearchGate or Academia.edu, to ensure the sustainability of peer-reviewed research in journal publications

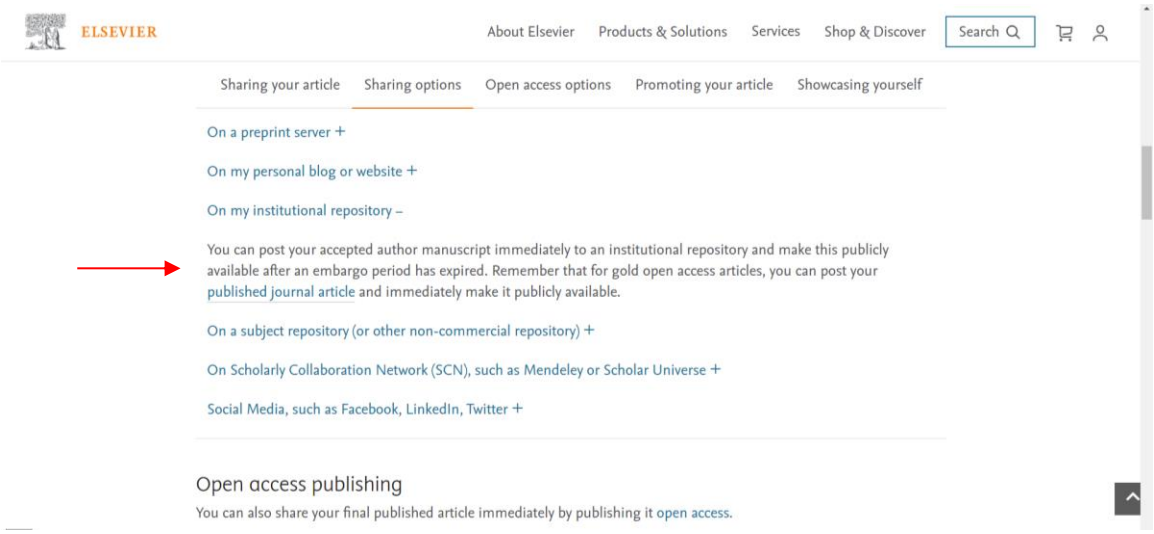
ELSEVIER
About Elsevier
Products & Solutions
Services
Shop & Discover
Search
Sharing your article
Sharing options
Open access options
Promoting your article
Showcasing yourself
On a preprint server +
On my personal blog or website +
On my institutional repository –
You can post your accepted author manuscript immediately to an institutional repository and make this publicly available after an embargo period has expired. Remember that for gold open access articles, you can post your published journal article and immediately make it publicly available.
On a subject repository (or other non-commercial repository) +
On Scholarly Collaboration Network (SCN), such as Mendeley or Scholar Universe +
Social Media, such as Facebook, LinkedIn, Twitter +
Open access publishing
You can also share your final published article immediately by publishing it open access.

Curriculum Vitae

Name: Rebecca Sullivan

Post-secondary Education and Degrees:

Western University
London, Ontario, Canada
2015-2021 PhD. Pathology and Laboratory Medicine
Collaborative Graduate Program in Molecular Imaging

Wilfrid Laurier University
Waterloo, Ontario, Canada
2011-2015 Hon. BSc Biochemistry and Biotechnology

Honours and Awards:

1. Alexander Graham Bell Canada Graduate Scholarship-Doctoral, NSERC, 2019-2021, $70,000
2. Word Molecular Imaging Congress Trave Stipend, WMIC, 2019, $350 USD
3. Women Scholar Award, WMIC, 2019, $300 USD
4. Molecular Imaging Travel Stipend, Western University, 2019, $400
5. Dr. Frederick Winnet Luney Graduate Research Award, Western University, 2019, $1.600
6. Dr. Frederick Winnet Luney Pathology research Scholarship, Western University, 2018-2019, $5000
7. Word Molecular Imaging Congress Travel Stipend, WMIC, 2018, $650 USD
8. Molecular Imaging Travel Stipend, Western University, 2018, $400
9. Best Poster Presentation, Cellular and Molecular Imaging Symposium, 2018, $50
10. Lawson Internal Research Fund – Studentship, Lawson Health Research Institute, 2017-2018, $15,000
11. Honourable Mention for Best Poster, Imaging Network of Ontario, 2017, $100
12. Best Basic/ Clinical Science Collaborative Poster Presentation, Western University, 2016, $100
13. Western Graduate Research Scholarship, Western University, 2015-2021, $7,000/year

Related Work Experience:

1. Graduate Teaching Assistant, 4100G One Health, Interdisciplinary Medical Sciences, Western University, January 2020 – April 2020
2. Graduate teaching Assistant, 4100G One Health, Interdisciplinary Medical Sciences, Western University, January 2019 – April 2019
3. Graduate teaching Assistant, 3900 Laboratory Course, Interdisciplinary Medical Sciences, Western University, September 2017 – April 2018
4. Summer Research Student, London Health Sciences Center, May 2014 – September 2015
5. Instructional Assistant, Fundamentals of Chemistry, Wilfrid Laurier University, January 2015 – December 2015

Peer Reviewed Publications:

1. **Sullivan R**, Randhawa V K, Lalonde T, Yu T, Kiaii B, Luyt L, Wisenberg G, Dhanvantari S. (2021). Regional Differences in the Ghrelin-Growth Hormone Secretagogue Receptor Signalling System in Human Heart Disease. CJC Open.4: 1-13.
2. Rice K, BatulK , Whiteside J, Kelso J, Papinski M, Pratasouskaya M, Wang D, S**ullivan R**, Bartlett C, Weadge J T, Van der Kamp M W, Moreno-Hagelsieb G, Suits M D, Horsman G P. (2019). The predominance of nucleotidyl activation in bacterial phosphonate biosynthesis. Nature Communications. 10, 3698 (2019). https://doi.org/10.1038/s41467-019-11627-6
3. **Sullivan R**, Randhawa V K, Stokes A, Wu D, Lalonde T, Kiaii B, Luyt L, Wisenberg G, Dhanvantari S. (2019). Dynamics of the Ghrelin/Growth Hormone Secretagogue Receptor System in the Human Heart Before and After Cardiac Transplantation. Journal of the Endocrine Society. 3(4): 748-762. http://dx.doi.org/10.1210/js.2018-00393
4. El-Sherif O, Xhaferllari I, Sykes J, Butler J, DeKemp R A, Renaud J, Yin H, Wilk B, **Sullivan R,** Pickering G J, Battista J, Wisenberg G, Prato F, Gaede S. (2019). ^{18}F-FDG Cardiac PET inflammation imaging in a canine model of radiation induced cardiac disease associated with breast cancer radiotherapy. American Journal of Physiology-Heart and Circulatory Physiology. 316(3): H586-H595. http://dx.doi.org/https://doi.org/10.1152/ajpheart.00273.2018
5. **Sullivan R**, McGirr R, Hu S, Tan A, Wu D, Charron C, Lalonde T, Arany E, Chakrabarti S, Luyt L, Dhanvantari S. (2017). Changes in the Cardiac GHSR1a-Ghrelin System Correlate With Myocardial Dysfunction in Diabetic Cardiomyopathy in Mice. Journal of the Endocrine Society. 2(2): 1-12. http://dx.doi.org/10.1210/js.2017-00433
6. **Sullivan R**, Schaus D, John M, Delport J A. (2015). A Mini Review of the Current status of Extended Spectrum Beta- Lactamases. Journal of Medical Microbiology & Diagnosis. 4(4): 203-205.

Selected Presentations:

National/ International

1. Word Molecular Imaging Congress 2020, October 2020, **Poster**, *Virtual*
2. The World Molecular Imaging Congress 2019, September 2019, **Oral**, *Montreal, Canada*
3. Canadian Cardiovascular Congress 2019, October 2019, **Oral**, *Montreal, Canada*
4. The World Molecular Imaging Congress 2018, September 2018, **Oral**, *Seattle, Washington, USA*
5. Canadian cardiovascular Congress 2017, October 2017, Vancouver, **Oral**, *British Columbia, Canada*
6. World Molecular Imaging Congress 2016, September 2016, **Poster**, *New York, New York, USA*

Local

1. The 18th Annual Imaging network of Ontario Symposium, March 2020, **Oral**, *Virtual*
2. London Health Research Day, April 2019, **Poster**, *London, Canada*
3. The 17th Annual Imaging Network of Ontario, March 2019, **Poster**, *London, Canada*
4. Pathology Research Day 2018, April 2018, **Poster**, *London, Canada*
5. The 16th Annual Imaging Network of Ontario, March 2018, **Oral**, *Toronto, Canada*
6. Southwestern Ontario Cellular and Molecular Imaging Symposium, May 2018, **Oral and Poster**, *London, Canada*
7. Talks on Friday, February 2018, **Oral**, *London, Canada*
8. The 15th Annual Imaging Network of Ontario, March 2017, **Poster**, *London, Canada*
9. London Health Research Day, March 2017, **Oral**, *London, Canada*
10. Pathology Research Day 2016, April 2016, **Poster**, *London, Canada*
11. 6th Annual Diabetes Research Day, October 2015, **Oral**, *London, Canada*